ENGINEERING A NOVEL MESOPOROUS SILICA-LIPID HYBRID CARRIER FOR ORAL PEPTIDE DELIVERY

MOHAMAD ANAS MAHER AL TAHAN

Doctor of Philosophy

ASTON UNIVERSITY

December 2023

Aston University

ENGINEERING A NOVEL MESOPOROUS SILICA-LIPID HYBRID CARRIER FOR ORAL PEPTIDE DELIVERY

Mohamad Anas Al Tahan

Doctor of Philosophy

December 2023

Thesis Summary

The cornerstone of drug administration routes is oral delivery due to its convenience, non-invasiveness, and safety. Yet, utilising this route for peptide oral delivery is quite challenging due to the harsh environment and limited permeability of the gastrointestinal tract. Nonetheless, many researchers have worked extensively to enhance the oral delivery of peptides using numerous approaches, such as lipids, physical approaches, and mesoporous silica.

Poor delivery and absorption through the intestinal epithelium constitute some of the key barriers. Hence, a novel carrier was formulated using mesoporous silica equipped with stearic acid needle-like structures on the surface, to enhance the peptide interaction with epithelial cells. This carrier was successfully constructed with microparticle silica after studying the factors that govern the peptide loading and the needles' presence on the surface. Subsequently, this carrier was loaded with a model peptide (octreotide acetate), and its absorption profile studied using Caco-2 cells. Octreotide absorption from the carrier was higher than the unloaded peptide. In addition, using this carrier has presented levels of permeation similar to values of permeation enhancers, which could be attributed to stearic acid needles presence on the surface that enhanced cell interaction.

The factors that affect protein loading into silica carriers were investigated by incorporating two proteins with different molecular weights into the carrier. The loading process was governed by diffusion, while loading efficiency seemed to be highly controlled by solvent's viscosity, polarity, and protein size. Furthermore, utilising imaging techniques such as confocal microscopy proved valuable in identifying protein's positioning after diffusion based on 3D imaging. Finally, the ability to compress silica into a dosage form was studied in addition to determining the release behaviour of protein from the carrier. Ultimately, compressing silica into tablets is achievable; however, this process is driven by the silica type, amount used, diluent composition, and compression force.

Keywords:

Protein Oral Delivery, Mesoporous Silica, Absorption, Permeation Enhancers, Cell Culture, Protein Diffusion, Tablets.

Acknowledgements

I would like to express my sincere thanks to my supervisor Dr Craig Russell and my associate supervisor Dr Ali Al-Khattawi, for their guidance, help and support during the three-year journey of my PhD. Additionally, all the academic staff at the School of Pharmacy must be thanked for their constant help and feedback during the three-year journey.

I would like to thank all the members of the technical team at Aston University who helped and assisted me during this project. Additionally, I would like to express my thanks to all my colleagues and friends for their motivation and support.

Last but not least, I would like to express my gratitude and forever thanks to my parents, who accompanied me during this journey and stood with me during every difficulty. If it were not for you, I would not be here, nor would I have achieved what I had.

List of Figures

List of Equations

List of Tables

Abbreviations

μm : micrometres

4-CNAB : 4-([4-chloro-2-hydroxybenzoyl]-amino) butanoic acid

5-CNAC : N-(5-chlorosalicyloyl)-8-aminocaprylic

Å : Angstrom

AFM : Atomic Force Microscopy

AMEs : Absorption-Modifying Excipients

ANOVA : One-Way Analysis of Variance

ATCC : American Type Culture Collection

BSA : Bovine Serum Albumin

C10: Sodium Caprate

C8: Sodium Caprylate

CLEC : Cross-Linked Enzyme Crystal

CMC Na : Coscarmellose Sodium

CODES : Colon Specific Delivery System

CPPs : Cell-Penetrating Peptides

D_0 : Diffusion

DC : Direct Compression

DCA : Deoxycholic Ccid

DDSs : Drug Delivery Systems

DEGEE : Diethylene Glycol Monoethyl Ether

DLS : Dynamic Light Scattering

DMEM : Dulbecco's Modified Eagle Medium

DMPC : 1,2-Dimyristoyl-sn-glycerol-3- phosphocholine

DOX : Doxorubicin

DSC : Differential Scanning Calorimetry

DSNs : Dendritic Silica Nanoparticles

DTPA : Diethylene Triamine Penta Acetic Acid

FBS : Fetal Bovine Serum

FDA : Food and Drug Administration

FET : Field-Effect Transistor

FnBPA : Fibronectin-Binding Protein A

FTIR : Fourier-Transform Infrared Spectroscopy

GH : Growth Hormone

GIPET : Gastrointestinal Permeation Enhancement Technology

GIT : Gastrointestinal Tract

GLP : Glucagon-Like Peptide

GRAS : Generally Regarded as Safe

HA2 : Hemagglutinin-2

HBSS : Hank's Balanced Salt Solution

HDV : Hepatocyte-Directed Vesicle

HPMC : Hydroxypropyl Methylcellulose

Hz: Hertz

IPEC-J2 : Small Intestinal Porcine Epithelial Cells

IUPAC : International Union of Pure and Applied Chemistry

K_B : Boltzmann Constant

LBL : Layer-by-Layer

LOD : Limit of Detection

LOQ : Limit of Quantification

LUMI : Luminal Unfolding Microneedle Injector

Mal-PEG-PCL : Maleimidyl-poly(ethylene glycol)-co-poly(ε-caprolactone)

MCC : Microcrystalline Cellulose

MDCK : Madin–Darby Canine Kidney

MDM2 : Mouse Double Minute 2 Homolog

MEM : Minimum Essential Medium

MLCK : Myosin Light Chain Kinase Signalling Pathways

mm : Millimetres

MMX : Multi Matrix

MSNs : Mesoporous Silica Nanoparticles

Mw : Molecular Weight

N_A : Avogadro's Number

nm : Nanometres

NOD : Non-Obese Diabetic

NPs: Nanoparticles

P(HEMA-co-MAA) : Poly (hydroxy ethyl methacrylate-co-methacrylic acid)

P(MAA-g-EG) : Poly (methacrylic acid-g-ethylene glycol)

Papp : Apparent Permeability

PBS : Phosphate Buffered Saline

PDCT : Peptide-To-Drug Converting Technology

PEG : Polyethene Glycol

PEs : Permeation Enhancers

P-gp : P-Glycoprotein

Phel : Phenylalanine

pHPMA : Poly-N-(2-hydroxypropyl) methacrylamide

PLA-PEG : Poly (lactic acid)– b-poly (ethene glycol)

PLGA : Poly(D,L-lactide-co-glycolide)

PMAA : Poly (methacrylic acid)

PMMMA : Poly [(methyl methacrylate)-co-(methyl acrylate)-co-(methacrylic acid)]

PNIPAm-MAA : Poly (N-isopropyl acrylamide-co-methacrylic acid)

POD ™ : Protein Oral Delivery ™

POPC : 1,2-Palmitoyl-oleoyl-*sn*-glycero-3-phosphocholine

PVP : Polyvinylpyrrolidone

RNase : Ribonuclease

RGD : Arginine–Glycine–Aspartic Acid

R_m : Solute Radius

RPM : Rotaions Per Minute

S.aureus : Staphylococcus Aureus

S/O/W : Solid-In-Oil-In Water

SB 15 : Santa Barbara 15

SB12 : Sulfobetaine 12

S_c : Molecular Surface Area

SEDDS : Self-Emulsifying Drug Delivery Systems

SEM : Scanning Electron Microscopy

SLN : Solid Lipid Nanoparticles

SNAC : Salcaprozate Sodium / N-(8-[2-hydroxybenzoyl]-amino) caprylic acid

SOMA : Self-Orienting Millimetre-Scale Applicator

SS_A : Specific Surface Area

SSTR2 : Specifically Somatostatin Receptor 2

T : Temperature

TAMSNs : Tannic Acid-Mesoporous Silica Nanoparticles

TEER : Trans-Epithelial Electrical Resistance

TFA : Trifluoracetic Acid

TJ : Tight Injections

TJMs : Tight Junction Modulators

TMC : N,N,N-Trimethyl chitosan

TML : Theoretical Maximum Pore Loading

TPE : Transient Permeability Enhancer

TPGS : D-α-Tocopherol polyethylene glycol 1000 succinate

V : Volume

VIP : Vasoactive Intestinal Peptide

VMD : Volume Mean Diameter

V_p : Pore Volume

WGA : Wheat Germ Agglutinin

X_m : Theoretical Amount Of Adsorbate For Monolayer Coverage

XRD : X-Ray Diffraction

γPGA : Gamma Poly (Glutamic Acid)

η : Viscosity

ρ : Density

θ : Theta

Chapter I

Introduction to Oral Delivery of Peptides and Associated Technologies

The term ‘’protein’’ was first introduced into the literature in 1838 by Gerardus Mulder, a Dutch chemist, in his publication ‘’On the composition of some animal substances” which was originally written in French (Murray et al., 2017). He used this term to describe a common complex that is present in egg albumin, gelatin, blood fibrin, and serum.

Proteins are made of aminoacids that are linked via α-peptide bonds that present the former in different structures: primary, secondary, tertiary, and quaternary. Yet, upon protein consumption and digestion in the gastrointestinal tract (GIT), they are broken into small peptides and free amino acids (Watford and Wu, 2018).

The primary structure is defined as the linear sequence of amino acids of the protein’s polypeptide chain, and this sequence is crucial for the protein as it determines the higher order of advanced structures of the protein, according to Anfinsen (1973). Secondary structure refers to the polypeptide backbone spatial conformation excluding the side chain, as regular secondary structures to numerous proteins are the α-helices and β-sheets (Sun et al., 2004). The tertiary is formed by the protein’s molecules folding into compact structures where the electrostatic interactions occur between the CH3 groups. The quaternary is based on forming a stable folded structure due to the interaction between two or more polypeptide chains (Soleymani et al., 2022).

Peptide drugs offer several significant advantages over small-molecule drugs. They exhibit greater specificity and more complex pharmacological mechanisms of action, allowing for targeted treatment of intricate diseases. Notable examples of successful peptide drugs include insulin, which is crucial for managing diabetes, and human growth hormone, that is used to treat various growth disorders. These attributes make peptide drugs highly valuable in modern medicine, enabling more precise and effective therapies for complex conditions (Gleeson et al., 2021). Yet, they are made into injection-based formulations rather than orally administered types since the primary goal in protein formulation development is to ensure and maintain the stability of the protein throughout its lifecycle, ensuring it remains active and effective. This involves stabilising the protein to endure the manufacturing processes without losing its integrity or activity. Additionally, the formulation must preserve the protein’s stability during transportation and storage, despite fluctuating temperatures and other stresses (Wang and Ohtake, 2019). Ultimately, the protein must remain stable and active until administered to the patient, ensuring its therapeutic efficacy. This comprehensive stabilisation approach is crucial for the success of protein-based therapeutics in clinical settings.

1.1. Peptides and their oral delivery

Peptide and protein-based formulations have progressed massively since they were commercially introduced in the 1920s with insulin formulation. The approval of recombinant insulin by the US Food and Drug Administration (FDA) in 1982 has paved the way for more proteins and peptides to be administered. However, 75% of protein/peptide formulations are administered parenterally, with more than 100 commercially available products in the US and Europe being injection-based formulations, and a very low number of orally administered peptides (Pandey et al., 2020). Therefore, the oral administration of peptides has been investigated and studied extensively because it offers immense advantages over the conventional ways of administration. It could increase patient compliance and acceptance since needles are not used and may have lower manufacturing costs considering that oral formulations do not require sterile manufacturing conditions (Tyagi et al., 2021, Shaji and Patole, 2008).

Many factors affect the bioavailability of an orally administered peptide. These factors can be classified based on the anatomy of the GIT as well as degradation and stability factors (figure 1.1).

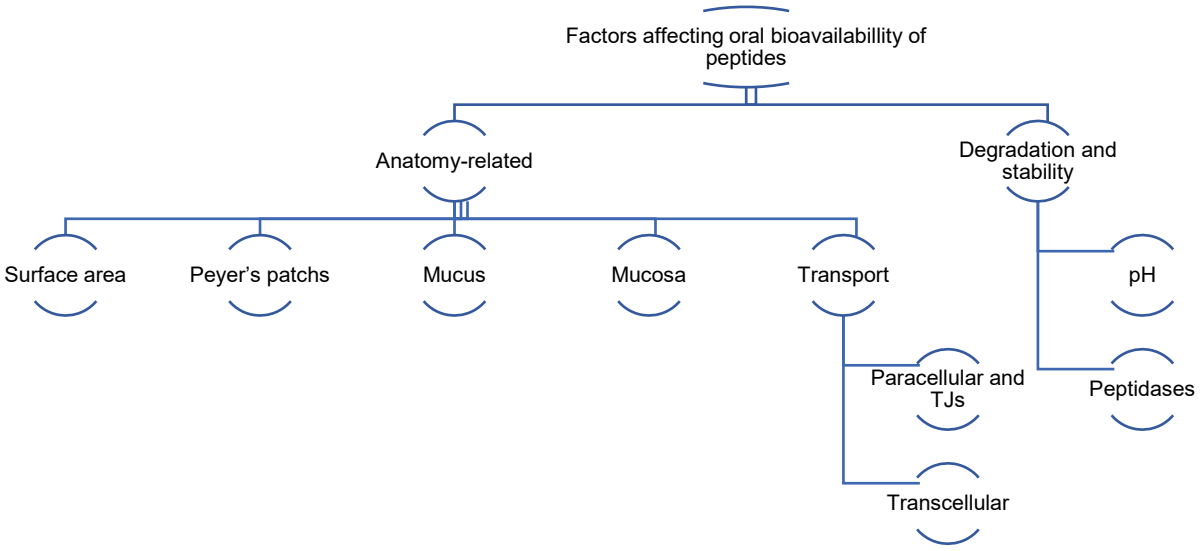

Figure 1.1. Factors affecting peptide stability.

The GIT anatomy-related factors include the GIT surface area and the presence of different barriers and components. One of the most critical factors that affect peptide bioavailability in the GIT is the absorption location and the surface area. This effect is evident in the small intestines, where the duodenum absorption rate is not as high as the rate of the jejunum and the ileum. Also, M and Goblet cells' presence in the intestines restricts peptide absorption based on molecule size, as only molecules with molecular size below 500 nm can pass this region via endocytosis (Dubey et al., 2021). The mucosa is one of the four layers of the intestines, and it contains a complex system of cross-linked mucin fibres, lumen microbiome, and lipids that prevent drugs from being absorbed (Ndayishimiye et al., 2020). On the other hand, the absorption of peptides is facilitated by Peyer's patches which are situated in the ileum. They facilitate peptide transport into the lymphatic system and evade the first-pass metabolism (Dubey et al., 2021).

Goblet cells secrete a viscoelastic gel layer that covers the GIT tract and protects the epithelia from exogenous pathogens, known as mucus (Dubey et al., 2021). This layer restricts pathogenic molecules from penetrating the cells, entraps foreign particulates via steric obstruction and adhesion, and works on immobilising and removing particles with cationic and hydrophilic properties (Lai et al., 2009, Wu et al., 2018). Moreover, mucus contains large amounts of enzymes that break down proteins and lipids, creating a degradation factor and a barrier against peptides entering mucus (Lundquist and Artursson, 2016). Once peptides are administered, they are transported via active diffusion (energy-dependent) and passive transport, with the latter being the most predominant way, and are divided into transcellular and paracellular routes (figure 1.2).

The paracellular route is based on the concentration gradient and utilizes the intercellular spaces between the epithelial cells. However, the presence of tight junctions (TJs) is the main restriction here, as they only allow the passage of small molecules with small molecular weight and hydrophilic properties (Markovic et al., 2022). On the other hand, the transcellular pathway differs from the paracellular route in terms of drug molecule passage. They will pass through the cytoplasm by traversing through the apical and basal membranes, where this route is more suited for molecules with hydrophobic properties (Wang et al., 2023). The carrier-mediated process is an active, energy-dependent form of transport that is substrate-specific, where it facilitates its passing via transport proteins on the apical and the basal membranes of the intestinal cells. As for large molecules, their transfer occurs through internalization via formed vesicles, a process identified as endocytosis. These vesicles are created by the outer membrane, enveloping and facilitating the ligand delivery before regaining their original shape. Endocytosis encompasses three types: receptor-mediated endocytosis, phagocytosis, and pinocytosis (Dubey et al., 2021).

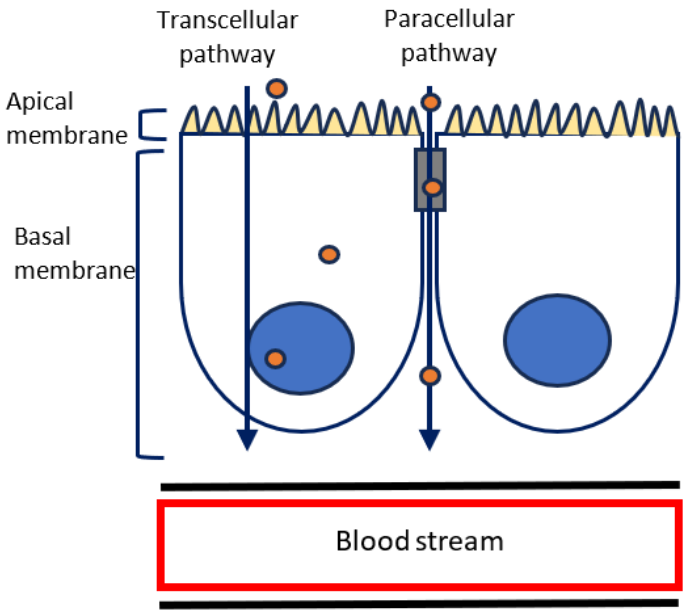

Figure 1.2. Drug molecules (orange circles) absorption via the transcellular and paracellular pathways in the intestinal mucosa to the bloodstream.

Another important factor for peptide stability in the GIT is the degradation attributed to the pH difference and the enzymes. The pH changes through the GIT from acidic to alkaline environment, and causes oxidation, de-amidation, and acid/base catalysed hydrolysis, which decreases the peptide activity drastically before reaching the absorption site (Dumont et al., 2019). The effects of pH on peptides depend on the amino acid sequence, as they are hydrolysed based on the acidic or amino groups in alkaline and acidic environments. Furthermore, the pH changes in the GIT are affected by numerous factors, including age, gender, and food. Usually, the pH of the gastric fluids in the stomach is between 1.5-3.5 in a healthy adult. The pH values are 6 in the duodenum due to carbonate neutralization, 7-8 in the ileum, and 8 in the colon. Yet, it can change if the patient suffers from inflammatory diseases or cancers. Generally, the colonic pH of patients with these diseases becomes more acidic (Zhu et al., 2021b). However, the pH degradation is not the only factor degrading peptides, as the different enzymatic activities participate extensively in that matter.

Peptides are vulnerable to degradation by the luminal enzymes (like pepsin, trypsin, and α-chymotrypsin), bacterial enzymes, pancreatic secretions, and the dipeptidases in the cytosol of the epithelial cells (Dumont et al., 2019). Enzymes in the brush border's microvilli contribute to peptide degradation. They include endopeptidase 24.11, endopeptidase-2, aminopeptidase N, and aminopeptidase A. Also, Peptides are degraded by pepsin in the acidic environment and trypsin, α-chymotrypsin and elastase in the alkaline environment, where the low

permeability in the intestinal epithelium reduces passing (Ndayishimiye et al., 2020, Dumont et al., 2019). Additionally, Pepsin degrades proteins into smaller peptide fragments through peptidic bond hydrolyzation. The remaining peptides are degraded by different types of peptidases (dipeptidase, aminopeptidase) into tripeptides, dipeptides and amino acids that are absorbed by the epithelium into the blood capillaries. Peptides are quickly degraded in gastric and intestinal fluids. However, some peptides such as cyclosporine desmopressin and octreotide are stable for 30 minutes and exist as commercial products: Neoral®, Minrin® and Mycapssa®, respectively (Zhang et al., 2016b, Sanchon et al., 2018, Miner-Williams et al., 2014, Cui et al., 2015, Wang et al., 2015, Zhu et al., 2021b).

As seen from the sections above, there are several barriers against peptide oral delivery, with the intestines and the intestinal components being the main barrier, where molecular weight and hydrophilic properties are assessed prior to absorption. Additionally, the characteristics of both transcellular and paracellular transport routes create an additional barrier. These previous barriers and drawbacks have led researchers to develop carriers to enhance oral peptide delivery.

1.2. Current research efforts and carriers to enhance oral peptide delivery

Several approaches and drug delivery systems (DDSs) have been developed or are under development to enhance oral peptide delivery. These approaches include using polymers, bacteria, lipid-based carriers, nanocarriers, targeting methods, modifying carriers, and different excipients in the formulation. The approaches are summarized in Figure 1.3 and will be discussed in the following few sections.

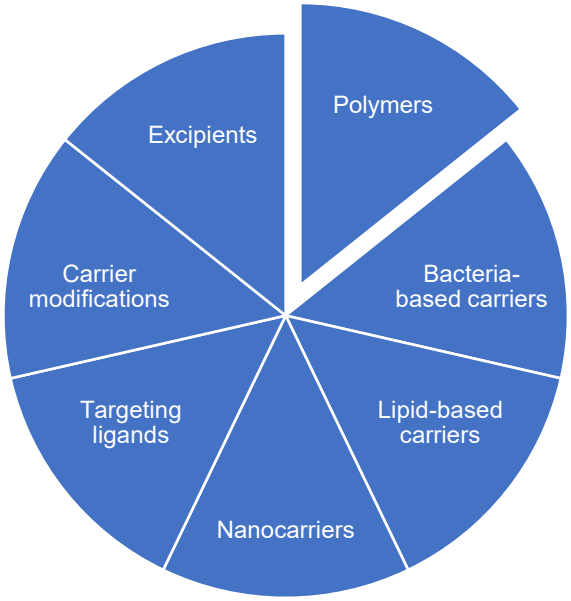

Figure 1.3. Current approaches used to enhance oral peptide delivery.

1.2.1. Using Polymers for enhancing peptide absorption and interaction with GIT cells

Polymers and polymeric nanoparticle systems have been used to enhance the characteristics of loaded drugs, targeting possibilities, bioavailability, and protection against enzymes (Zu et al., 2021). Usually, polymers are used because of their mucoadhesive properties that prevent the occurrence of a sudden concentration gradient. The previous increase ensures passive drug uptake and prohibits any pre-systemic metabolism of the peptides between the absorption membrane and the DDS (Bernkop-Schnurch et al., 2005). Furthermore, polymers can be used as pH-responsive carriers, where they release the drug at a specific pH level depending on the polymer's interaction with GIT fluids and on the ionization of functional groups that are attached to the polymer (Wang and Zhang, 2012).

In that context, He et al. (2019) characterized polymers used for peptide delivery based on their mechanism and composition, as described below. They are listed as pH-responsive polymer-based DDSs, mucoadhesive polymers-based DDSs, and polymer-drug composites.

pH-responsive polymer-based drug delivery systems are widely used because they release the therapeutic drug based on the pH difference and rise between the stomach and the intestines. This induces the deprotonation of the carboxylic groups within the polymer structure, leading to electrostatic repulsions and subsequent swelling of the polymer matrix. This swelling is succeeded by an expansion in the mesh size of the matrix, facilitating the release of the drug (Wagner et al., 2018). These polymers have been studied as carriers for oral vaccine delivery. Examples include the development and use of Poly [(methyl methacrylate)-co-(methyl acrylate)-co-(methacrylic acid)]-poly(D,L-lactide-co-glycolide) (PMMMA-PLGA) where it protected the antigen from degradation. It also secured a targeted delivery at the large intestines, shielding the nanoparticles from intestinal uptake due to PMMMA carboxylic group ionization (Zhang et al., 2016a). Additionally, mannan-modified poly (hydroxy ethyl methacrylate-co-methacrylic acid) P(HEMA-co-MAA) was used as an oral vaccine carrier, where the carrier protected the drug load against degradation and released it in the alkaline environment. Additionally, an increased macrophage internalisation was evident due to mannan addition (Duran-Lobato et al., 2014). Yoshida et al. (2017) used Poly (methacrylic acid-g-ethylene glycol) [P(MAA-g-EG)] hydrogel to deliver ovalbumin orally into rats' intestines, and their carrier managed to increase the levels of anti-ovalbumin IgG levels, where less than 10% were released in pH 1.2 within 2 hours, compared to 50% in the intestines.

The utilization of mucoadhesive polymers improves drug absorption by prolonging the retention time and enhancing oral bioavailability by accumulating drug molecules at various absorption sites. (Cardoso et al., 2021). Many types of mucoadhesive polymers, including chitosan, have been extensively used and studied. Erel et al. (2016) reported that developing insulin-loaded chitosan-sodium triphosphate nanoparticles managed to lower the glucose levels of Albino rats. Their findings indicated a reduction in glucose levels by up to 31.3% within the initial 3 hours, an effect sustained for 8 hours, as opposed to subcutaneous insulin, which lowered glucose levels to 40% but returned to 100% after 8 hours. This action was attributed to the mucoadhesive properties of the positively charged chitosan that interacts with mucin electrostatically, thus, enhancing absorption.

Polymers can also be used to formulate polymer-drug composites, where the benefits of several components are combined. Araujo et al. (2014) formulated an encapsulated glucagon-like peptide 1 (GLP-1) in chitosan and other polymers for oral delivery. Their formulation consisted of PLGA, witepsol E85 lipid, porous silicon, and chitosan. The *In vitro* results

presented no drug release for the formulation with PLGA and chitosan at pH 1.2. This was attributed to GLP-1 acquiring a strong positive charge at acidic pH due to its isoelectric point (pI) is 5.4 and interacting with the negative charge of PLGA. These previous actions decreased drug release due to strong attraction forces between PLGA and GLP-1. On the other hand, at higher pH values, the drug release reached 28 ± 1.6% after 6 hours, compared to 5% at pH 1.2. The difference in the release is attributed to the drug acquiring a less positive charge in the alkaline environment, which decreases the interaction with the negatively charged PLGA. Thus, more amounts of drugs are released.

1.2.2. Bacteria-based carriers to enhance binding and absorption

The use of bacteria-based carriers for oral delivery provides numerous advantages, one of which is producing mucosal immune responses upon oral administration of peptide vaccines. Also, Bacteria-based carriers have been studied and tested for the delivery of DNA vaccines (Takahashi et al., 2020). There are many types of bacteria-based carriers for oral delivery; lactic acid bacteria and Aracheosomes are among the most common bacteria-based carriers used for oral peptide delivery approaches.

Many strains of lactobacillus adhere tightly and efficiently to the epithelial cell walls. These strains survive the transit through the GIT, which makes them a suitable vector for peptide-loading applications. The interaction between lactic acid bacteria and the target cells can be increased by fusing adhering factors to the therapeutic proteins, enhancing the interaction. Examples include fibronectin-binding protein A (FnBPA), a virulence factor from *staphylococcus aureus* (S.aureus) that facilitates the adherence of bacteria to host cells through binding to fibronectin (Plavec and Berlec, 2019).

Archaeosomes are liposomal delivery systems synthesized from the membrane lipids of several types of Archeobacteria that contains diether or tetraether lipids (Patel et al., 2000). Archaea are unicellular microorganisms that is different from bacteria and eukaryotes as they lack the presence of peptidoglycan in the cell wall (Gaci et al., 2014). Archeobacteria-based drug delivery systems have been investigated because they are reported to be stable at high temperatures, different pH levels, and in the presence of phospholipases and bile salts (Bajracharya et al., 2019). Li et al. (2010) compared the glycaemic effects of insulin-loaded liposomes and archaeosome-insulin complex on rats. Their results revealed minor burst insulin release in achaeosomes-based carriers compared to insulin-loaded liposomes, where the burst release in archaeosomes carriers in acidic pH was less than 50%, compared to 75% release for liposomes. The difference in release rates can be attributed to archaeosomes

protecting insulin from degradation, where the negative charge of archaeosomes and their rigid lipid packing contribute to stability and low leakage of insulin in the GIT.

Bacteria-based delivery systems can be considered as possible vectors for peptide oral delivery. Nevertheless, they cannot be applied to all peptides, as some peptides might interact or degrade upon interacting with them. Hence, more biocompatible vectors are needed, like lipid-based carriers.

1.2.3. The use of lipid-based carriers to enhance peptide oral delivery

Lipid-cell interaction is a significant factor in designing lipid-based carriers because it affects their morphology, size, and lipophilicity. Therefore, many researchers have studied the interaction of lipid-based materials with cells and how the interaction could be repairable.

Margolis et al. (1982) suggested a new liposome-cell interaction apart from endocytosis, adhesion, and fusion. Their hypothesis is based on the liberation of intraliposomal substances upon liposomes contact deterioration at the cell surface, resulting in the intraliposomal substances being taken by cells. This interaction could be partnered with monolamellar liposomes transforming into multi-layered structures. Many researchers have studied the effect of lipid addition on the interaction with cells using phospholipids. Zhang et al. (2020) Modified kinked nanowires of field-effect transistor (FET) probes with phospholipids, and this modification inserted the probe spontaneously through the cell membrane. Also, they had previously developed coated U-shaped silicon nanowire arrays. The coating was composed of phospholipids that mimicked the cell membrane, and allowed the nanowire to be inserted into multiple cells in parallel without damaging them (Zhang et al., 2020). It has also been reported that the phospholipid-coated kinked nanowires can penetrate the cells without damaging them (Kruskal et al., 2015). Furthermore, the use of phospholipid-based materials for nanoprobes have been examined for intracellular imaging and sensing. The main component of the used phospholipids was 1,2-dimyristoyl-sn-glycerol-3- phosphocholine (DMPC) because it offers protection for the cells (Gao et al., 2012, Jiang et al., 2012).

Lipid-based carriers are becoming crucial in oral delivery as they increase drug stability, enhance oral drug absorption, and are efficient in entrapping hydrophobic molecules (El Moukhtari et al., 2021). Many lipid-based carriers are used for peptide delivery, such as nanocapsules, liposomes, solid lipid nanoparticles, micro/nanoemulsions, and self-emulsifying drug delivery systems (SEDDS). These carriers are summarized in figure 1.4 below and are explained in the sections below.

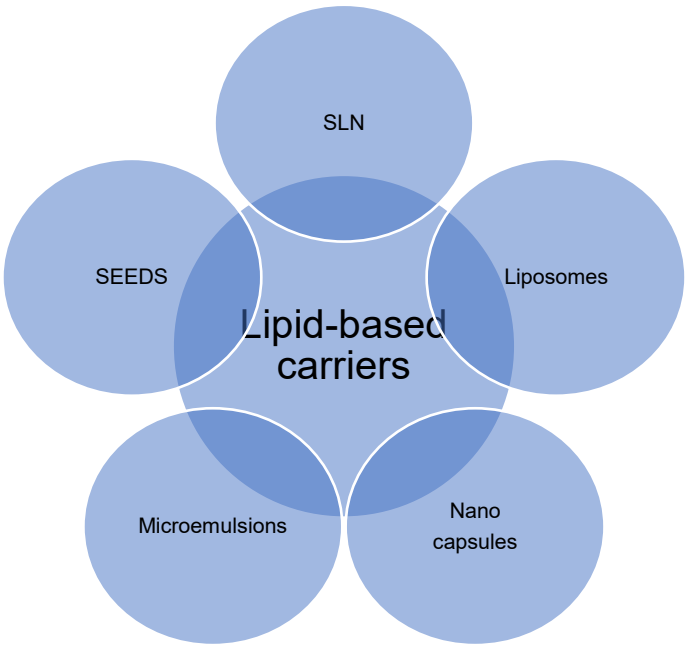

Figure 1.4. Lipid-based carriers that are used to enhance oral peptide delivery.

Nano capsules are nanostructures containing a liquid core that is usually oil, surrounded by a polymer coating that controls peptide release. An example is the use of reversed-micelles lipid nano capsules to encapsulate exenatide, where the formulation was tested *In vitro* in human L-cells and murine L-cells. The results revealed an increase in endogenous secretion of GLP-1, an enhanced oral bioavailability of 4%, and an improvement of glucose tolerance. Also, polyethene glycol (PEG)-Chitosan nanocapsules have been used, as well as lipid nanocapsules incorporating reverse micelles, which in turn were loaded with plesctasin derivative AP138. The previous loading protected the drug from enzymatic degradation (Xu et al., 2020b, Niu et al., 2016, Ndayishimiye et al., 2020, Dumont et al., 2019, Prego et al., 2006).

Liposomes can entrap peptides in their aqueous core, and the efficiency of the interaction is affected by the ionic and hydrophobic interaction with liposomal contents. Examples include osmolarity-sensitive liposomes, wherein the release of components is based on the osmolarity difference between the inside and outside of liposomes. This approach, without the inclusion of permeation enhancers, has the potential for peptide oral delivery applications (Minami et al., 2020). Modified liposomes were investigated for their uses in peptide oral delivery, and examples include using wheat germ agglutinin (WGA)-carbopol-coated liposomes. Makhlof et al. (2011) developed WGA-carbopol modified liposomes for the oral delivery of calcitonin. Their findings revealed an enhanced uptake by Caco-2 cells for the modified liposomes compared to the non-modified counterparts, and the pharmacological efficacy of the modified lipids was demonstrated to be 20 times higher than that of the non-modified liposomes.

Solid lipid nanoparticles (SLNs) are another type of nano-based carriers made from synthetic, natural, or semi-synthetic lipids, including triglycerides, partial glycerides, fatty acids, and waxes. An emulsifier layer is incorporated to provide stability when dispersed in water and to increase the peptide stability in lipids (Niu et al., 2016). Fan et al. (2014) reported using modified SLN for the oral delivery of oral calcitonin, where they used a peptide ligand CSKSSDYQC (CSK) that has a high affinity to goblet cells. Their bioavailability tests presented high results for the modified SLN (12.41 ± 3.65%) compared to the non-modified (5.07 ± 0.54%). This observation suggests the possibility of applying the previous approach for peptide oral delivery.

Micro/nanoemulsions have attracted attention to their use, considering their ability to encapsulate hydrophilic peptides in simple water in oil (W/O) or W/O/W emulsions. Examples include forming solid-in-oil-in water (S/O/W) emulsion alongside a peptide coated with surfactant for oral delivery using porous silica particles (Altaani et al., 2020, Toorisaka and Nonaka, 2018, Niu et al., 2016). Khaleel Basha et al. (2021) conducted a study using alginate/Aloe vera gel-coated nanoemulsions to deliver insulin orally. Their results presented an increase in insulin translocation (20%-25%) across Caco-2 cells monolayers.

Self-emulsifying drug delivery systems SEDDS, micro (SMEDDS) and nano (SNEDDS) are formulations that self-emulsify when dispersed in gastrointestinal fluids upon gentle dispersion to form emulsions, micro emulsions, or nano emulsions. SMEDDS contain a high percentage of surfactant, about 30-60%, oily phase of around 20%, a hydrophilic co-surfactant, and sometimes include a co-solvent. SMEDDS differ from SEDDS based on the percentage of the oily phase, the size of the produced droplets with size being less than 200 nm, and the microemulsion being translucent. One of the critical considerations in SEDDS is the dilution in the GIT because an O/W emulsion through the initial dilution may invert to W/O or W/O/W emulsion. The main advantage of these emulsion systems is the absence of organic solvents and high shear conditions, which could destabilise peptides during formulation. Neoral® is a formulation that was developed using SNEDDS technology as an improved version of a commercially available product called Sandimmune®. Sandimmune® was the first oral preparation of cyclosporin A with an oral bioavailability between 25–30%. However, high cytochrome metabolism activity and intestinal epithelial P-glycoprotein (P-gp) efflux of cyclosporin caused sandimmune degradation and led to the Neoral® development. Neoral® utilises medium-chain length polyoxyethylene castor oil derivatives and medium-chain length mono- and di-triglycerides. These lipid materials increase intestinal permeability, which results in the inhibition of P-gp efflux. (Aguirre et al., 2016, Han et al., 2019, Niu et al., 2016).

Lipid-based carriers provide an improvement over the bacteria-based ones since lipid carriers are made from materials that are usually biocompatible. Lipid-based carriers enhance the bioavailability of orally administered peptides through encapsulation, entrapment, and targeting when using a specific ligand like CSK. However, these carriers are susceptible to pH degradation and cytochrome metabolism. Consequently, more research should focus on improving these properties and using different carriers in a smaller range, like nano-based materials.

1.2.4. The use of nanocarriers to enhance the bioavailability of orally administered peptides

Nanotechnology-based carriers have been used for different delivery systems, mainly due to their small size, biocompatibility, and versatility to be easily functionalized (Raguraman et al., 2021). Some nanotechnology-based carriers include fucoidan and chitosan nanoparticles (NPs), mesoporous silica, nanosponges, and casein. These carriers are presented in figure 1.5 below and discussed in the following sections.

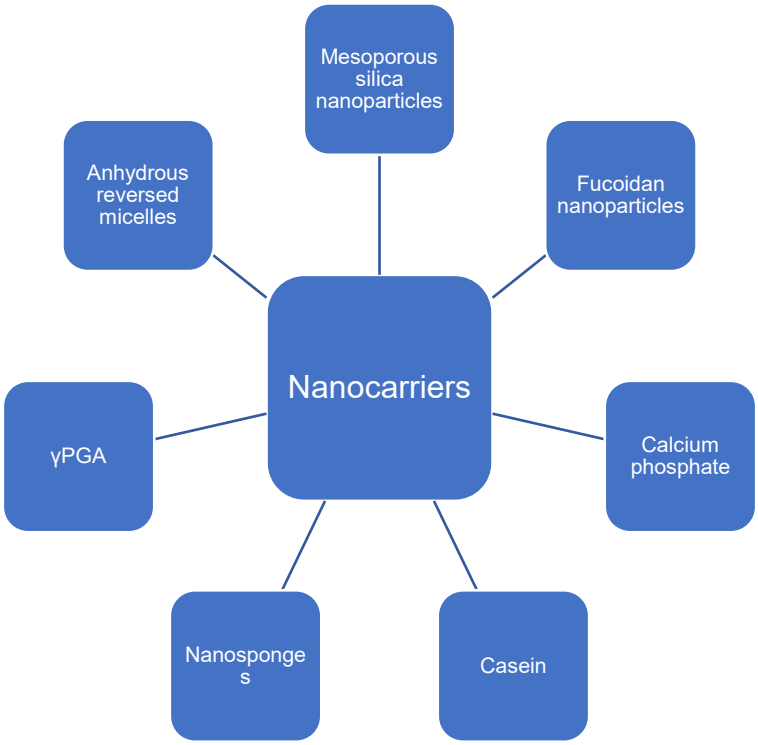

Figure 1.5. Nanotechnology-based carriers for enhancing peptide oral delivery.

Formulating nanoparticles from fucoidan and chitosan has been investigated. Fucoidan is an anionic sulphated heparin-derivative polysaccharide, that possesses a pH-sensitive polymer profile because of its acidic functional groups and the response to pH changes (Coutinho et al., 2020). Tsai et al. (2019) reported using fucoidan and trimethyl chitosan (TMC) nanoparticles to enhance the bioavailability of oral insulin. The carrier protected insulin from degradation, enhanced the transepithelial permeation of insulin due to chitosan activity, and inhibited α-glucosidase activity in hydrolysing α-glucosidic linkages owing to fucoidan effects at ratios of 33.2%.

Mesoporous silica nanoparticles (MSNs) and derivatives have been used, and many novel carriers composed of mesoporous silica nanoparticles have been reported. The silica nanoparticles were modified to be zwitterion functionalized. The modification was done by adding deoxycholic acid (DCA) and coating with sulfobetaine 12 (SB12) to improve mucus permeation and transepithelial absorption characteristics. The SB12 secures neutral and hydrophilic surfaces that are crucial for enhancing mucus permeation. Deoxycholic acid, on the other hand, provides a hydrophobic cationic surface, causing the novel carrier to acquire neutral and hydrophilic surfaces from both (Gao et al., 2021). Another study has been conducted using silica nanoparticles, where dendritic MSNs were used as carriers for the oral delivery of insulin in the form of tablets. The mesoporous nanoparticles were coated with succinylated β-lactoglobulin, to manufacture a pH-responsive tablet, in which mesoporous coating prevented the degradation and premature release of insulin. Also, MSNs were coated with poly (methacrylic acid-co-vinyl tri ethoxysilane) containing insulin to form another pH-sensitive carrier for oral delivery. The results showed only 13% release in simulated gastric fluid and a rapid glucose reduction for the first 2 hours (Abeer et al., 2020). The use of mesoporous carriers will be further investigated in section 1.3.2.

Nanosponges are mesh-like structures with dimensions smaller than 1 μm. (Pandey et al., 2018). There are many types of nanosponges, including cyclodextrin-based nanosponges, which are polymeric materials formulated through a cross-linking agent with cyclodextrin (α, β and γ). Nanosponges can entrap both hydrophilic and lipophilic molecules due to the formed complex network, where the complexation action occurs in the internal cavities of cyclodextrins as well as the interstitial volumes between them. Insulin was incorporated within nanosponges made from β-cyclodextrin and crosslinked with pyromellitic dianhydride. Insulin was absorbed at the intestinal level in non-obese diabetic (NOD) mice, and it was tested *In vitro*, where the results showed a minimal release of 2% at gastric pH.

Enhancing the characteristics of micelles has been investigated for improving the oral delivery of insulin. Lyophilized anhydrous reversed micelles were synthesized by freeze-drying W/O

emulsion. The reversed micelles were constructed with insulin and phosphatidylcholine being in the aqueous phase, and insulin stability was maintained by using mild sonication. This system delivers insulin in a slow-release manner when administered orally, with less than 12% release after 24 hours of administration (Bajracharya et al., 2019, Wang et al., 2010).

Chitosan and gamma poly (glutamic acid) (γPGA) nanoparticles-based drug delivery system has been reported in which γPGA nanoparticles were covalently conjugated with diethylene triamine penta acetic acid (DTPA). DTPA chelates metal cations like calcium and zinc, disrupting tight junctions, enhancing paracellular permeability and inhibiting the metallopeptidases' proteolytic activity in the intestinal lumen. Another example includes combining nanoparticles and targeting ligands, like poly (lactic acid)– b-poly (ethene glycol) (PLA-PEG) block copolymer-based nanoparticles. This complex incorporates insulin with Fc-thiol surface ligand groups that target neonatal FcRn receptors in murine intestines (Aguirre et al., 2016). The use of calcium phosphate nanoparticles has been investigated for oral insulin delivery aside from their primary role as carriers for vaccine delivery. The release studies showed a negligible 2% release at gastric pH levels and a sustained release in alkaline environments for 8 hours (Ramachandran et al., 2009, Lin et al., 2017, Park et al., 2011).

Casein has been introduced to formulate a novel carrier for oral insulin. The carrier has been designed to contain casein, PEG, and insulin in the form of calcium phosphate nanoparticles. Casein is crucial in the formulation because it is acid-resistant and protects insulin passage in the small intestine due to its mucoadhesive properties, while calcium phosphate reduces acid-related degradation (Park et al., 2011).

Nanotechnology-based carriers are widely used and studied for their peptide oral delivery. They can inhibit enzymes like α-glucosidase and release the drug in a slow manner in acidic pH as in the case of fucoidanand TMC nanoparticles. However, they may cause the same side effects as traditional carriers, like inflammation and accumulation in different tissues. Also, nanoparticles effects are more potent due to their small size and large surface area (De Jong and Borm, 2008). So, more attention is focused on developing carriers and strategies where the drug accumulates in the right place, like targeting.

1.2.5. The use of targeting ligands to enhance oral peptide delivery

Targeting has been considered as a novel strategy for enhancing the availability of drugs. There are many types and examples of targeting carriers. The section below focuses on three main targeting ligands: enterocytes, goblet cells, and colon targeting. The types of targeted cells are presented in figure 1.6 below.

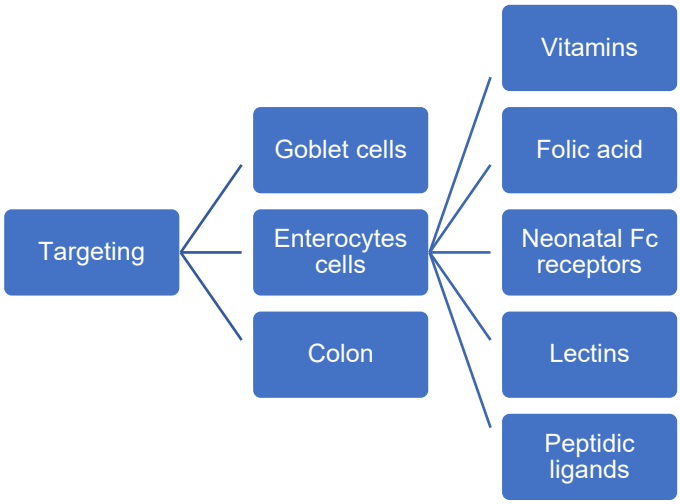

Figure 1.6. Targeting strategies and approaches to enhance the bioavailability of oral peptide preparations.

The utilization of enterocytes as targeting ligands has been proposed, wherein the drug entry is linked to receptor-mediated endocytosis. In this mechanism, the interaction between the ligand on the DDS surface and the receptor initiates the endocytosis process (Xu et al., 2020a). Enterocytes recptors are classified according to them:

Vitamins are vital components of enterocytes receptors. The family of vitamin B is extensively used in targeting due to its water solubility. B12 is considered amongst vitamin B family as the best ligand for targeting. It can be complexed with dextran nanoparticles to enhance the uptake of poorly soluble peptides and proteins as this new complex will protect insulin against gut proteases (Xu et al., 2020a, Chalasani et al., 2007).

The use of neonatal Fc receptors was proposed, in which a novel carrier was created using poly PLA-PEG copolymer nanoparticles containing the Fc of the IgG on the surface. Also, the surface of maleimidyl-poly(ethylene glycol)-co-poly(ε-caprolactone) (Mal-PEG-PCL) nanoparticles was modified with IgG Fc to encapsulate SP141, a mouse double minute 2 homolog (MDM2) inhibitor (Wang et al., 2019b).

Wheat germ agglutinin (WGA) is highly used because of its specific binding to N-acetyl-D-glucosamine and sialic acid residues. It has been found that WGA-bovine serum albumin (BSA)

conjugates have a higher binding affinity to Caco-2 cell monolayer, equal to 19 times more than non-conjugated BSA.

Arginine–glycine–aspartic acid (RGD) is a common ligand for targeting integrin receptors, like the αvβ3 receptor. The latter is a transmembrane glycoprotein that is expressed on Caco-2 cells. Modified N,N,N-trimethyl chitosan (TMC) nanoparticles were used to deliver insulin orally. PEG-b-PCL micelles were modified with HAIYPRH (7pep) because of the high affinity of 7 pep towards the transferrin receptor, and the results showed higher intracellular uptake of the loaded cargo (The transferrin receptor) comapred to non modified particles (Xu et al., 2020a).

Goblet cells are the second most predominant cells in the epithelium (Zhang et al., 2015), and targeting them provides an excellent technique for delivering therapeutics into the epithelium. In that context, it has been proven that the peptide CSKSSDYQC (CSK) can specifically target Goblet cells effectively (Kang et al., 2008). Jin et al. (2012) used TMC-insulin-loaded nanoparticles and attached CSK to enhance the oral delivery of insulin, where CSK was complexed with TMC to enhance the uptake of insulin. Their results proved that CSK addition enhanced the recognition of goblet cells and increased the hypoglycaemic effects in rats up to 1.5 folds, compared to the unmodified TMC-insulin nanoparticles.

Colon targeting is studied due to the low proteolysis activity compared to other parts of the intestines. According to some studies, the colon proteolytic activity is 20-60 times lower than the ileum and the high sensitivity of the colonic apical membrane to permeation enhancers (PEs) compared to the intestines (Aguirre et al., 2016). An example of a commercially available colon drug is Gengraf®, which is an FDA-approved oral dosage form of cyclosporin, bioequivalent to Neoral® and formulated as an orally administered colon-targeting drug (Tsang et al., 2003, Amidon et al., 2015).

Although targeting approaches are beneficial for peptide oral delivery, they cannot be implemented for all peptides and target all tissues, as only some tissues contain markers where targeting moieties adhere. For that reason, different approaches can be employed in which the properties of the peptide to enhance its oral bioavailability.

1.2.6. Physical and chemical modification of the oral peptide carriers

There are several types of modification, either physical or chemical. For instance, using additional components and macro/micro molecules is considered a very efficient modifying technique. Figure 1.7 summarizes the modification techniques. The modification methods are derived into physical and chemical-based methods in the section below.

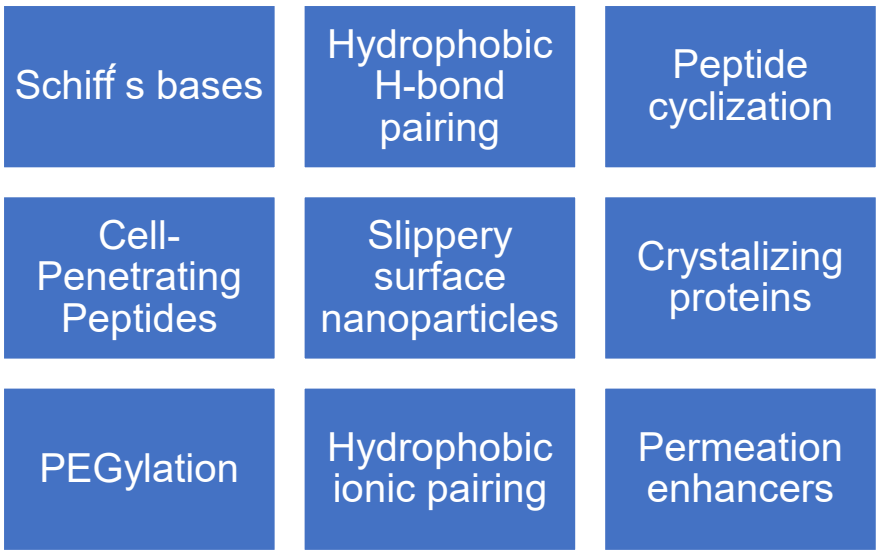

Figure 1.7. Schematic of different modification methods to enhance oral peptide delivery.

1.2.6.1. Chemical Modifications

Chemical modification can take different forms, enhancing the bioavailable properties of hydrophilic drugs. One of the most common chemical modifications is Schiff́ s bases, which is based on forming an imine bond between the primary amino groups and the carbonyl groups of aldehydes. The hydrophilic peptide is polymyxin B, and the lipophilic aldehyde is cinnamaldehyde that possesses high lipophilic characteristics and low toxicity. The polymyxin B-cinnamaldehyde conjugates will be incorporated into a self-emulsifying drug delivery system. The overall purpose of the process is to enhance the oral bioavailability profile of the SNEDDS containing the peptide-aldehyde conjugate (Dizdarevic et al., 2019).

Another form of chemical modification is the use of hydrophobic H-bond pairing. This technique enhances the permeability of drugs by discarding the H-bond donor and acceptor substructures. The technology was applied to leuprolide with the addition of sucrose esters. It improved the lipophilicity of the drug, its permeability, and the binding of non-ionic surfactants to the peptide surface without denaturing the peptides (Nazir et al., 2020). The hydrophobic ionic pairing approach is different from the previous technique. It is based on pairing peptides

with a hydrophobic counter ion, thus turning them into highly oil-soluble hydrophobic agents (Abdulkarim et al., 2019).

Cross-Linked Enzyme Crystal (CLEC®) technology was developed by St. Clair and Navia (1992) and was introduced for oral peptide delivery to maintain bioavailability. This technology includes crystallizing and chemically cross-linking the enzymes with macromolecules (Park et al., 2011). Altus (USA) used CLEC® technology to for possible formulation, but it has not progressed (Muheem et al., 2016).

One of the techniques, known as macrocyclization, changes the peptide's chemical structure. It is used to transform linear peptides into cyclic peptides to enhance their stability. There are four types of macrocyclization: side chain-to-side chain, side chain-to-tail, head-to-side chain, and head-to-tail. However, the bioavailability of macrocycles is limited because of the high amide content accompanying a large polar surface area. To overcome this when synthesizing macrocycles libraries, leads are generated with potential improved oral bioavailability due to high degrees of N-methylation and a lower number of hydrogen bond donors (Aguirre et al., 2016).

1.2.6.2. Physical modifications

Physical modifications take many forms and focus on using additives to the carrier rather than modifying the structure. Examples include using slippery-surfaced nanoparticles, PEGylation, permeation enhancers, and cell-penetrating peptides. One of the most frequently employed and extensively studied modification techniques is centred on the penetration mechanism, aiming to enhance permeability through various means. One such approach involves the utilization of cell-penetrating peptides (CPPs).

CPPs are short peptides of less than 30 amino acids that enhance the mucosal uptake of the nanoparticles. Using cyclic CPPs is favoured because they are more stable and are less susceptible to hydrolytic effects by peptidases. Also, CPPs are used as permeation enhancers, where CPP-mediated delivery has been reported to take place via multiple endocytosis ways. These include macropinocytosis, caveolae-mediated and clathrin-mediated pathways (He et al., 2019, Gedawy et al., 2018, Han et al., 2019, Uhl et al., 2020). Another form of penetrating particles are the mucus-penetrating particles. They pass through GIT barriers by entering the adherent mucus layer through penetration. They penetrate the layers deep enough before adhering, in contrast to the adhesion particles that adhere to the surface (Liu et al., 2021).

Enhanced mucus permeation can be achieved using slippery surface nanoparticles. This idea was derived from viruses that contain inert neutral surfaces and possess a capsid shell that is densely charged but neutral to avoid any interactions with mucus (hydrogen bonding, electrostatic). There are two approaches for creating slippery surface NPs: the first is through coating the particle with a neutral hydrophilic polymer (PEG). The second method involves creating an inert surface through the combination of two oppositely charged polymers. The interaction between these polymers leads to the precipitation of the polyelectrolyte polymer, thereby forming a densely neutral surface (Abdulkarim et al., 2019).

PEG is highly studied and used to modify peptide-based formulations since peptides-branched chain PEG conjugates possess enhanced thermal stability, higher resistance, and a higher pH than linear types. PEG coating improves the stability of the nanocarrier upon contact with the mucosal fluid and facilitates macromolecules transport through the intestinal epithelia. (Aguirre et al., 2016, Abdulkarim et al., 2019, Prego et al., 2006, Park et al., 2011).

1.2.6.2.1. Permeation enhancers

Enhancing the permeability can be achieved with intestinal permeation enhancers (PEs). These compounds facilitate the transition of macromolecules across the GIT by transiently altering the epithelial barrier (Maher et al., 2021). Permeation enhancers, also known as absorption-modifying excipients (AMEs), are incorporated into the formulation. Depending on their type, they can either operate on the transcellular or paracellular route and enhance the bioavailability of orally administered peptides as a result (Dahlgren et al., 2021, Tyagi et al., 2021).

However, some sources differentiate between AMEs and PEs based on the intended purpose of addition. AMEs are not intentionally added to increase the bioavailability and affect the fraction extracted from the gut lumen even though their chemical structure allows them to operate for that purpose. PEs, on the other hand, are intentionally added to improve the bioavailability of orally administered peptides (Maher and Brayden, 2021). Brunner et al. (2021) classified the permeation enhancers based on their interaction with tight junctions into non-specific and specific, with the latter containing two subtypes based on the generation:

The first is Non-specific PEs that include surfactants, bile salts, chitosan and its derivatives, and fatty acids. The other, specific or termed target-specific tight junction modulators (TJMs), are also classified into two subgroups (generations), each containing several members. The first-generation PEs target non-TJ proteins, like cytoskeleton and enzymes. Meanwhile, the second-generation PEs interact with proteins in the TJs, like Claudin occludin, e-cadherin, and

zonula occludens (Brunner et al., 2021). Figure 1.8 below lists the permeation enhancers listed above.

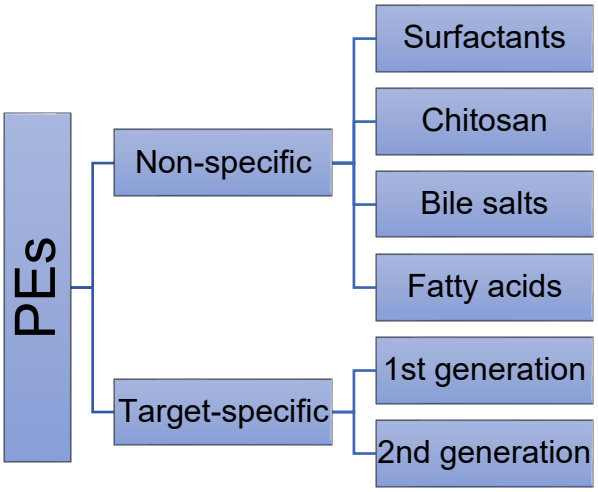

Figure 1.8. Permeation enhancers based on Brunner et al. (2021) classification identifying the type and generations.

In addition, Maher et al. (2016) categorised permeation enhancers based on their action site regarding intestinal absorption. For instance, they can operate on either paracellular or transcellular routes. This is attributed to the more significant challenge of reversibly opening tight junctions between cells compared to the non-specific perturbation of the intestinal mucosa. However, less than 5% of transcellular PEs have advanced to clinical trials for peptide oral formulations. This is associated with the safety concerns of these compounds not being adequately addressed for human clinical trials, along with considerations for the recovery of epithelial cells as they might harm them (Maher et al., 2016).

Permeability enhancers (PEs) have been investigated to tackle the poor oral permeability of peptides. These PEs can enhance the absorption of molecules in two ways; transcellular or paracellular, as reported earlier. The first is based on disrupting the cell membranes, while the paracellular route is based on opening the tight junctions between the cells (Maher et al., 2016). Medium-chain fatty acids have attracted attention for their use as potential PEs. Among them are sodium caprate (C10), sodium caprylate (C8), and its derivative salcaprozate sodium SNAC. C8 is included in the formulation of (Mycapssa®, Chiasma), an FDA-approved oral formulation of octreotide for the treatment of acromegaly, while C10 has not been added to any FDA-approved drug. Yet, it is an excipient in a long-acting basal insulin formulation designed by Novo Nordisk that is currently in Phase II (Twarog et al., 2022).

These permeation enhancers interact with lipid bilayers differently depending on their hydrophobic properties, their charge, and their chain length, according to Kneiszl et al. (2022).

Negatively charged PEs like SNAC tend to interact less with cell membranes than neutral PEs like caprate. Moreover, PEs with long chains tend to have a lower number of molecules expulsion from the membrane where they operate, which is due to the PE interacting better with the 1,2-palmitoyl-oleoyl-*sn*-glycero-3-phosphocholine (POPC) moieties in the membrane. Furthermore, SNAC expresses more expulsions than other C8 PEs due to the presence of the salicylamide region in its structure (Kneiszl et al., 2022).

In addition, SNAC, a caprylate derivative as mentioned above, has a generally regarded as safe (GRAS) status and is present in the commercially approved product of Rybelsus (Buckley et al., 2018). Compared to sodium caprate, SNAC was developed following the former licensing by two companies, and most notably by Emisphere (NJ, USA) as their main component for their Eligen® carrier technology. One thing to note is that SNAC contains a higher distribution of functional hydrophilic groups in its structure compared to sodium caprate. This translates to SNAC being less efficient in interacting with phospholipid membranes than sodium caprate, which results in high concentrations of SNAC to be used to improve permeation (Twarog et al., 2019, Kneiszl et al., 2022).

Rybelsus® is the first oral-based formulation for the delivery of semaglutide, which was developed by Novo Nordisk. It consists of the active API (semaglutide) with a permeability enhancer (SNAC), where the latter's amount is 300 mg compared to 7 or 14 mg of the drug. The inclusion of the PE in the formulation adjusts the pH around the tablet, which protects it from pepsin-related degradation. Additionally, it enhances the permeability of semaglutide across the stomach mucosa (Fattah et al., 2020). The effects of SNAC on improving semaglutide permeability and protection will be detailed in the following section.

There have been many theories regarding SNAC's mode of action. For instance, it has been proposed by Eligen Scientists that SNAC works on the passive transcellular pathway through hydrophobization. This is conducted through dipole-dipole noncovalent interaction between SNAC and the drug, causing conformational changes that expose the hydrophobic regions and thus, favouring transcellular permeation (Twarog et al., 2019). This was also found by early research where Malkov et al. (2005) found that SNAC acts on the transcellular pathway upon increasing the permeability of insulin by enhancing its lipophilic properties. Additionally, they found that SNAC has protected insulin from trypsin digestion, where they attributed this effect to SNAC's binding to the surface of insulin and halting enzymatic access. Additionally, Ding et al. (2004) found that SNAC interacts with APIs where the former's aromatic ring and specifically the 2-hydroxybenzamide fraction is inserted between the drug's structure, increasing the complex hydrophobic properties and decreasing its hydration.

The effect of SNAC in Rybelsus® has been reported by Buckley et al. (2018). SNAC causes a temporary increase in the pH around the tablet once it is in the stomach. This pH increase reduces the conversion of pepsinogen to pepsin, which protects the drug from degradation. Furthermore, semaglutide is protected against pepsin by SNAC, and the solubility of the drug is increased. Upon being in close contact with the gastric epithelium, API molecules cross the gastric mucosa in an increased concentration-dependent flux via a transcellular mechanism. This is related to incorporating SNAC molecules into the lipid membrane of the gastric cells and fluidising the plasma membrane in the gastric epithelium (Aroda et al., 2022).

Moreover, SNAC causes the drug molecules to be in monomeric forms, where they are absorbed transcellularly after SNAC molecules fluidise the gastric epithelium. The absorption of semaglutide occurs only in the transcellular route, as the tight junctions were not affected by SNAC. The effects of SNAC on monomerising semaglutide are crucial for absorption as fatty acid acylated glucagon like peptides 1 (GLP) tend to be formed in oligomers, which affect their absorption (Buckley et al., 2018).

In addition, Buckley et al. (2018) found that increasing the concentrations of SNAC while maintaining a constant amount of semaglutide has shifted the drug molecules towards monomerisation. They attributed their findings to SNAC's ability to weaken the self-association interactions between the drug molecules. To elaborate, semaglutide forms oligomers due to its amphiphilic nature, where these oligomers are held together via noncovalent hydrophobic interactions. When SNAC is added to the formulation, it changes the solution's polarity in the stomach, weakening the hydrophobic interactions within semaglutide oligomers, and thus, monomers are formed.

One crucial factor to consider is that the absorption-enhancing activity of SNAC is agent-dependant, which means that the co-formulation of SNAC and drug is more important than the administration of the drug-SNAC. This was evident when liraglutide was formulated with SNAC, and there was no flux increase across the gastric epithelium in *In vitro* models. This could be attributed to liraglutide's stronger membrane-binding properties that decreased transcellular permeation, as well as liraglutide'e tendency to oligomerize, which is the opposite of SNAC's effect in monomerizing drugs (Aroda et al., 2022, Buckley et al., 2018).

Kneiszl et al. (2022) studied the effects of the PE type on enhanced permeability. They concluded that increasing the number of carbon chains in the structure of the PE lengthens the time where the PE interacts with membranes. They found that more caprate (C10) molecules are inserted into the membrane compared to caprylate (C8) or its derivatives (SNAC). Additionally, the presence of the salicylamide region in SNAC reduces its time to stay

inside the membrane due to increased solubility. Furthermore, they found that SNAC had a higher number of molecule expulsions compared to C8-based PEs, which was due to its decreased interaction with membranes, as reported earlier. Furthermore, according to Kneiszl et al. (2022) SNAC presents the lowest PE-PE interaction as it does not form aggregates upon increasing the concentrations at the point of contact. This might explain why higher amounts of SNAC are needed to enhance permeability compared to other PEs.

Modifying the drug is vital to enhance its characteristics. Nevertheless, this approach is not sufficient to ensure a higher bioavailability profile when administered orally. Also, every formulation contains different excipients that contribute to its efficiency and efficacy. Consequently, understanding and identifying excipients that enhance the activity of peptide oral DDSs is essential. Different excipients will be discussed in the following sections.

1.2.7. Excipients significantly contributing to oral peptide DDS activity

The pharmaceutical industry has been developing excipients to enhance the properties of the administered drugs. Using excipients applies to both high and low-molecular-weight APIs. The newly developed and used excipients for oral peptide delivery can either be used through a new system or by applying additives to the formulation. Figure 1.9 below identifies different excipients that are used in oral peptide formulations.

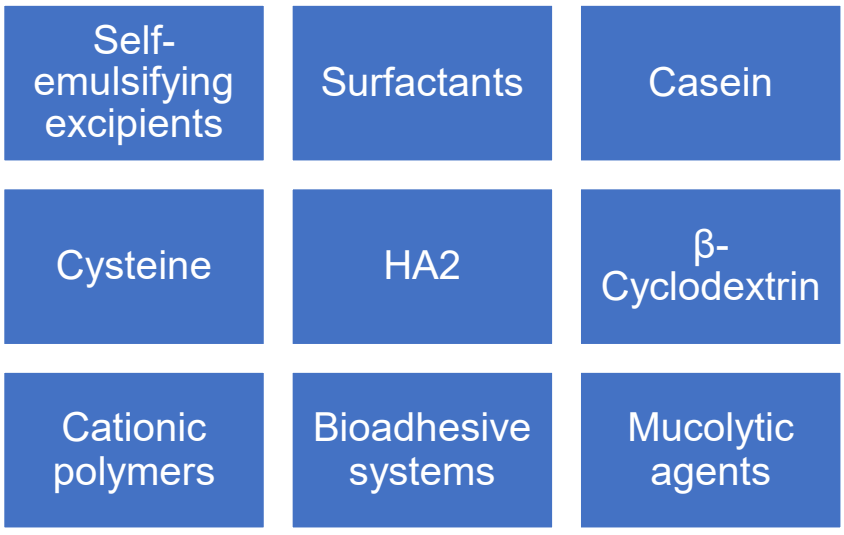

Figure 1.9. Schematic of used excipients that enhance the properties of oral peptide DDSs.

Using different excipients provides the DDS with numerous characteristics based on the added material properties. These excipients can be self-emulsifying, like Labrasol®, which is composed of mono-, di-, triglycerides, and mono- and di- fatty acid esters of PEG (Ukai et al.,

2020). McCartney et al. (2019) tested Labrasol® in rats, and their *Ex vivo* and in situ methods presented reversible opening of the tight junctions and the ability to permit the passage of compounds with a molecular weight close to insulin. Their results showed that Labrasol increased the apparent permeability of fluorescein isothiocyanate insulin up to 1.8×10^{-6} cm·s^{-1} compared to control insulin 0.4×10^{-6} cm·s^{-1} when Labrasol was added at a concentration of 4 mg/ml**.** Furthermore, the enhancement of permeability by Labrasol is correlated with molecular weight. Labrasol demonstrated a 19-fold increase in permeation for fluorescein isothiocyanate dextran 4000. However, one crucial factor to consider is that the enhanced permeation effect is active until the molecular weight reaches 40 kDa. Moreover, surfactants can be classified within this category, particularly when employed in supersaturated SEDDS. In this context, low concentrations of surfactants are utilized, and a precipitation inhibitor is incorporated into the formulation (Abdulkarim et al., 2019).

Proteins and their derivatives can be used as excipients to enhance the properties of peptide oral DDS, and an example of added proteins is casein. Casein is included in insulin formulations due to its acid-resistant nature, serving to protect insulin from premature passage through the small intestine. This protective effect is attributed to the mucoadhesive properties of casein (Park et al., 2011). On the other hand, amino acids, like cysteine, can be used as additives. It has been found that modifying Eudragit L100 nanoparticles with cysteine enhances the mucoadhesion properties. The enhanced adhesion is related to the formed covalent bonds between the thiomers and mucus glycoproteins, specifically the cysteine-rich subdomains (Liu et al., 2021).

Polymers are extensively used as drug carriers or additives, with PLGA as an example. Cationic polymers are used for drug delivery to the stomach, as they are ionized in low pH values and swell to release the drug. Anionic hydrogels, in comparison, collapse in structure because their pKa is higher than the pH of the stomach. This action protects the encapsulated cargo against degradation while in the acidic environment. Upon reaching the intestine and the colon, cationic polymers are ionized and release the drug in a controlled manner (Ibeanu et al., 2020). Anionic polymers, on the other hand, can be used when they are modified with thimoers. Thiomers improve the mucoadhesive properties of anionic polymers like polyacrylica and cationic polymers like chitosan. The formation of disulphide bonds improves the mucoadhesive properties 140 folds compared to unmodified polymers (Gedawy et al., 2018).

Various materials can be employed, irrespective of their nature, whether oligosaccharide-based or otherwise. In this category, β-Cyclodextrin is a promising candidate as an additive in orally administered peptides. β-Cyclodextrin has been found to stabilize insulin structure by forming an inclusion complex with the insulin molecules' hydrophobic cavity (Wong et al.,

2018). Song et al. (2017) formulated carboxymethyl-β-cyclodextrin grafted chitosan nanoparticles as a potential oral peptide carrier, and they used BSA as their model protein. Their results presented a low release of BSA in simulated gastric fluid (< 18% over 72 hours) compared to a higher release of 70.48% in simulated colonic fluid.

Hemagglutinin-2 (HA2) is an endosomal escape agent studied as an excipient for formulations intended for oral delivery. It has been found that HA2 enhances the bioavailability of DDS because it achieves lysosomal escape in cells (Yin et al., 2020). Similarly, Shi et al. (2021) incorporated HA-2 and CSK into chitosan-poly-N-(2-hydroxypropyl) methacrylamide (pHPMA) nanoparticles for liraglutide oral delivery. Their findings presented an improved bioavailability profile in rats 10.12% compared to 4.15 % of subcutaneously administered liraglutide, making these excipients good candidates for further studies and development.

Mucolytic agents are being studied for their effects in enhancing the availability of orally administered drugs. Mucolytic agents reversibly destroy the mucin network, which enhances NPs diffusion across the mucosal barrier. The previous mechanism operates three types of mucolytic agents: the first type breaks the disulphide bonds in the mucin network, while the second breaks peptide bonds. Additionally, The third hydrolyses the entangled DNA tangles in the mucin network. Papain was used as a mucolytic agent to improve the intestinal permeation of polyacrylic acid NPs. Surface modification can be combined with mucolytic agents to produce a synergistic effect (Abdulkarim et al., 2019).

The excipients mentioned above enhance the properties of peptide oral formulations in numerous ways, including adjusting tight junctions, forming complexes, mucin network reversible destruction, ionization and release. The previous excipients and modifications were used to design new peptide oral delivery technologies that either made it to the market or are currently under development. These new technologies will be discussed in the following sections.

1.3. New oral peptide delivery technologies on the market

This section will characterize the newest oral delivery technologies that enhance the effect and action of available products and DDSs or are newly introduced novel carriers. The characterization is based on the properties of the commercial products.

1.3.1. Newly developed technologies enhancing the properties of oral peptide tablets

One of the most studied and developed oral products is tablets. Therefore, many research groups and companies have developed new technologies that enhance oral tablets' functionality for peptide delivery. Developing oral formulations containing insulin has been highly studied and requested. Many companies have developed novel technologies that enhance the oral bioavailability of orally administered insulin. These technologies differ in manufacturing procedure and are summarized in figure 1.10 below.

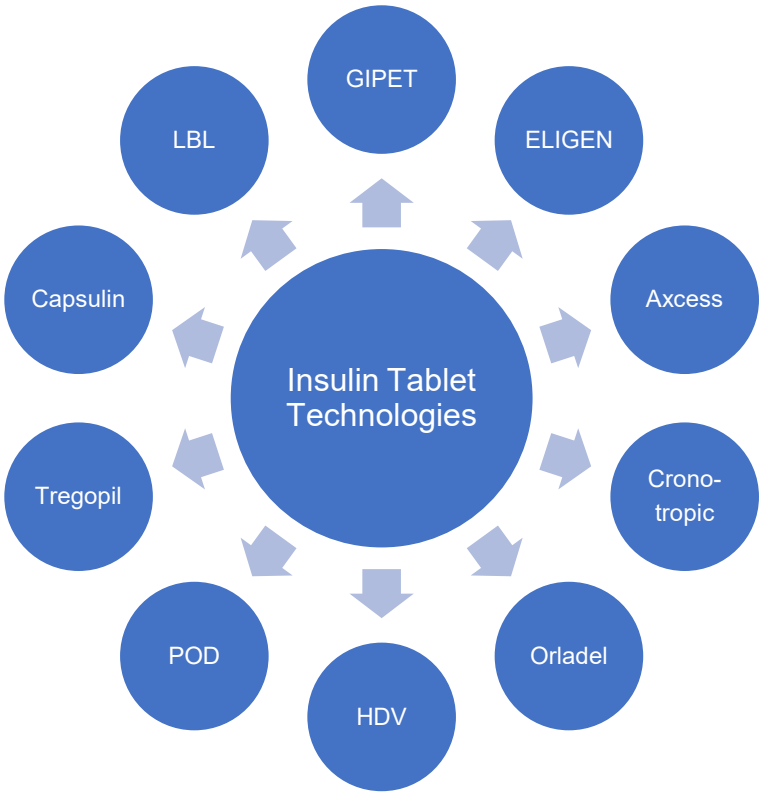

Figure 1.10. Tablet-based technologies for delivering oral insulin.

Merrion Pharmaceuticals produced a novel technology called the Gastrointestinal permeation enhancement technology (GIPET). It utilises the combination of lipoidal excipients like Labrasol and medium-chain fatty acids and their derivatives in the form of a capsule or coated tablet (Brown et al., 2019). Novo Nordisk has used GIPET technology to develop oral insulin I338, which is currently in Phase II clinical trial (Halberg et al., 2019).

Emisphere has developed a new technology called Eligen. It is based on the use of benzoyl and salicyloyl derivatives of caprylic acid and their salts for oral delivery: salcaprozate sodium: (SNAC), N-(5-chlorosalicyloyl)-8-aminocaprylic acid (5-CNAC), 4-([4-chloro-2-hydroxybenzoyl]-amino) butanoic acid (4-CNAB) and N-(10-[2-hydroxybenzoyl]amino) decanoic acid (Brown et al., 2019). Malkov et al. (2005) implemented Eligen technology for an oral insulin formulation while using SNAC. The *In vitro* results indicated an oral absorption of insulin transcellularly without disrupting the tight junctions. Also, SNAC has increased the lipophilicity of insulin, which assists in its diffusion through the cell membrane.

Proxima Concepts, Ltd. (London, United Kingdom), and Diabetology, Ltd. (London, United Kingdom) have developed Axcess. This technology utilizes aromatic alcohols as permeation enhancers and solubilizers to enhance transcellular transport for drugs intended for oral administration (Brown et al., 2019). It is used for developing an enteric-coated oral tablet of insulin called Capsulin™ IR, which is currently in clinical Phase II (Diabetology, 2021, Proxima, 2021).

Chronotropic ™ is a novel oral delivery for oral insulin in the form of a tablet that Dexcel Pharma Technologies has developed as a two-pulse colonic device. The device is composed of an outer layer coating of hydroxypropyl methylcellulose (HPMC), an adjuvant intermediate layer and an erodible HPMC layer surrounding the core. Including a comastate mesylate as a protease inhibitor and sodium glycocholate as an absorption enhancer creates a lag phase between the adjuvant and protein release proxima (Choonara et al., 2014).

ORLADEL is a novel technology that is based on using carbohydrate-based polymer coating with vitamin B12 as a matrix to encapsulate insulin. B12 protects insulin from enzymatic degradation and facilitates transport through the intestines (Park et al., 2011). Macrulin™ is a novel oral pill for the oral delivery of insulin that is currently in phase II trials (Spoorthi Shetty et al., 2023). The new technology is based on the concept of using lipid-based w/o microemulsions, where insulin is in the aqueous phase, and the oily phase is composed of cholesterol, lecithin, and non-esterified fatty acids. (Park et al., 2011).

Hepatocyte-directed vesicle (HDV) is a novel carrier intended for the oral delivery of insulin that has been designed by Diasome Pharmaceuticals in the form of an oral insulin gel capsule.

The carrier is within the nano range and is composed of a phospholipid bilayer with hepatocyte-targeting molecules (Easa et al., 2019). The Phase 2 OPTI-1 Clinical Trial were presented at the 80th Annual American Diabetes Association Virtual Scientific Sessions in 2020 (Diasome, 2021).

Oramed Pharmaceuticals. Inc has designed the ORMD-0801 capsule for delivering oral insulin. It is manufactured through Protein Oral Delivery ™ (POD) technology, wherein an enteric coating is applied around the capsule. Absorption enhancers and protease inhibitors are also incorporated alongside insulin in the core (Easa et al., 2019). Additionally, Oramed has announced the enrolment and randomizing of 25% of the 450 patients scheduled for Phase 3 ORA-D-013-2 trial of ORMD-0801for treating type 2 diabetes (Oramed.Inc, 2021).

Tregopil is an insulin tablet that has been developed by Biocon and is called Biocon's oral insulin tablet IN-105 or Tregopil, but is currently in Phase II/III study (Biocon, 2021). Tripogil, is modified insulin in the form of an insulin analogue, where polyethene glycol is covalently bonded to the free amino acid group on the Lys-β29 residue through a non-hydrolysable amide bond. This modification enhanced the stability, decreased the degradation due to the steric hindrance, and improved solubility (Easa et al., 2019). In addition, Diabetology has developed an oral tablet of insulin called Capsulin™, still in clinical trials phase II. The formulation is composed of unmodified insulin within an enteric-coated capsule. This work is based on the principle of Axcess™ technology that contains aromatic alcohols as permeation enhancers and a solubilizer (Easa et al., 2019).

Layer-by-layer technology (LBL) was first introduced by Decher (1997) to form two and three-dimensional polymeric coatings. The technology is composed of thin films that are generated by the deposition of oppositely charged species, making microcapsules, microgels and films. This technology was implemented in developing a multicomponent system containing Insulin, dextran sulphate and chitosan, which were deposited on the core of insulin-dextran sulphate macroaggregates (Dragan and Dinu, 2019, Alkekhia et al., 2020). Huang et al. (2015) used LBL technology to report a novel carrier intended for oral delivery. The novel carrier is composed of an iron oxide core coated by a layer of amphiphilic triblock copolymer poly (maleic acid) and octadecene. It is also loaded with doxorubicin (DOX) and indocyanine green as model drugs, where casein is deposited as the final layer. *Ex vivo* experiments on mice cells presented enhanced doxorubicin absorption in the small intestines and improved microvilli translocation *In vivo* imaging results revealed the safe transit of the carriers through the stomach and their accumulation in the intestines. The fluorescent signal persisted in the stomach for 7 hours, whereas the casein-modified particles exhibited a signal for the drug in the intestines after 3 hours of administration.

One formulation that never came to the market is Bows Pharmaceutical AG's oral insulin formulation. It was composed of insulin embedded within dextran to produce a matrix in a capsule. The last update regarding this formulation was from November 2010 (Easa et al., 2019).

Researchers have focused on colon targeting by developing many oral administration-based systems. Most of these technologies are dedicated to oral tablets. Colon technologies are summarized in figure 1.11 below and explained in the following sections.

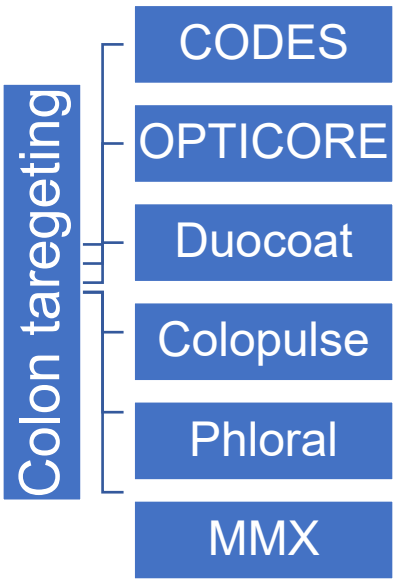

Figure 1.11. Developed technologies that enhance colon tablets properties.

Targeting the colon has been introduced through Colon Specific Delivery System CODES ™ technology. It was developed by Yamanouchi Pharmaceutical Co., Ltd. (Tokyo, Japan) as a tablet. The delivery system consists of lactulose in the core, that is surrounded by two acrylic-based films polymers. The inner coating is acid-soluble made from Eudragit E, and the outer coating is an enteric polymer made from Eudragit L, where an HPMC layer separates the two films of coating. The release mechanism of the drug is based upon the following: the enteric coating protects the carrier from gastric fluids and dissolves in the alkaline environment in the intestines. In the colon, the bacteria degrade the lactulose in the core, creating organic acid that lowers the pH of the tablet surroundings, dissolving the acid-sensitive coating and resulting in drug release. The studies have shown that CODES-insulin tablets have decreased glucose levels when absorption enhancers are supplemented with the tablet (Choonara et al., 2014, Gedawy et al., 2018).

OPTIORE™ is a tablet with three layers of coating, where the tablet's core is composed of the drug, and an example would be using 5 amino silicic acid. The first layer is an isolation layer

that separates the drug core (acidic) from the first enteric coating. This layer is composed of HPMC and a plasticizer triethyl citrate. The next layer is composed of either HPMC or Eudragit with glycerol monostearate, talc, and sometimes triethyl citrate.

Another colon targeting system is Duocoat®, a double-layer system with two enteric polymers: where the inner is partially neutralized. The system was used for targeting the proximal small intestine or the ileocolon. Colopulse® is an additional developed system incorporating swellable agents (sodium starch glycolate) in the enteric coating, facilitating the colon's delivery (Varum et al., 2020). Phloral® is a dual-action technology intended for drug delivery to the colon, combining a pH-responsive polymer and a bacterial-responsive polymer to form a coating for tablets or capsules. When the carrier reaches the colon, the bacterial-responsive polymer is dissolved in the presence of the microbiota. The change in pH initiates the dissolution of the pH-responsive polymer, releasing the drug. This product has reached clinical trials phase 3 (Ibeanu et al., 2020, Pharma, 2021a).

Cosmo Pharmaceutical Inc. (Lainate, Italy) have engineered Multi Matrix (MMX®), a novel technology intended to target the colon in delayed-release tablets (CosmoPharamceuticals, 2021). It utilizes hydrophilic and lipophilic materials with a pH-dependant coating. (Sandborn et al., 2007). MMX® has been employed for oral delivery of low molecular weight heparin. It comprises an enteric coating crafted from acrylic copolymers, conferring MMX with characteristics helpful to colon targeting and the capability to deliver the drug throughout the length of the colon (Choonara et al., 2014).

Enhancing the bioavailability of orally administered peptide-based tablets has been studied by researchers. They have developed numerous technologies that enhance the characteristics of oral peptide tablets. These technologies are summarized in figure 1.12 below and described in the following sections.

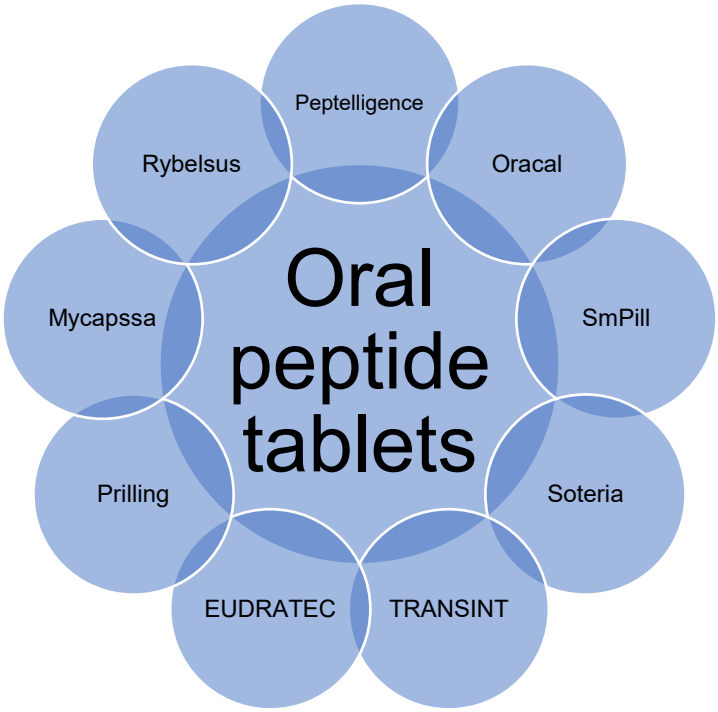

Figure 1.12. Current and under development technologies for tablet-based peptide delivery.

Peptelligence™ is one of the technologies developed for the oral delivery of peptides in the form of a tablet that utilises two components currently in phase III. The first is a permeation enhancer that loosens the tight junctions and acts as a surfactant. The other component is citric acid, which plays a vital role in chelating calcium ions. The tablet is coated with an enteric coating that protects it from gastric degradation and dissolves in the intestines. There, citric acid and the permeation enhancer are released, where the latter loosens the tight junctions, and citric acid lowers the pH of the intestinal environment to protect the drug from peptidases and protease degradation. Another form of Peptelligence™ is Oracal®, an oral formulation developed by Tarsa Therapeutics, and is intended for the oral delivery of salmon calcitonin. Oracal® is composed of granular citric acid, salmon calcitonin, and an enteric coating of Eudragit (Choonara et al., 2014, Brown et al., 2019, Zizzari et al., 2021, Peptelligence®, 2021, Peng et al., 2023).

SmPill was an innovative carrier under development by Sublimity Therapeutics, reached clinical phase II but was abandoned due to not presenting favourable results. The novel technology was designed for the oral administration of cyclosporin, with the candidate being ST-0529. The carrier, known as Single Multiple Pill or SmPill, encapsulates the drug in a soluble state while surrounded by a solid minisphere (Sublimity, 2021, Awad et al., 2022).

Soteria® is a novel technology that transforms injectable drugs into orally administered pills. The drug delivery system is composed of the primary drug combined with a dual-action enhancer in the core, followed by Phloral coating. The dual enhancer protects the drug from degradation, and the drug particles reach the intestinal walls. The permeation of the drug is facilitated by the dual enhancer (Ibeanu et al., 2020, Pharma, 2021b).

The TRANSINT permeability enhancer developed by Applied Molecular is based on truncated exotoxin technology. This technology targets the intestinal submucosa by using cholix-toxin-derived fusion molecules. One of their projects aims to administer interleukin 10 in tablet forms using a biopolymer called AMT-101, intended for treating inflammatory bowel diseases. However, the project has failed to progress to phase III (Brown et al., 2019, AMT, 2023). Evonic Industries has introduced a new technology called EUDRATEC PEP to enhance the bioavailability of oral peptides. It consists of the active drug, permeation enhancers, and an enteric coating (Kanugo and Misra, 2020, Enovic, 2021).

The prilling process is a microencapsulation technique that suits protein loading. This process protects the protein from thermally induced degradation and formulates the protein in the form of microparticles (de Kruif et al., 2016). The process is based on dropping a polymeric solution that contains the drug into a hardening bath, which in turn entraps the API by the formed hydrogel. The process was conducted by prilling a polymeric solution of mono-N-carboxymethyl chitosan and BSA into the hardening bath containing calcium chloride to produce hydrophilic microgels. The study aimed to study the effects of using a non-aqueous hardening bath on the bioavailability of oral administered proteins encapsulated within the previous complex. The bath comprised a co-solvent, a glyceride with different chain lengths, and a complementary excipient: either peppermint oil or PEG (De Kruif et al., 2015).

Mycapssa® is an oral dosage form of octreotide acetate. It comes in the form of sustained-release capsules and is developed by Chiasma, via the transient permeability enhancer (TPE®) technology (Zhu et al., 2021b, Chiasma, 2021). This drug has been introduced to the market. The API in Mycapssa is Octreotide, a somatostatin analogue for the treatment of acromegaly (Bhutani et al., 2021). Another example for a commercially available product using TPE technology is Rybelsus®, the first oral formulation for delivering semaglutide. This formulation combines the active pharmaceutical ingredient (semaglutide) with a permeability enhancer (SNAC), as mentioned previously (Buckley et al., 2018). Table 1.1 below summarises the technologies mentioned above.

TPEs are compounds that modulate intestinal epithelium permeability. Examples include sodium caprate, N-[8-(2-hydroxybenzoyl) amino] caprylate (SNAC), which is an acylated

amino acid, and medium-chain glycerides and derivatives (Vinarov et al., 2021). TPEs are the key factors within the formulation in Mycapssa, where sodium caprylate serves as the TPE. It enhances the permeation through the tight junctions via the paracellular route by reversibly modulating molecules passage. In Mycapssa, octreotide is blended with a hydrophilic powder, and the two ingredients are suspended in a mixture of excipients, which includes sodium caprylate, resulting in an oily suspension (Zizzari et al., 2021, ChiasmaTPE, 2021).

Another example of the utilisation of TPE includes enteric-coated tablets/capsules. These dosage forms contain the lyophilised API mixture with C_8/C_{12} and povidone. The previous mixture is suspended in an oily phase composed of polysorbate 80, glyceryl monocaprylate, and glyceryl tricaprylate (Maher et al., 2016).

Upon reviewing the preceding technologies and tablet-based carriers, it can be asserted that the technology behind Mycapssa® and Rybelsus® stands out as the most advanced and sought-after solution. This is attributed to the fact that both Mycapssa and Rybelsus already exist on the market as an FDA-approved products.

Table 1.1. The status of available and under development technologies for peptide-based tablets.

Technology/product	API	Components	Phase	Reference
Peptelligence	Calcitonin	Citric acid as PE	Phase III	(Peng et al., 2023)
Oracal	Calcitonin	Enteric coated capsule of Eudragit	Completed Phase III in 2012	(Zhu et al., 2021c)
SmPill	Cyclosporine A	Solid minisphere	Abandoned after Phase II	(Awad et al., 2022)
TRANSINT	Interleukin 10	Biopolymer	Failed to reach Phase III	(AMT, 2023)
Mycapssa	Octreotide	Sodium caprylate as PE, based on TPE technology.	In the market	(Larsen et al., 2024)
Rybelsus	Semaglutide	SNAC as PE, based on TPE technology.	In the market	(Buckley et al., 2018)

Aside from the previous technologies for peptide oral tablets, researchers have focused on developing carriers in many forms. These carriers enhance the properties of the DDS upon addition.

1.3.2. Novel carrier technologies and additives to oral DDS

The use of novel carriers has been investigated for protein and peptide oral delivery. Most of the focus was on insulin, as many carriers were designed to administer oral insulin. The novel additives are mentioned in figure 1.13 below and described in the following sections.

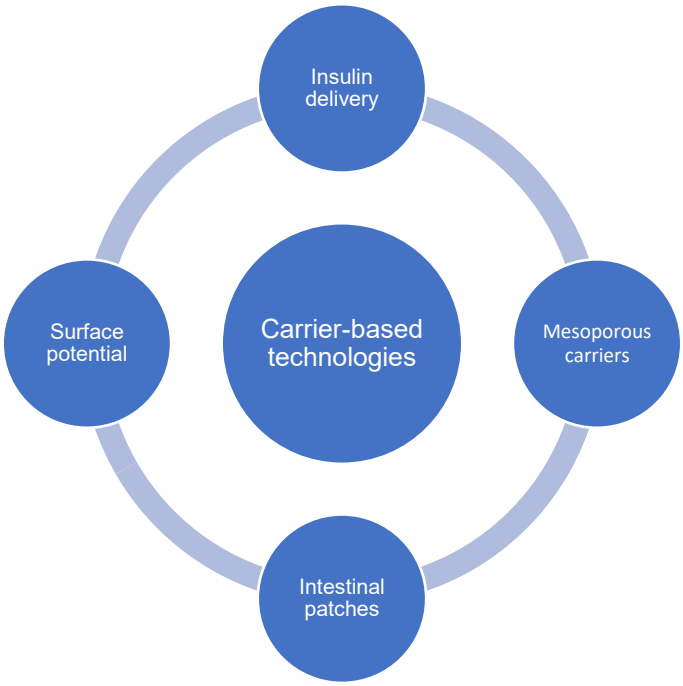

Figure 1.13. Carrier-based technologies and additives to oral peptide DDSs

1.3.2.1. Novel carriers for insulin delivery

The Canadian company Generex Biotechnology has developed an oral insulin formulation Generex Oral-lyn™ to be administered as a buccal spray during meals and is currently in phase III clinical trials. This dosage form delivers insulin via RapidMist™, a similar device to the ones used in delivering metred doses for asthma. The formulation comprises a combination of surfactants functioning as absorption enhancers along with insulin micelles (Easa et al., 2019).

Preparing nanofibers through electrospinning is a conventional preparation method. It involves using electric fields to draw out charged threads with a diameter within the nano range from the polymer solution. This technology has been used to deliver insulin orally using electrospun nanofibers derived from fish sarcoplasmic proteins, which are soluble in water. However, the resultant nanofibers are insoluble in aqueous mediums but are degraded in the presence of

proteolytic enzymes. This technique is helpful for colon targeting and in the case of poorly soluble drugs (Ahadian et al., 2020, Brown et al., 2019).

Chuang et al. (2015) developed a bubble carrier system for oral insulin delivery that generates nanosized CO_2 bubbles while water passes through the shell and expands until it contacts the mucous and releases the drug. The bubble carrier is a capsule-based system composed of diethylenetriamine penta acetic acid (DTPA) dianhydride, sodium bicarbonate, a surfactant, and an enteric polymer that coats the capsule and fills its interior. Furthermore, research has explored the utilization of a self-assembled bubble carrier system for oral delivery. This innovative carrier system is created using DTPA dianhydride, a surfactant (SDS), sodium bicarbonate, and insulin. The mixture is coated with an enteric coating and then encapsulated in a capsule. Upon interaction with fluids, the system releases its components, forming bubbles that play a crucial role in transporting insulin (Kanugo and Misra, 2020).

Oshadi Drug Administration has pioneered the development of a novel carrier, known as the Oshadi carrier, based on inorganic particles for the oral administration of insulin. This innovative carrier incorporates insulin and proinsulin C-peptide, forming a non-covalent association with silica nanoparticles. This system employs a non-biodegradable carrier, raising considerations about the removal of the carrier from the body without accumulation. The carrier has successfully completed phase 2 clinical trials (Brown et al., 2019).

Micro delivery devices have been investigated as potential carriers for the oral delivery of insulin. Microcapsule-based drug delivery systems have been studied as potential candidates. Microcapsules can be formulated using different methods like W/O/W double emulsion, self-assembly, complex coacervation, and LBL. Insulin microcapsules can be formulated using natural or synthetic polymers (Wong et al., 2018), and Ma et al. (2000) used polylactide microcapsules as insulin carriers. Polylactide microcapsules were able to protect insulin against enzymatic degradation in the intestinal tract and reduce glucose levels to 68% of control glucose levels.

Another form of microcapsules can be formulated using ragweed pollens, proposed as carriers of proteins intended for oral delivery. Lale and Gill (2018) developed an oral protein microcapsule carrier using ragweed pollens. Their carrier was composed of an enteric polymer Eudragit L100-55 as the core matrix with BSA as a model protein. Eudragit protects the protein from acidic degradation and achieves a pH-dependent release in the intestines (Lale and Gill, 2018). The release studies indicated a 24% release of BSA at pH 1.2 for the formulation with pollen and Eudragit, in contrast to a 64% release from carriers made solely from pollen. Additionally, the carrier slowly released BSA in pH 6.8, where 45% were released in the first

hour, compared to approximately 6% from the carrier made from Eudragit. These results might indicate that the pollen-Eudragit carrier provides a controlled and prolonged release profile.

Silicon wafers are used to make micro containers intended for oral insulin delivery, with sodium caprate C10 to enhance paracellular permeation (Jorgensen et al., 2019). One of the new strategies focused on using polydimethylsiloxane containers loaded with poly (N-isopropyl acrylamide-co-methacrylic acid) (PNIPAm-MAA) nanoparticles. The drug release is related to pH changes; upon pH decrease, channels in the matrix are formed due to the nanoparticles shrinking, causing drug release (Mandsberg et al., 2020).

Hydrogels are studied for their possible uses as carriers for insulin intended for oral delivery. Poly (methacrylic acid) (PMAA)-based insulin-loaded hydrogel microparticles are used since they offer pH-sensitive swelling behaviour (Wong et al., 2018). The previous carrier was modified to contain methyl-β-cyclodextrin/insulin complex into hydrogel microparticles of PMAA-chitosan-PEG, and the formulation reported an enhanced insulin oral bioavailability where less than 15% of insulin was released in 1.2 pH within 2 hours (Sajeesh et al., 2010).

1.3.2.2. Intestinal patches and surface potential as novel carriers

Researchers also focused on using technologies that enhance the characteristics of DDSs intended for oral delivery. An example would be intestinal patches containing a backing, pH-sensitive, and mucoadhesive layer. There are many types of intestinal patches: the two-layered patch contains a backing layer and a drug-loaded mucoadhesive layer, including a chitosan ethylene diaminetetraacetic acid hydrogel layer to provide good adhesion properties. The three-layer patch contains a pH-sensitive layer in addition to the previous two, while the four-layer patch contains a middle layer that separates the drug-loaded and the pH-sensitive layer. The patch adheres to the intestinal wall based on the cationic polymers' attachment with the mucin's negatively charged residues. Also, hydrogen bonds and polymer chain entanglement contribute to patch adherence (Ahadian et al., 2020).

Lyndra Therapeutics developed a polymeric scaffold that fits inside a capsule. The capsule releases the drug in the stomach after breaking, and the drug is infused with poly(ε-caprolactone) polymer structure. The previous complex is a self-expanded structure and takes the form of stellate or a star-like shape. The expanded form is retained without passing through the pylorus until pH-dependent linkers are degraded (Brown et al., 2019).

Enhancing the interaction between nanocarriers and negatively charged mucin can be achieved through the carriable surface potential technique, which is based on the use of polyphosphate chitosan nanomicelles with SEDDS. Phosphate is hydrolysed by alkaline

phosphatase, which inverts the zeta potential of the surface from negative to positive. These changes enhance the interaction with the negatively charged membrane and prevent back diffusion (Wang et al., 2020). Le-Vinh et al. (2019) prepared micelles from phosphorylated chitosan-stearic acid conjugates and tested the zeta potential changes and interaction with Caco-2 cells. Their results revealed an enhanced mucus permeation properties up to 6 folds in comparison to unphosphorylated micelles. Their results provide a platform for further developments in oral peptide delivery.

1.3.2.3. The use of mesoporous carriers

Researchers have been aiming to use a GRAS, biocompatible, low-toxic material for oral delivery with mesoporous silica micro/nanoparticles possessing these characteristics. Porous materials are materials with small holes in their structure, and these holes can be either ordered or disordered. The matrix is the skeletal portion of the material, as seen in figure 1.14 below (Kumar et al., 2017). According to the International Union of Pure and Applied Chemistry (IUPAC), the porous materials are classified into three categories based on the size of the pores (McCusker et al., 2003):

1. Microporous materials: the diameter of the pores is less than 2 nm.
2. Mesoporous materials: the pore diameter is in the range between 2-50 nm.
3. Macroporous materials: the pore diameter is larger than 50 nm.

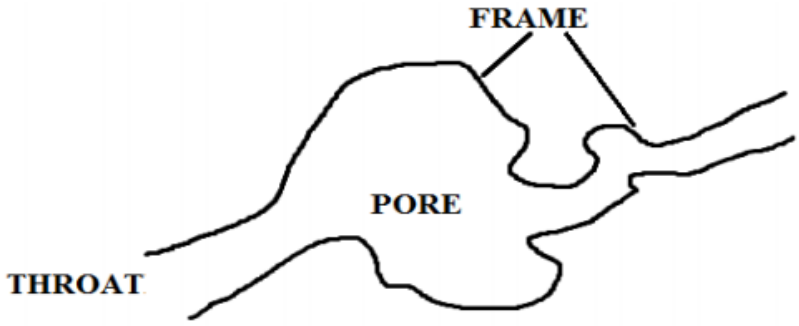

Figure 1.14. Skeletal matrix of the mesoporous carrier (Kumar et al., 2017).

There are two categories of mesoporous materials: silicon-based and non-siliceous mesoporous materials. Silicon-based mesoporous materials are called mesoporous silica and can be divided into modified and pure silicates (Kumar et al., 2017).

Mesoporous silica was discovered by Yanagisawa et al. (1990) in Japan, and it was subsequently industrially produced by Mobil Corporation Laboratories. Among the most common products were MCM-41, MCM-48, and MCM-50, where MCM stands for Mobil Crystalline Material. The types mentioned above are parts of the Molecular 41 Sieves (M41S) family (Rahmat et al., 2010). One of the most famous mesoporous silica carriers is Santa Barbara 15 (SBA 15), an MSN type that was invented by a research group in the United States (Zhao et al., 1998a, Zhao et al., 1998b). Due to their surface area and tuneable pore size, mesoporous silica carriers provide an excellent candidate for drug loading and incorporation as these characteristics contribute to formulation flexibility (Le et al., 2019).

The tuneable size, high surface, and porous structure of silica provide a good carrier for peptides, where loading efficiency can reach up to 20%, depending on the peptide. Additionally, silica nanoparticles, and MSNs in particular, have been found to protect peptides from enzymatic degradation if they remain inside the pores (Braun et al., 2020).

Proteins can be incorporated into these carriers. However, in non-ordered mesoporous silica, access to pores might be limited because of the long diffusion pathways that result from the disordered structures (Liu et al., 2000, Wan and Zhao, 2007). He et al. (2020) reported loading mesocellular silica foam with insulin for oral delivery applications in mice. Their loading results showed that the insulin loading of the carrier was up to 43%. Also, 87% of the protein was released after the lysozyme-modified carrier was incubated for 30 minutes with pancreatin. Moreover, the digestion time of insulin was twice as long as that of plain insulin, and only 1/40-1/20 of the secondary conformational changes were observed compared to Zn2+-incubated plain insulin. Moreover, Abeer et al. (2019) developed porous dendritic silica nanoparticles (DSNs) for the oral delivery of exenatide. Their results demonstrated a high loading capacity of 35%-40%. Also, the Caco-2 cell tests presented that chitosan-coated DSN presented 1.7 times higher transport in comparison to free exenatide.

Ariga et al. (2003) proposed the development of novel, regular-structured nanocomposites made from silica-peptides, termed proteosilica. These structures can be acquired by filling the pores of mesoporous silica with peptides and amino acids using two methods. The first is via preparing mesoporous composites between silica and peptides that are carrying surfactants. On the other hand, the other method is composed of covalently immobilising the silica backbone with surfactants, followed by hydrolysis to remove alkyl tails. Their work resulted in the production of proteosilica films, where the amino acids were immobilised inside the pores in a weakly-bonded state. Additionally, the amino acids would bind easily with external molecules at activated hydrogen bonding sites. In that context, Omar et al. (2017) reported the fabrication of a mesoporous silica-based multifunctional biodegradable magnetic hybrid nanovector for protein delivery into cancer cells. Their carrier provided pH-triggered release that was actuated magnetically. The protein was released at pH levels around 5 with reversible actuation due to the magnetic attachment.

The use of silica nanoparticles enhances the permeability of proteins. It was found that negatively charged 50 nm silica nanoparticles enhance the permeability through integrin-mediated TJs remodelling. Integrin receptors are strongly connected with permeation through myosin light chain kinase signalling pathways (MLCK). Activating MLCK acts as a stimulator of the cytoskeleton myosin phosphorylation, in which tight junctions are rearranged and opened due to the contraction and tension caused by myosin (Abeer et al., 2020).

The previous technologies are considered great candidates for delivery. However, the development of needle-based delivery devices has revolutionised peptide delivery. The needle-based devices/carriers are used for diagnosis or treatment, and they are orally ingestible microdevices with the exact injection mechanism. Although their action is based on puncturing, the used needles are in the micro range.

1.3.3. Swallowable devices and needle-based carriers used for oral delivery and diagnosis

Using microneedles for delivering drugs has been studied and developed since the 1980s. Many applications have been reported in which needles are used, including transdermal applications and vaccine delivery. Recently, this approach has been examined to deliver proteins and peptides since they possess low oral bioavailability. Understanding the interaction between injection-based carriers and the intestinal tissues is crucial, as their application can be invasive (Zizzari et al., 2021). The sections below will focus on the most advanced and developed swallowable devices and injection-based carriers for peptide oral delivery purposes. Figure 1.15 below summarizes the carriers.

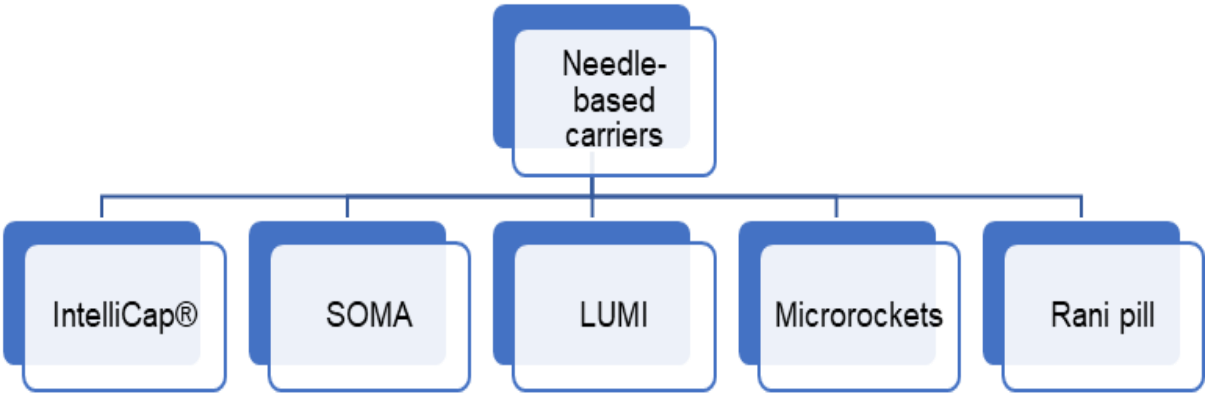

Figure 1.15. Orally swallowable devices and needle-based carriers for peptide oral delivery.

To begin, IntelliCap® technology offers delivery at specific pH levels and temperatures when programmed to be real-time controlled or triggered. Additionally, it provides the ability to monitor the changes in pH and temperatures. It is loaded with liquid drug formulation and releases the drug in 24 hours, where the release mechanism depends on the microprocessor controlling a motor. The motor is connected to a spindle that moves the piston to release the drug (Mandsberg et al., 2020, Tatlić et al., 2020). Figure 1.16 represents a schematic of IntelliCap components.

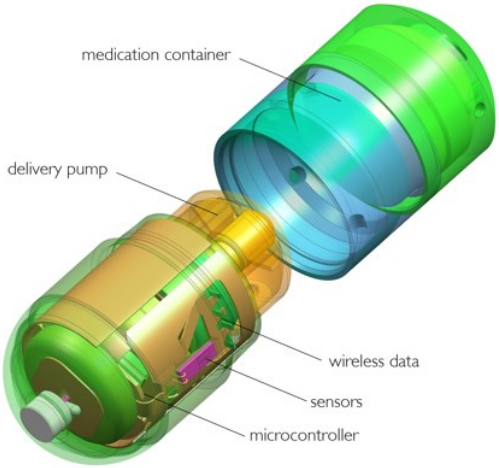

Figure 1.16. Schematic of Intellicap components (Tatlić et al., 2020).

Two of the most advanced and mentioned needle-based carriers in literature are the luminal unfolding microneedle injector (LUMI) and the Self-orienting millimetre-scale applicator (SOMA).

The luminal unfolding microneedle injector (LUMI) is an engineered carrier intended for delivering biologics orally, where one form was constructed to deliver insulin. The device is made in the form of a capsule that is packed along with three degradable arms made from polyvinylpyrrolidone (PVP), each containing insulin-loaded microneedles and a PEG-coated actuator. The capsule is coated with poly(methacrylic acid-co-ethyl acrylate) that dissolves at pH levels above 5.5, where the PEG coating is dissolved, and the device is pushed out of the capsule. The arms adhere to the walls of the intestines and deliver the drug (Brayden et al., 2020, Drucker, 2020, Ahadian et al., 2020, Mandsberg et al., 2020). The self-orienting millimetre-scale applicator (SOMA) is an ingestible carrier inspired by the self-righting tortoise shell, where this carrier delivers the drug into the stomach lining. The drug delivery process is initiated from the fluid-induced dissolution process, where pressurized insulin is injected from the biopolymer shaft-fused tip by a stainless-steel spring. The difference between SOMA and LUMI is that the first carrier does not depend on gastric emptying to release the drug and delivers the drug to the gastric epithelium. Also, LUMI has not been ready for oral delivery.

(Drucker, 2020, Brown et al., 2019, Mandsberg et al., 2020, Brayden et al., 2020). Figure 1.17 presents a schematic of the components of both carriers.

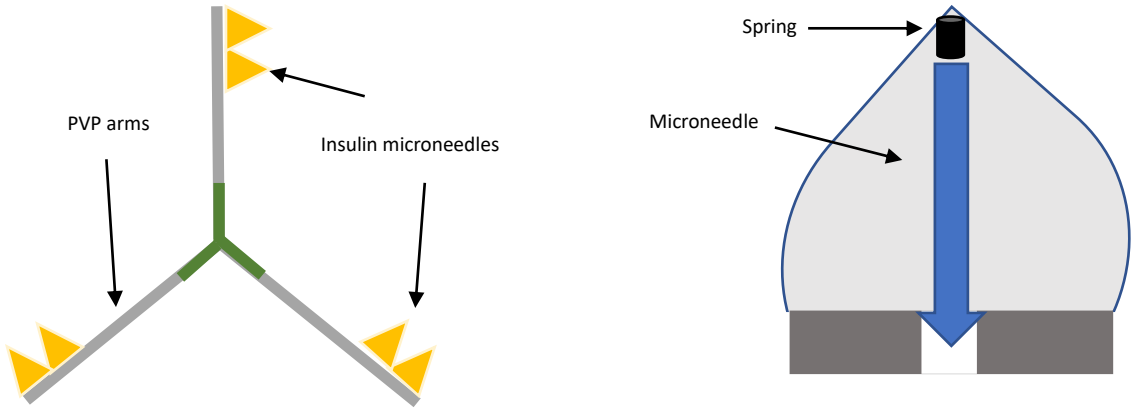

Figure 1.17. Schematic of LUMI (left) identifying the three degradable arms (grey) that carry insulin-loaded microneedles (yellow) .SOMA on the right showing the spring (black piece) and the microneedle to deliver insulin (blue arrow).

Microrockets or micromotors are novel self-propelled microdevices intended to be dissolved in the stomach. They were used to deliver doxorubicin in a controlled manner, where the carrier consisted of a poly(aspartic acid) microtube and a thin layer of iron as the coating surrounding the zinc core. Doxorubicin was absorbed into the poly(aspartic acid) layer through electrostatic interaction, and the movement of the carrier was regulated by zinc particles. These particles generated hydrogen bubbles in acidic pH, preventing the oxidation of iron molecules (Ahadian et al., 2020, Zhou et al., 2019). Retrospectively, microneedles have been proposed for animal *In vivo* testing. Traverso et al. (2015) reported the formation of a microneedle that delivered insulin orally to swine. Their microneedle was made with 25G needles that protruded from the surface.

Rani Therapeutics developed the ‘’Robotic pill’’ or Rani pill. This formulation is covered with an outer cellulose coating that is intended to dissolve in pH levels ranging between 6.5 and 7.0. The dissolution serves as an activator for a chemical reaction within the pill, leading to the inflation of a balloon with carbon dioxide. This inflation, in turn, triggers the deployment of sugar-based microneedles loaded with the drug, allowing them to pierce the intestinal wall (Aguirre et al., 2016, RaniTherapeutics, 2021). Another technology that utilises gas release for delivery is the balloon delivery system, which is a self-actuated-balloon microneedle device. The release depends on mixing reactants A and B, where the reaction produces gas that expands the polymer balloon and pushes a needle that injects the lining (Mandsberg et al., 2020).

1.3.4. Challenges with marketed and novel approaches for oral peptide delivery

The use of different carriers and additives to peptide oral formulations modernized DDSs in which many formulations are either in the market or in clinical trials. Nevertheless, some challenges accompany this development. For instance, most formulations are developed in the form of a tablet, which is understood considering it is the most commonly used approach. Yet, other DDS types are less focused on, like buccal patches, syrups, and inhalers. Moreover, these newly developed technologies are not applicable to all peptides and proteins since some of them are based on using specific materials, like Axcess technology that utilises aromatic alcohols. Some peptides might interact with aromatic alcohols and degrade as a result. Additionally, some technologies require the drug to be in a specific form, like the surface potential technique where SEDDS is used. An essential factor to consider is the interaction between the drug and the components of SEDDS, like the co-solvents and whether the drug can be turned into an SEDDS.

The needle-based carrier systems revolutionised drug delivery systems. However, there are many considerations and drawbacks that researchers draw. For example, the puncturing mechanism of the carrier can cause irreparable damage to the tissues where the carrier is administered, especially if the needle size is in the micron range. Also, causing injury to the tissue correlates with the previous problem, as the inflicted injury might affect the integrity of the tissues, allowing passage of toxins and microparticles that are generally restricted.

Another critical factor related to the puncturing mechanism is patients' compliance, which is a vital consideration in the formulation, as some patients fear using needle-based carriers. Another factor to consider is the formulation materials, which can pose challenges in the development process. The components in the carrier could cause possible toxicity and interactions, as some materials might be toxic towards certain tissues, and cause metal toxicity. Also, some carriers are inapplicable to *In vivo* usage for therapeutics and are only intended for *In vitro* testing and diagnosis. Furthermore, needle-based carriers are made of non-biodegradable components, which leads to the carrier being excreted by faeces. Moreover, the applicability of the needle-based carriers to administer drugs is essential when designing a novel formulation. These carriers are limited to specific therapeutics, indicating that they cannot be universally applied to all drugs and therapeutic proteins. Interactions within the carrier, whether chemical or physical, pose obstacles to their use with all types of drugs.

As mentioned above, there are several techniques to enhance the bioavailability of administered drugs through the use of permeation enhancers or different additives like mesoporous silica and lipid-based carriers. This project will focus on designing a novel carrier for the oral delivery of proteins, and the investigated protein will be octreotide. The characteristics of this protein, as well as its bioavailability and absorption will be investigated in the following section. Furthermore, the recent studies and works regarding the oral delivery of octreotide will be reported to elaborate on the gaps and the need to implement novel carriers for administration.

1.4. Octreotide as a model protein and its formulations

This section will elaborate on octreotide and the available formulations in the market, as well as the orally available products and developments regarding the oral delivery of octreotide.

1.4.1. The development of octreotide as a somatostatin analogue

Octreotide is an octapeptide with 8 amino acids, that was synthesized as a long-acting analogue of somatostatin that has been used since 1984. This analogue is more specific towards growth hormone (GH) without the adverse effects on insulin and glucagon. It is referred to as selective mini-somatostatin (SMS 201-995) or SMS (Plewe et al., 1984). The first report of SMS was by Bauer et al. (1982), as in their design, they developed an octapeptide with more specific properties toward GH, minimizing its impact on insulin and glucagon. The FDA approved the use of octreotide in 1989 for managing and treating malignant vasoactive intestinal peptide (VIP)-secreting tumours and carcinoid syndrome. Octreotide is more potent than the normal somatostatin in suppressing peptide-based hormones (Brown, 1990). The chemical structure of octreotide and the amino acid sequence are defined in figure 1.18 below

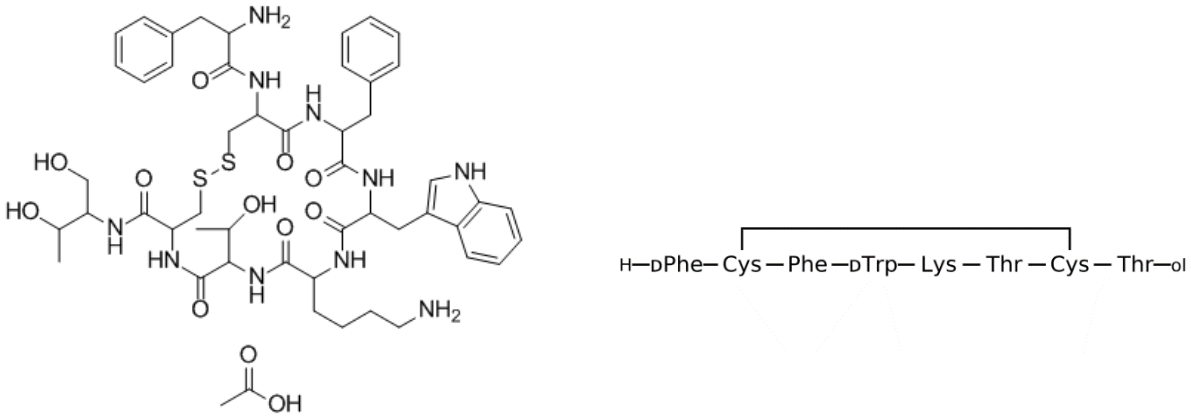

Figure 1.18. Octreotide chemical structure and amino acid sequence (Octreotide, 2023).

Octreotide or octreotide acetate (the acetate-based salt of the synthetic octapeptide) is more potent and stable than the naturally available somatostatin. Apart from inhibiting several hormones like GH, insulin, and glucagon, it is used for treating carcinoid syndrome and GIT endocrine tumours. In addition, it has a high affinity towards somatostatin receptors, specifically somatostatin receptor 2 (SSTR2) and receptor 5. Moreover, it is used for its antitumor effects in hepatocellular carcinomas where high-affinity SSTRs are over expressed. Furthermore, octreotide is used for disease control between the onset and administering

radiotherapy, as well as as an adjuvant for pre- and postoperative therapy. However, octreotide has a short *In vivo* half-life of 2 hours, and the therapeutic effects are drastically reduced at the end of infusion or subcutaneous injection (Wang et al., 2016).

1.4.2. The bioavailability and absorbance of octreotide

Tanabe et al. (2015) reported that the presence of the disulphide bonds and the preservation of the cyclic structure in octreotide are essential for the peptide to maintain its biological activity. Moreover, considering the peptidic structure of octreotide (figure 1.18), the amide bonds that connect the intramolecular amino acids are easily hydrolysed. The hydrolysis activity is prompted in the presence of an alkaline environment where the disulphide bond is dissociated, creating two resulting primary degradants (Li et al., 2020). This supports Ryu and Na (2009) results, as they found that the degradation of octreotide is faster in alkaline environments. They found that the degradation follows first-order kinetics, and at 37 ℃, where the half-life of octreotide is 123.8, 288.8, 52.9, and 9.6 days at pH 2.5, 4, 7.4, and 9, respectively. They concluded that the most favoured pH level is 4, which helps maintain the disulphide bond. The disulphide bridge restricts the active tetrapeptide fragment, which is crucial for activity. The aromatic side chain of phenylalanine (Phel) protects the active fragment from enzymatic attacks, while the chain occupies a similar region to Phe6 that is available in somatostatin. The carboxylic function in octreotide Thr-COOH is responsible for the stability of enzymatic degradation when reduced to an alcoholic function (Pohl et al., 1995).

The work of Bauer et al. (1982) was based on modifying a conformationally stabilised fragment of naturally occurring somatostatin. This fragment is the extended parallel β sheet that has residues at the β turn consisting of TrP8-Lys9 residues. The SMS was found to be highly resistant to degradation, whether by enzymes or tissue homogenates. The engineering of SMS went through numerous steps and trials for the product to emerge. The main point was to enhance the chemical structure of the cyclic peptide Cys-Phe-(D)Trp-Lys-Thr-Cys . The work focused on adding different chemical groups in the N-terminal (A) and the C-terminal (B) as seen in the structure: A-Cys-Phe-(D)Trp-Lys-Thr-Cys-B. The aromatic side chain is essential in protecting the disulfide bridge against enzymatic attack, while the D-Thr(ol) is responsible for having the natural L-configuration, where it takes the place of Thr12 in the native hormone.

However, octreotide has a low bioavailability which is attributed to several reasons. For instance, the limited absorption sites in the intestines may contribute to its low bioavailability, affecting the passage of the drug. Moreover, the interaction with the contents in the intestines, such as pancreatic or biliary fluids, can impact its stability (Fricker et al., 1992). Moreover, octreotide uptake from brush border membrane vesicles isolated from the jejunum was higher than the uptake from ileum vesicles. The protein uptake from the jejunum-isolated vesicles after 15 seconds was around 1.75 nmol/mg compared to 1.2 nmol/mg from ileum vesicles. This difference is attributed to specific peptide-membrane interaction and a Na^+/H^+ exchange system that produces a proton gradient and Na^+ dependency. Additionally, octreotide acetate is highly hydrophilic, and its molecular weight is relatively high (1kDa), which creates a barrier against intestinal permeability, and thus, low oral bioavailability (Pohl et al., 1995).

1.4.3. Oral delivery of octreotide

Several attempts were made to enhance the bioavailability of orally administered octreotide, which was administered with absorption enhancers like bile salts *In vivo* for rats and healthy volunteers. It has been found that the inclusion of these enhancers has distorted the membrane, increasing octreotide's permeability. However, this approach has not been investigated further towards a solid dosage form development due to the harmful effects of the bile salts-based permeation enhancers (Thanou et al., 2000).

There have been injectable-based formulations of octreotide for acromegaly treatment. One of which is Sandostatin LAR. This injectable formulation was developed using PLGA microspheres as a monthly intramuscular injection delivery system. However, one drawback is the long lag time of 14 days, which is the time that the amount reaches the therapeutic concentration in plasma. This downside was tackled by administering daily injections of octreotide to cover the 14-day period (Erfani Jabarian et al., 2013). Nonetheless, due to recent research studies, patients prefer non-injectable-based therapies and oral formulations.

Moreover, administering octreotide via Sandostatin is painful because it uses low-gauge needles. These reasons led scientists to develop octreotide in oral-based formulations using novel technologies. An example is Chiasma's Mycapssa, which employs the transient permeability enhancer technique mentioned earlier. In this formulation, octreotide is presented as an oily suspension that is combined with the intestinal permeability enhancer sodium caprylate (C_8) (Fattah et al., 2020). Over the years, numerous attempts were conducted by researchers to develop orally administered forms of octreotide which will be discussed next.

One article has explored delivering octreotide orally for *In vivo* experiments in pigs. This study used superporous hydrogel polymers as the carriers for octreotide delivery, as reported by (Dorkoosh et al., 2002). They reported loading octreotide into PEG 6000 microparticles, which were later installed to the interior part of the porous hydrogel. Additionally, octreotide was also loaded into minitablets that were later added into the exterior part of the porous hydrogel. However, the tablets contained several excipients like TMC and lactose. After loading the two composites into Eudragit S100 enteric-coated tablets, they found that the formulation without TMC (installed to the interior part) had presented a bioavailability of 8.7% compared to the minitablet-based formulations with 12.7%. This increase could be related to the effect of TMC that causes gelation and slows the release.

Also, Chaisma (the company behind the commercial product Mycapssa) has conducted an experiment on the effects of fats and food on the bioavailability of octreotide. This experiment consisted of giving 20 mg Mycapssa to volunteers who either took the drug 30 minutes after having a high-fat meal or after 10 hours of fasting. The results concluded that the group with the high-fat meal presented a 90% decrease in bioavailability compared to the levels of the fasting groups. The researchers concluded that the presence of food particles in the intestines can negatively affect the drug absorption as it obstructs the PE from intestinal wall localisation (Maher and Brayden, 2021).

Bonengel et al. (2018) reported the incorporation of octreotide with an SEDDS to study its bioavailability in pigs. They ion paired octreotide with a surfactant, deoxycholate, followed by incorporating this pair in an SEDDS. This complex presented an increase in relative bioavailability of 4.9% compared to octreotide administered in a solvent. They attributed their results to the properties of the SEDDS. Octreotide within the SEDDS carrier can pass the mucus barrier more efficiently due to the deoxycholate properties and the charge that favours the interaction with cells. At pH 6.8 in the intestines, octreotide is positively charged due to the presence of the amino acids. In addition, the mucus barrier will be negatively charged, affecting the permeation, considering the difference in charge. However, SEDDS has a neutral charge which will shield the octreotide from the interaction with mucus and, thus, enhances its uptake and bioavailability.

Chatzitaki et al. (2023) reported the fabrication of a 3D-printed octreotide acetate tablet for oral delivery. Their formulation provided a prolonged release and enhanced the permeability of the drug from 0.9 μg/cm^2 after two hours to 1.6 μg/cm^2. They attributed this increase to the presence of the used inks in printing tablets, which were carbopol and HPMC. In that context, carbopol has been reported to enhance the paracellular transport of drugs by opening the tight junctions, and it has no toxic effects against Caco-2 cells. Furthermore, the previous materials

were included due to their mucoadhesive properties and protection effects against enzymatic degradation.

Furthermore, Fattah et al. (2020) studied the effects of SNAC on the permeability of octreotide across human colonic mucosa. They found that using SNAC in ascending concentrations (20-40mM) has significantly increased the apparent permeability of octreotide from 1.3 * 10^{-6} to 2.1 10^{-6} and 2.7 10^{-6} cm^2/s when SNAC amount was 0, 20, and 40 mMol, respectively. Additionally, the trans-epithelial electrical resistance (TEER) values have decreased upon adding octreotide and octreotide-SNAC in the two previous concentrations. This decrease was proportional to SNAC increase, where the 40mMol has caused the highest decrease (60%) compared to 0 mMol (20%). This is related to the effects of SNAC on the cells and the reduction on TEER values, as reported by Twarog et al. (2019). Additionally, they studied the effects of the different permeability enhancer concentrations on the cells after treatment with SNAC. They found that the villi tips were damaged when SNAC was used in 20 mMol, while there was an erosion event when the concentration increased to 40 mMol. It can be theorized that SNAC may not be as potent as other PEs in enhancing permeability, given that certain PEs have been observed to increase permeability at lower concentrations. Another aspect supporting the previously reported theory is the ratio of SNAC to the peptide in Rybelsus formulation, which was almost 21:1 SNAC to peptide (Fattah et al., 2020).

As reported above, octreotide has a low bioavailability, and the use of permeation enhancers has been considered for improving the oral absorption. However, using surfactants can cause cell toxicity and high doses of permeation enhancers are not preferred. Therefore, using a different approach with another drug delivery system can be beneficial.

1.5. Research aim and objectives

As discussed above, there are numerous technologies that deal with the oral delivery of peptides, with needle-based systems like SOMA and LUMI being amongst the most novel. However, their disadvantages regarding size and the use of nonbiodegradable needle-based systems could present a drawback for administering. Furthermore, octreotide acetate as a somatostatin analogue has great potential for use, with an FDA-approved available formulation in the market. This project aims to design a mesoporous silica lipid-based carrier as a novel approach for the oral delivery of octreotide. The objectives of this work can be listed according to the chapters where they are reported below.

Chapter 2:

- To design a novel-lipid mesoporous hybrid carrier via investigating stearic acid loading over a range of concentrations.
- To characterise the morphology, thermal properties, and size of the developed carrier using SEM imaging, DSC, and laser diffraction.
- To examine the parameters that govern crystal formation at different stearic acid concentrations using thermal and crystallographic methods.

Chapter 3:

- To develop and validate an HPLC method for octreotide acetate detection.
- To design SYLOID-stearic-octreotide complex and characterise the fluorescence and morphological properties.
- To conduct *In vitro* permeability tests using Caco-2 cells.
- To examine the effects of different permeation enhancers on the complex permeability across Caco-2 cells.

Chapter 4:

- To evaluate the loading efficiency and investigate the factors that govern protein-silica loading.
- To assess the impact of the solvent viscosity, protein size, and polarity on loading.
- To quantify protein diffusion into SYLOID using confocal fluorescence microscopy.

Chapter 5

- To investigate the factors that govern mesoporous silica tabletting.
- To design a tablet containing silica-peptide for oral delivery by investigating different silica concentrations and excipients.
- To examine the effects of different excipients and silica ratios on tabletting properties.
- To assess the different effects of compression on the morphological properties of silica.

Chapter 2

Formulation and Characterisation of a Mesoporous Silica Microparticle-Lipid Hybrid Carrier

Introduction

Mesoporous silica are widely used as carriers for different materials as they possess adjustable porous structure, high loading capacity, and tuneable surface area, as well as relatively high silanol density (Lerida-Viso et al., 2023). In addition, mesoporous silica are employed for oral delivery and tailored for targeting purposes through the optimisation of their shape and surface properties. This can be achieved by surface modifications via numerous functional groups and active targeting (Pamshong et al., 2023). Despite their advantages, mesoporous silica carriers may encounter challenges such as premature drug release before reaching the target site, making them susceptible to cellular uptake and potentially reducing the effectiveness of the carried active pharmaceutical ingredient (API). However, these drawbacks can be mitigated through (silica-capping) by employing gatekeepers that control the pore opening and release of loaded materials through stimuli-responsive interactions (Kheirkhah et al., 2022; Gupta et al., 2023). The addition of gatekeepers such as peptides and lipids enhances the surface characteristics of silica particles, as some of these keepers are added to target a specific tissue or organ, enhancing the interaction with tissues (Cai et al., 2020, Ahmadi et al., 2022). There are several types and strategies for silica-capping, where lipids can be used as gatekeepers, and the cargo release mechanism is based on the oxidation and reduction of the lipid (Bakhshian Nik et al., 2020). Additionally, using lipid-based materials as capping agents enables an easy surface functionalisation of the silica carrier with numerous ligands (Zhu et al., 2021a).

As mentioned above, mesoporous silica capping can be achieved using different materials, and one of the promising candidates is stearic acid. According to the International Union of Pure and Applied Chemistry (IUPAC), stearic acid or octadecanoic acid is a long-chain saturated fatty acid containing 18 carbon atoms as in the molecular formula $C_{18}H_{36}O_{2,}$ and with a molar mass of 284.48 $g.mol^{-1}$. Stearic acid is highly biocompatible and possesses low cytotoxicity (Negahban et al., 2021, Patti et al., 2021). Like many lipid-based materials with a crystalline structure, stearic acid displays polymorphism. A case in which different crystal forms are constructed depending on the arrangements of molecules (Ajito et al., 2016). While there are four polymorphs of stearic acid, the majority of peer-reviewed literature typically refers to it as a three-polymorph material (A, B, and C). Polymorph C is often considered the most stable and is obtained through crystallization with a polar solvent (Calvo and Cepeda, 2008, Beckmann et al., 1984).

Stearic acid has been reported as a capping material for mesoporous silica nanoparticles (MSNs) to enhance drug delivery or change silica's properties (Zhou et al., 2022). Yuan et al. (2012) prepared chitosan-stearic acid micelles with doxorubicin and incorporated them into

mesoporous silica nanoparticles (MSNs). There are several formulation techniques to incorporate stearic acid into mesoporous silica, including solvent evaporation. Santa Barbara 15 (SBA-15) mesoporous silica was used to construct stearic acid -SBA composites through ethanol solution impregnation with subsequent evaporation. Another example of mesoporous silica-stearic acid complexes was investigated using tannic acid-mesoporous silica nanoparticles (TAMSNs), and the resultant complex was acquired through hot ethanol impregnation with subsequent evaporation (Mitran et al., 2019). Additionally, Gao et al. (2021) reported using stearic acid as a hydrophobic coating for MSNs to overcome the barriers to protein's oral delivery, considering that hydrophobic surfaces are preferred for better internalisation into the cells.

These properties make stearic acid and mesoporous silica great candidates for constructing a carrier based on their properties. Using lipids or lipid-like needle crystals in the formulation could facilitate cellular penetration in a non-destructive manner as Almquist and Melosh (2010) reported. The use of phospholipids to enhance cellular penetration has also been investigated through the addition of lipid-based stacks onto stealth atomic force microscopy (AFM) probes. The work aimed to view how modified probes can enhance the penetration of cells for mimicking transmembrane proteins. The latter group showed that the modified AFM probe penetrated the lipid bilayer in a non-destructive manner. This occurred through the interaction between the modified hydrophilic probe, featuring hydrophobic attachments, and the hydrophobic core region within the lipid membrane. Their results showed that the breakthrough distance of the probe (2.9 ± 0.3 nm) was less than the hydrophobic layer thickness (3.1 nm), indicating that the hydrophilic probe inhabits the hydrophilic gaps of the membrane, while the hydrophobic attachments reside naturally through the lipid core. Figure 2.1 below presents a schematic of the modified AFM probe and its non-destructive interaction with cells.

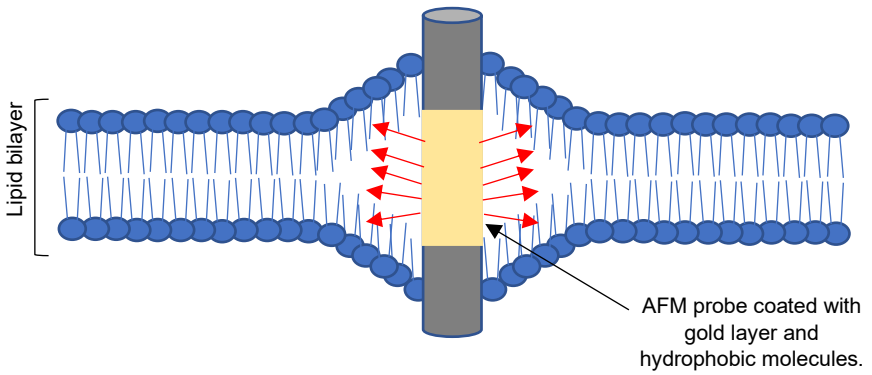

Figure 2.1. Schematic of modified AFM probe based on (Almquist and Melosh, 2010) design presenting the interaction between the modified probe and lipids bilalyer. The AFM probe is coated with a layer of gold (grey rod with yellow layer), and the hydrophobic functional molecules (red arrows) are interacting with the hydrophobic core of the lipid bilayer.

Based on the above observations by other researchers on non-destructive cellular penetration by lipidic probes/needle-like materials, the work detailed in this chapter aims to to create a novel lipid-mesoporous hybrid carrier for oral peptide delivery. This carrier will be made from a mesoporous carrier particle (SYLOID) and stearic acid. SYLOID offers the capacity to load peptides within its pores and act as a base for needle-shaped crystals of stearic acid. These are intended to facilitate attachment and reversible non-destructive penetration of epithelial cells in the GIT.

Objectives are to:

- Design a novel-lipid mesoporous hybrid carrier via investigating stearic acid loading over a range of concentrations.
- Characterise the morphology, thermal properties, and size of the developed carrier using SEM imaging, DSC, and laser diffraction.
- Examine the parameters that govern crystal formation at different stearic acid concentrations using thermal and crystallographic methods.

2.1. Materials and methods:

2.1.1. Materials:

Stearic acid with bulk density 400-500 kg/m^3 and ethanol absolute 99.8% (HPLC grade) were purchased from Sigma-Aldrich (Dorset, UK) Mesoporous silica SYLOID ® XDP 3050 (specific surface area of 310 m^2/g, average pore size of 22.4 nm, pore volume of 1.74 cm^3/g) was kindly provided by W.R. Grace and Co (Worms, Germany).

2.1.2. Methods:

2.1.2.1. Preparation of mesoporous SYLOID-lipid hybrid formulations

The preparation of hybrid lipid- mesoporous silica microparticles was conducted through two different formulation techniques: the evaporation-based method and melting under vacuum. In the evaporation-based method which was adapted from Fan et al. (2017), stearic acid was suspended in ethanol at concentrations ranging between 0.6 – 14 mg/ml and left on a magnetic stirrer while covered for 10 minutes at 25**°**C until complete dissolution. SYLOID XDP 3050 was added to the stearic acid-ethanol solution and left to stir for 2 hours at 25°C while also being covered, where the amount of stearic acid to SYLOID ranged between 20-140% w/w. The suspension mixture is spattered on a watch glass and left to dry in a laboratory oven at 50 ℃ for 1 hour. After drying, the samples were kept in glass vials for post-formulation characterisation.

Melting under vacuum utilised a vacuum oven OVA031(UK)**.** SYLOID was placed in a glass vial, and stearic was added at 80% w/w of SYLOID. The samples were put in the oven at 115°C and 500 mbar for 1.5 hours. The samples were left to cool at room temperature for 1 hour or via immersing the glass vial in ice for 15 minutes.

2.1.2.2. Morphology of the hybrid silica lipid particles

The morphology of the particles was assessed via Scanning electron microscopy (SEM) imaging. The surface of the drug-loaded mesoporous silica particles was examined by Philips XL30 ESEM FEG (Hillsboro, OR, USA), operating at 10 kV under a high vacuum. Before SEM imaging, samples were coated with gold by a sputter coater. Approximately 1 mg of each sample was placed onto a double-sided adhesive strip on a sample holder. SEM images were captured at different magnifications.

2.1.2.3. Particle size analysis using laser diffraction

Sympatec laser diffraction (Sympatec, Germany) was used to determine the particle size of the formulations. The instrument was equipped with the vibratory feeder VIBRI, RODOS/L dispersion unit, and the compact laser diffraction sensor HELOS/BR. The used lens was the R3 Fourier lens (f=100 mm) with a measuring range between 0.5-175 µm. The analysis parameters were as follows: PAQXOS 5.0 was employed as the software to analyse the results, the dispersion pressure was set to 1 bar, vacuum to 22 mbar, the feed rate as 50%, and the optical concentration ≥ 1%. All size analysis runs were done in triplicate for all formulations.

2.1.2.4. Thermal characterisation of silica -stearic formulations

The thermal properties of samples were characterised by the Differential Scanning Calorimetry DSC instrument TA Q200 (New Castle, DE, USA). Each sample was accurately weighed into a Tzero low-mass aluminium pan. The sample weight was 2.5 ± 0.1 mg, and the sample was heated in the range of 25-100°C at a scanning rate of 10°C/min under a nitrogen flow of 50 ml/min. Tzero low-mass pans and Tzero aluminium lids were used. TA universal analysis 2000 software (version 4.5) was employed to analyse the resulting DSC thermograms.

2.1.2.5. Fourier-transform infrared spectroscopy (FTIR) analysis

Investigation of molecular interactions was assessed using Nicolet™ iS™ 5 FTIR (Thermofisher, Waltham, USA) equipped with an ID5 diamond attenuated total reflectance (ATR) accessory. Before scanning, a background scan was collected, then approximately 30 mg of the powders were placed on the diamond plate, and the spectrum was obtained by taking 36 scans in the region 500-3500 cm^{-1} at 4 cm^{-1} resolution. Atmospheric suppression and advanced ATR corrections were implemented after scanning. OMNIC™ was used for spectra analysis.

2.1.2.6. X-ray Diffraction (XRD)

XRD data were collected on a 3rd generation Malvern Panalytical Empyrean equipped with multicore (iCore/dCore) optics, providing Cu Kα1/2 radiation, and a Pixcel3D detector operating in 1D scanning mode at a range between 5-65 2θ, step size of 0.05° and a count time of 1 s. For low angle measurements, a beam knife was used to reduce the air scatter. Data were analysed using OriginPro 2021b software.

2.1.2.7. Helium pycnometry

The amorphous density of stearic acid was determined based on the method of Bavnhoj et al. (2019). Prior to analysis, the material was heated in a Heratherm oven (Thermo) at 10 ℃ above the melting point for 30 minutes, followed by quench cooling following the sample removal from the oven. The samples were grounded and weighed into the aluminium sample holder for analysis. Multipycnomter from Quantachrome instruments (USA) was used for amorphous density determination, where the samples were purged with dry helium. Three consecutive measurements were taken, and results are presented as mean ± SD.

2.1.2.8. Nitrogen porosimetry

Surface area and pore volume of the formulations were determined using NOVAtouch LX2, Quantachrome instruments (Anton Parr, USA). Prior to analysis, samples were degassed for 18 hours at 30 ℃. Specific surface area was acquired using standard BET (Brunauer, Emmett, Teller) model, by means of Nitrogen adsorption at 1 bar nitrogen gas with a relative pressure p/p_0 in the range 0.05-0.3. Pore volume was determined using BJH (Barrett, Joyner, and Halenda) adsorption and BJH desorption methods. Kurk-Jaroniec-Sayari model (Kruk et al., 1997) was used to calculate the pore size distribution of the carrier, considering that it is suitable for mesoporous silica carriers. Touchwin software (version 1.2 x) was used to retrieve data.

2.1.2.9. Fluorescence imaging

Confocal microscopy (TCS SP8, Leica Microsystems, GmbH) was used for imaging. A 405 nm diode laser and a white light laser at 70% power were used to image fluorophores AlexaFluor 532. The excitation and emission wavelengths for stearic acid were 520-739 nm. For each channel, HYD detectors were used. A 20X dry APO lens was used for imaging, and all images were taken at 2048*2048 resolution with the imaging speed set at 200 Hz. The laser powers, gain, and emission wavelengths were kept consistent for quantification purposes. 3D image for the particle is generated, where the two planes are merged. For image analysis, LAS X 3.0 (Leica Microsystems GmbH) and Fiji (Schindelin et al., 2012) software applications were used.

2.1.2.10. Statistical analysis

Statistical analyses of data were performed with SPSS 28 program by using one-way Analysis of Variance (ANOVA) coupled with a Tukey post-hoc test. All experiments were conducted in triplicate. All data was presented as mean ± SD, and P-value < 0.05 is considered statistically significant.

2.2. Results and discussion

The design of a novel mesoporous silica carrier with a needle-like formation of stearic acid on its surface commenced via investigating different stearic acid loading methods. Scanning electron microscopy (SEM) imaging was used to study and define the structure and morphological properties of SYLOID XDP 3050 particles and differentiate between the stearic acid loading approaches. The particle size of the used carrier was 59 µm, with an average pore size of 25 nm and a surface area of 320 m^2/g as reported in literature (Vranikova et al., 2020a, Solomon et al., 2021). Figure 2.2 below shows the particle population (A), individual particle shape (B), and the pores of the silica carrier (C). SYLOID XDP 3050 is a form of non-ordered mesoporous silica microparticles, which means that the pore sizes differ from each other. This difference can be seen in figure 2.2 C, where the red arrows point towards the mesopores, while the red circles indicate the formation of the pores by the aggregation of nano-silica spheres.

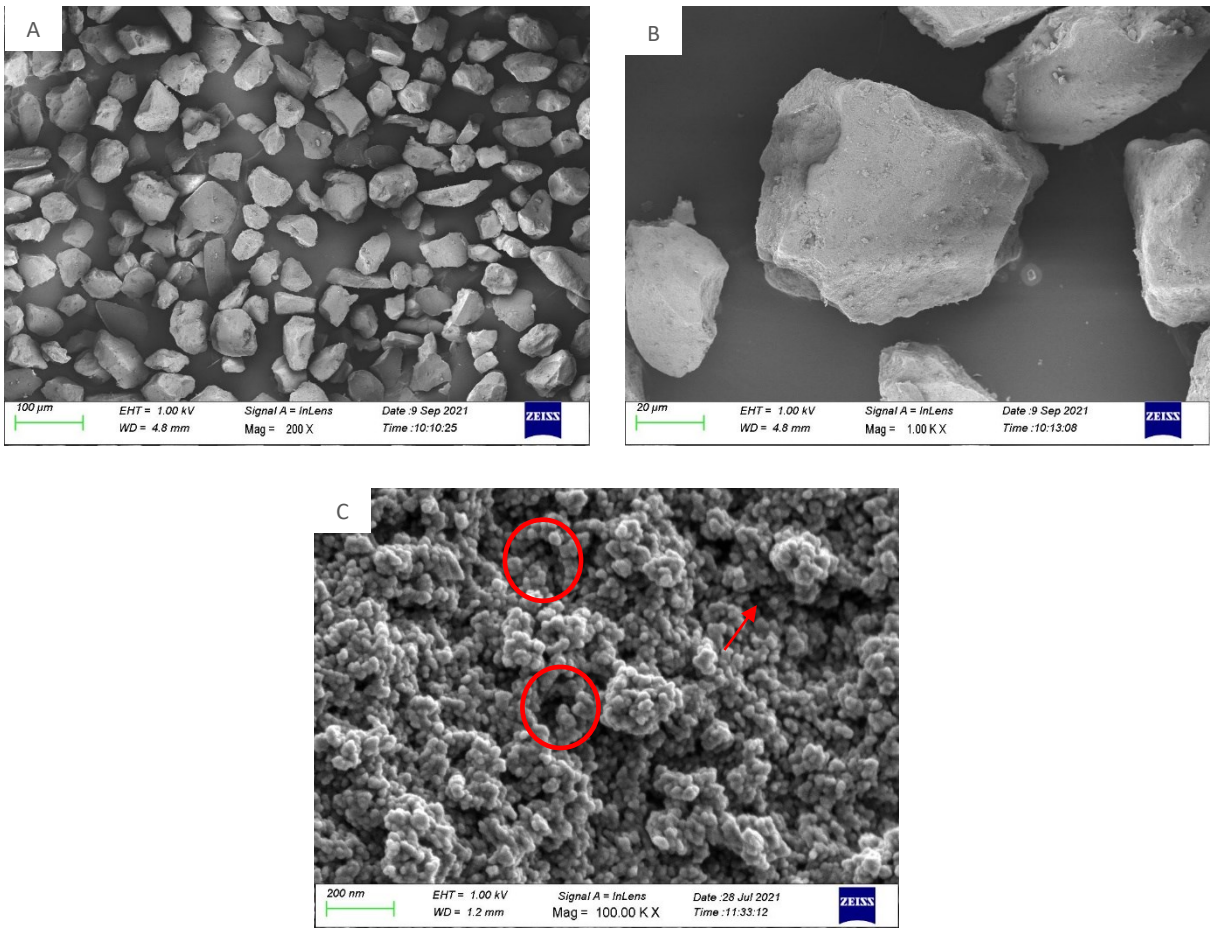

Figure 2.2. . SEM imaging of SYLOID XDP 3050 at different magnifications, presenting the particle population (A), morphology (B), and pores (C). The red circles and arrow identify the mesopores.

Two cooling approaches were tested to define the effect of cooling speed on the morphological appearance of SYLOID in vacuum-based loading. After the formulation process in the vacuum oven, the powders were cooled fast in ice, or slowly at room temperature.

Figure 2.3 below provides a comparison between two of the loading methods (ethanol loading and vacuum). The formulations in the melting method were left to cool slowly at room temperature (B) or cooled fast in ice (C). As seen in figure 2.3 in the ethanol method (A), the pores seem more diminutive in size and occupied with nanoparticles that seem to coat/fill the pores or cap them as the red arrows point. However, this observation is not evident in picture (B), where the pores seem more intact and not capped. Nevertheless, picture (C) indicates the capping of the pores with relatively large masses of nanoparticles.

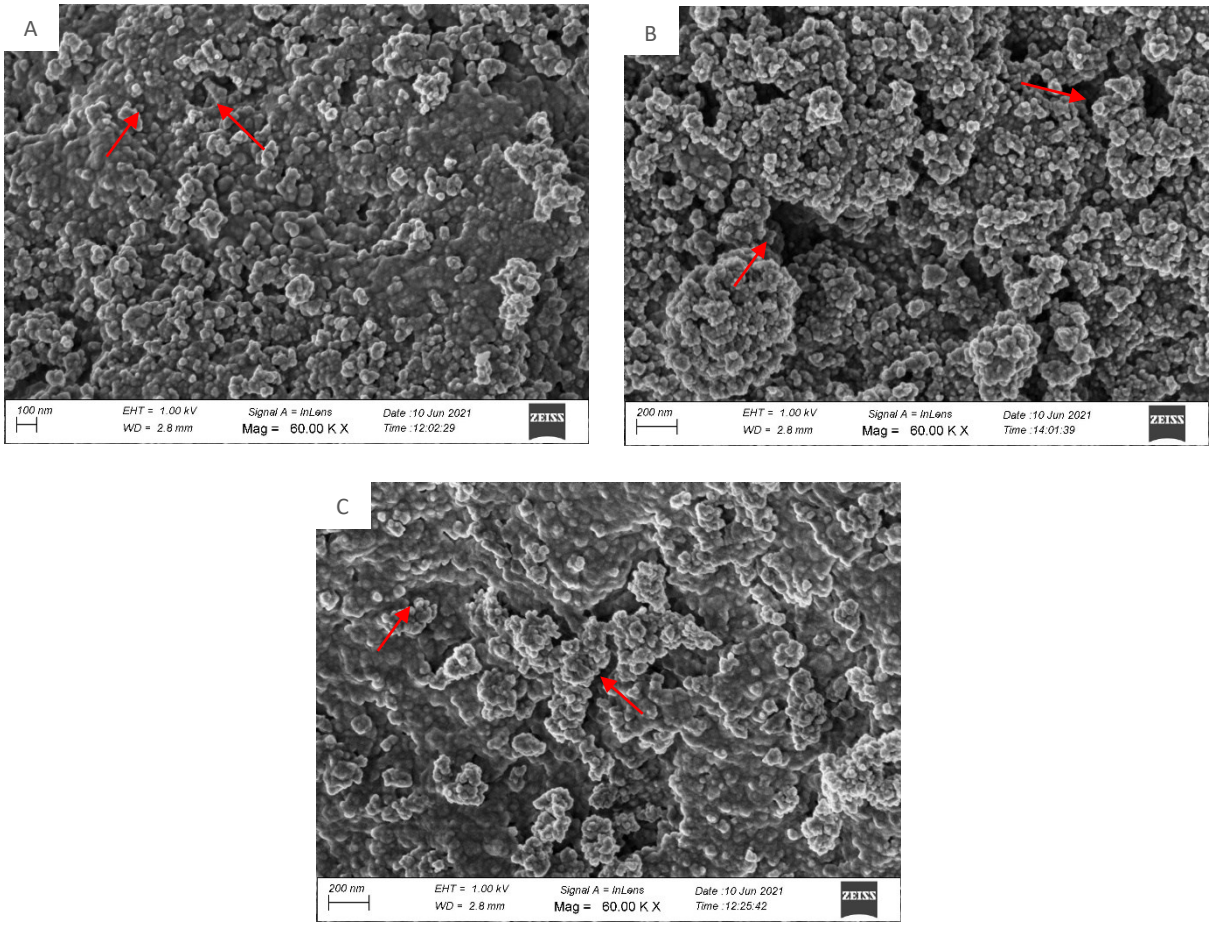

Figure 2.3. SEM imaging of Syloid-stearic 80% w/w acid of different formulations: ethanol evaporation (A), melting under vacuum and cooling at room temperature (B), and melting under vacuum and fast cooling (C).

The differences in the previously observed figure 2.3 could be attributed to the formulation method. In the ethanol evaporation, the stearic acid particles seem to have formed inside the pores, probably due to a mechanism similar to solvent impregnation (Mitran et al., 2019, Fan et al., 2017). The solvent was able to convey stearic acid into the internal porous structure of the carrier. On the other hand, the melting-vacuum method with fast cooling led to a cover of particles on the silica surface due to fast solidification rather than the formation of stearic acid particles within the pores. However, the melting-vacuum method with slow cooling showed no evident capping of the pores compared to the previous two methods, which indicates the potential separation of stearic acid from the silica particles. This was also confirmed via visual observation of the powder bed (figure 2.4), which appeared to have formed two distinct layers rather than a homogenous powder blend. The previous observations indicate that the evaporation method was more efficient than the melting-vacuum methods to cap silica using 80% w/w stearic acid concentration. Thus, the ethanol method was investigated further, and formulations were tested within a concentration range between 20-140% (stearic:SYLOID) w/w.

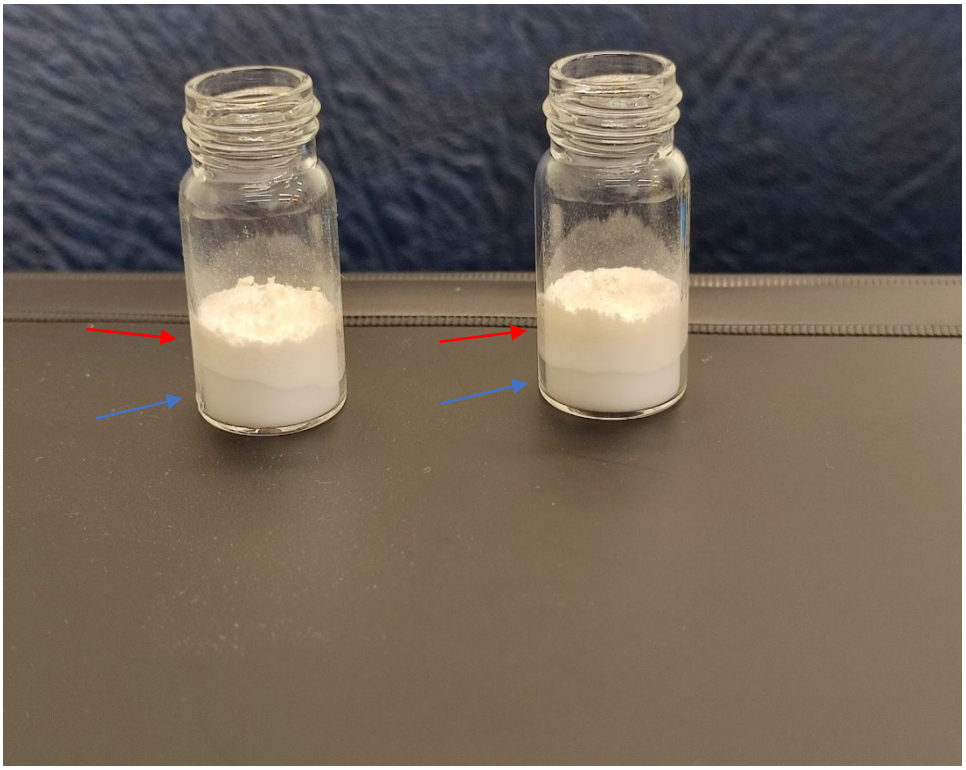

Figure 2.4. SYLOID-stearic formulation prepared via the vacuum method at 80% concentration, where powders cooled fast in ice (right), and slow at room temperature (left). Red and blue arrows point towards the two acquired layers of powder.

To further explore stearic acid effect on the porous structure of SYLOID, images were taken at high magnifications for all formulations, and presented in figure 2.5 A-G.

Figure 2.5 A-G below shows high magnification images of the pores of SYLOID after loading with stearic acid at 20-140% w/w via the ethanol evaporation method. The silica pores seem to be increasingly capped upon higher stearic acid loading, and nano-sized masses of stearic acid precipitate on the surface where the red arrows point. In formulations E, F and G, where loading is 100, 120, and 140% w/w, respectively, the pores seem more capped with less prevalence of the darker areas representing less pore availability than formulations A, B, C and D (20-80% w/w). This could be attributed to the higher amounts of stearic acid, in which stearic acid nanoparticles occupy the pores and cap them.

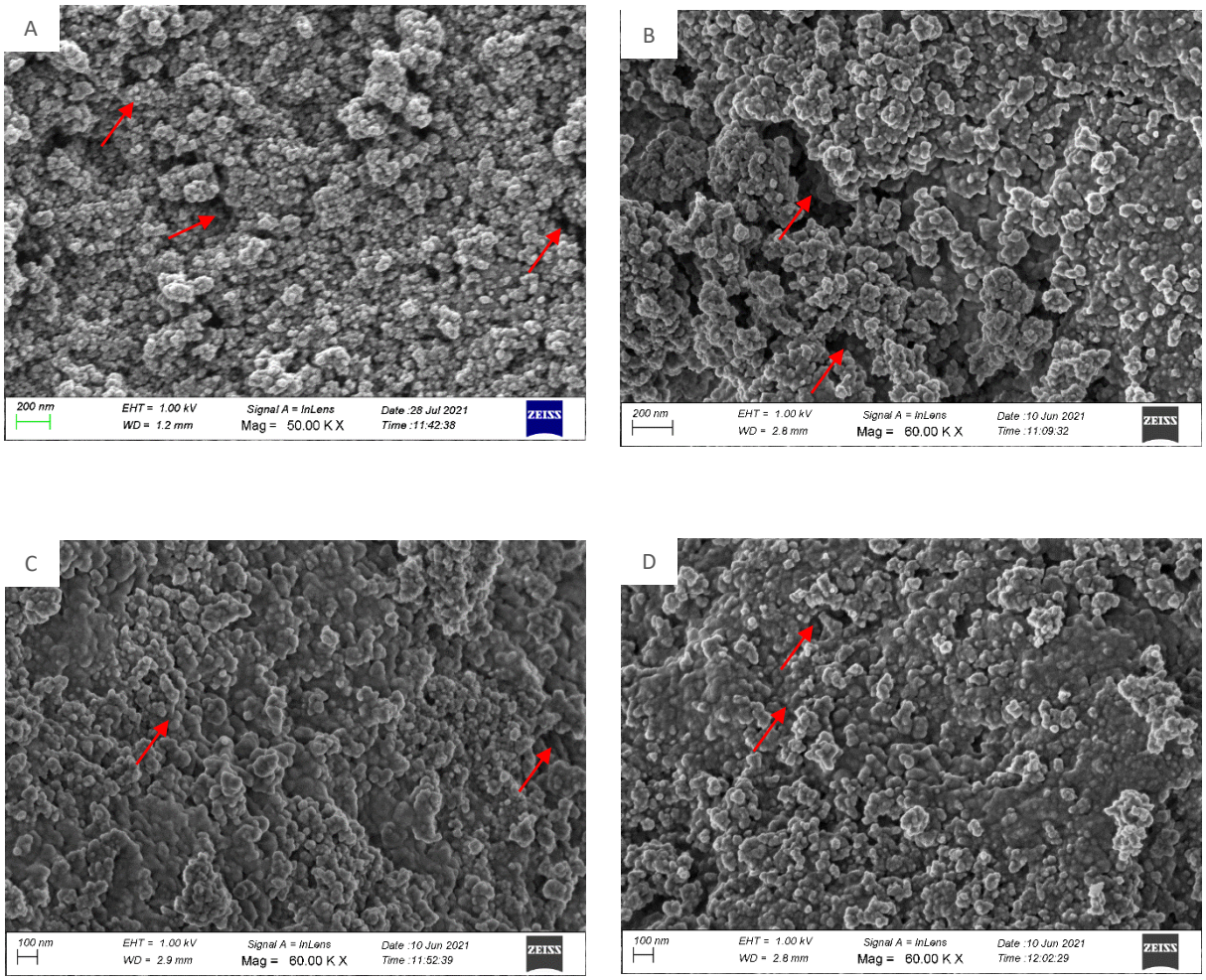

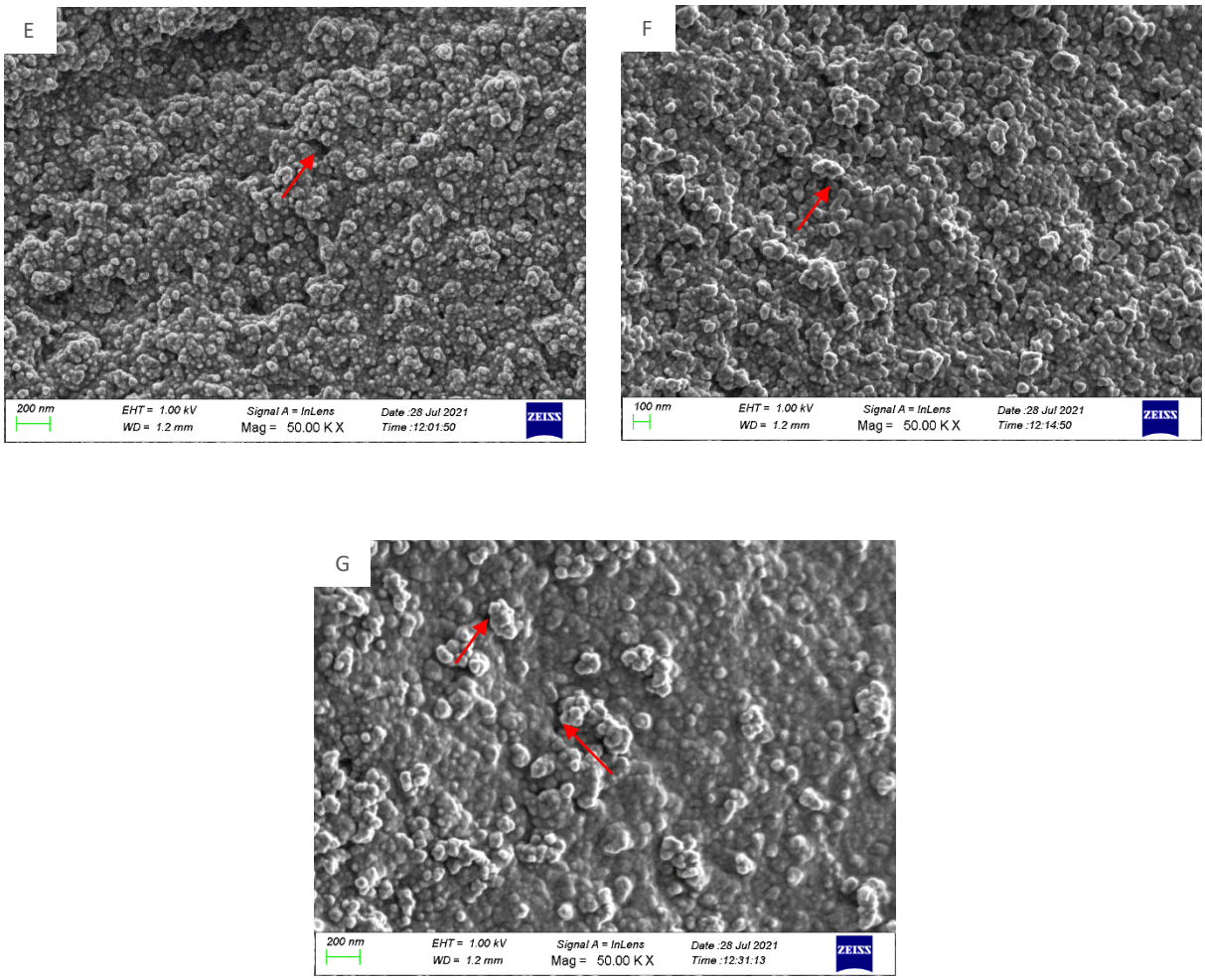

Figure 2.5. High magnification SEM imaging for samples containing different stearic acid concentrations: 20% (A), 40% (B), 60% (C), 80% (D), 100% (E), 120% (F), and 140% (G). Red arrows identify mesopores that are capped with stearic acid increase.

To further highlight stearic acid interaction with silica's surface, low magnification images were taken for the carrier surface and presented in figure 2.6 below.

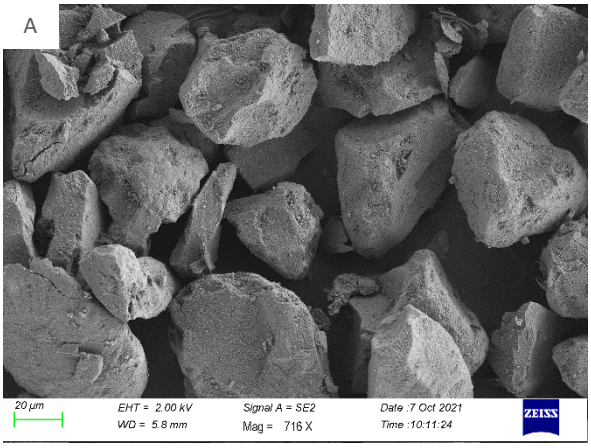

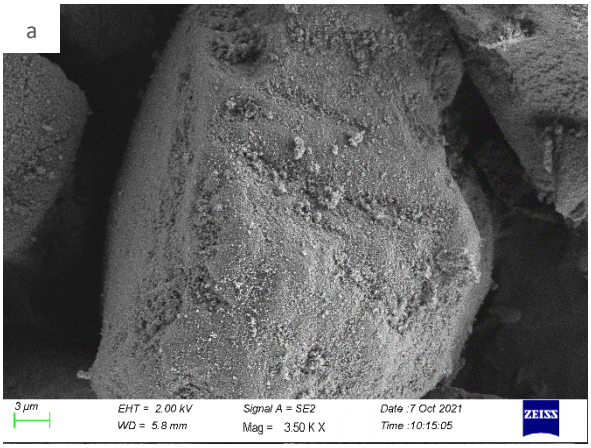

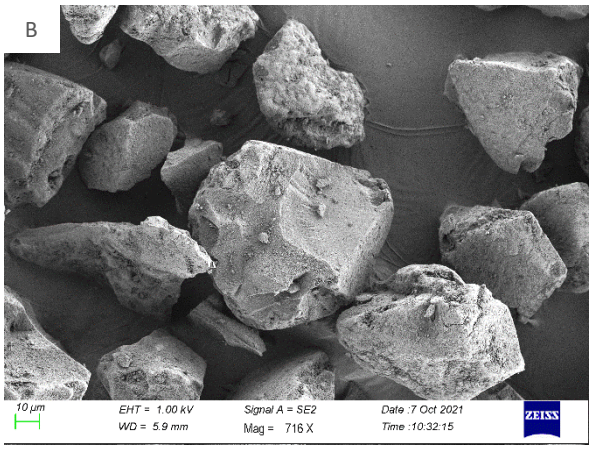

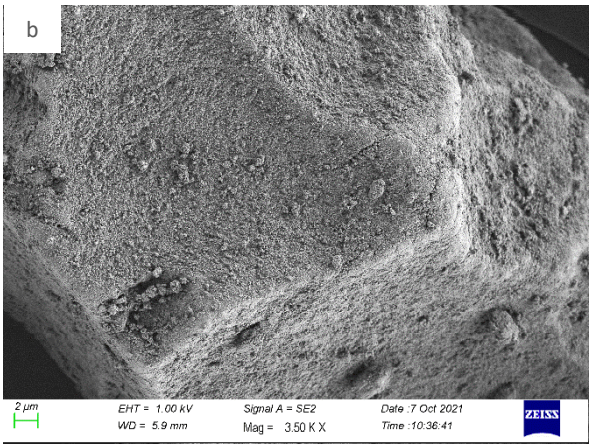

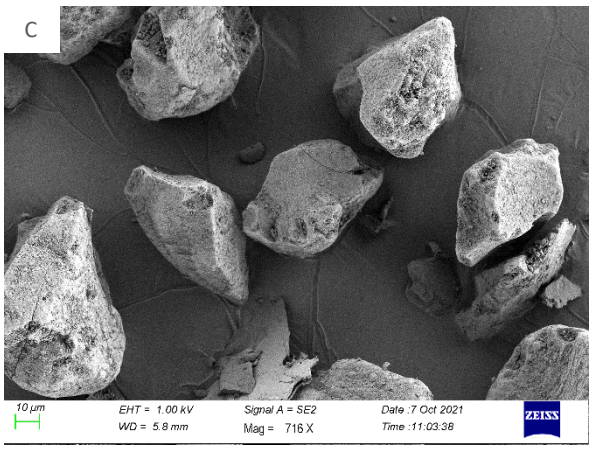

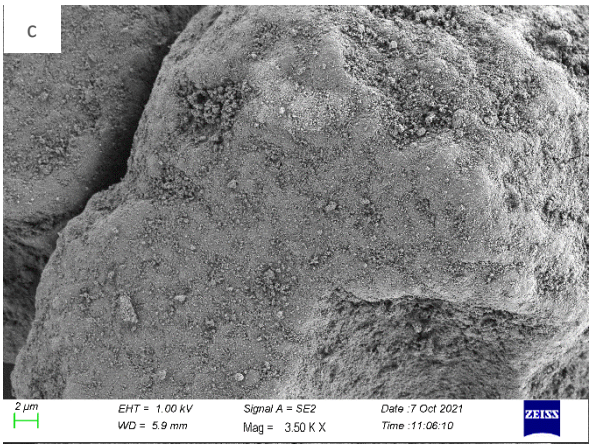

D

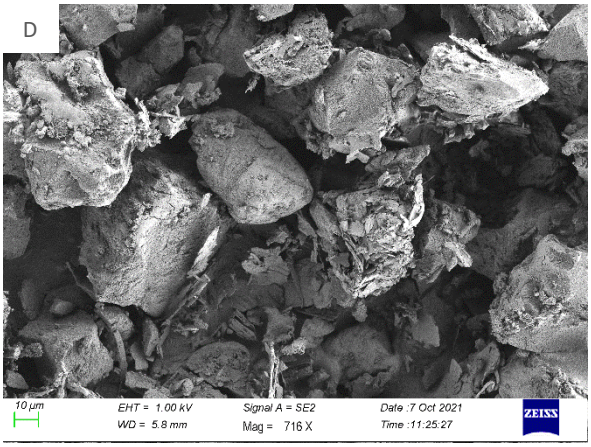
10 µm
EHT = 1.00 kV
WD = 5.8 mm
Signal A = SE2
Mag = 716 X
Date :7 Oct 2021
Time :11:25:27
ZEISS

d

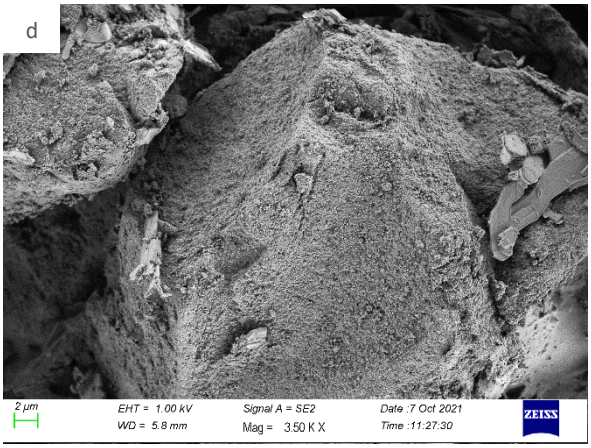
2 µm
EHT = 1.00 kV
WD = 5.8 mm
Signal A = SE2
Mag = 3.50 K X
Date :7 Oct 2021
Time :11:27:30
ZEISS

E

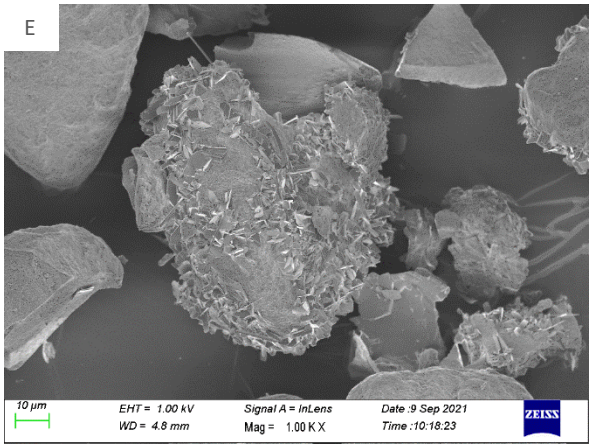
10 µm
EHT = 1.00 kV
WD = 4.8 mm
Signal A = InLens
Mag = 1.00 K X
Date :9 Sep 2021
Time :10:18:23
ZEISS

e

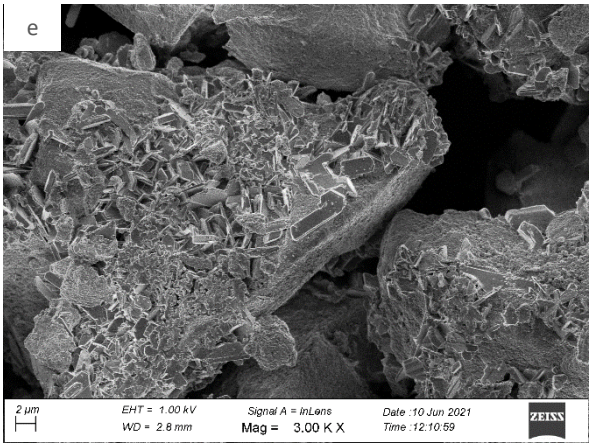
2 µm
EHT = 1.00 kV
WD = 2.8 mm
Signal A = InLens
Mag = 3.00 K X
Date :10 Jun 2021
Time :12:10:59
ZEISS

F

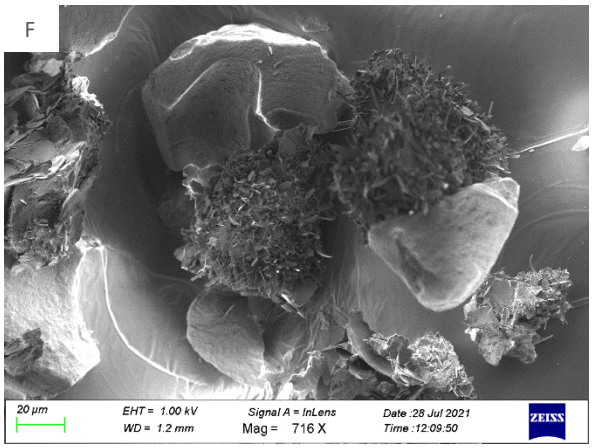
20 µm
EHT = 1.00 kV
WD = 1.2 mm
Signal A = InLens
Mag = 716 X
Date :28 Jul 2021
Time :12:09:50
ZEISS

f

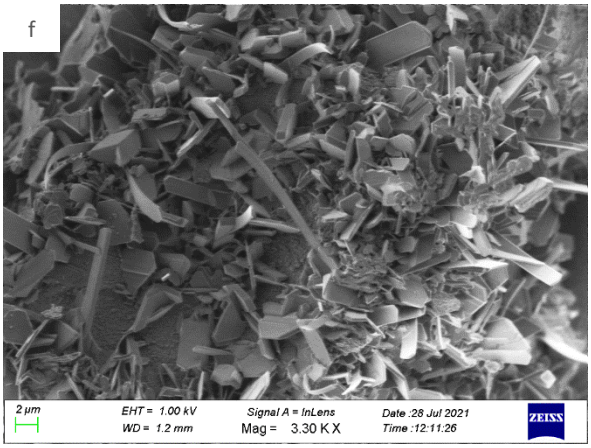
2 µm
EHT = 1.00 kV
WD = 1.2 mm
Signal A = InLens
Mag = 3.30 K X
Date :28 Jul 2021
Time :12:11:26
ZEISS

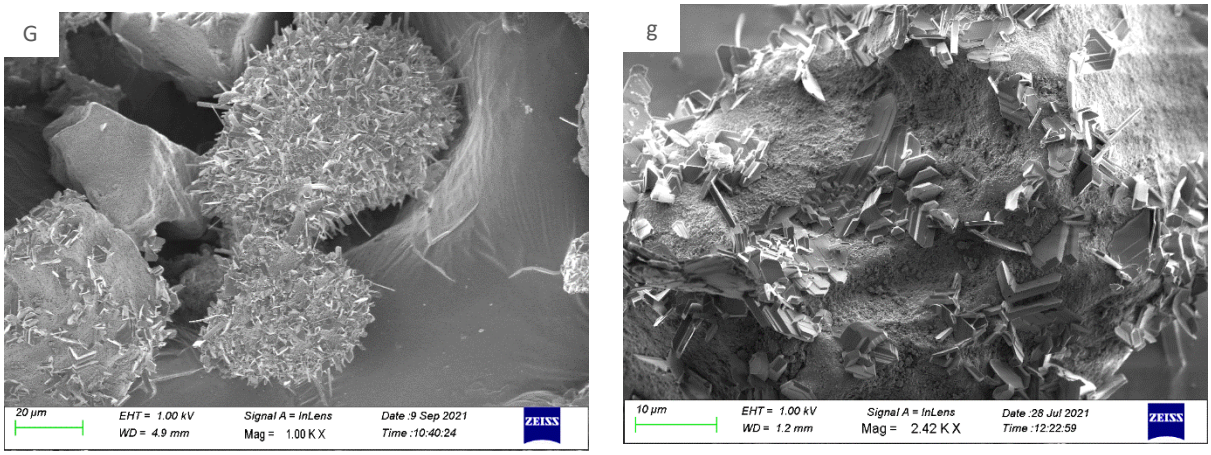

Figure 2.6. Low magnification SEM surface imaging for SYLOID-stearic particles in different concentrations, where 20% (A), 40% (B), 60% (C), 80% (D), 100% (E), 120% (F), and 140% (G). Upper-case letters present low magnified surface images, and lower-case letters present magnified images focusing on the surface of the particles.

As seen in figure 2.6 above, the surface of the silica carrier seems very similar to unloaded SYLOID (figure 2.2) in the formulations that contain stearic acid in concentrations between 20-60% w/w. However, when the amount increased to 80%, small crystal-like structures were evident on the surface even though they were not very apparent. However, upon increasing stearic acid concentration to 100%, needle-like structures started to appear on the surface of silica particles, which is attributable to stearic acid crystallisation (figure 2.6 E-G). These structures are consistent with stearic acid crystal habits observed in the literature (Beckmann et al., 1984), where needle-like formations are expected. According to the SEM investigations, this observation of needle-like morphologies at concentrations exceeding 100% is probably related to the capping of mesopores, as the two phenomena seem to coincide (Zhou et al., 2022).

Furthermore, it can be observed that silica particles with higher stearic acid loading presented a more significant needle-like structure population area and larger crystals. This could be seen by comparing Figure 2.6 E and F, where the stearic acid amounts are 100% and 120%, respectively. When stearic acid is overloaded, in this case, more than 100% w/w with respect to the carrier, it blocks the pores or caps them, followed by the remaining stearic acid crystallising on the surface of the carrier.

The analogy of this would be a container filled to its total capacity, and the remaining liquid/material beyond capacity starts to overflow. The stearic acid within pores is expected to be inhibited from significant crystallisation due to spatial confinement (Huo et al., 2021).

However, the excess on the surface is free to crystallise into large crystals. One possible hypothesis is the formation of nano stearic acid aggregates in the mesopores upon drying as described below.

These stearic acid nanoparticles within the pores solidify and interconnect to close the pores, while the remaining stearic acid then uses the near-surface nuclei of stearic acid to grow into directional needle-like shapes, similar to stearic acid and stearyl alcohol needle formations in oleogels (Blach et al., 2016). It could be noticed that the stearic acid crystals are mostly perpendicular in their formation plane to that of the carrier surface. This constitutes preliminary evidence supporting the notion that these crystals originated from the near-surface nuclei of stearic acid, as opposed to independently crystallizing outside the carrier and subsequently adhering to it. If the latter were true, then most stearic acid particles would be seen lying flat on the surface of the carrier rather than perpendicular to it due to a preferable adhesion profile in that flat orientation.

To further support this finding, the theoretical amount for monolayer coverage and the theoretical maximum load of the carrier were calculated. These values are beneficial to present an idea of the theoretically required amount of the adsorbate to cover the carrier in a monolayer and the amount that will present a theoretical maximum load (Dening and Taylor, 2018).

The surface area of stearic acid can be calculated using the largest two dimensions of the stearic acid molecule, which are 5.59 and 9.36 Å based on the short and long axis length (Malta et al., 1971), making a total theoretical molecular surface area of 52.32 $Å^2$. The previous number can be used to calculate the quantity of stearic that will achieve a theoretical monolayer coverage of SYLOID using equation (2.1) that is derived from Dening and Taylor (2018):

$$X_m = \frac{SS_A \times 10^{20} \times Mw}{S_c \times N_A}$$

Equation 2.1. The theoretical monolayer coverage.

Where X_m is the required stearic acid quantity to cover the adsorbate (SYLOID) in a monolayer (g/g), SS_A is the specific surface area of the adsorbate (m^2/g), Mw is the molecular weight of stearic acid (g/mol), S_c id the molecular surface area of the adsorbent ($Å^2$), and N_A is Avogadro's number. By applying the previous equation and assuming that the entire surface area of SYLOID is accessible for stearic adsorption, the stearic acid quantity for monolayer deposition is 0.2591 g/g. This amount means that for achieving a theoretical monolayer coverage of SYLOID using stearic, the loading ratio would be 25.91% (w/w).

Another aspect to consider is the theoretical maximum pore loading. The previous value can be calculated using the following equation (2.2) adapted from Hong et al. (2016).

$$TML = \left[\frac{V_p \times \rho_{stearic}}{1 + V_p \times \rho_{stearic}}\right] \times 100\%$$

Equation 2.2. The theoretical maximum pore loading.

Where TML is the theoretical maximum load of the porous carrier, V_p is the pore volume of the silica carrier (cc/g), and $\rho_{stearic}$ is the true density of the loaded material (stearic acid), which was calculated using helium pycnometry. By applying the previous equation (2.2), the TML value will be 64.32%, which indicates that at a loading concentration of 64.32% (w/w) of stearic acid, the theoretical maximum load of the SYLOID pores could be potentially reached. The difference in loading methods could affect the actual drug load of the carrier, where the slow evaporation of the loading solvent can facilitate nucleation inside the pores of the carrier, occupying the pores in the process (Charnay et al., 2004).

Even though formulations with low stearic acid amounts did not exhibit needle-like formations, stearic acid can still be located within the pores. FTIR analysis was conducted to investigate the presence of stearic acid in the different formulations. In addition, particle size distribution was assessed to determine the effects of stearic acid concentration on the size of the SYLOID-stearic hybrid particle.

2.2.1. FTIR analysis and particle sizing

FTIR was used to investigate the presence of stearic acid inside the silica carrier. Figure 2.7 below presents the spectra of all formulations with SYLOID and stearic acid as reference.

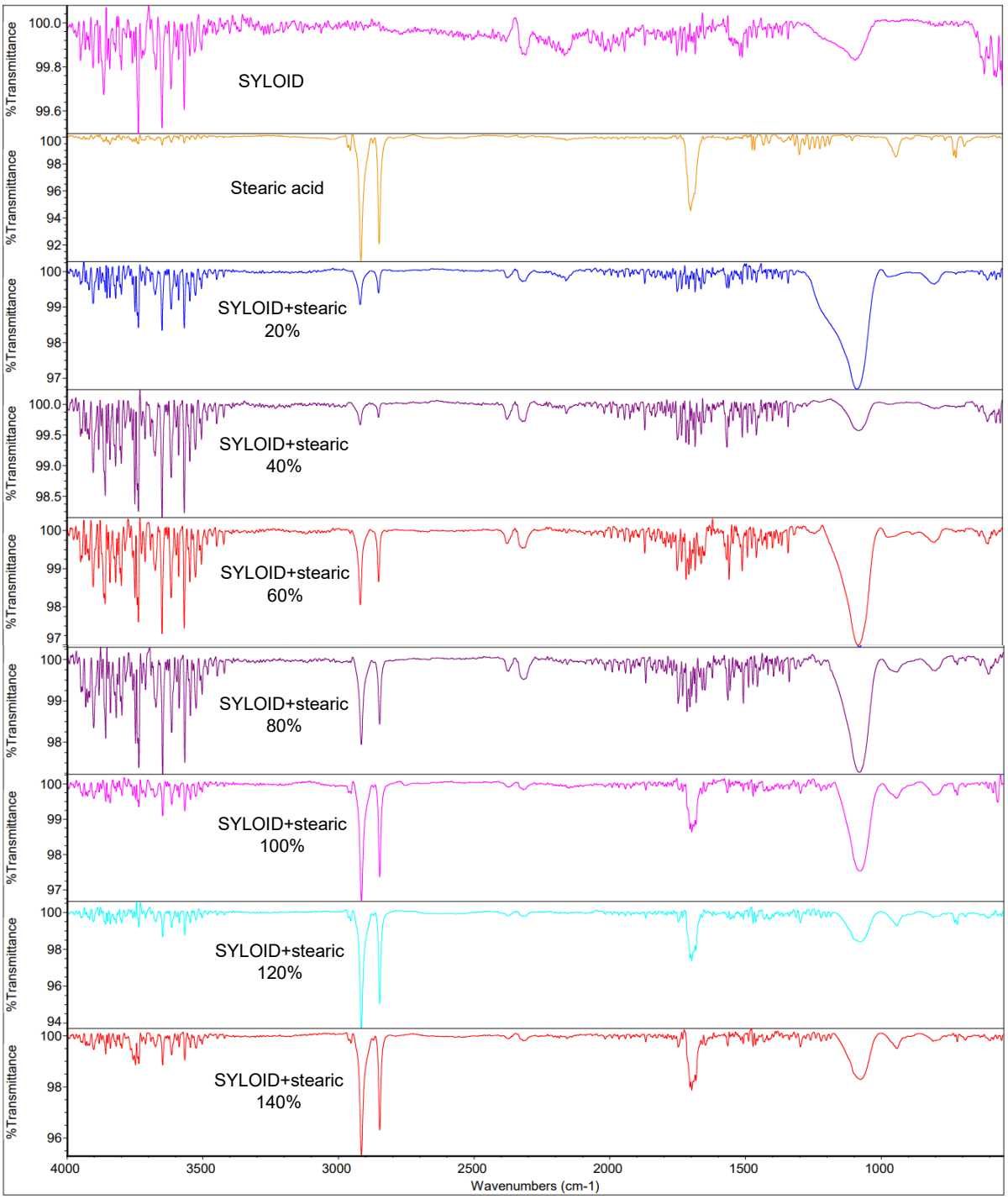

Figure 2.7. FTIR profile for formulations containing different concentrations of stearic acid.

As seen from figure 2.7 above, for the spectrum of SYLOID, a broad band at 1075 cm^{-1} corresponds to the asymmetric stretching of the siloxane group (Si-O-Si). In addition, the peaks at 800 cm^{-1} and 970 cm^{-1} correspond to the symmetric stretching vibration of Si-O and Si-OH, respectively (Baan et al., 2019). The strong bands at 2850 and 2925 cm^{-1} are related to symmetric and antisymmetric stretching of the methylene group, while the band at 1700 cm^{-1} is associated with the carboxylic group (Teixeira et al., 2007). The intensity of the CH3 group increases as the stearic acid amount in the formulation increases (20-140%). Also, the carboxyl group intensity increases from 100% stearic acid w/w. Additionally, the increased intensity is related to the presence of stearic acid inside the porous structure and on the surface.

To further elaborate on the effects of stearic acid's increased concentration on silica, particle size analysis was conducted using laser diffraction.

2.2.2. Particle sizing

Particle size analysis was used to confirm the previous observations from SEM, where particle diameter is potentially bigger due to the formation of surface needles (Figure 2.8 below).

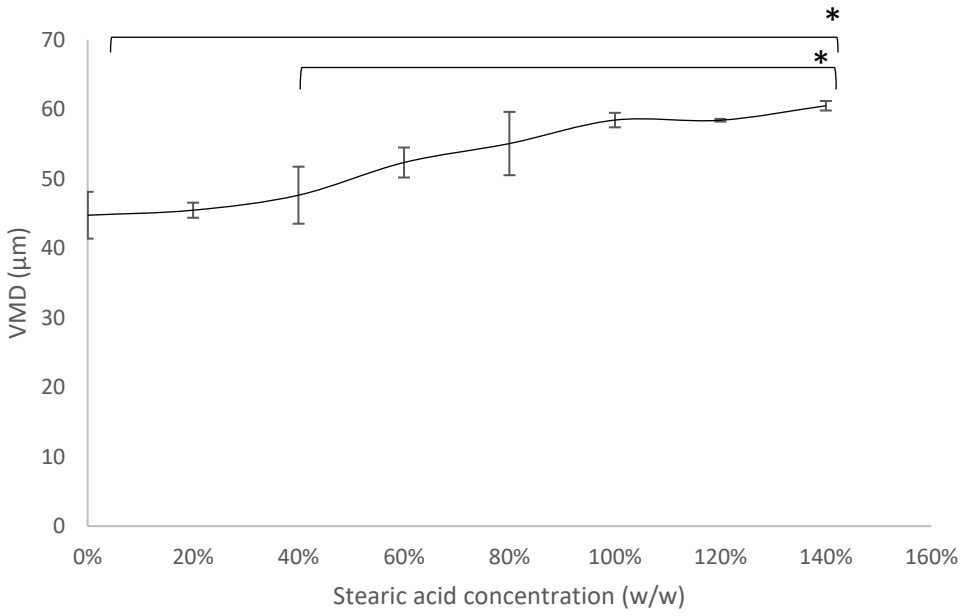

Figure 2.8. Graph outlining the relationship between stearic acid concentration (X axis) and particle size mean (Y axis). Error bars represent standard deviation (n=3) and (*) representing significant difference (p<0.05).

Indeed, the particle size of the prepared particles significantly increased (ANOVA, $p<0.05$) as the amount of loaded stearic acid increased. The volume mean diameter (VMD) for the empty carrier (SYLOID) is 44.74 ± 3.36 µm, and has gradually increased to 60.5 ± 0.68 when stearic acid amount was 140% w/w. The increase in size could relate to the formation of needle-like structures on the surface of the particles. These needles could have increased the size of the carrier particles by a few micrometres, as seen in the above SEM images.

To further support the presence of stearic acid needle-like structures at a certain concentration, confocal imaging was employed to detect stearic acid considering its autofluorescence properties.

2.2.3. Confocal microscopy

Some lipids tend to possess autofluorescence related to their oxidation and forming oxidised species, resulting in a long wavelength absorption. Subsequently, a fluorescence excitation within a broad spectral range is enabled (Semenov et al., 2020). For this reason, confocal microscopy was employed to highlight the presence of loaded stearic acid in the porous structure. Figure 2.9 presents 3D-genertaed images for SYLOID-stearic formulations.

SYLOID XDP 3050 is a mesoporous carrier that is non-fluorescent material. However, as shown in figure 2.9 A-G below, the surface of the carrier presents minor fluorescence properties (2.9 A), which is related to stearic acid. Moreover , upon increasing stearic acid amount within the formulation, the fluorescence is more apparent and seems to increase (2.9 A-D). However, when stearic acid is above 100%, non-uniformed structures are evident on the surface of the carrier, which are stearic acid needle-like structures that have been discussed previously (2.9 E). Furthermore, upon increasing the amount beyond 100% (2.9 F-G), the fluorescence potency increased, and clusters of fluorescent materials seemed to be crystallising on the surface, which was related to the needles' presence. This further supports the previous findings that needle-like structures tend to form on the surface of SYLOID at higher concentrations of stearic acid (100%).

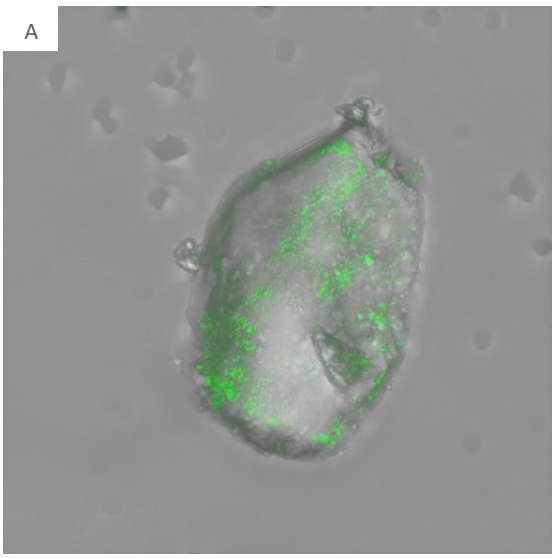

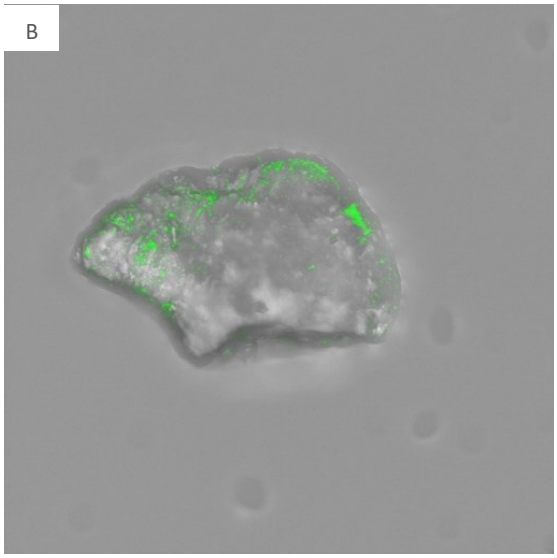

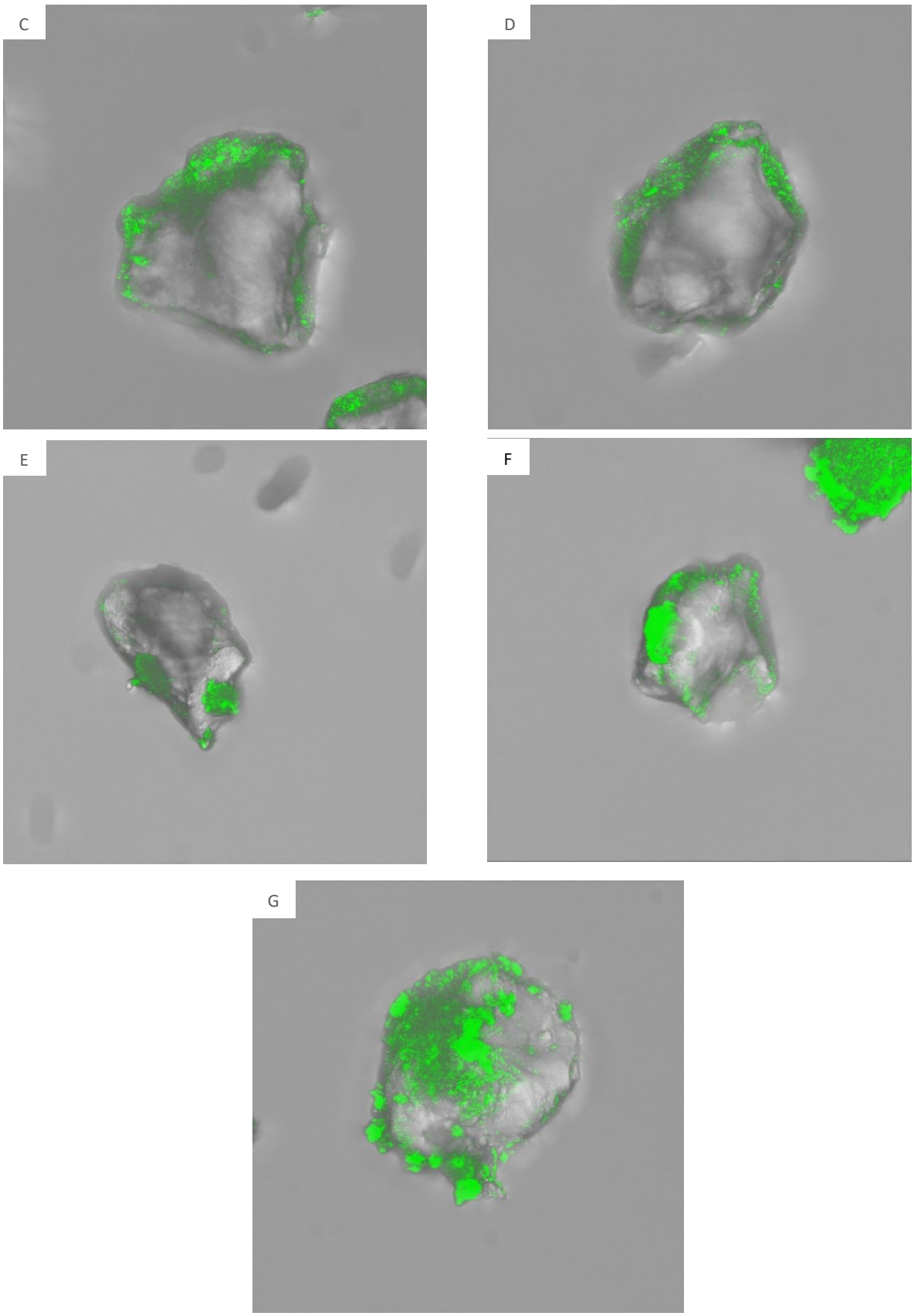

Figure 2.9. 3D confocal imaging of SYLOID-stearic in different concentrations (w/w) showing stearic auto fluorescence; SYLOID -stearic 20% (A), SYLOID -stearic 40% (B), SYLOID -stearic 60% (C), SYLOID -stearic 80% (D), SYLOID -stearic 100% (E), SYLOID -stearic 120% (F), SYLOID-stearic 140% (G).

2.2.4. Thermal and solid-state properties of SYLOID-stearic formulations

DSC was used to investigate the loading and thermal properties of stearic acid within silica (Figure 2.10). The DSC profiles were acquired at temperatures below 100°C to avoid sublimation of stearic acid (Sagiri et al., 2015).

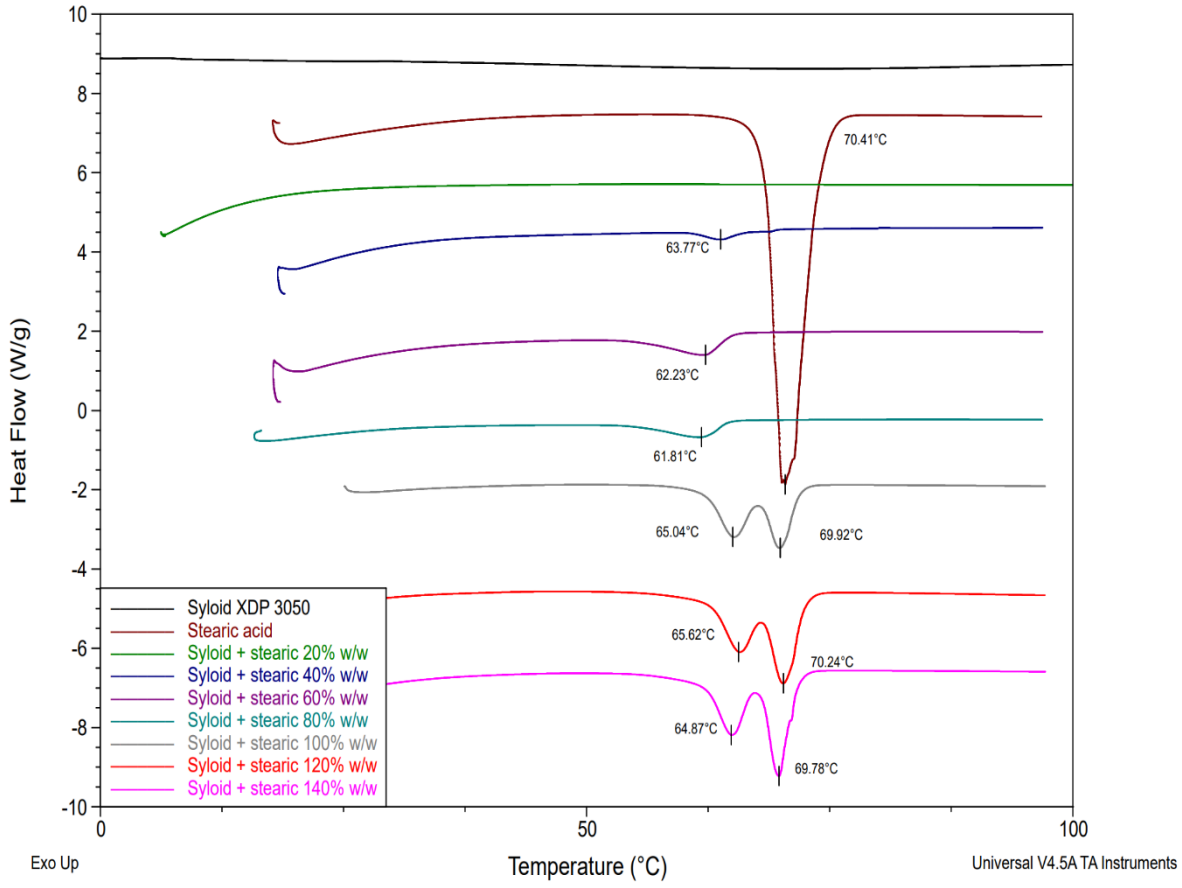

Figure 2.10. DSC profile of SYLOID-stearic formulations in different concentrations identifying the melting points of stearic acid in its unloaded form and within SYLOID.

Stearic acid has three polymorphs, A, B, C, with the C polymorph being the most stable (Beckmann et al., 1984, Calvo and Cepeda, 2008). Having different polymorphs indicates potentially different physiochemical properties, including melting points (Zhou et al., 2018). In figure 2.10 above, stearic acid showed a melting point of 70.41°C, which is similar to the melting point (69.51°C) that Lin et al. (2019) have reported and similar to the melting point of pure C form as reported in the literature (Zhu et al., 2007).

The formulation with 20% stearic acid w/w does not present an endothermic peak, indicating either no presence of stearic acid in the formulation or low amounts. Upon increasing the percentage of stearic acid, an endothermic activity is evident indicating the melting of stearic acid, and its intensity is increased as the percentage of stearic acid increases within the formulation. Yet, the melting point is around 62°C, which differs from stearic acid's (70.41°C). This indicates that the loaded stearic acid within the carrier could be in a different polymorph or amorphous, considering SYLOID's ability to convert materials from crystalline to amorphous form (Le et al., 2019).

However, the endothermic peak becomes sharper and more apparent, which is seen in formulations containing 100%, 120% and 140%, indicating that the incorporated stearic acid could be in a crystalline form. This finding supports the SEM results, which showed crystalline growth in formulations with stearic acid percentages exceeding 100%. Moreover, formulations containing 100, 120, and 140% present another endothermic activity with a melting point that is similar to stearic acid, indicating the presence of stearic acid in two forms. The second endothermic activity supports the observation in SEM results, where crystal-based needle-like formations are observed on the surface of silica.

DSC data confirmed the presence of stearic acid within SYLOID pores and the crystal behaviour of formulations with stearic acid amounts exceeding 100% w/w, where needle-like formations were observed using SEM. However, the endothermic event in DSC for formulations containing 80% stearic acid w/w and less was not confirmed to be crystal-related. Therefore, XRD analysis was used for further clarification of solid-state properties.

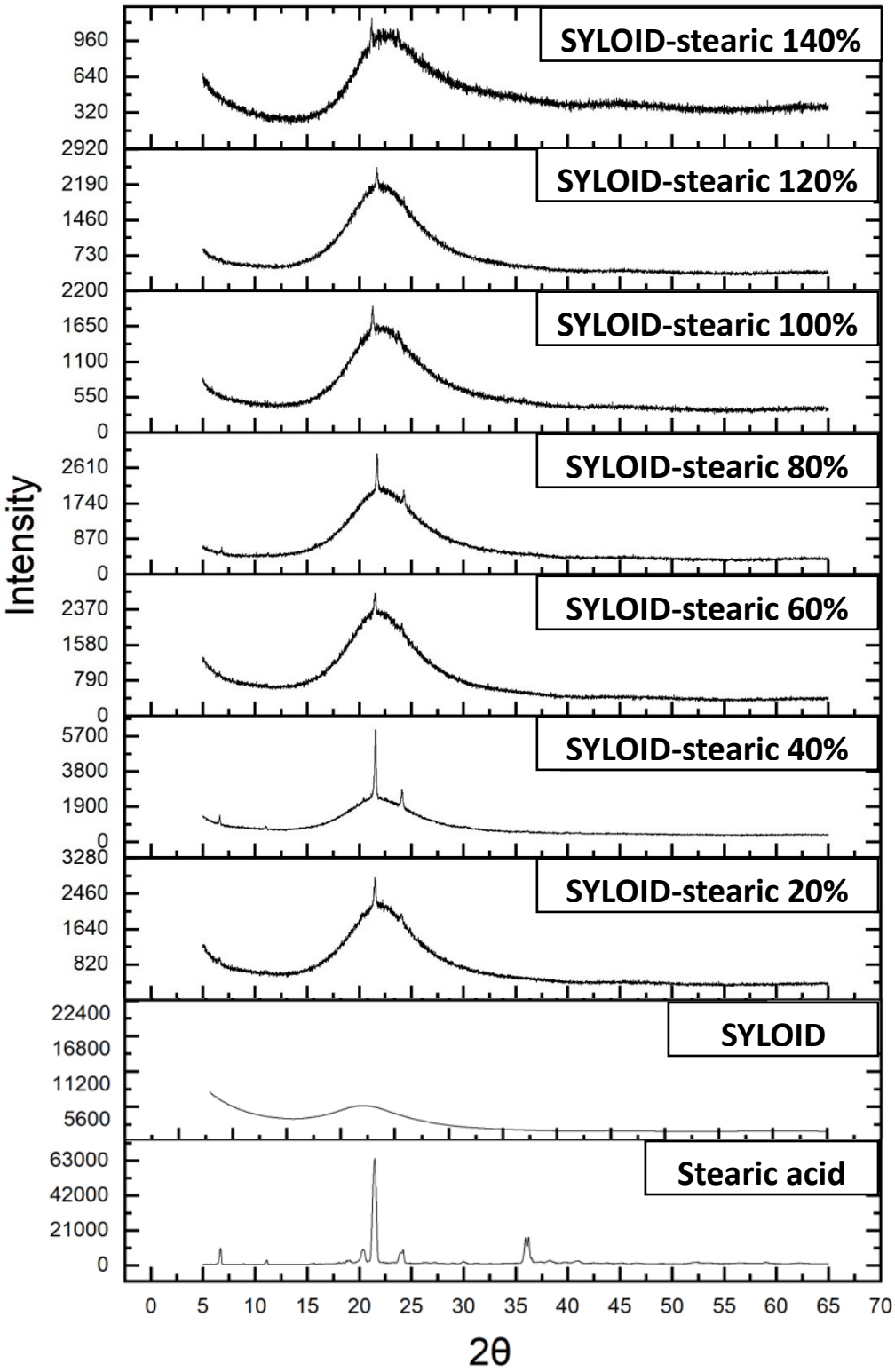

Figure 2.11. XRD analysis for SYLOID-stearic acid formulations in different concentrations presenting the Bragg peaks associated with stearic acid crystal form.

As seen in figure 2.11 above, SYLOID had no Bragg peaks and presented a halo which is supported by literature considering its amorphous form (Baan et al., 2019). Stearic acid diffractogram contains several Bragg peaks around 6°, 21°, and 36° confirming the crystal structure of the lipid. Additionally, the peak at 21° is associated with polymorph C, as reported by Garti et al. (1980), indicating that stearic acid crystal structure and supporting the data from DSC. Formulations containing stearic acid present a reading with a halo, representing SYLOID as reported in the literature (Vranikova et al., 2020b). Also, all SYLOID-stearic acid formulations presented a Bragg peak at 21°, indicating the presence of crystalline stearic acid in the formulations. This finding supports DSC results for formulations containing 100%, 120%, and 140% that the second peak in the thermogram represents the needle-like formations on the surface that were first observed via SEM. As for formulations containing (20- 80% stearic acid w/w), the peak indicates the presence of stearic acid crystals, and in this case, nanocrystals, which could have formed during the evaporation process. These crystals could have caused the endothermic event in DSC, even though they were not evident in SEM, considering the high sensitivity of XRD analysis. These previous findings confirm the crystal structure of stearic acid and that the needle-like formations on the surface of silica particles are stearic acid crystals.

2.2.5. Surface area and pore volume

Nitrogen porosimetry was utilised to assess the surface area and pore volume of SYLOID-stearic acid formulations and to view how increasing stearic acid amount would affect both.

Table 2.1. Surface area and pore volume of SYLOID-stearic acid formulations in different concentrations.

Formulation	Surface area (m^2/g)	Pore volume (cc)
SYLOID XDP 3050	340.44	2.10
SYLOID-stearic 20% w/w	229.90	1.99
SYLOID-stearic 40% w/w	215.08	1.48
SYLOID-stearic 60% w/w	210.19	1.46
SYLOID-stearic 80% w/w	168.54	1.12
SYLOID-stearic 100% w/w	93.19	0.62
SYLOID-stearic 120% w/w	93.26	0.59
SYLOID-stearic 140% w/w	86.46	0.55

SYLOID XDP is a non-ordered mesoporous silica carrier that presented the surface area and pore volume of 340.44 m^2/g and 2.1 cc, respectively. As seen from table 2.1 above, the increase in stearic acid loading led to a decrease in the surface area and pore volume of the carrier due to the occupation of the mesoporous channels inside the porous matrix with stearic acid molecules (Hong et al., 2016). This indicates that stearic acid populates the pores and covers the surface of silica. Moreover, the decrease in the surface area upon using 20% stearic acid aligns with the calculated amount of stearic acid to cover the carrier surface in a monolayer (25.91%) (please refer to section 2.2.1). The pore volume of SYLOID-stearic 20% is similar to SYLOID which indicates that stearic acid has only partially incorporated the porous structure. Furthermore, the pore volume and surface area of SYLOID-stearic formulations decrease as stearic acid concentration increases, indicating that the pores of SYLOID are being filled with stearic acid, and the surface is covered. This is further supported by both SEM (figure 2.5 A-G and 2.6 A-G), as well as confocal imaging (figure 2.9 A-G). In addition, the lowest pore volume and surface area value is associated with the formulation containing 140% stearic acid, which is related to stearic acid needle-like structures crystalising on the surface.

Conclusions

This chapter reports the development of a Mesoporous SYLOID-stearic acid hybrid carrier using SYLOID XDP 3050 as a mesoporous silica microparticle. Two methods were utilised; vacuum and ethanol evaporation, with the latter being more efficient in capping the mesopores in the silica structure. The carrier incorporated stearic acid in different concentrations w/w (20-140%).

The morphology of the carrier was assessed via SEM and presented an increase in pore capping as stearic acid amount increased. Furthermore, at concentrations above 80%, needle-like structures of stearic acid were evident on the silica surface, which resulted from the pores being fully capped and stearic acid crystallising on the surface. Additionally, the size of the hybrid carrier increased as stearic acid amount increased, which was assessed using laser diffraction.

The presence of stearic acid inside the silica carrier was further supported using FTIR due to the presence of the carboxylic group on the silica surface and confocal microscopy due to stearic acid autofluorescence which further supported the needle-like structures growth on SYLOID's surfaces.

DSC results highlighted the presence of stearic acid inside the carrier in two polymorphs due to the endothermic activity. In addition, a second melting peak was evident for formulations that contained concentrations above 80%, which was related to the melting of the needle-like structures on the silica surfaces, further supporting their presence in a crystal form. XRD analysis has supported the crystal nature of stearic inside the carrier due to its Bragg peaks at certain 2θ values (21°).

Nitrogen porosimetry was used to evaluate the pore size and surface area of the SYLOID-stearic hybrid carrier. It showed a trend in which the pore volume and surface area decreased as the amount of stearic acid increased, and the smallest values were associated with SYLOID-stearic 140% w/w.

The newly developed SYLOID-stearic acid carrier will be used for peptide delivery, where different protein loading mechanisms will be investigated while preserving the formed needle-like structures in the following chapters. Additionally, the effects of needles on protein permeability will be addressed with the addition of different permeability enhancers.

Chapter 3

Formulation and In Vitro Testing of Novel Mesoporous Silica-Lipid-Protein Complex for Oral Delivery.

Introduction

The evaluation of oral absorption serves as the cornerstone of oral drug delivery, the most prevalent administration route. This physiological process occurs in the intestines following oral administration. However, many factors affect the intestinal absorption, where the intestinal transit, gastric emptying, drug dissolution, particle size, and permeability impact bioavailability. These factors can be studied using *In vitro* and *In vivo* models to predict drug absorption, distribution, metabolism, and excretion (Agoram et al., 2001, Vinarov et al., 2021). However, using *In vitro* models for evaluating absorption is preferred to *In vivo* studies, considering the latter's high costs and the ability to use different models that mimic different areas of absorption (Fedi et al., 2021).

In vitro models are used for the early stages of drug development as they offer more insight towards drug absorption and mimic the conditions within the GIT. Following the *In vitro* tests, both *In vivo* and *Ex vivo* models are used for the following stages as they offer more robustness, complexity, compatibility, and similarity to human conditions. Yet, the correlation between *In vitro* and *In vivo* tests is crucial for successful drug development (Xu et al., 2021). However, the use of *In vitro* models does not substitute for *In vivo* studies. Yet, they consist of multiple transport systems that combine their effects in reflecting the organ in an *In vivo* situation and the feasibility of reproduction in a lab setting (Fritsch et al., 1999). Additionally, the use of *In vitro* cell lines is widely recognised as the first line to predict drug responses as preclinical models. Furthermore, they are utilised for understanding the mechanisms of the drug actions where the access to clinical samples is either limited or their cost is high (Niu and Wang, 2015).

According to Sarmento et al. (2012), there are different *In vitro* cell models that are categorised by the absorption site that they are intended to mimic. Examples of these include vaginal and rectal models like C-33A cervical monolayers, nasal and pulmonary models like Calu-3 and 16HBE14o- as airway epithelium, ocular models like the human corneal epithelium HCE-T cell model, skin models like EpiSkin model, and intestinal model like Caco-2 cell line.

There are numerous types of intestinal *In vitro* models as reported by Pereira et al. (2016); Caco-2, MDCK (Madin–Darby canine kidney), IPEC-J2 (pig jejunum epithelial cells), TC7 (Caco-2 subclone), 2/4/A1 (rat fetal intestinal cells), and IEC-18 (rat intestinal cell line).

Caco-2 cell models are considered the gold standard for intestinal permeability studies because they express absorptive intestinal cell characteristics. Despite their colonic origin, considering they are derived from human colorectal carcinoma cells, they possess enzymatic

activity and lack a passive membrane (Maubon et al., 2007, Pereira et al., 2016). However, they present several limitations: absence of mucus at the apical side, high P-glycoprotein (P-gp) efflux, and higher trans-epithelial electrical resistance (TEER**)** value (~500 Ω cm^2) compared to the values of 12–69 Ω cm^2 in the human intestines (Beloqui et al., 2016). Another model for intestinal permeability studies is TC-7 cells, which are subclones of Caco-2 that are the second most used cell line for permeability. According to Pereira et al. (2016), they are a more homogenous population with developed intercellular junctions. Yet, they have been found to be unsuitable for intestinal absorption studies for highly lipophilic and poorly absorbed drugs (Turco et al., 2011).

Another alternative is the Madian-Darby canine Kidney (MDCK) cell line, which has been investigated as an alternative for Caco-2 cells. However, its non-human origin and the over-expression of P-gp can be a barrier to implementing this cell line as a complete alternative to Caco-2 cells (Jin et al., 2014). An additional example is the small intestinal porcine epithelial cell line (IPEC-J2) which is derived from the epithelium of neonatal piglets' jejunum. This alternative has potential for *In vitro* experiments, yet it is still being validated for its use as a cell line for permeability studies (Geens and Niewold, 2011). The 2/4/A1 cell line originates from rats and has the ability to develop monolayers similar to Caco-2. Additionally, paracellular studies can be conducted using this cell line since the pore sizes of the tight junctions between the cells are similar to their counterpart in the human intestines. Nonetheless, the lack of active transport processes limits their use (Pereira et al., 2016). Another rat-based cell line is the IEC-18, which is used for paracellular transport and permeability studies. However, these cells are not differentiated as Caco-2 cells, and carrier-mediated transport is absent (Pereira et al., 2016).

According to Bednarek (2022), The permeability of materials through cellular monolayers is conducted using cell culture inserts or as termed (transwell supports system). This system consists of cells cultured on a microporous semipermeable membrane to form a confluent monolayer. The membrane acts as a support for the cells without affecting the diffusion across the cells. It is situated between two fluid compartments, facilitating the passage of solutes through the membrane. The upper compartment is the apical side, which represents the luminal part of the intestinal cells, while the basolateral compartment represents the abluminal part of the epithelial cell lining. These transwells are inserted into multiwells and seeded at a specific number of cells per well, depending on the area of the well and the cell line. Figure 3.1 below presents a schematic of the transwell.

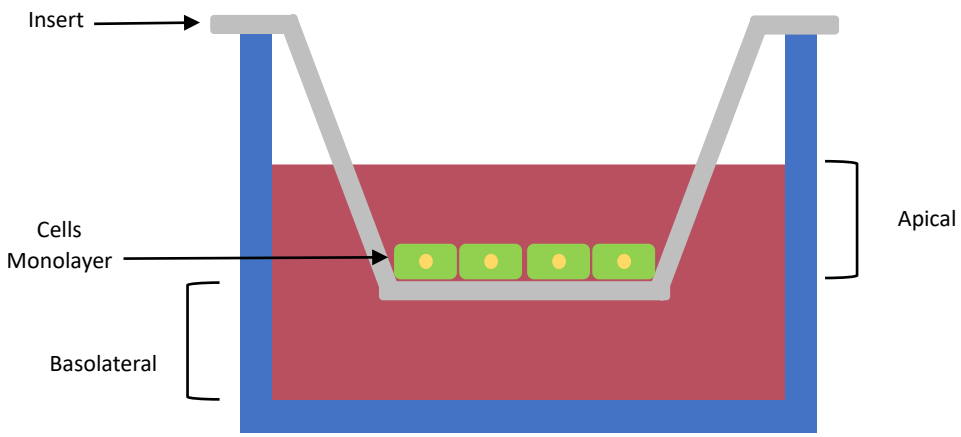

Figure 3.1. Transwell for permeability study identifying apical and basolateral chambers, with the monolayer of the cells.

Peptide analogues are not favoured for solid dosage forms due to their physiochemical properties (molecular weight and size) that make transmucosal absorption challenging (Thanou et al., 2000). The main problem associated with the oral delivery of octreotide is its low bioavailability (as discussed in Chapter 1), which results from its high molecular weight and hydrophilic properties (Florea et al., 2006). There have been several attempts to enhance octreotide's bioavailability using permeation enhancers (PEs), like sodium caprylate in the commercially available product Mycapssa (Fattah et al., 2020). Yet, the oral bioavailability of octreotide in Mycapssa is 0.8%, and the amount of added permeation enhancers is high (Berg et al., 2022). However, the use of silica as carriers for octreotide oral delivery has not been reported, nor have lipid-based carriers been used as a delivery system for octreotide delivery.

As reported above, Caco-2 cell line is the optimum candidate for evaluating intestinal absorption. Therefore, it will be used to assess the permeability of a protein (octreotide) from a newly developed silica-lipid-protein complex. This complex will be based on the work of the previous chapter.

This chapter aims to design a mesoporous silica-lipid complex for the oral delivery of octreotide acetate. The used silica carrier will be a mesoporous microparticle (SYLOID XDP 3050), and the lipid is stearic acid. The SYLOID-stearic-octreotide complex will be formulated where the presence of the needle-like structures on the surface must be maintained, as they are the hypothesised approach for enhancing the drug's permeability. The loading method is solvent evaporation, and the used solvent is ethanol considering the solubility of both stearic acid and octreotide.

Objectives are to :

- Develop and validate an HPLC method for octreotide acetate detection.
- Design SYLOID-stearic-octreotide complex and characterise the fluorescence and morphological properties.
- Conduct *In vitro* permeability tests using Caco-2 cells.
- Examine the effects of different permeation enhancers on the complex permeability across Caco-2 cells.

3.1. Materials and Methods

3.1.1. Materials

Stearic acid with bulk density 400-500 kg/m^3, Ethanol absolute 99.8% (HPLC grade), acetonitrile 99.8% (HPLC grade), D-α-Tocopherol polyethylene glycol 1000 succinate BioXtra, water soluble vitamin E conjugate (TPGS), Trifluoracetic acid (TFA) 99% (HPLC grade) were purchased from Sigma-Aldrich (Dorset, UK). Mesoporous silica SYLOID ® XDP 3050 (specific surface area of 310 m^2/g, average pore size of 22.4 nm, pore volume of 1.74 cm^3/g) was kindly provided by W.R. Grace and Co (Worms, Germany). Octreotide acetate lyophilised powder with a molecular weight of 1.079 kDa was purchased from Stratech (Cambridgeshire, UK). Polypropylene containers were purchased from Agar Scientific (Essex, UK). Sodium 8-(2-hydroxybenzamido) octanoate (SNAC) MW 301.31 g/mol was purchased from AmBeed (Illinois, USA). Dulbecco's modified eagle medium (DMEM) high Glucose GlutaMax supplement, fetal bovine serum (FBS), penicillin-streptomycin (5000 U/ml), minimum essential medium (MEM) non-essential amino acids solution (100x), L-glutamine (200 mM), trypsin/EDTA, hank's balanced salt solution (HBSS), amphotericin B, and gentamycin were purchased from Fisher Scientific (UK). 12 mm Transwell® with 0.4 µm Pore Polycarbonate Membrane Insert were purchased from Corning (Denmark).

3.1.2. Methods

3.1.2.1. HPLC method development for detecting octreotide acetate:

HPLC analysis and detection for octreotide acetate was adapted from (Park and Na, 2008) and conducted using Agilent 1200 series at a UV wavelength of 280 nm. The column was a Gemini C18 (Phenomenex) with the following specifications: 150 mm, 4.5 mm, 5 µm, 110 Å. The injection volume was 50 µl and a flow rate of 0.8 ml/min. Mobile phases were: A (water + 0.1% TFA) and B (acetonitrile + 0.1% TFA) with an analysis run time of 6 minutes. The concentration for the mobile phases starts at 70:30 A:B and decreases to 55:45 A:B at 3.6 minutes. Then, the concentration increases back to 70:30 A:B. Stock solution of octreotide acetate was made by dissolving 1.6 mg/ml, and a serial dilution was made prior to each sample batch analysis. The method validation and development are discussed in the following sections.

3.1.2.2. Caco-2 cells preparation and growth for permeability studies.

Caco-2 cells were originally from the American type culture collection (ATCC) at a passage level of 47 and revived into T-75 cm^2 flasks. The cell media was made using DMEM as the base with L-glutamine (11 ml), penicillin-streptomycin (2.5 ml), amphotericin B (1 ml), gentamycin (1 ml), MEM non-essential amino acids (5.5 ml) and FBS (50 ml). The cells were maintained in an incubator at a temperature of 37 ℃ with a humidified air atmosphere at 5% CO_2. The media solution was changed with 15 ml every other day for 3 weeks or until the cells reached 75% confluence.

3.1.2.3. Caco-2 cells passaging

When the cell confluence exceeded 75%, the cell media was disposed of, and the flask was rinsed with HBSS twice to remove any media remnants. A mixture of Trypsin and HBSS was made where Trypsin/HBSS ratio was 1/4, and 5 ml was added to the cells, followed by incubating for 5 minutes to activate the trypsin and detach the cells. After 5 minutes, 5 ml of the media was added to the cells to deactivate the trypsin and gently agitated for 4 minutes to induce faster cell detachment. Detached cells were then transferred into new flasks for regrowing.

3.1.2.4. Transwell plate seeding

Caco-2 cells were rinsed with HBSS, then treated with HBSS/Trypsin 4/1 solution and kept in the incubator for trypsinisation. Following that time, 5 ml media was added, and the cells were collected and centrifuged at 5000 rpm for 10 minutes using MSE Mistral 3000i (Sanyo, UK) to acquire the cell mass. The supernatant fluid was discarded, and the cells were resubstituted with 1 ml of media. Caco-2 cells were seeded at a density of 1.2 * 10^5 cells/cm^2 onto 12-well permeability supports. Cells were cultured in an incubator at a temperature of 37 ℃ in a humidified air atmosphere at 5% CO_2. Media was changed every other day over 4 weeks, where 0.5 and 1 ml were added to the apical and basolateral compartments, respectively.

3.1.2.5. TEER value calculation and assessment

The transepithelial electrical resistance (TEER) values were measured using the EVOM manual (WPI, USA) at room temperature after seeding the cells into the transwells. The TEER values were also taken before and after the permeability studies to ensure the integrity of the cells. Before taking the TEER value, the apical and the basolateral compartments were washed with HBSS twice. The cell resistance values (R_{Cells}) can be calculated using both the

resistance values of the cells monolayers on the membrane ($R_{Membrane}$) and the resistance value of the membrane without cells (R_{Blank}) using equation 3.1 below:

$$R_{Cells} = R_{Membrane} - R_{Blank}$$

Equation 3.1. The cell resistance value.

The TEER values of the cell monolayers can be calculated using equation 3.2 below.

$$TEER\ (\Omega) = R_{Cells} * A_{Membrane}$$

Equation 3.2. The TEER values of the cell monolayers.

Where the $A_{Membrane}$ is the area of the insert (1.12 cm^2).

3.1.2.6. Permeability study

The release and transport of octreotide were assessed with the additives: SNAC at different concentrations (5, 10 and 30 mMol) and TPGS at 1 mMol. Further, the silica-octreotide stearic complex permeability was assessed with both. The apical and basolateral compartments were rinsed with HBSS twice prior to the start of the permeability study. Then, 0.5 and 1 ml were added to apical and basolateral compartments, respectively. Samples (150 µl) were taken from the basolateral compartment (except for the experiment where the efflux of octreotide was assessed, where the samples were taken from apical compartments), and the volume of the compartment was maintained at 1 ml by substituting with HBSS. The time points of the study were 5, 10, 20, 40, 60, 90, and 120 minutes. The samples were put into HPLC vials for HPLC analysis. Each study was done in triplicate, and results are presented as mean ± SD.

3.1.2.7. Apparent permeability

The intestinal apparent permeability is related to the drug's flux on a concentration gradient across intestinal cells. This value is used to predict drug transport across cell barriers based on several factors. It is used for determining protein permeability investigations as it proves good for *In vitro* examinations, as reported by Dahlgren and Lennernas (2019). Apparent permeability (Papp) can be calculated using equation 3.3 according to Palumbo et al. (2008):

$$Papp = \left(\frac{V_r}{AC_0}\right)\left(\frac{dC}{dt}\right)$$

Equation 3.3. Apparent permeability.

Where V_r is the basolateral chamber volume (ml), A is the surface area of the filter transport (cm^2), and for the used transwell, it is 1.12 cm^2, C_0 is the initial concentration of the drug in the apical compartment (mg/µl), and $\frac{dC}{dt}$ is the initial slope of the cumulative concentration of the drug against time.

3.1.2.8. Formulation of silica-peptide and silica-peptide-stearic complex

3.1.2.8.1. SYLOID-Octreotide complex

The formulation of silica-octreotide was conducted by dissolving octreotide in ethanol at concentrations ranging between 1-3 mg/ml, followed by the addition of SYLOID (where octreotide/SYLOID ratio was 10, 20, and 30% w/w) and kept on a magnetic stirrer for 2 hours. The sample is transferred into a watch glass and left in the vacuum hood for 4 hours to dry at room temperature.

3.1.2.8.2. SYLOID-Octreotide-stearic acid complex

SYLOID-Octreeotide-stearic complex was made via a solvent evaporation method:

Stearic acid was dissolved in ethanol in a polypropylene container, followed by the addition of octreotide, then SYLOID was added into the mixture, where the amounts were as follows: stearic:SYLOID and octreotide:SYLOID were 120% and 30% w/w, respectively. The mixture was kept stirring at room temperature for 2 hours and then transferred into a glass watch to dry at room temperature for 4 hours. Samples were taken and stored in polystyrene Bijou containers at -20 ℃ for further analysis.

3.1.2.9. Drug load quantification and recovery

The actual drug load was calculated by adding 5 mg of the peptide-silica complex into 10 ml of distilled water in a polypropylene plastic container and left on a magnetic stirrer for 2 hours. Samples were taken from the container at the previous time interval and filtered into HPLC vials using a 0.2 µm syringe filter for analysis, while the remaining contents in the container were discarded. The presented results are based on the recovery percentage.

3.1.2.10. Fluorescence imaging

Confocal microscopy (TCS SP8, Leica Microsystems, GmbH) was used for imaging. A 405 nm diode laser and a white light laser at 70% power were used to image fluorophores

AlexaFluor 405 and AlexaFluor 620 for octreotide and stearic acid, respectively. The excitation and emission wavelengths for octreotide were 385-562 nm, while for stearic acid they were 520-739 nm. For each channel, HYD detectors were used. A 20X dry APO lens was used for imaging, and all images were taken at 4096*4096 resolution with the imaging speed set at 100 Hz. The laser powers, gain, and emission wavelengths were kept consistent for quantification purposes. 3D image for the particle is generated, where the two planes are merged. For image analysis, LAS X 3.0 (Leica Microsystems GmbH) and Fiji (Schindelin et al., 2012) software was used.

3.1.2.11. Morphology of the developed complex

The morphology of the particles was assessed via Scanning electron microscopy (SEM**)** imaging. The surface of the drug-loaded mesoporous silica particles was examined by Philips XL30 ESEM FEG (Hillsboro, OR, USA) operating at 10 kV under a high vacuum. Before SEM imaging, samples were coated with gold by a sputter coater. Approximately 1 mg of each sample was placed onto a double-sided adhesive strip on a sample holder. SEM images were captured at different magnifications.

3.1.1.1. Fourier-transform infrared spectroscopy (FTIR) analysis

The molecular inetarctions were assessed using same method from section 2.1.2.5.

3.1.1.2. Thermal properties of the complex

The thermal properties were assessed using same method from section 2.1.2.4.

3.1.1.3. Statistical analysis

Statistical analyses of data were assessed using same methos in section 2.1.2.10.

3.2. Results and discussions

3.2.1. Development and validation of an HPLC method for octreotide detection

The development and validation of the HPLC method for octreotide acetate detection is based on Park and Na (2008) method. An acclaim C-18 column 3*75 mm with a particle size of 3 µm was used, while the mobile phases consisted of water and acetonitrile, both acidified with TFA at 0.1%. and the run time was 5 minutes.

Following the method of Park and Na (2008), a sample containing 1.6 mg/ml of octreotide dissolved in distilled water was run, and the retention time was 4.6 minutes, as seen in figure 3.2 below.

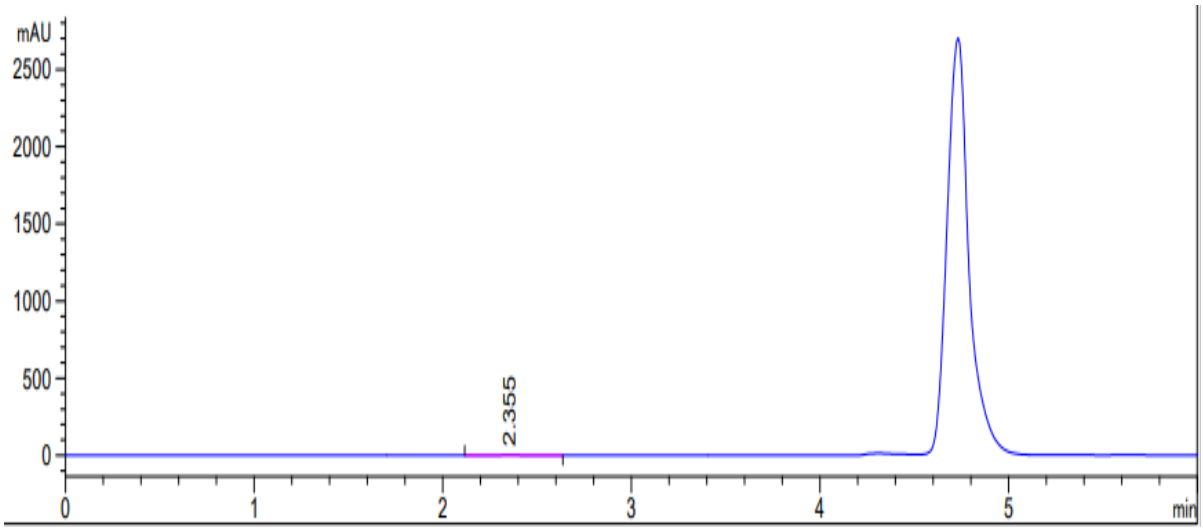

Figure 3.2. Retention time and peak of octreotide acetate using Park and Na (2008) method.

Following the acquirement of octreotide peak at 1.6 mg/ml, 9 calibration standards were made from serial dilution of the stock solution (1.6 mg/ml) and were run in triplicate to produce a calibration curve seen in figure 3.3 below.

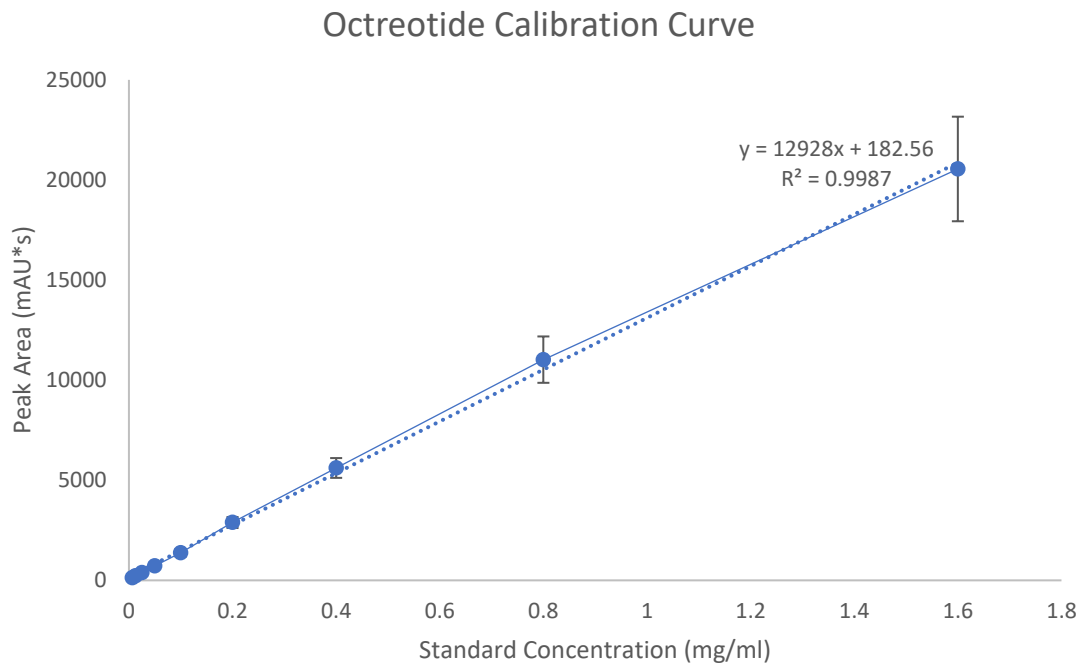

Figure 3.3. Calibration curve of octreotide acetate with the modified method. Error bars represent standard deviation (n=3).

Following the calibration curve, the produced linearity was R^2 0.9987, while the sample at the highest concentration (1.6 mg/ml) had a high standard deviation. The chromatogram of all dilutions was overlayed to see how the retention time might be different, and they are produced in figure 3.4 below.

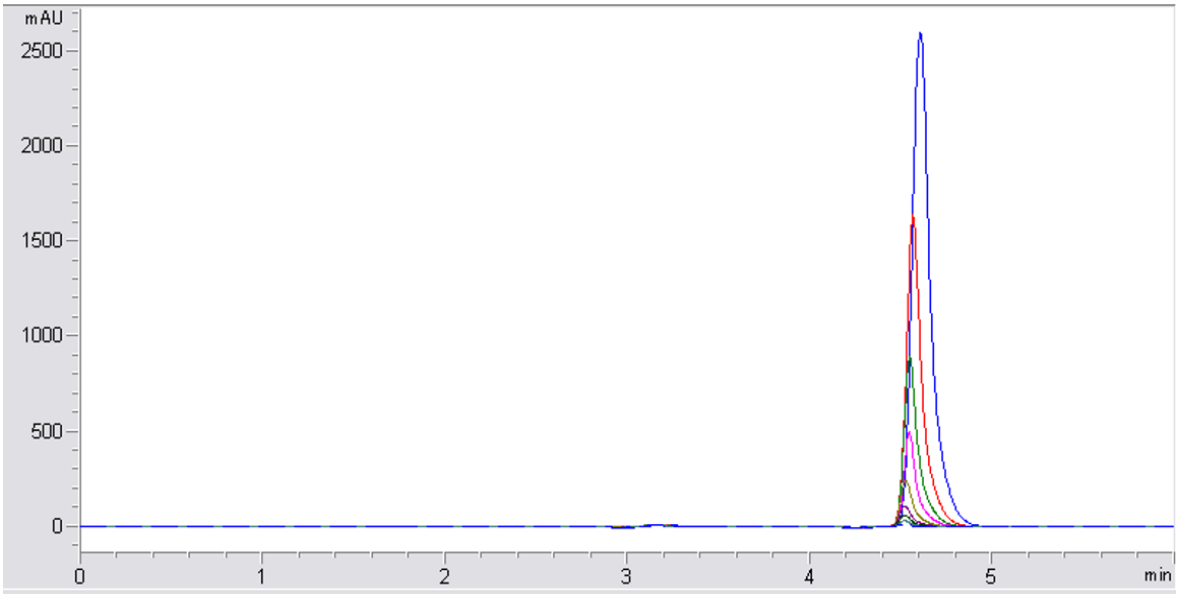

Figure 3.4. Chromatograms of all dilutions of octreotide acetate using the modified method.

As seen from figure 3.4 above, the retention time of the samples seems consistent except for the stock solution sample. Therefore, a new calibration curve was made by excluding the first sample and checking the linearity, as presented below in figure 3.5

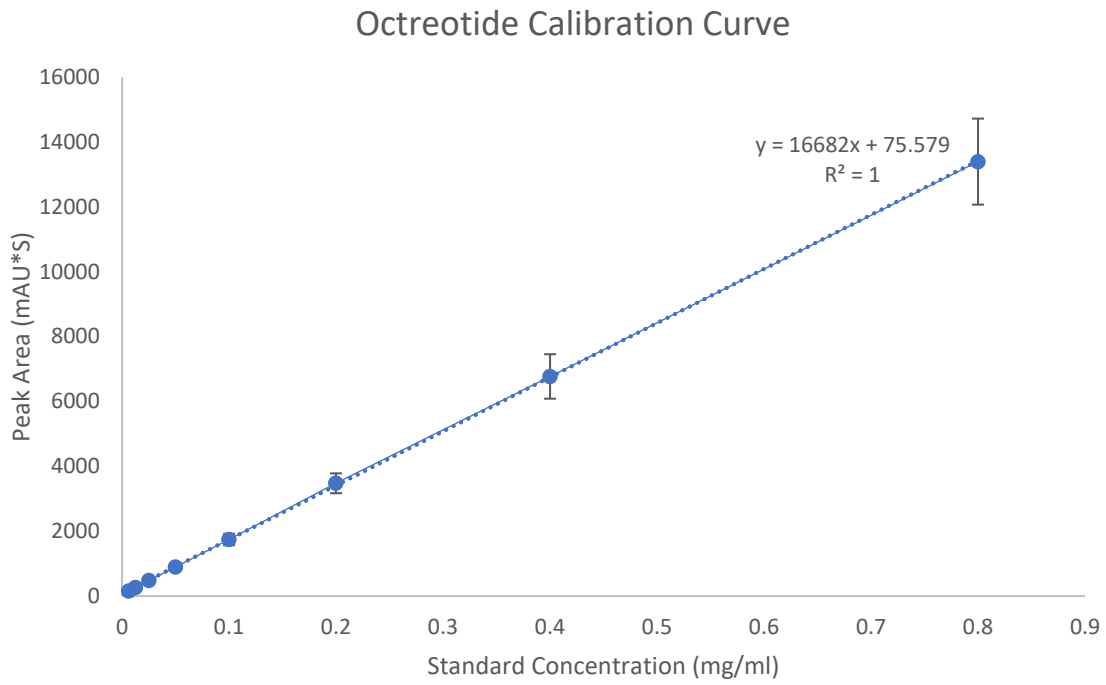

Figure 3.5. Calibration curve of the new serial dilutions after excluding the sample with the concentration of 1.6 mg/ml. Error bars represent standard deviation (n=3).

As seen from figure 3.4 above, the linearity of the calibration curve is $R^2 = 1$.

The recovery accuracy for the HPLC method was assessed by choosing three concentrations from the calibration curve over nine determinations. The recovery percentage is presented in table 3.1 below according to ICH guidelines (EMA-ICH-Q2R2, 2023).

Table 3.1. Octreotide acetate HPLC method accuracy data.

Octreotide standard concentration (mg/ml)	**Recovery (mean)**
0.8	99.8 %
0.2	101.96 %
0.1	100.08

The precision of the HPLC method was carried out by taking three concentrations runs in triplicate to assess repeatability, and the results are presented in table 3.2 below:

Table 3.2. Octreotide acetate HPLC method precision assessment.

Octreotide standard concentration (mg/ml)	Found concentrations (mg/ml)	RSD
0.8	0.79	1.02 %
0.2	0.2	0.8 %
0.1	0.1	0.7 %

The limit of detection (LOD) and limit of quantification (LOQ) were further calculated. LOD refers to the lowest analyte concentration that can be detected by the HPLC method as a distinguished signal from background noise. LOD is calculated through equation 3.4:

$$LOD = \frac{3.3\,\sigma}{S}$$

Equation 3.4. Limit of detection for developed HPLC method.

Where σ is the standard deviation of the y-intercept, and S is the slope of the calibration curve. Based on this, the limit of detection of this method for octreotide is 6.25 µg/ml.

The LOQ refers to the minimum concentration of the sample that can be accurately analysed and is calculated through equation 3.5.

$$LOQ = \frac{10\,\sigma}{S}$$

Equation 3.5. Limit of quantification for developed HPLC method.

Based on the equation above, LOQ is 14.9 µg/ml.

In summary, a developed HPLC method has been validated according to ICH guidelines for octreotide acetate detection. Since the HPLC method has been validated, the next step was to load octreotide into the silica carrier via the ethanol evaporation method with/without stearic acid and permeation enhancers and check the effects of permeation enhancers on octreotide permeability.

3.2.2. SYLOID-peptide-stearic complex formation

The silica-peptide complex was first made by dissolving the peptide in different concentrations and checking the recovery percentage. Figure 3.6 below presents the recovery values.

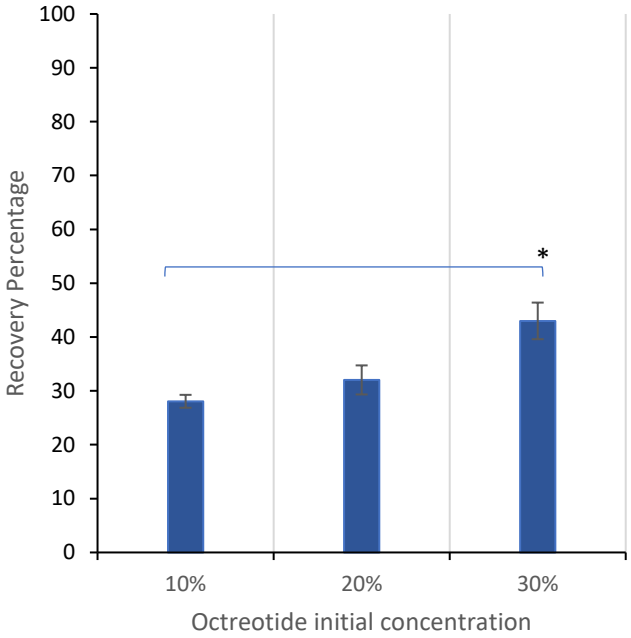

Figure 3.6. Recovery percentage of SYLOID-octreotide in different loading concentartions (10, 20, and 30% w/w) . Error bars representing standard deviation and (*) representing significant difference ($p<0.05$).

As seen from figure 3.6 above, the recovery percentage increases with the increase in loading concentration. However, the highest recovery (43%), is associated with the loading concentration of 30% w/w. These values could be related to the used solvent, and its properties. For instance, the viscosity of the solvent affects loading as well as the polarity, where solvents with low hydrogen bonding abilities affect loading.This is related to silanol groups interacting with each other instead of the solvent, which causes them to flocculate and decrease protein loading efficiency (Raghavan et al., 2000). The effects of the solvent on loading efficiency are discussed in detail in the following chapter.

The 30% loading concentration was used for further experiments as it gave the highest recovery percentage.

Secondly, the complex was made by adding the three components together at these ratios: octreotide 30%, stearic acid 120% and SYLOID. The recovery percentage was calculated and it was 54%, which is higher than the SYLOID-octreotide on its own.

To investigate the presence of stearic acid in the formulation, DSC, FTIR, confocal microscopy, and SEM were used to confirm its presence and the morphological properties.

3.2.3. Molecular interactions of SYLOID-stearic-octreotide

As seen in figure 3.7 below, the spectrum of SYLOID is similar to the aforementioned in section 2.2.1. The strong bands at 2850 and 2925 cm^{-1} are related symmetric and antisymmetric stretching of the methylene group, while the band at 1700 cm^{-1} is associated with the carboxylic group (Teixeira et al., 2007). Octreotide, on the other hand, contains the hydroxyl group (-OH) that presents a peak at 3000 cm^{-1}.

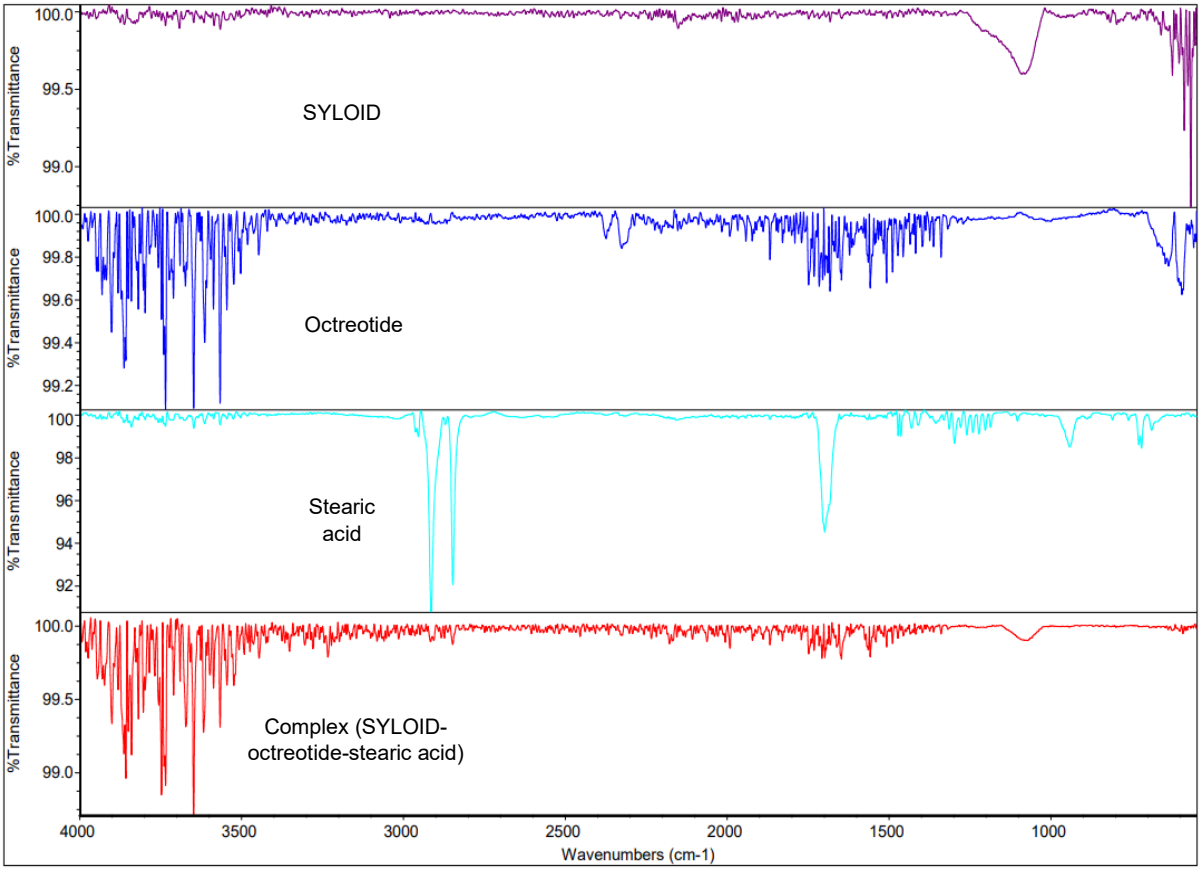

Figure 3.7. FTIR spectrum of the complex with octreotide, SYLOID, and stearic as a reference.

Moreover, both the C=O and -NH groups correspond to peaks at 1650 and 1540 cm^{-1}, respectively, which specifies the presence of octreotide (Chatzitaki et al., 2023). The FTIR data helps in detecting the presence of a specific chemical group in the formulation. However, to study the morphological properties of the carrier, SEM was used to establish if stearic acid has formed needle-like structures on the surface.

3.2.4. Thermal properties and behaviour

DSC was used to investigate the thermal properties of the materials within the silica carrier. Figure 3.8 (A-B) below presents the thermograms of the complex with the components as well as of octreotide for comparison.

SYLOID XDP 3050 is an amorphous mesoporous silica microparticle that shows no thermal activity upon increasing temperature (Koch et al., 2020). Stearic acid shows an endothermic activity with a peak at 71°C , which is similar to the melting point (69.51°C) that is reported by Lin et al. (2019). This endothermic peak is present in the complex, which indicates the presence of stearic acid in the formulation. Additionally, octreotide presents a weak endothermic activity that is related to its melting at 150°C that is supported by literature (Wang et al., 2019a), where it is more apparent in 3.8 B. Furthermore, the complex shows an endothermic activity at 69°C, which is associated with the melting of stearic acid. This indicates the presence of stearic acid crystals within the formulation, which might imply that stearic acid presents needle-like structures on the surface, as seen in Chapter 2. This can be further explored using SEM imaging to investigate the morphological properties of the silica carrier.

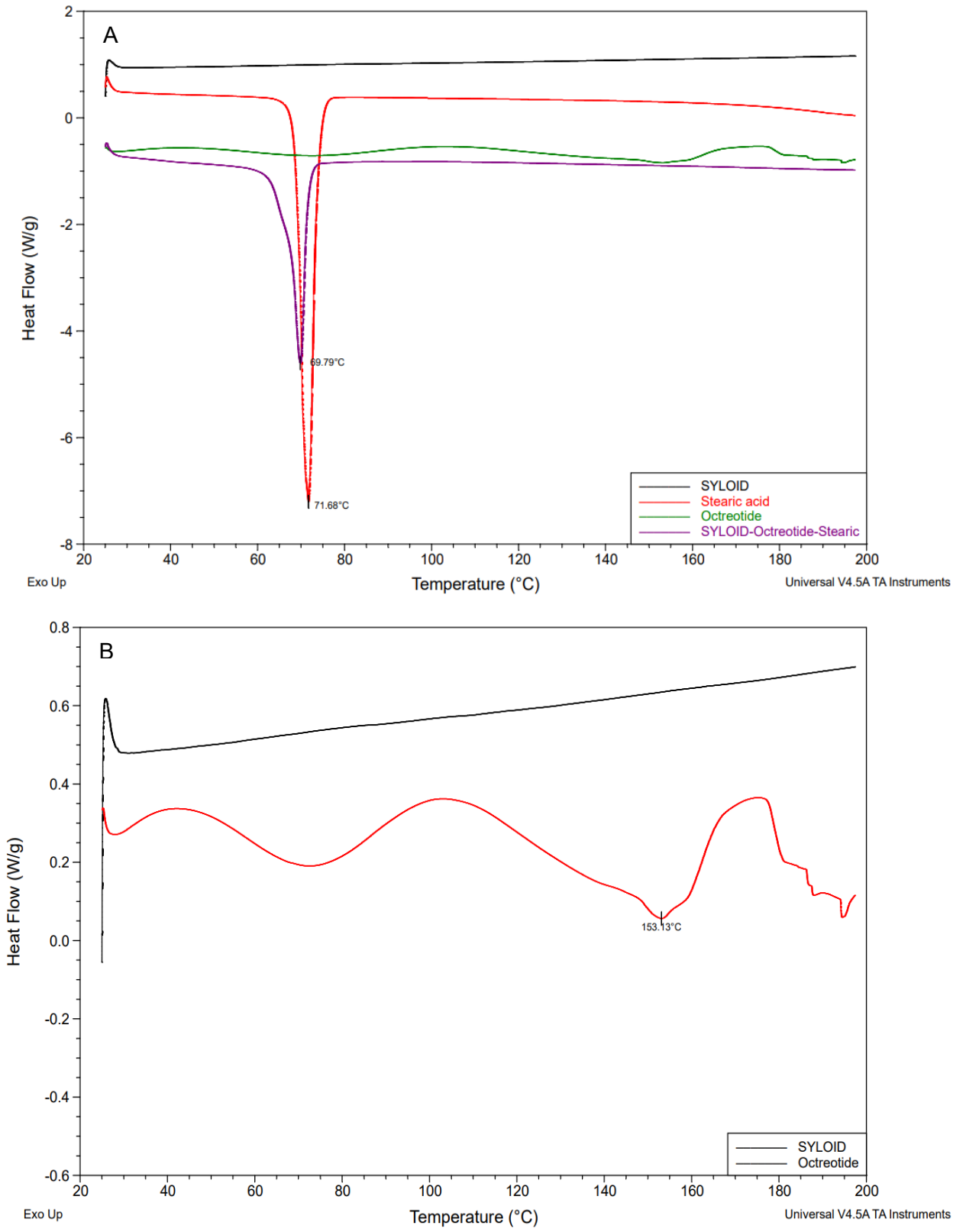

Figure 3.8. DSC thermograms of the complex in comparison to stearic acid, SYLOID, and octreotide (a) identifying the melting points. (B) is a thermogram of octreotide and SYLOID showcasing the melting point of octreotide.

3.2.5. Fluorescence properties

SYOILD XDP 3050 is a mesoporous silica carrier that presents no fluorescent properties. However, octreotide acetate is an octapeptide that shows fluorescence between 395 and 460 nm according to Wang et al. (2019a). Furthermore, the presence of the amino acid tryptophan in octreotide's structure facilitates the fluorescence imaging of the protein (Sy et al., 2001, Vivian and Callis, 2001). Stearic acid on the other hand, is a fatty acid that presents autofluorescence properties due to the lipid oxidation, and its fluorescence happens at a broad spectral range (Semenov et al., 2020). The fluorescence imaging was conducted to present a preliminary indication on the presence of octreotide and stearic acid due to their aforementioned properties. Figure 3.9 below presents images taken of 3D generated model of the silica-lipid-octreotide complex at different planes.

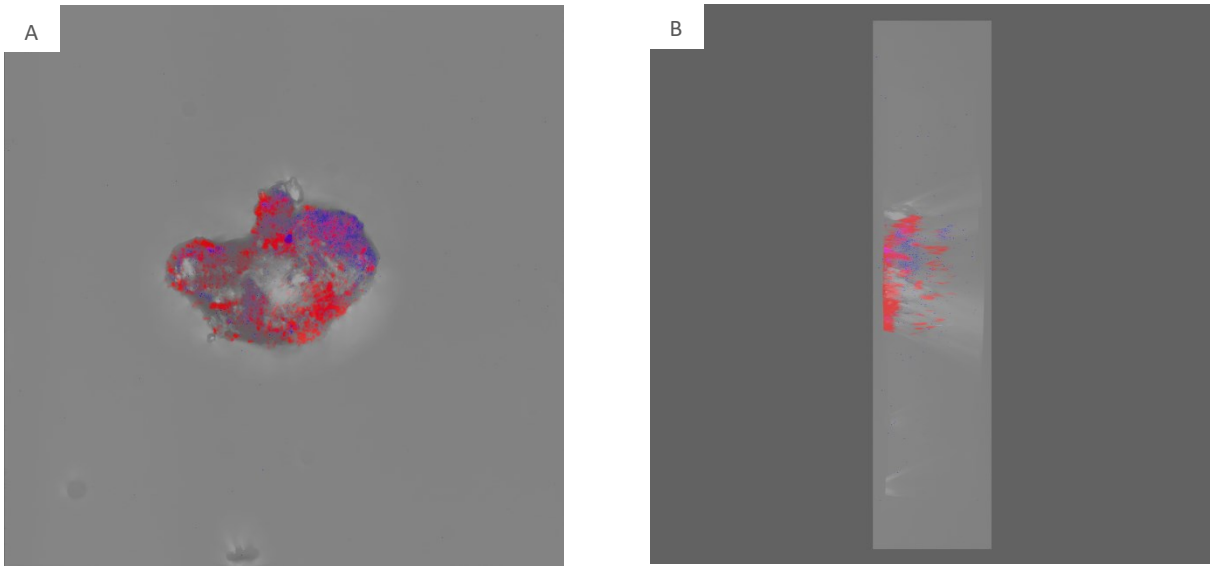

Figure 3.9. 3D confocal fluorescence images showing stearic acid autofluorescence from the needle-like structures on the surface of the carrier (red) and octreotide (blue). Anterior plane (A), and the longituidinal plane (B) showing the distribution of octreotide and stearic acid around the carrier.

As seen from figure 3.9 above, the red fluorescence is related to the autofluorescence properties of stearic acid, while the blue colour relates to the fluorescence of octreotide at the used fluorophore. Figure 3.9 A shows that stearic acid seems distributed on the surface while octreotide is inside the carrier (B) as it is taken from a different plane. This establishes that both stearic acid and octreotide are incorporated within the carrier.

SEM imaging was used to check the morphological properties of the silica surface and determine the shape of stearic acid.

3.1.1. Morphology and surface structure of the designed complex

SEM imaging was used to further support the FTIR, DSC and fluorescence results regarding the presence of stearic acid needle-like structures on SYLOID's surface. Figure 3.10 below presents SEM images for the complex (SYLOID-stearic acid-protein), where (A) is the individual particle shape and surface of SYLOID XDP 3050, (B) is the particle population of the complex, and (C) is a magnified image identifying the needle-like structures of stearic and octreotide crystals.

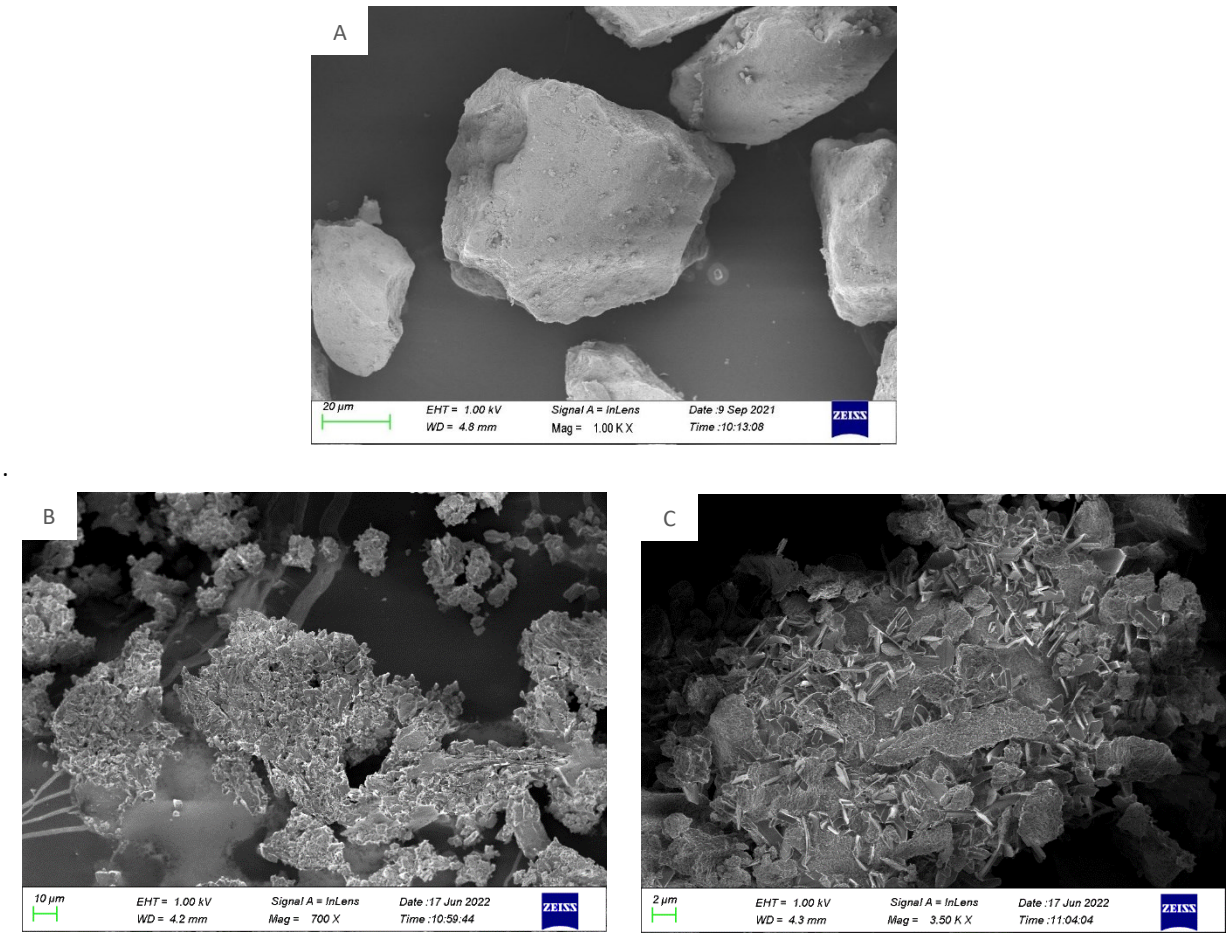

Figure 3.10. SEM surface imaging showing SYLPOID XDP 3050 morphology (A), the SYLOID-stearic acid-octreotide complex particle population (B), and higher magnified image of the complex showing stearic acid needle-like structures and (C) octreotide recrystallisation on the surface.

As seen from figure 3.10 above, the surface of the silica carrier is smooth and shows no crystal growth (A), which is supported by literature as Solomon et al. (2021) reported since SYLOID XDP 3050 is a non ordered mesoporous silica carrier that has a size of 59 µm and a smooth particle surface.

As reported in the previous chapter, upon stearic acid addition, needle-like structures are evident on SYLOID's surface when stearic acid concentration exceeds 100% w/w. The stearic acid concentration used in making the complex was 120%, to ensure that the needle-like structures are present. Upon adding both the protein and stearic acid, a similar observation was evident as stearic acid has crystallised on the surface of the carrier (B) in needle-like shapes. Additionally, the complex seems to have compact-like formations on the surface of SYLOID (C), which is related to octreotide crystallising on the surface. These results further supported previous findings (figure 3.9 A-B), where stearic acid had shown fluorescent properties and octreotide's fluorescence around and inside the silica carrier.

Following the characterisation of the formed SYLOID-stearic-octreotide complex, the next sections will focus on the Caco-2 cells growth and preparation for the permeability study.

3.1.2. Preparation and growth of Caco-2 cells

Caco-2 cells were chosen for the permeability study, considering their properties that resemble the intestinal cells (Maubon et al., 2007). Caco-2 cells are dethawed before use and added to the flasks to grow and reach confluence. Figure 3.11 below presents the chronological growth of the cells from the moment they were dethawed and transferred to the flasks (A) until they reached full confluence (D).

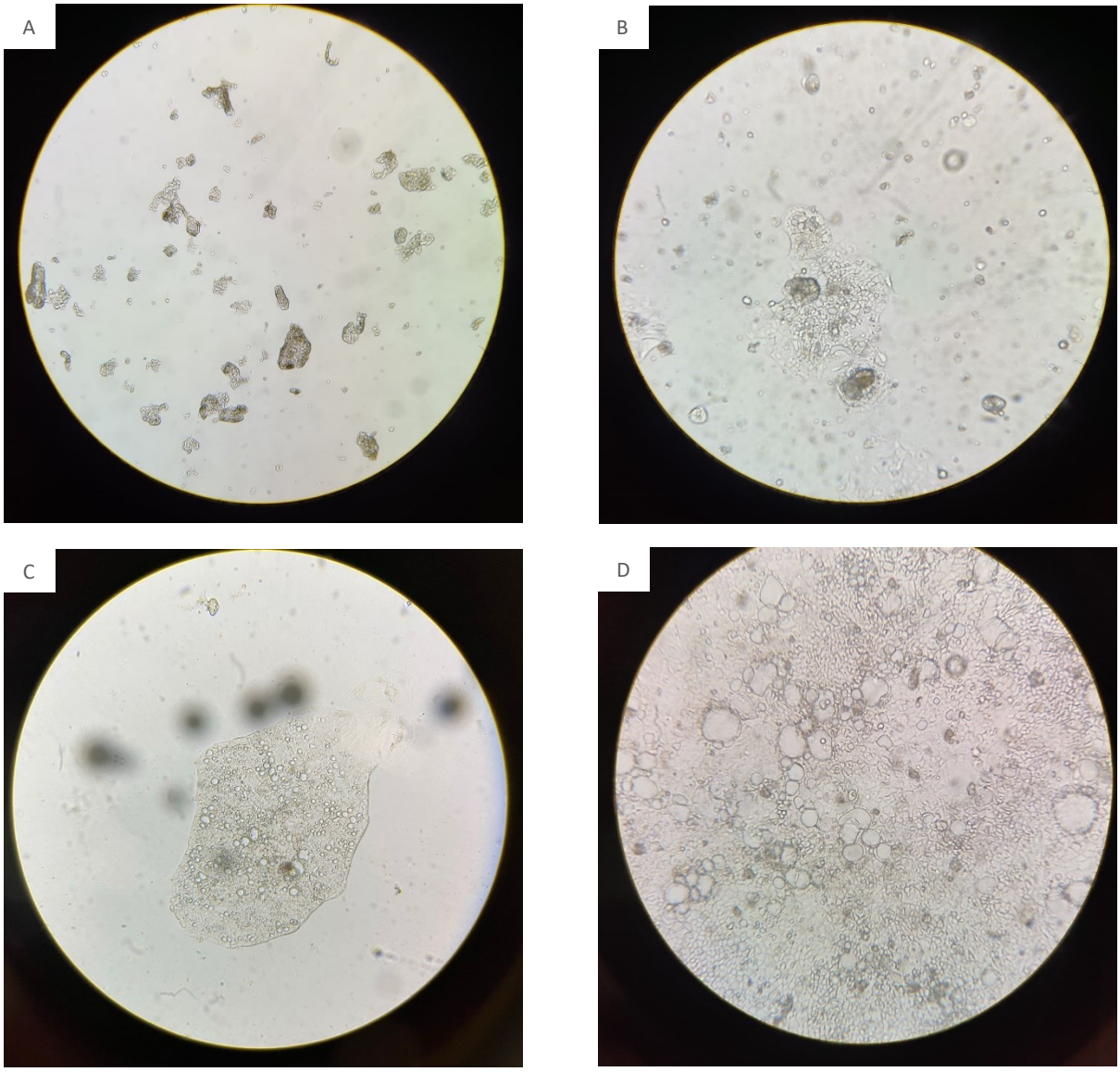

Figure 3.11. Chronological growth of Caco-2 cells, where they were transferred to the flasks after dethawing (A), after 6 days (B), after 12 days (C), and upon reaching full confluence (D).

As seen from figure 3.11 above, cells have gradually grown until they have reached the required confluence for seeding into the transwells.

3.1.3. Caco-2 cells culture for investigating permeability

For octreotide acetate permeability investigations, membrane supports were seeded at a density of 1.2 * 10^5 cells/cm^2 and allowed to develop. It is important for the cell density not to exceed 5 * 10^5 cells/cm^2, as it causes multilayers to form rather than a monolayer, which causes a disorganisation of the cell layers (Panse and Gerk, 2022). Cells were maintained, and the media was changed every other day to keep the cells viable. It took between 7 to 10 days for the cells to fully confluence the transwell. As mentioned above, Caco-2 cells are a great candidate for evaluating transcellular and paracellular absorption, considering the presence of tight junctions between the cells. However, a microscope cannot be used to inspect the integrity of the cells. Another non-invasive technique that is regularly used, called trans-epithelial electronic resistance (TEER) measurement, can be implemented. This is applied to ensure the integrity of the Caco-2 cells monolayer prior to the permeability study. The TEER value was checked every other day after the media change to ensure the validity and viability of the cells. The TEER values are identified in figure 3.12 below.

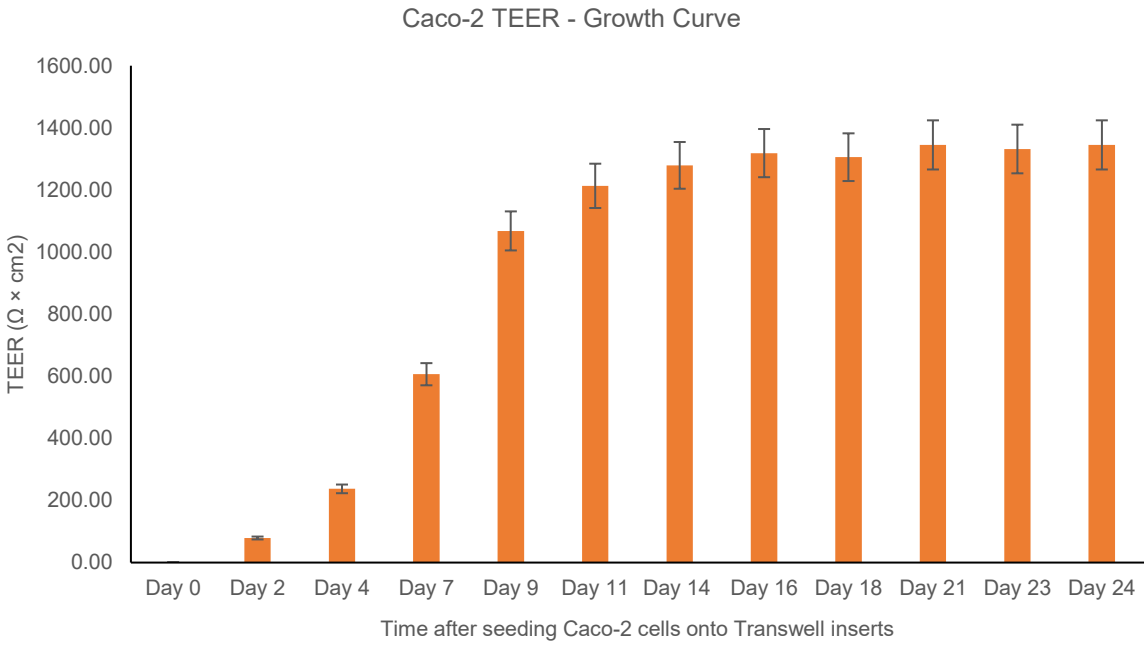

Figure 3.12. TEER value increase within 3 weeks until cells reached required confluence for permeability studies. Error bars present standard deviation.

As seen in figure 3.12 above, the TEER values increased until they peaked at 16 days (1318 Ω), and the values were maintained around this number. These readings align with the literature as the TEER values for Caco-2 cells when measured using the EVOM/Chopstick system (Srinivasan et al., 2015). Additionally, the TEER readings of Caco-2 cells increase as the passage number of the used cells increases prior to seeding, and the optimum passage

range for permeability experiments should be between 30 and 65 (the used cells had a passage number of 47). Furthermore, permeability studies for cells after seeding can be conducted after 3-4 weeks after the monolayers have fully grown. (Panse and Gerk, 2022).

The TEER values were measured directly before the permeability study, after finishing, and after 24 hours, and the results are presented in figure 3.13 below.

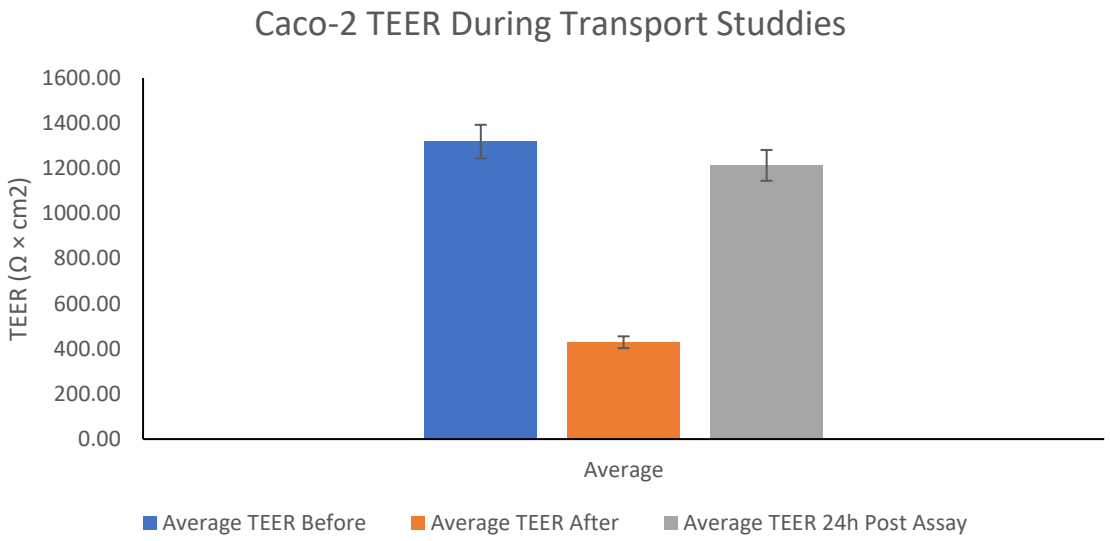

Figure 3.13. Average TEER values before the permeability study, after finishing the studey, and after 24 hours with HBSS incubation showing Caco-2 cells viability. Error bars present standard deviation.

As seen from the figure above, the TEER values have decreased after finishing the experiments, which is expected as the presence of the formulations inside the apical compartment changes the electrical resistance between the two compartments. Additionally, the used materials have been reported to decrease the TEER values, since SNAC has been found to decrease TEER values upon addition to Caco-2 cells (Brayden et al., 1997). However, after 24 hours of incubation using HBSS, the TEER values have increased to 1213 Ω, which aligns with Pires et al. (2021) results. According to them, Identifying TEER values before and after assessing permeability is important to ensure that the monolayer integrity was not affected during the study. Furthermore, a decline in TEER values may be observed upon completion of permeability studies. However, following a 24-48 hour incubation period with HBSS, the TEER should increase, approaching the initial value before the study.

3.1.4. Octreotide release and permeability

The Caco-2 cell model was used to evaluate the permeability with the addition of two permeability enhancers (SNAC and TPGS). The permeability study was conducted in different stages: evaluating the permeability of octreotide on its own and with the addition of SNAC at three concentrations (5, 10, and 30 mMol). The next step involved checking the permeability of octreotide in different formulations: loaded in SYLOID, co-loaded with stearic acid as the complex (SYLOID-octreotide 30%-stearic acid 120%), physically mixed with preprepared SYLOID-stearic 20%, and a physical mixture of stearic acid with octreotide. Finally, the complex's permeability was assessed with the incorporation of SNAC, TPGS, and both. The permeability studies are presented below as transported drug percentage (%) against the time of the release study.

The permeability of octreotide was first assessed by the apical-basal and basal-apical permeability, and the percentage of the transported amount is presented in figure 3.14 below. The apical-basal transported amount is presented while the basal-apical transport were not added as all values presented 0% drug transport.

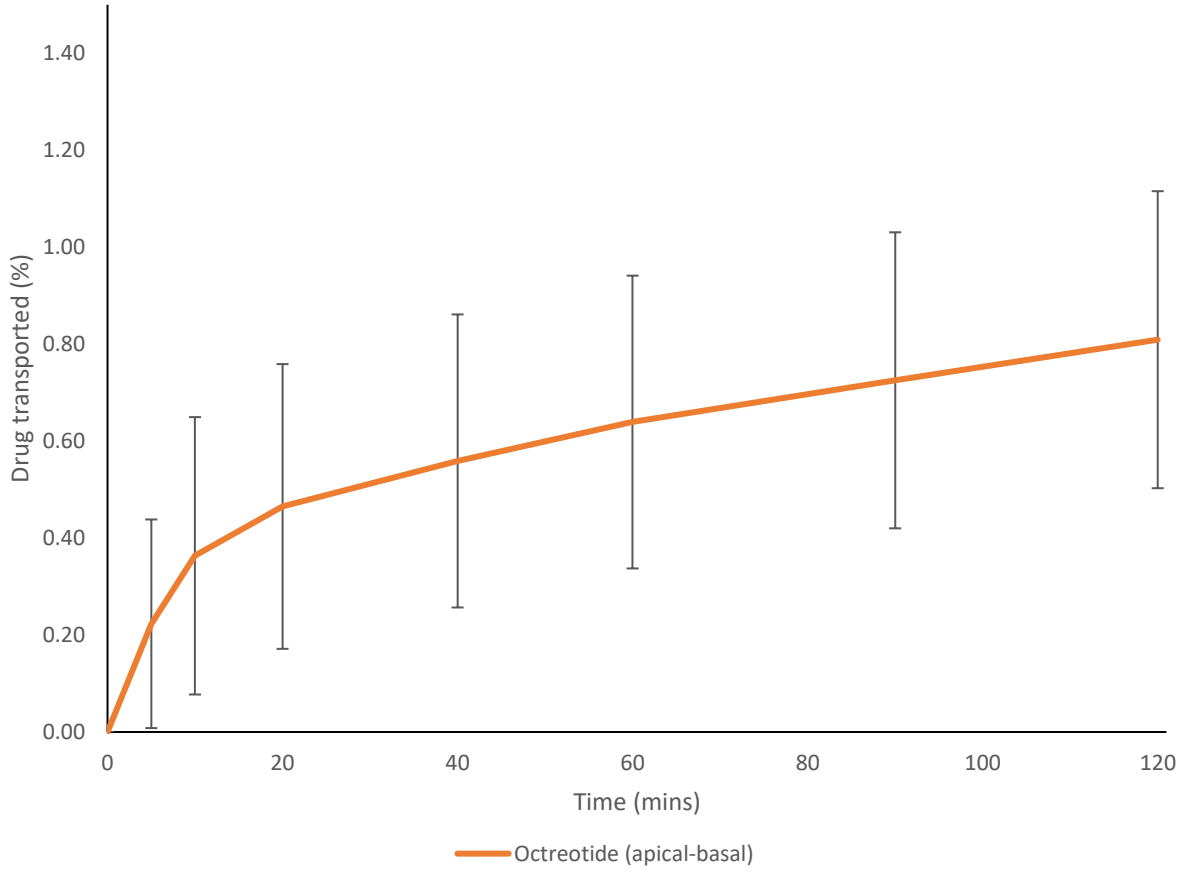

Figure 3.14. Drug transport percentage (%) of octreotide acetate across time within 2 hours. Error bars represent standard deviation (n=3).

As seen from the figure above, there is an increase in octreotide's absorption as time increases. However, it is relatively low, where the highest amount achieved after 2 hours was 0.8%. This aligns with previous findings reported by Florea et al. (2006) as they found that the maximum absorbed amount is less than 1%. This could be attributed to the high molecular weight of octreotide as well as its hydrophilic properties, which make the absorption challenging (Thanou et al., 2000). Following the assessment of the permeability of octreotide, SNAC was used as a potential permeability enhancer in three concentrations (5 mMol, 10, mMol, and 30 mMol), and the transported amount is reported in figure 3.15 below.

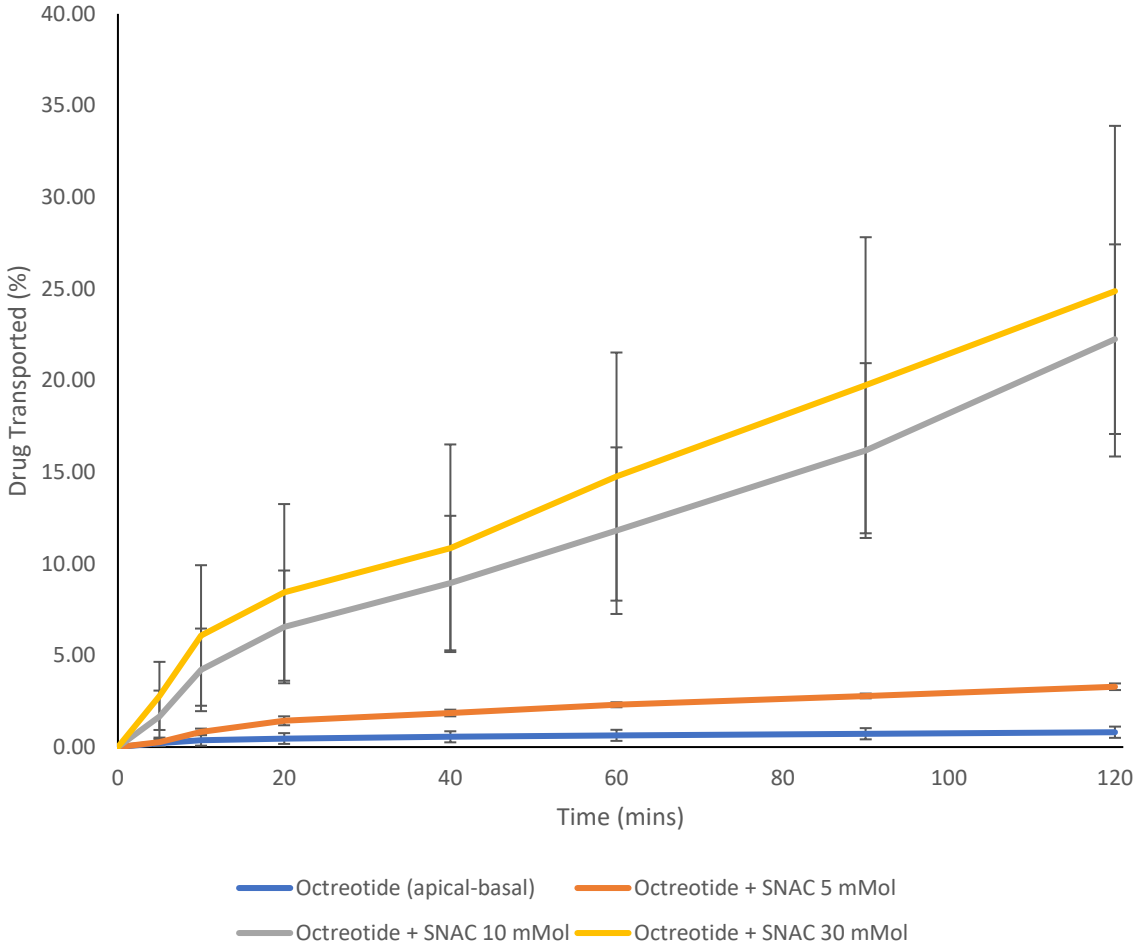

Figure 3.15. Drug transport percentage (%) of octreotide acetate with different SNAC concentrations (5, 10, and 30 mMol). Error bars represnet standard deviation (n=3).

As seen from figure 3.15 above, the use of SNAC has significantly increased the amount of the transported drug. When the SNAC concentration was 5 mMol, the amount of the transported drug increased gradually until the permeation study was finished, where the highest achieved value was 3.28%. This has shown a 4-fold increase compared to octreotide. Upon increasing the amount of SNAC to 10 mMol, a sharp increase in the amount of the transported drug occurred. At the beginning of the study, 2.7% of the drug was absorbed after 5 minutes compared to 0.22% and 0.27% when SNAC concentration was 0 and 5 mMol, respectively, where the highest amount achieved after 2 hours increased to 22%. In addition, Upon increasing SNAC to 30 mMol, the percentage of the transported octreotide was 2.79% at 5 minutes and reached 24.86% after the study finished.

The highest amount is associated with the use of SNAC 30 mMol (24%) compared to octreotide's amount (0.8%). Additionally, increasing SNAC concentration increased the overall

transported amount from 3.2 to 24% when SNAC amount was 5 and 30 mMol, respectively. This is related to SNAC's effect in increasing the transcellular permeability, where the increase in transported amount with increased SNAC's amount aligns with findings in literature (Twarog et al., 2020). This is due to SNAC's structure and the higher interaction with cells upon increasing its amount. Even though increasing SNAC's amount increases permeability, upon increasing the amount beyond 30 mMol, Caco-2 cell-cytotoxicity can occur. In addition, at SNAC amounts above 10 mMol, cell viability begins to decline, as reported by Twarog et al. (2020). Therefore, the 10 mMol was used for further experiments.

Based on the findings from these experiments, the 10 mMol concentration of SNAC will be used with formulations. The next set of samples will contain octreotide, the complex, and physical mixtures of octreotide with different components of the silica complex.

TPGS was chosen at a concentration of 1 mMol to decrease the possibility of damaging the Caco-2 cells. Collnot et al. (2006) found that TPGS 1000 starts to affect the integrity of Caco-2 cells at concentrations starting from 625 µMol, reaching its peak effect at 10 mMol. They attributed the results to TPGS 1000 amphiphilic properties, where it interacts with cellular lipid membranes. It can also be due to TPGS inhibitory effects, as it was shown to inhibit the P-gp and cause the drugs to accumulate inside the cells (Kumbhar et al., 2022).

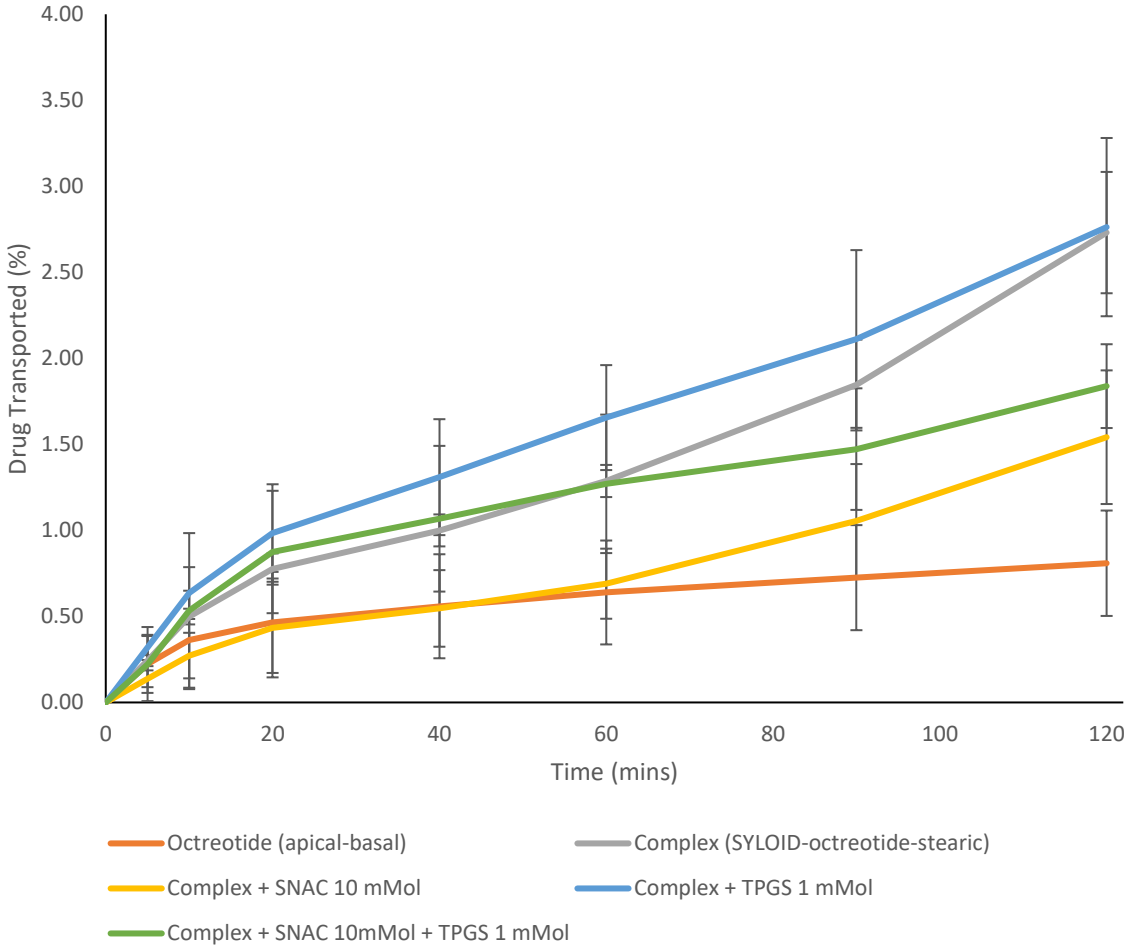

Figure 3.16. Drug transport percentage (%) of octreotide acetate from different formulations: octreotide as a reference, the complex (SYLOID-octreotide-stearic), the complex + SNAC 10 mMol, the complex + TPGS 1 mMol, the complex + SNAC 10 mMol + TPGS 1 mMol. Error bars represent standard deviation (n=3).

As seen from figure 3.16 above, The amount of transported drug differed based on the used formulation. For instance, when the complex (SYLOID-stearic-octreotide) was used, the amount of the drug that was transported using the complex increased from 0.24 to 2.73% at 2 hours. This amount is 3 folds higher than octreotide's transport (0.8%). When SNAC amount was 10 mMol, the transported amount was 1.54% after 2 hours, which was higher than octreotide but lower than the complex. The sample with TPGS had a transported amount of 2.76% as the highest achieved value. However, when the two permeation enhancers were used, the transported amount was 1.83%, lower than the complex's and the complex-TPGS transport.

As reported above, using the complex has significantly enhanced the transported amount ($p<0.05$) compared to octreotide. After 2 hours, the highest transported amount was 2.73% compared to 0.8%. This could relate to the presence of the needle-like structures and

octreotide on the surface of the carrier. Moreover, as seen in the SEM and confocal imaging, octreotide seemed to crystallise on the surface as well as on the needles. We theorise that the needles on the surface of the carrier have resulted in an increase of the transported protein, where they interact with the cells and release the drug that has crystallised on them as well as the drug inside SYLOID. It can be related to octreotide being amorphous inside the carrier, as SYLOID has been found to contain the drug in an amorphous form (Le et al., 2019).

Nevertheless, the use of both TPGS and SNAC with the complex resulted in a reduction in the absorbed amount compared to the complex alone, albeit higher than when the complex was with SNAC. This could be related to the fact that using both permeability enhancers has made the cells reach the limit for permeability. The use of agents has accumulated the side effects of both, as mentioned above, which could be the reason for the decrease compared to TPGS.

The reason for the enhanced recovery could relate to the inclusion of stearic acid. When stearic acid is added to the formulation, octreotide could crystallise either inside the pores (based on confocal images) or on the needle-like structures of stearic as seen from the SEM imaging. Furthermore, one minor factor that might affect the loading and recovery is sticking on the glass watch. The formulation that contained stearic acid was easier to acquire compared to the ones that had no stearic. It is related to the stickiness of peptides on glass, as well as the stearic acid effect as a lubricant (Krajewski et al., 1996, Goebel-Stengel et al., 2011).

To further investigate the effects of stearic acid needle-like structures on permeability, different combinations were made using silica, protein, and stearic acid in numerous formulations and in physical mixtures. The values of the transported amounts are identified in figure 3.17 below.

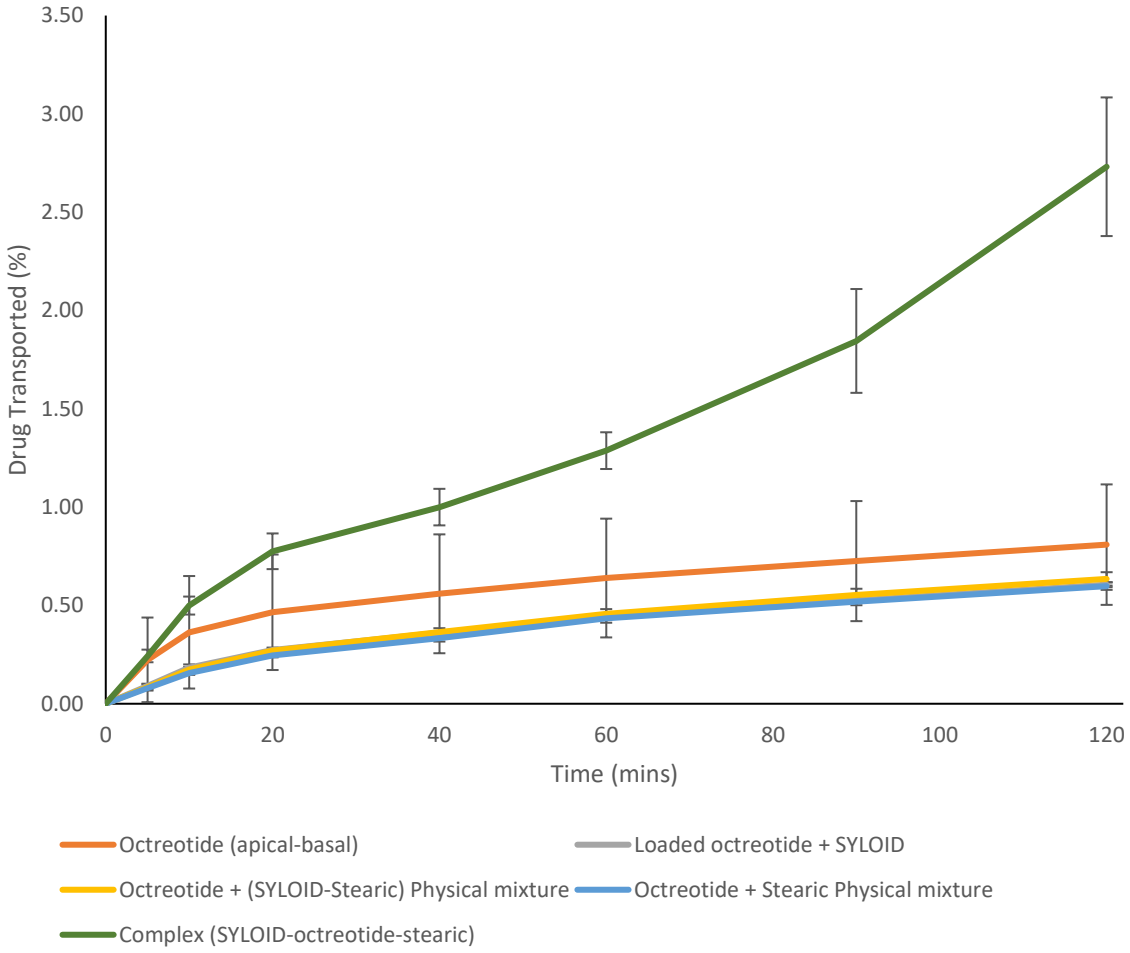

Figure 3.17. Drug transport percentage (%) of octreotide acetate from differnt formulations: octreotide as a reference, octreotide with (SYLOID-stearic acid) in a physical mixture, the complex, octreotide loaded in SYLOID, and a physical mixture of octreotide and stearic acid. Error bars represent standard deviation (n=3).

As seen from figure 3.17 above, the transported amount of octreotide from formulations containing silica-octreotide, octreotide-stearic physical mixture, and octreotide with SYLOID-stearic in physical mixture presented low drug transported compared to octreotide and the complex. The highest transported amount was 0.62% for octreotide-(SYLOID-stearic) in a physical mixture compared to 0.8% of octreotide.

These differences could be related to the low recovery of octreotide-SYLOID that is due to solvent viscosity and interaction with the carrier (this will be further investigated in the next chapter). Additionally, the addition of stearic acid on its own to octreotide can affect the permeability considering the hydrophobic properties and the presence of octreotide in crystal form compared to octreotide being amorphous form as SYLOID contains the drug in amorphous form as reported by Le et al. (2019). Additionally, when octreotide was added to a pre-prepared SYLOID-stearic in a physical mixture, it was not incorporated inside the carrier, even though the needles were evident. However, the complex comprising all three

components exhibited the greatest enhancement in the transported amount. This can be attributed to the amorphous state of octreotide within the carrier, both internally and recrystallised on the carrier's surface, thereby rendering the drug readily accessible for direct absorption. Therefore, upon comparing the octreotide-(SYLOID-stearic) with the complex, it can be seen that the needles on the carrier's surface have positively contributed to enhancing the permeability of octreotide across Caco-2 cells. The effect of the hydrophobic properties of stearic acid on the drug transport could be interpreted by the floating powders. During the experiment, the formulations containing stearic acid as a physical mixture floated inside the apical chamber due to stearic acid's hydrophobic properties.

3.1.5. Apparent permeability

The apparent permeability (P app) will be calculated after assessing the transported amount of octreotide from different formulations. This value is used to predict drug transport across cell barriers and determine protein permeability as it proves useful for *In vitro* examinations, as reported by Dahlgren and Lennernas (2019).

The apparent permeability values (log P app) for the formulations are detailed in graph 3.18 below.

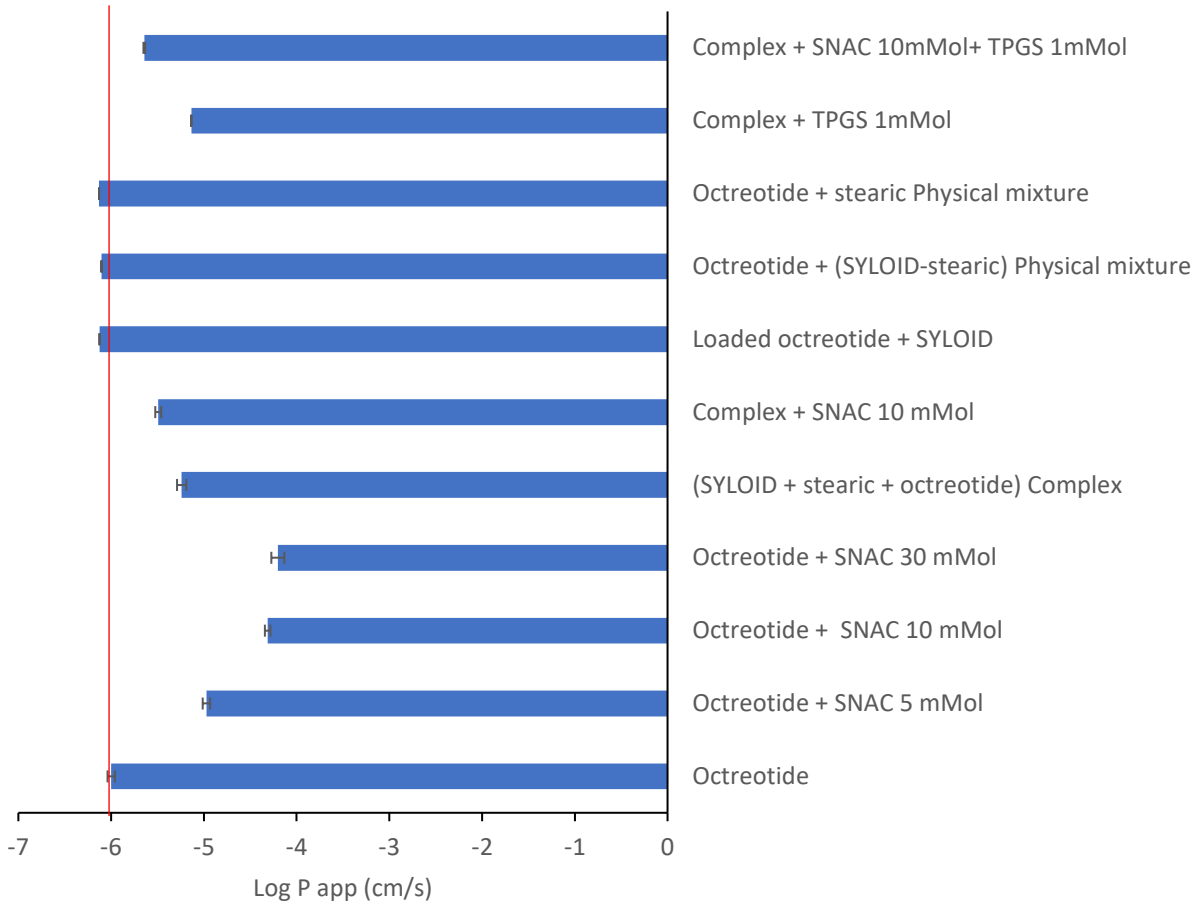

Figure 3.18. Apparent permeability values (log) of octreotide from different formulations and different permeability enhancers. The threshold of drug absorption (10^{-6} cm/s) is indicated by the red line. n=3 and error bars represent standard deviation.

As seen from the figure above, the apparent permeability of octreotide is $1*10^{-6}$ cm/s and the log P app is -5.99 cm/s, which is the limit that is considered for drugs to be poorly permeable. This aligns with Berg et al. (2022) results, considering that octreotide has a low permeability. Additionally, the P app value seemed to increase as the amount of SNAC added to octreotide increased as the values (log P app) increased from -4.97, -4.31, -4.2 cm/s when SNAC amount with octreotide was 5, 10, and 30 mMol, respectively. This is related to SNAC's effect as a permeation enhancer (Twarog et al., 2020) as the highest value is associated with SNAC at 30 mMol. Furthermore, the complex value was -5.23 cm/s which is higher than octreotide's, but yest lower than the values with SNAC. However, it has significantly increased the absorption of octreotide. This enhanced permeation is theorised to be related to the needle-like structures of stearic acid that facilitate the interaction with the cells. Moreover, as seen

from both confocal imaging and SEM, octreotide was present on the surface of the carrier and occupied the porous structure.

However, when SNAC was added to the complex, the permeability of octreotide decreased as the value (-5.49 cm/s) has decreased in comparison to the complex's, yet it was higher than the octreotide's (-5.99 cm/s), indicating that it has enhanced octreotide's absorption but bot as efficient as the complex. This could be related to the higher presence hydrophobic materials (stearic acid) and SNAC which causes the enhanced permeability effect to reach its limit, thus decreasing absorption. When TPGS was added to the complex, the value was found to be -5.13 cm/s, higher than both octreotide's and the complex's, which is due to TPGS effects as a permeation enhancer and surfactant as reported in the literature, where it interacts with lipid membranes and causes the drug molecules to accumulate inside the cells (Kumbhar et al., 2022).

To further elaborate on stearic acid inside the complex interacting with cells, octreotide was added into SYLOID, stearic, and SYLOID-stearic in different combinations. The log P app values have decreased below -5.99 cm/s, indicating a decrease in permeability. These values could relate to stearic acid having strong hydrophobic properties to enhance permeation on its own, but when incorporated into the carrier it increases permeability. Additionally, considering the solvent properties, when octreotide was loaded into SYLOID, the loading efficiency was not high. These factors will be further investigated in the next chapter. When octreotide was added physically into SYLOID-stearic, the permeability decreased below octreotide's value. This could be related to the drug not being incorporated into the complex as the drug can be in an amorphous form and crystallised on the surface of the drug, being ready to be released (Le et al., 2019), as reported above.

The formulation with the highest P app is octreotide with SNAC 30 mMol, which was expected considering SNAC effect in enhancing the permeability of octreotide. Additionally, as SNAC's amount increases, the apparent permeability increases and the log P app decreases, an anticipated outcome considering SNAC's effect as a permeation enhancer (Twarog et al., 2020). Additionally, the use of the complex has significantly increased the apparent permeability of octreotide compared to the use of octreotide on its own, based on what has been reported earlier. Yet, using the complex with TPGS or with SNAC has increased the apparent permeability of the drug. Additionally, the Papp values of the complex with TPGS and SNAC are higher than the complex's, which might be due to TPGS effects in interacting with lipid membranes and causing the drug molecules to accumulate inside the cells (Kumbhar et al., 2022). Yet, upon using both permeation enhancers with the complex, the P app has decreased compared to the complex, indicating a decrease in permeability. This could be

related to the cells being saturated with the addition of both materials as well as the presence of stearic acid. This high increase in lipophilic materials might counteract the permeation-enhancing effects of both, resulting in decreased permeability (Frallicciardi et al., 2022).

Based on the reported findings, the complex has significantly increased the permeability of octreotide and can compete with the use of different permeation enhancers. Additionally, the use of this complex could be investigated further for different proteins and for *In vivo* trials.

Conclusions

This chapter reports the fabrication and *In vitro* testing of a silica-lipid-protein complex for oral delivery. The silica carrier was mesoporous SYLOID XDP 3050, while the lipid was stearic acid, and the protein was octreotide acetate.

The design of this novel complex was based on the previous chapter's findings regarding the presence of needle-like structures on the surface of the carrier. Therefore, the stearic acid ratio was 120% w/w of SYLOID's. The loading method was solvent evaporation, and preliminary loading experiments were conducted to find the optimum octreotide/SYLOID ratio using three different loading concentrations: 10, 20, and 30 w/w.

For octreotide acetate analysis and detection, a new HPLC method has been developed and validated according to the ICH guidelines, where the LOQ and LOD were 14.9 and 6.25 µg/ml, respectively. Octreotide was chosen at a concentration of 30% w/w to SYLOID as it presented the highest recovery. The complex was made using 120% stearic acid and 30% octreotide acetate w/w via solvent evaporation.

The post-formulation analysis included FTIR, DSC, confocal microscopy, and SEM. FTIR results have indicated stearic acid and octreotide presence based on their specific wavenumbers. DSC has presented an endothermic activity for the complex, where the melting point was similar to stearic acid, indicating the presence of needle-like structures on the surface. Furthermore, the fluorescence 3D imaging has shown the distribution of stearic acid around the carrier surface, while octreotide's presence inside and on the carrier surface was also confirmed based on its fluorescence.

SEM imaging was implemented to confirm the presence and shape of the stearic acid structures on the surface of SYLOID. The images showed that the needle-like structures were present on the carrier's surface due to stearic acid recrystallisation. In addition, compact-like structures of octreotide acetate have been found embedded within stearic acid needles.

Following the development and characterisation of the new complex, *In vitro* tests were conducted using Caco-2 cells. The cell line was maintained and grown in flasks prior to seeding in transwells. The permeability of octreotide was similar to previous findings in the literature (>0.8%). SNAC was added as a permeation enhancer in three concentrations, and it has significantly improved octreotide's permeability. A concentration of 10 mMol was chosen for further studies with TPGS at 1 mMol.

The complex has significantly increased octreotide's permeability, so SNAC and TPGS have done, even though this increase was not as high as the increase associated with using SNAC with octreotide. This could be due to the presence of the needle-like structures that facilitate the interaction between the carrier and the cells. Yet, using both permeation enhancers has decreased the permeability, which might be due to the cells being saturated with hydrophobic moieties from the PEs and stearic's presence.

The next chapter will focus on the factors that affect protein loading into mesoporous silica carriers, where the solvent and the protein size will be investigated.

Chapter 4

Solvent Evaporation-Based Method for Loading Model Proteins into Mesoporous Silica Microparticles for Oral Delivery.

Introduction

Researchers and pharmaceutical companies have long sought the oral delivery of peptides/proteins due to its enhanced patient compliance, cost-effectiveness, convenience, and non-invasiveness compared to injection-based delivery (Tyagi et al., 2021). However, there are many barriers against the oral administration of biomolecules, including pre-absorption challenges, namely degradation due to both pH difference in the Gastrointestinal tract (GIT) and enzymatic activity, which cause decreases in the bioavailability of orally administered products (Dubey et al., 2021, Zhu et al., 2021b).

Some of the previous barriers have been successfully evaded resulting in a couple of FDA-approved products like Rybelsus® and Mycapssa® for the oral delivery of Semaglutide and Octreotide acetate, respectively (Zhang et al., 2021). Both products were manufactured with novel technology that utilises novel compounds called permeation enhancers, which facilitate the transport of the drug molecules through the intestinal epithelium (Maher and Brayden, 2021).

Apart from the previous technologies, pharmaceutical companies and formulation scientists are searching for versatile, generally regarded as safe (GRAS) and biocompatible materials, with mesoporous silica falling into this category. It possesses several advantages that make it sought after for peptide delivery, such as large surface area, tuneable pore size and high pore volume (Singh et al., 2022). Mesoporous silica exists under the classification established by the International Union of Pure and Applied Chemistry (IUPAC), which has been produced for porous materials (McCusker et al., 2003).

There are two general categories for mesoporous silica loading strategies: Solvent-free and solvent-based methods. The first includes physical mixing, melting, co-milling, and microwave irradiation. The second consists of adsorption, solvent evaporation, incipient wet impregnation, supercritical fluid technology, co-spray drying, and chaperone assistance (Trzeciak et al., 2021, Seljak et al., 2020, Le et al., 2019). Regardless of the loading approach, mesoporous silica protects peptides from enzymatic degradation if they remain inside the pores (Braun et al., 2020). Furthermore, they protect biomolecules from bacterial decomposition and contribute to formulation flexibility, making them a good candidate for biomolecule loading (Lei et al., 2013). Loading the active pharmaceutical ingredient (API) into the mesoporous carrier should be proceeded by immobilising the drug. This is usually conducted via mechanical work by allowing the API to melt and using the capillary forces to attract the melted material into the pores. Another approach utilises impregnation and drying, termed as the incipient method. The carrier pores are dosed with the drug, and this step is

followed by subsequent drying, which results in the pores being filled with the material. One similar method utilises the same concept of the immersion, but with small amounts of the solvents and without filtration, basically solvent evaporation, by immersing the carrier in API solution (Soltys et al., 2019).

However, many factors affect the efficiency of protein loading into mesoporous silica. For instance, pore volume is crucial in determining protein loading. Increasing the pore size of mesoporous silica nanoparticles (MSNs) Santa Barbara 15 (SBA-15) from 8.2 to 11.4 nm increased bovine serum albumin (BSA) loading efficiency from 15 to 27%. Moreover, Zhang et al. (2014) reported that silica vesicles presented an increase up to two times in ribonuclease (RNase) loading when the pore size increased from 3.9 nm to 6 nm.

Furthermore, the difference in the characteristics of mesoporous silica can affect the loading efficiency and release. For instance, MCM-48 is a mesoporous silica nanoparticle with a pore size of 3.7 nm, its pore structure is 3D-bicontinuous cubic, and the release is in first-order kinetics. SBA-15, on the other hand, has a 2D-hexagonal pore system with a size of 8.8 nm, and the release follows zero-order kinetics. Another factor that might indirectly affect protein loading is the temperatures in which silica carriers are produced. Peptide loading into mesoporous silica can be affected by the hydrothermal ageing temperature, which is used for silica gel ageing before calcination, as found by Qi et al. (2012). They reported that increasing the hydrothermal temperature increased pore volume, and the porous structure changed, affecting protein loading.

The solvent used in API loading plays a crucial role during formulation, as the solvent properties dictate the interactions between the solute and the mineral surface of the carrier (Charnay et al., 2004). For instance, choosing a suitable solvent is one of the most critical factors. It has been reported that using a polar solvent will decrease the loading of a hydrophobic API, as they will compete to interact with silica surfaces (He et al., 2017). Moreover, non-polar solvents are more suitable for loading hydrophobic APIs into mesoporous silica nanoparticles due to the formation of hydrogen bonds between the drug molecules and silanol groups (Hillerström et al., 2014). Additionally, Charnay et al. (2004) found that the polarity of the solvents affects the material adsorption on the surface of the silica-based carrier.

Furthermore, the protein concentration in the loading solvent can affect loading efficiency. For instance, the loading capacity of MSNs can increase to 80% compared to 10% upon increasing the drug concentration in loading solutions (Croissant et al., 2016). Additionally, the solubility of the drug in the loading solvent can affect the loading efficiency depending on the drug's properties, as good solubility indicates better interaction between the drug molecules and the solvent (Soltys et al., 2019).

As for protein properties, they can affect mesoporous silica loading, where large size, surface charge, and fragile tertiary structures reduce loading efficiency (Shi et al., 2019). Loading is highly affected by molecular size and surface charge. Small molecular-weight proteins can occupy the pores better than high molecular-weight ones, as small proteins can ingress internal surfaces, while large proteins are limited to external surfaces (Vidaurre-Agut et al., 2019). Concerning the molecule's charge, the surface of silica carriers is covered with Si–OH groups, which usually act as an adsorption site and provide the carrier with a negative charge. This facilitates the interaction with positively charged molecules based on electrostatic interactions. Nevertheless, negatively charged molecules can be loaded more efficiently when a chaotropic agent is applied when it screens the repulsion and allows higher loading (Mamaeva et al., 2013). Upon loading the protein into the carrier, the capping approach can control the release of biomolecules from MSNs. It includes utilising gate keepers that cap the mesopores in the structure and release the components upon interacting with a specific stimulus (Mekaru et al., 2015).

Once the silica-peptide complex has passed most of the GIT parts towards the intestines, it faces another barrier: absorption. The restricted absorption across the intestinal epithelium presents a significant barrier, where large molecules with lipophilic properties cross the intestinal barrier via the transcellular route. On the other hand, small molecules with hydrophilic properties cross via the paracellular route, which contains tight junctions (Shipp et al., 2022).

The process that affects the successful oral delivery of a silica-peptide complex is summarised in figure 4.1 below based on the process of formulation and administration.

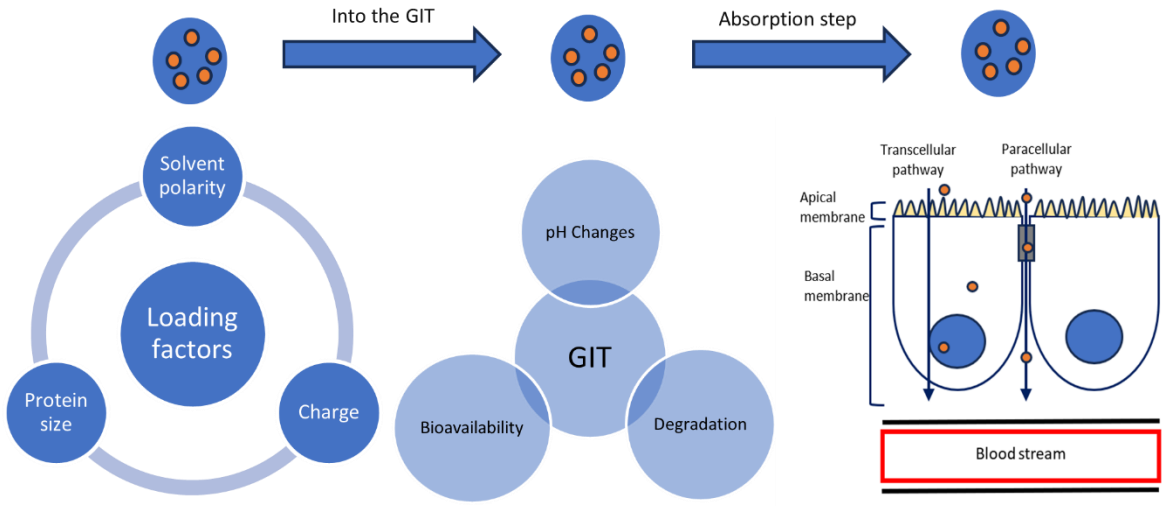

Figure 4.1. The process of delivering a successful silica-peptide complex orally with the affecting factors of each step: factors affecting silica loading (left), followed by the factors affecting the peptide (middle), and the absorption routes for peptides whether transcellular or paracellular (right). The blue sphere represents the silica carrier, while the small orange circle is the loaded peptide.

This chapter aims to formulate silica-protein complexes by loading a silica carrier with two different proteins via the solvent evaporation method. The silica is a mesoporous microparticle (SYLOID XDP 3050), and the two proteins are octreotide acetate and BSA, having different molecular weights: 1 kDa and 67 kDa for octreotide and BSA, respectively. The loading will be conducted using three solvents for both proteins: methanol, ethanol, and water.
Objectives are to:

- Evaluate the loading efficiency and investigate the factors that govern protein-silica loading.
- Assess the impact of the solvent viscosity, protein size, and polarity on loading.
- Quantify protein diffusion into SYLOID using confocal fluorescence microscopy.

4.1. Materials and methods

4.1.1. Materials

Ethanol absolute 99.8% (HPLC grade), methanol absolute 99.9% (HPLC grade), acetonitrile 99.8% (HPLC grade), and Bovine serum albumin (BSA) fraction V molecular weight 68 kDa were purchased from Sigma-Aldrich (Dorset, UK). Octreotide acetate lyophilised powder with a molecular weight of 1079.29 Da was purchased from Stratech (Cambridgeshire, UK). Polypropylene containers were purchased from Agar scientific (Essex, UK). Mesoporous silica SYLOID XDP 3050 (specific surface area of 310 m^2/g, average pore size of 22.4 nm, pore volume of 1.74 cm^3 /g) was kindly provided by W.R. Grace and Co (Worms, Germany).

4.1.2. Methods

4.1.2.1. Preparation of mesoporous silica-peptide complex formulations

Preparation of peptide-mesoporous microparticles was conducted through the solvent evaporation method using three solvents; water, ethanol, and methanol. Peptides were dissolved in the solvent at concentrations ranging between 0.5 – 2 mg/ml, followed by the SYLOID XDP 3050 addition to the mixture. The mixture was left on a magnetic stirrer for 2 hours while covered. The suspension mixture was transferred into a watch glass and left in the fume hood for the solvents to evaporate. After solvent evaporation, the samples were kept in plastic containers for post-formulation characterisation. The theoretical loading of both peptides to SYLOID was 5, 10, and 20% w/w.

4.1.2.2. Drug load quantification and recovery

Actual drug loaded was calculated using the same method in section 3.1.2.9.

4.1.2.3. HPLC methods for analysis

HPLC analysis for octreotide acetate was adapted from (Park and Na, 2008) and conducted using Agilent 1200 series at a UV wavelength of 280 nm. The column was a Gemini C18 (Phenomenex) with the following specifications: 150 mm, 4.5 mm, 5 µm, 110 Å. The injection volume was 50 µl at a flow rate of 0.8 ml/min. Mobile phases were: A (water + 0.1% TFA) and B (acetonitrile + 0.1% TFA) with analysis run time of 6 minutes. The concentration for the mobile phases starts at 70:30 A:B and decreases to 55:45 A:B at 3.6 minutes. Then, the concentration increases back to 70:30 A:B.

BSA analysis is adapted from (Umrethia et al., 2010) and was conducted using WATERS 2695 at excitation and emission wavelengths of 280 and 350 nm, respectively, and an injection volume of 100 µl. The column was Jupiter® C5 with the following specifications 5 µm, 300 Å, 4.6 mm , and 250 mm. Mobile phases were A (water + 0.1% TFA) and B (acetonitrile + 0.1% TFA) at a flow rate of 1ml/min, and the gradient was as follows: A:B from 95:5 to 35:65 in 20 min, followed by a 2-minute recovery to initial conditions. Both HPLC methods were validated according to ICH Q2R2 guidelines (EMA-ICH-Q2R2, 2023).

4.1.2.4. Solvent and loading phase viscosity calculation.

Viscosity of the loading solvents and the loading phase (solvent-protein) was calculated using a micro viscometer MicroVISC (RheoSence, USA). 50 µl Samples were taken using microVISC disposable pipettes (100 µl), and the used chip was A05 (microVISC Chip, 0-100 cP 50 µm flow channel). The sample runs were conducted at room temperature, with a cleaning cycle running after each formulation to rinse and dissolve any particulates. Each sample was run in triplicate, and results are presented as mean ± SD mPa.s.

4.1.2.5. Protein fluorescence intensity identification

Confocal microscopy (TCS SP8, Leica Microsystems, GmbH) was used for imaging. A 405 nm diode laser and a white light laser at 70% power were used to image fluorophores AlexaFluor 405 and AlexaFluor 532 for octreotide and BSA, respectively. The excitation and emission wavelengths for octreotide were 385 and 562 nm, while for BSA, they were 520-739 nm. For each channel, HYD detectors were used. A 20X dry APO lens was used for imaging, and all images were taken at 4096*4096 resolution with the imaging speed set at 100 Hz. The laser powers, gain, and emission wavelengths were kept consistent for quantification purposes. 3D image for the particle is taken, and the fluorescence intensity of the middle plane is calculated. The particle is divided into four sections; and the highest intensity value for each section is taken. Ten particles were imaged for fluorescence intensity, and the mean values were used for determining intensity value. For image analysis, LAS X 3.0 (Leica Microsystems GmbH) and Fiji (Schindelin et al., 2012) software was used.

4.1.2.6. Morphological properties of the formulations

Images were taken using the Environmental Scanning Electron Microscope mode of the ThermoFisher Scientific Quattro S microscope equipped with a field emission filament (FEG). The images were taken in low vacuum mode in variable pressure between 85 and 105 Pa, with an acceleration voltage of 3 kV and 3 -3.5 spot size.

4.1.2.7. Protein dispersions particle size analysis

Sympatec laser diffraction (Sympatec, Germany) was used to determine the particle size of the non-dissolved protein dispersions in loading solvents (ethanol and methanol). The instrument was equipped with a compact laser diffraction sensor HELOS/BR and CUVETTE wet dispersion system. CUVETTE 50 ml extension was used, and the R5 Fourier lens (f=100 mm) with a measuring range between 0.5 - 875 µm. 30 ml sample was used, and the run started at a trigger condition of ≥ 1% Copt (optical concentration) for 100 ms, where it was sonicated for 5 seconds at 100% power and stirred at 1200 rpm throughout the analysis. The median diameter (VMD) was recorded for all samples, in which all measurements were done in triplicate, reported as VMD (µm) ± SD. PAQXOS 5.0 was employed as the software results analysis.

4.1.2.8. Dynamic light scattering (DLS) analysis.

For the size analysis of the dissolved protein in the loading solvents, Dynamic light scattering (DLS) measurements was performed using the NanoBrook Omni from Brookhaven Instruments Corporation (Holtsville, NY, USA). Eppendorf disposable plastic cuvettes (#952010051) were used for analysis (Mississauga, ON, Canada). The apparatus was set to an angle of 90° at 25°C and the measurement time was 120 seconds with three measurements of each sample was taken, and the values were reported as the mean effective diameter (nm) ± SD.

4.1.2.9. Surface area and pore volume evaluation

The surface area and pore volume of the formulations were assessed similar to method in section 2.1.2.8. without the degassing step.

4.1.2.10. Fourier-transform infrared spectroscopy (FTIR)

The molecular inetarctions were assessed using same method from section 2.1.2.5.

4.1.2.11. Statistical analysis

Statistical analyses of data were assessed using same methos in section 2.1.2.10.

4.2. Results and discussion

4.2.1. Actual drug load quantification and recovery

Actual drug load quantification of both molecules in their respective solvents was investigated via HPLC, where figure 4.2 below identifies the recovery percentage from octreotide and BSA silica complexes.

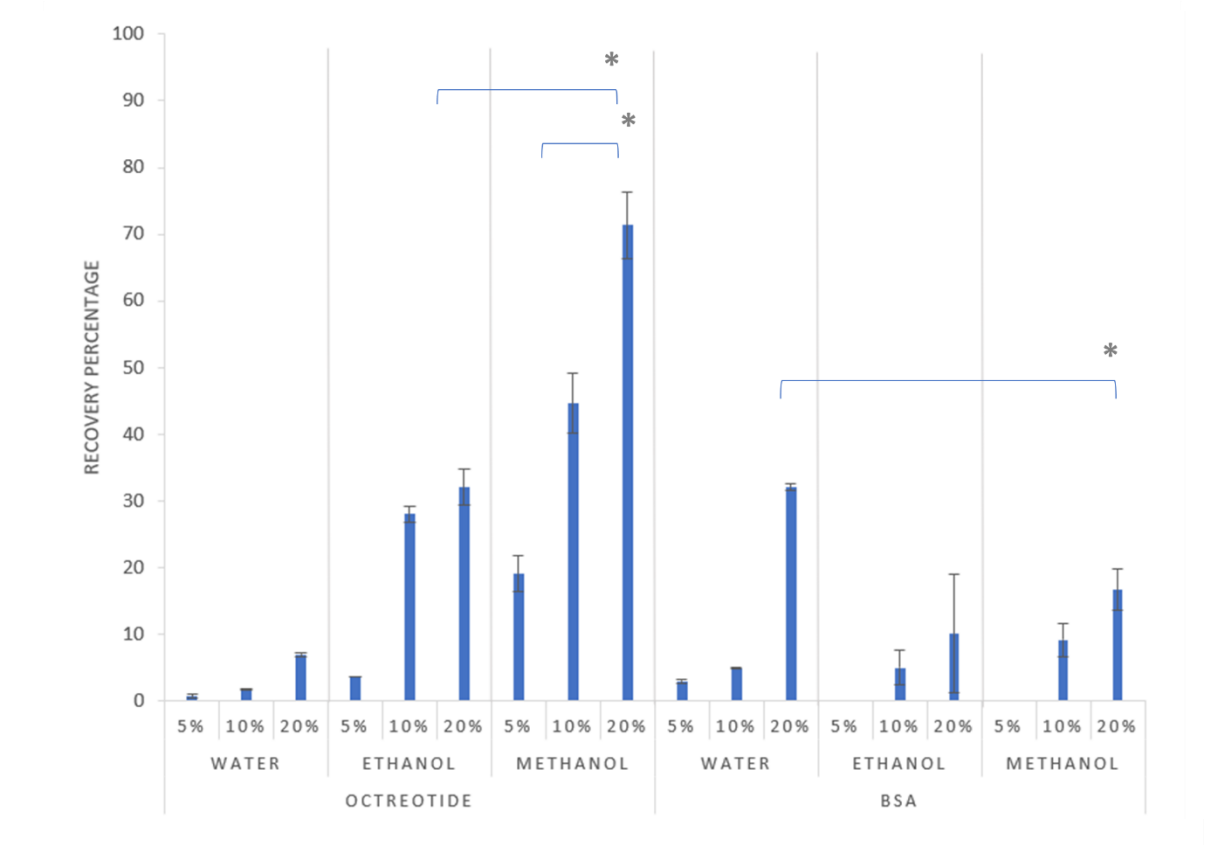

Figure 4.2. Recovery percentage of formulations after 2 hours at different theoretical loadings, 5%, 10%, and 20% drug load respectively for each solvent, with error bars representing standard deviation and (*) representing significant difference ($p<0.05$).

As seen from figure 4.2 above, octreotide's recovery percentage increases as the drug concentration increases in the loading solvents, with the lowest recovery associated with water at the initial loading concentration 5% (w/w). However, upon using methanol as the loading solvent, the recovery was 19, 44, and 71% for concentrations 5, 10 and 20% w/w, respectively, as the higher concentration significantly increased the recovery percentage ($p < 0.05$). Moreover, ethanol presented a similar pattern for the loading concentration-recovery relation, where the highest recovery was 32% when the loading concentration was 20%. These

differences are related to the difference in solubility of octreotide in the three solvents, which is addressed in section 4.2.2.

As for BSA, the recovery seems lower in comparison to octreotide results, as the highest achieved recovery (32%) is associated with the sample being dissolved in water at a concentration of 20% w/w. The recovery of BSA in the three solvents followed a similar pattern to octreotide, where the recovery percentage increased as the loading concentration increased, which significantly increased the recovery percentage ($p < 0.05$). Though, upon using methanol and ethanol as the loading solvents, the recovery was 0% at an initial loading concentration of 5%. The highest recovery for both solvents is 16% and 10% for methanol and ethanol, respectively. The differences in recovery are related to several factors including solvent properties, the API's molecular size and solubility in the loading solvent, and diffusion-related factors.

4.2.2. Effects of solvent polarity and protein solubility on loading

The solvent used in API loading plays a crucial role during formulation, as the solvent properties dictate the interactions between the solute and the silanol groups on the surface of the carrier (Charnay et al., 2004).

The used solvents have different polarities, which are 10.2, 5.1, and 4.3 for water, methanol and ethanol, respectively (Fishersci-polarity, 2023). In addition, silica surfaces are negatively-charged and polar due to the presence of hydroxyl groups on the surface that are crucial in interaction with the solvent upon loading (Yildirim et al., 2013). Moreover, Octreotide acetate has 14 hydrogen bond donors and 16 hydrogen bond acceptors, which will cause water molecules to compete with octreotide to interact with the polar surface of silica and form hydrogen bonds with the negatively charged silanol groups. Thus, decreasing the loading efficiency as a result. Methanol, on the other hand, is less polar than water, which will cause octreotide to form more hydrogen bonds with the silanol groups and enhance the loading efficiency (Hillerström et al., 2014). In addition, the solubility of octreotide in methanol is higher than in water (LAMBERT et al., 2003), which might affect the loading since it is based on reaching the equilibrium state followed by the solvent evaporation, leaving the drug inside the pores (Koch et al., 2022). As for samples loaded with ethanol, the low recovery is related to the solvent's weak hydrogen bonding abilities and the interactions between silanol groups on the surface, which decreases loading efficiency (Raghavan et al., 2000).

BSA samples, on the other hand, presented lower recovery compared to octreotide samples. The low values are attributed to several factors including protein aggregation, loading viscosity, solubility, protein molecular size and diffusion, which is the most prominent factor. However, the recovery was lower for methanol and ethanol than their counterpart in water-based loading, where it was 32%, 10%, and 16% for water, ethanol, and methanol, respectively. This is related to the low solubility of BSA in both ethanol and methanol compared to water, where the solubility of BSA in alcohol-based solvents decreases as the solvent concentration increases (Yoshikawa et al., 2012). Besides, ethanol causes BSA aggregations due to the strengthened electrostatic interactions enforced by the solvent (Kayser et al., 2020).

Additionally, ethanol can cause protein aggregation by disrupting hydrophobic interactions due to a lower dielectric constant of 25 compared to 80.4 of water (Feng et al., 2022, Mohsen-Nia et al., 2010, De Sousa et al., 2017). The aggregation can also be caused by structural perturbations, which expose aggregation-prone sequences and force them to associate with other proteins to form non-native dimers, usually described as nucleation or the initial aggregation event. The previous changes are induced by solvent-caused undesired

conditions, e.g., organic solvents, where ethanol and methanol are used in this case. In addition, another factor that might lead to aggregation is protein-protein interaction, which is a concentration-dependent factor. This is related to the decreasing average inter-protein distance upon increasing the protein concentration, thus, crowding proteins (Wang and Roberts, 2018). The previous findings are related to the decrease in recovery for BSA formulations in both ethanol and methanol-based loading.

Other factors contributing to differences in loading and recovery include; viscosity, diffusivity, and protein molecular size.

4.2.3. Effects of viscosity and protein size on diffusivity

Carrier loading is associated with the API molecules diffusing into the porous structure, which is governed by the Stokes-Einstein equation (Equation 4.1) where the particles are spherically shaped (Thompson and Williams, 2021).

$$D_0 = \frac{k_B T}{6\eta\pi R_m}$$

Equation 4.1. Stokes-Einstein equation.

Where K_B is the Boltzmann constant, T is temperature, η is the viscosity, and R_m is the solute radius. The previous equation can be used to determine protein diffusivity in solutions (Lu et al., 2011), where it is disproportional to the radius and viscosity. According to Erickson (2009), the protein radius (R_m) can be acquired upon assuming that it will take a spherical shape by calculating the occupied volume by protein mass (V) as seen in equation 4.2:

$$V = 1.212 * 10^{-3} * M$$

Equation 4.2. The occupied volume by protein mass.

Where M is the molecular weight in Da. After calculating the protein mass, R_m can be calculated as seen in equation 4.3 below:

$$R_m = \sqrt[3]{(\frac{3V}{4\pi})}$$

Equation 4.3. Equation 4.3. Protein molecule radius.

The viscosity of the solvents was 0.55, 0.89, and 1.096 mPa.s for methanol, water and ethanol, respectively (Thompson et al., 2006, Gonçalves et al., 2010). As mentioned above, the viscosity of the loading solvent affects the mass transfer between the solvent and the loaded system. Moreover, the viscosity of the loading phase was calculated and the results are presented in table 4.1 below.

Table 4.1. Dynamic viscosity values of the loading solvents containing BSA and octreotide at different loading concentrations.

Dynamic Viscosity (mPa.s)						
Concentration	Octreotide			BSA		
	Water	Methanol	Ethanol	Water	Methanol	Ethanol
5% w/w	1.12 ± 0.00	0.69 ± 0.00	1.27 ± 0.01	1.12 ± 0.04	0.7 ± 0.01	1.3 ± 0.00
10% w/w	1.08 ± 0.01	0.65 ± 0.01	1.26 ± 0.02	1.32 ± 0.01	0.71 ± 0.00	1.34 ± 0.03
20% w/w	1.11 ± 0.00	0.68 ± 0.02	1.26 ± 0.01	1.37 ± 0.04	0.71 ± 0.01	1.3 ± 0.01

By applying equations 4.1 and 4.2, the radius for BSA and octreotide will be 2.69 and 0.67 nm, respectively, and the diffusivity values are presented in table 4.2:

Table 4.2. BSA and octreotide diffusivity values (m^2/s) in loading solvents.

Solvent	Octreotide	BSA
Methanol	$5.92*10^{-10}$	$1.47*10^{-10}$
Water	$3.66*10^{-10}$	$9.13*10^{-11}$
Ethanol	$2.97*10^{-10}$	$6.73*10^{-11}$

As seen from tables 4.1 and 4.2 above, octreotide's diffusivity in methanol is the highest ($5.926*10^{-10}$ m^2/s), which is related to the viscosity of both methanol and methanol-octreotide phase as well as the high solubility of octreotide (40 mg/ml). As for BSA, the diffusivity is the lowest when ethanol is the loading solvent ($6.731*10^{-11}$ m^2/s). This is related to the low solubility of BSA in ethanol as well as the large radius (2.69 nm). These findings support the HPLC recovery results, where octreotide formulations with methanol had the highest recovery percentage.

The protein dispersions in the loading solvents were analysed using laser diffraction and dynamic light scattering for dissolved proteins (octreotide in all solvents and BSA in water) to investigate protein aggregation further.

Octreotide acetate has dissolved completely in the three solvents, which aligns with its high solubility (LAMBERT et al., 2003). As for BSA, it has dissolved in water, which is expected, considering its high solubility in water (Masuelli, 2013). However, BSA did not dissolve in both methanol and ethanol regardless of its concentration, and the particle size was 223.63 and 231.06 µm in ethanol and methanol, respectively. This supports the aggregation of BSA in

high concentrations and the HPLC results, where the recovery of 5% loading w/w for was 0% and for 20%, it was 10% and 16% for ethanol and methanol, respectively (Molinier et al., 2021).

FTIR was used to determine the molecular interactions and the presence of both proteins.

4.2.4. Molecular interactions of SYLOID-proteins

The FTIR spectrum for both octreotide and SYLOID has been discussed previously in sections 2.2.1. and 3.2.3.

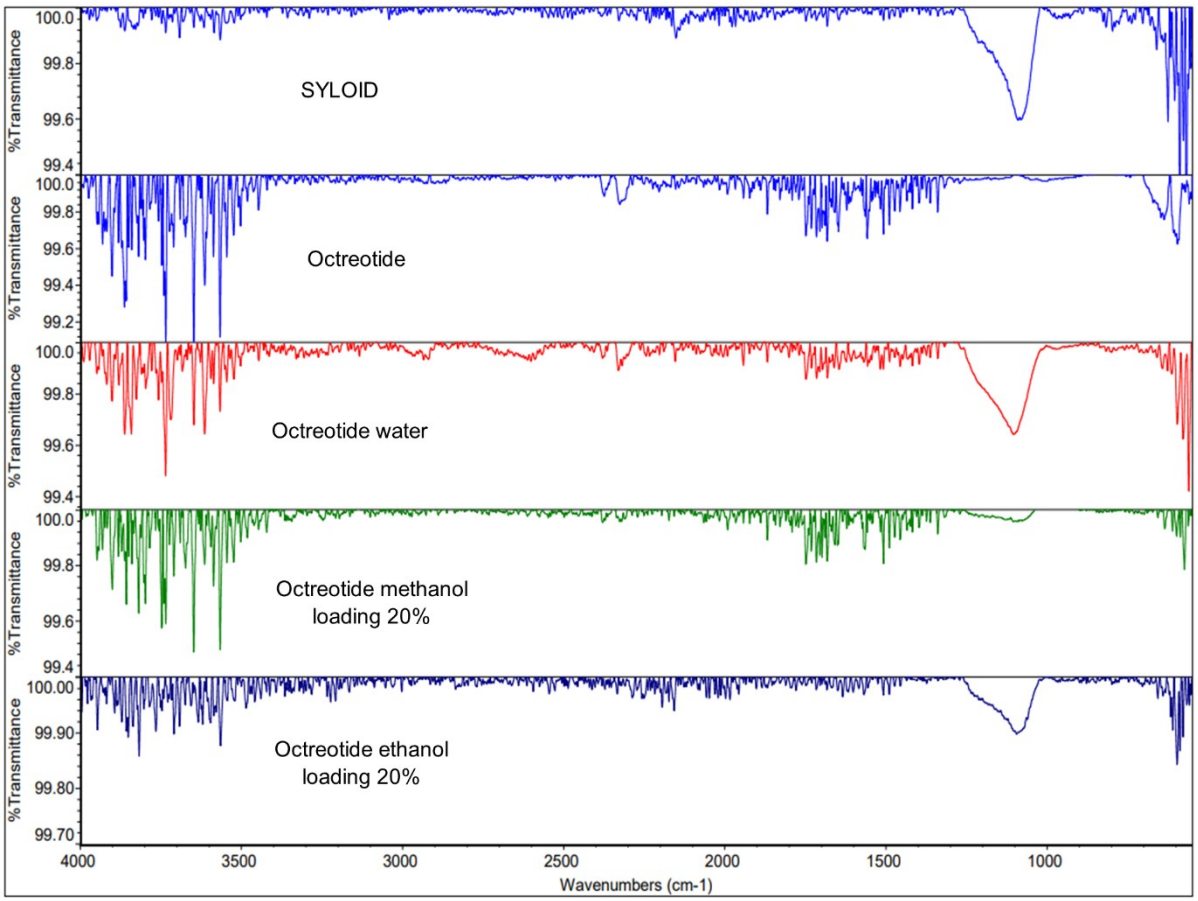

Figure 4.3. FTIR spectrum of octreotide-silica formulations for the three solvents at a loading concentration of 20% w/w.

The presence of the amino groups at 3500 cm^{-1} specifies the presence of octreotide in the three formulations. Moreover, the decrease in intensity of the broad band at 1075 cm^{-1} for methanol-based samples indicates an interaction between the siloxane groups and octreotide that could have masked the signal. This further supports that octreotide has diffused and formed new bonds with siloxane groups from methanol more efficiently than ethanol and water.

As for BSA samples (figure 4.4), the carbonyl group corresponds to a strong peak at 1650 cm^{-1}, while the bands at around 1375 and 1450 cm^{-1} correspond to CH and CH2 (Shourni et al., 2022). Moreover, the stretching of the amide bond at 1670 cm^{-1} indicates that BSA had adsorbed on the surface of the silica carrier.

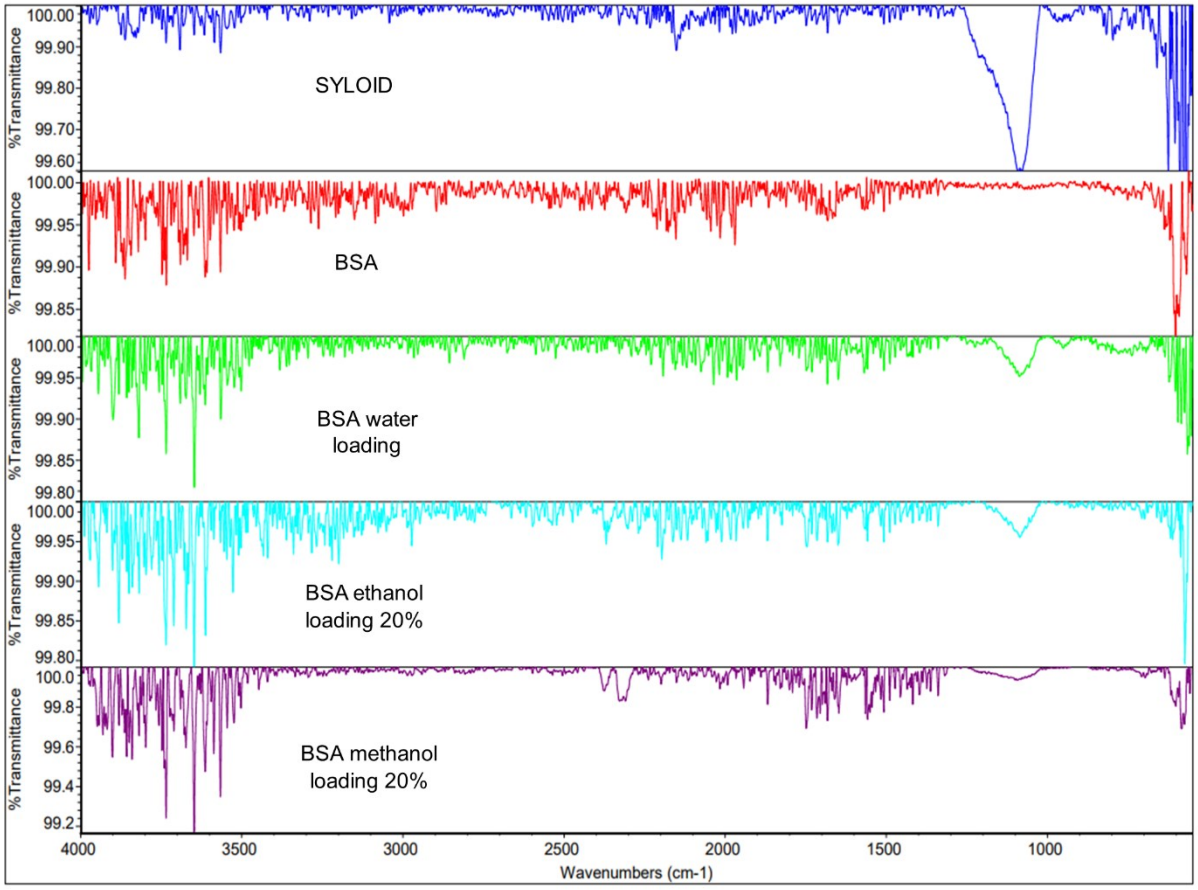

Figure 4.4. FTIR spectrum of BSA-silica formulations for the three solvents at a loading concentration of 20% w/w.

The previous results showcase protein presence on the carrier. However, the efficiency of loading and protein diffusion into SYLOID was not determined. Therefore, fluorescence confocal microscopy was used to determine the previous points.

4.2.5. Fluorescent properties of proteins and diffusion into silica carrier

Confocal microscopy has been reported to study the diffusion of proteins into silica carriers based on fluorescence intensity as reported by Lu et al., 2011. Therefore, fluorescence imaging has been used. The presence of tryptophan in the structure of both BSA and octreotide has assisted in identifying fluorescence due to its presence in both proteins (Sy et al., 2001, Vivian and Callis, 2001). Figure 4.5 (A-C) shows plain SYLOID, octreotide and BSA, respectively, where SYLOID presents no fluorescence while octreotide (blue) and BSA (green) are fluorescent.

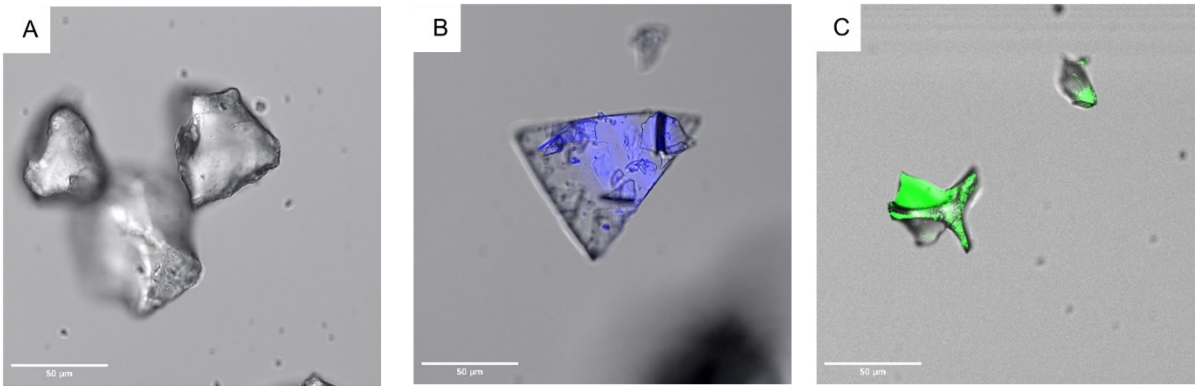

Figure 4.5. Fluorescence behaviour of peptides and silica via confocal microscopy where (A): SYLOID XDP, (B): octreotide, (C): BSA.

Figure 4.6 below presents the surface fluorescence of all formulations. It can be seen that octreotide samples (A-I) tend to present more surface fluorescence compared to BSA (J-R). Moreover, octreotide samples prepared with methanol had a higher fluorescence than those prepared with ethanol and water, which can be seen in 4.6 (A-C) compared to 4.6 (D-F) and 4.6 (G-I). In addition, surface fluorescence seems to increase as the loading concentration increases. For instance, octreotide loaded in methanol at a loading concentration of 20% w/w (A) presents higher surface fluorescence in comparison to lower loading concentrations: (B and C). Moreover, octreotide loaded via water had the lowest surface fluorescence properties (G-I), with 5% loading presenting the lowest fluorescence amongst octreotide formulations (I).

As for BSA, BSA samples seem to have lower surface fluorescence (4.6 J-R) compared to octreotide samples. Furthermore, it seems that the protein is concentrated on the sides of the silica carrier, and the fluorescence intensity decreases with the decrease in loading concentration (J-I). These results might offer an initial insight into the interaction between the protein and SYLOID. To further study the diffusion of proteins into silica carriers and evaluate the efficiency of the process, 3D imaging was implemented, and the middle plane fluorescence

intensity was assessed. Figures 4.7 and 4.8 below present the fluorescence intensity values of the middle plane across the particle.

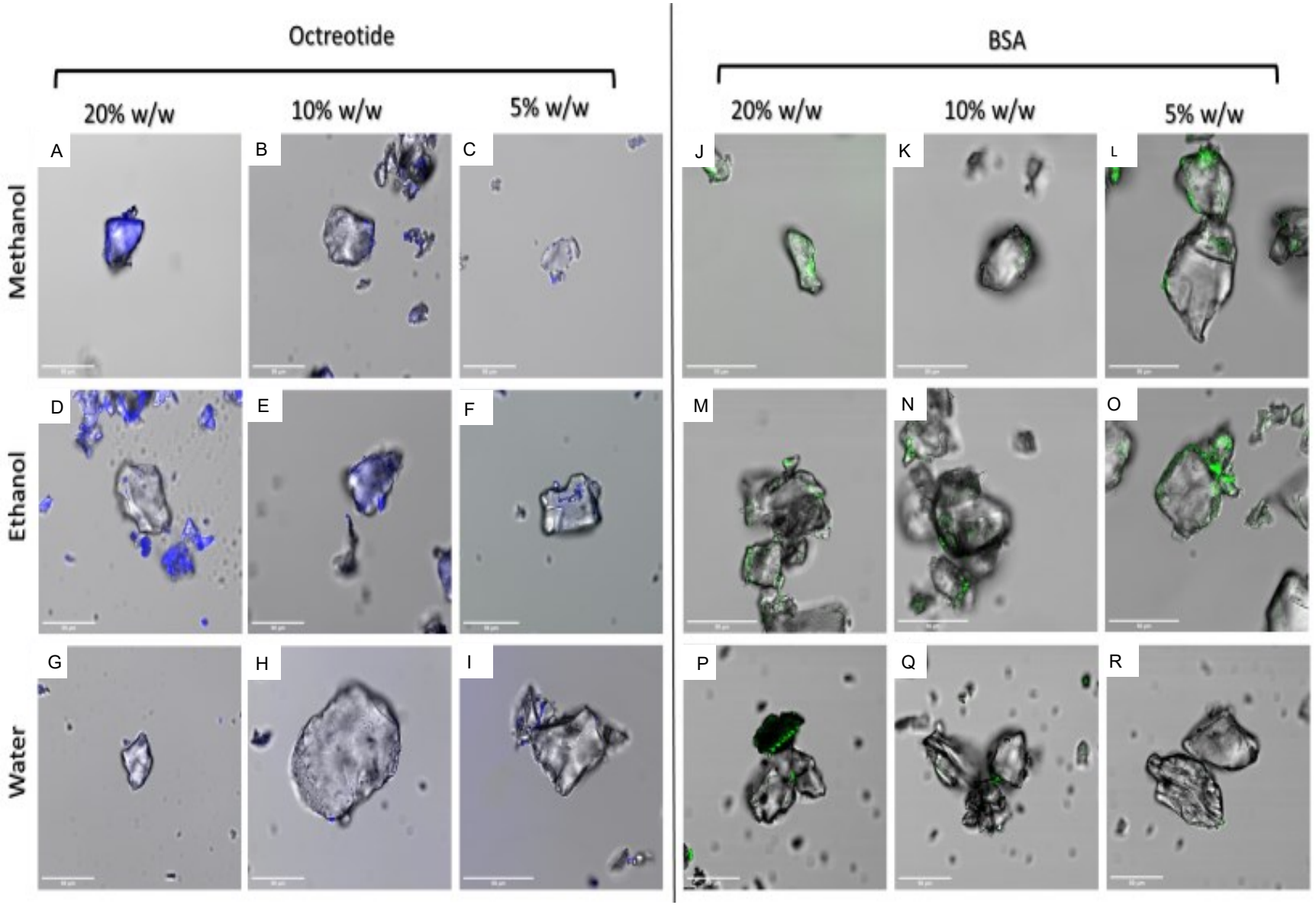

Figure 4.6. Fluorescence properties of silica-peptide formulations. octreotide loaded in methanol (A: 20% loading, B: 10% loading w/w, C: 5% loading w/w), ethanol (D: 20% loading, E: 10% loading w/w, F: 5% loading w/w), water (G: 20% loading, H: 10% loading w/w, I: 5% loading w/w), BSA loaded in methanol (J: 20% loading, K: 10% loading w/w, L: 5% loading w/w), ethanol (M: 20% loading, N: 10% loading w/w, O: 5% loading w/w), and water (P: 20% loading, Q: 10% loading w/w, R: 5% loading w/w).

As seen in Figure 4.7 upon using methanol as the loading solvent, octreotide diffused equally into all parts of the silica particle at 20% w/w (A). Upon decreasing the loading concentration, the fluorescence intensity decreases but maintains a thorough diffusion into the carrier (B-C). However, upon using ethanol and water, octreotide seems to have inhabited the sides of the carrier with a low diffusion manner regarding the loading concentrations. In addition, water presents very low diffusion into the carriers' centre when the loading concentration is 5% w/w. The difference in diffusivity is related to the solvent viscosity and the peptide solubility. For instance, methanol has the lowest viscosity and presents the highest diffusivity, as calculated above ($5.926*10^{-10}$ m^2/s), compared to water ($3.662*10^{-10}$ m^2/s) and ethanol ($2.973*10^{-10}$ m^2/s). Additionally, it has been reported that octreotide has a solubility of 40, 10.04, and 28.85 mg/ml in methanol, ethanol and water, respectively (LAMBERT et al., 2003). The low solubility of octreotide in ethanol and the highly polar properties of water will affect the loading efficiency. These results further support the recovery results, where methanol presented the higher percentage at 20% loading w/w, while water at a loading concentration of 5% presented the lowest recovery (3%)

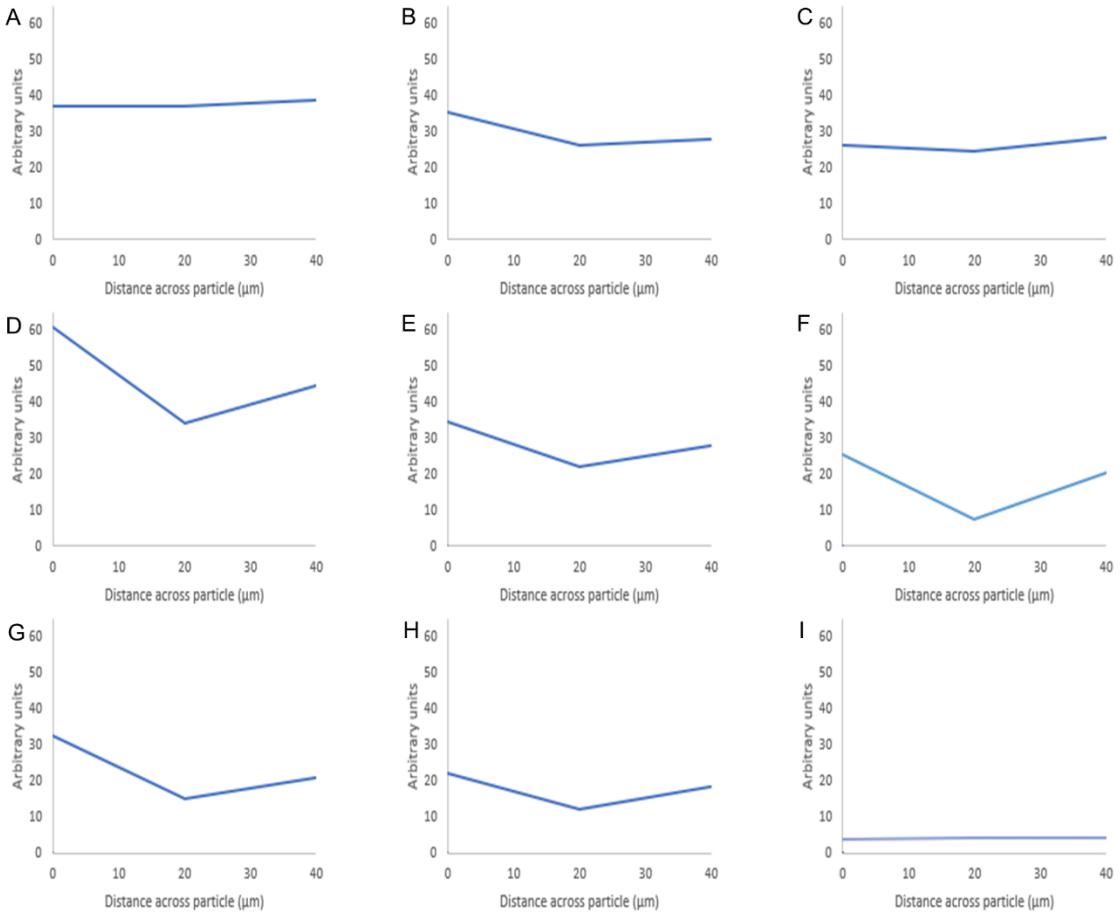

Figure 4.7. Fluorescence intensity values of octreotide-silica formulations. The intensity value for each particle is the average intensity of 10 particles where the (Y) axis represents the arbitrary units and the (X) axis resembles the distance taken across the middle plane of the particle after 3D imaging. The first row presents methanol-based loading: 20% w/w (A), 10% w/w (B), 5% w/w (C), while the second row presents ethanol-based loading: 20% w/w (D), 10% w/w (E), 5% w/w (F), and the third row is water-based loading 20% w/w (G), 10% w/w (H), 5% w/w (I).

As for BSA, the protein seems to be present on the edges as fluorescence intensity values are high around the particle's sides. This is apparent for the three solvents as the protein seems to occupy mainly the edges upon loading using ethanol at a 20% w/w (G). The protein's presence on the edges is related to the low solubility in ethanol and methanol and the effects of the previous solvents on its aggregation as mentioned above. In addition, the larger radius of BSA (2.69 nm) compared to octreotide (0.67 nm) contributes to these observations as BSA would struggle to occupy SYLOID's non-ordered pores.

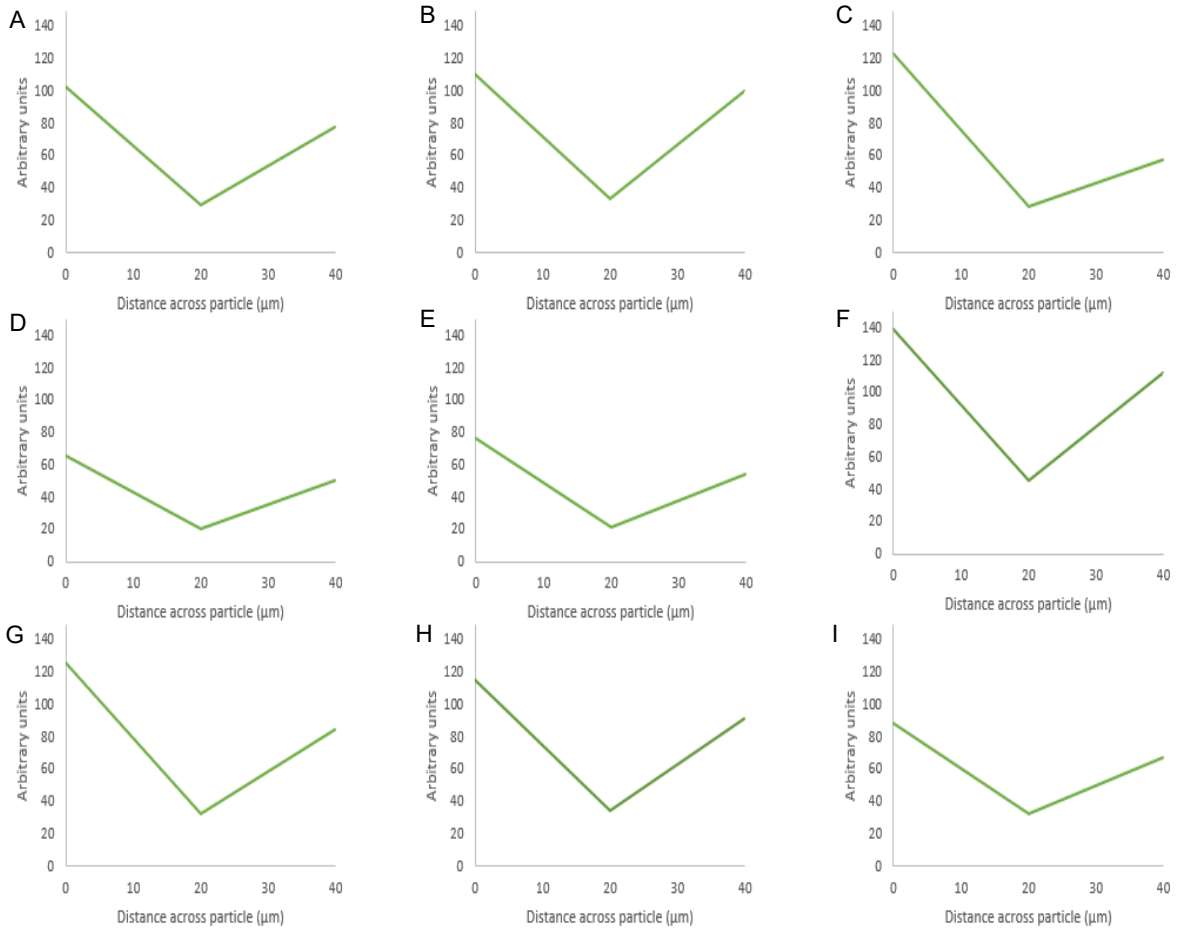

Figure 4.8. Fluorescence intensity values of BSA-silica formulations. The intensity value for each particle is the average intensity of 10 particles where the (Y) axis represents the arbitrary units and the (X) axis resembles the distance taken across the middle plane of the particle after 3D imaging. The first row presents methanol-based loading: 20% w/w (A), 10% w/w (B), 5% w/w (C), while the second row presents ethanol-based loading: 20% w/w (D), 10% w/w (E), 5% w/w (F), and the third row is water-based loading 20% w/w (G), 10% w/w (h), 5% w/w (I).

These findings support the results presented earlier regarding the recovery percentage where octreotide formulations and especially methanol-based loading, had the highest recovery. Nitrogen porosimetry was used to further corroborate how proteins occupy the carrier, which is explained in the following section (4.2.6).

4.2.6. Effects of loading parameters on surface area and pore volume

Surface area and pore volumes were calculated for the peptide-silica formulations to assess the effects of loading solvent and concentration on them. Table 4.3 below presents the surface area and pore volume of the formulations.

SYLOID XDP 3050 is a non-ordered mesoporous silica carrier that has a multi-directional and non-uniform pore structure. It has a pore volume of 1.75 cc/g and a surface area of 285 m^2/ g, supported by literature (Waters et al., 2018). Moreover, the porous network is non-homogenous and contains interconnected pores (Hussain et al., 2017, Baumgartner and Planinsek, 2021). The table below shows that the pore volume decreases as the loading concentration increases for all solvents. In addition, for octreotide-based formulations, the lowest pore volume corresponds to methanol loading at 20% w/w, meaning that the drug has occupied the porous structure more efficiently than other solvents. Furthermore, the low pore volume of methanol loading samples supports the fluorescence intensity results, where the protein has diffused evenly into the carrier. In addition, the highest calculated pore volume corresponds to the water-based formulation at a loading concentration of 5%. This is related to the polar properties of water and the competition with octreotide to interact with the silica groups on the surface. Additionally, the surface area decreases with the increase in loading concentration, which might be related to the protein adsorption on the silica surface.

As for BSA samples, BSA loaded in methanol at 5% w/w presented the highest pore volume of 1.71 cc/g, as it is related to the low amount of the drug inside the silica carrier. However, the lowest pore volume is related to water-based loading at 20% w/w, which contributes to the drug inside the porous structure. In addition, ethanol-based loading formulations presented a similar observation where the pore volume decreased as the loading concentration increased. Even though BSA has very low solubility in ethanol, some crystals might inhabit the porous structure of SYLOID and decrease the pore volume. The surface area results present a similar pattern to octreotide's formulations, where it decreases as the drug loading concentration increases, which might be related to the drug adsorbing on the surface and decreasing the surface area.

Table 4.3. Surface area and pore volume of peptide-silica formulations

Loading solvent	Initial loading Concentration (w/w)	Octreotide		BSA	
		Surface area (m^2/g)	Pore volume (cc/g)	Surface area (m^2/g)	Pore volume (cc/g)
Water	5%	283.89	1.77	229.82	1.38
	10%	258.18	1.48	210.62	1.31
	20%	208.22	1.41	170.82	1.17
Methanol	5%	224.87	1.42	271.09	1.71
	10%	231.61	1.38	246.40	1.36
	20%	203.53	1.20	193.02	1.48
Ethanol	5%	225.80	1.38	216.98	1.44
	10%	211.38	1.35	245.20	1.43
	20%	217.55	1.24	215.16	1.24

Following the analysis of the surface area and pore volume, SEM imaging was implemented to elaborate on protein adsorption on the carrier's surface and the changes to its morphological properties.

4.2.7. The morphological properties of the carrier and the peptide silica complex

The formation of crystals on the silica carrier and the difference in morphological features can be seen in figure 4.9 (A-H), where silica (A and B), octreotide (C) and BSA (D) were imaged as reference for comparison.

SYLOID 3050 is a non-ordered mesoporous silica where the pore size varies between particles (A). Also, the particle's surface is usually smooth (B). Octreotide acetate presents crystal morphology under the microscope (C), compared to the large crystals of BSA (D), which is supported by literature (Majorek et al., 2012).

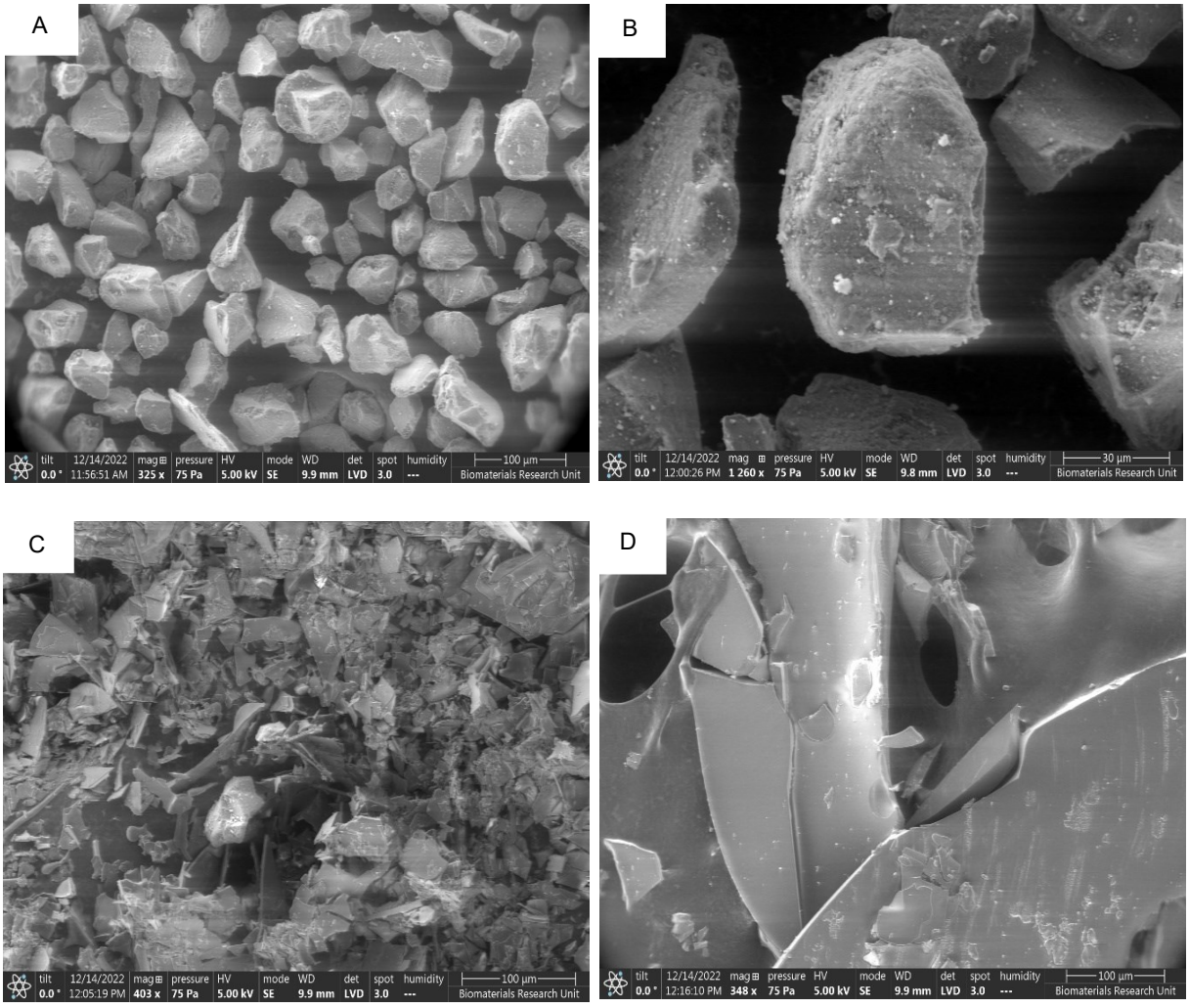

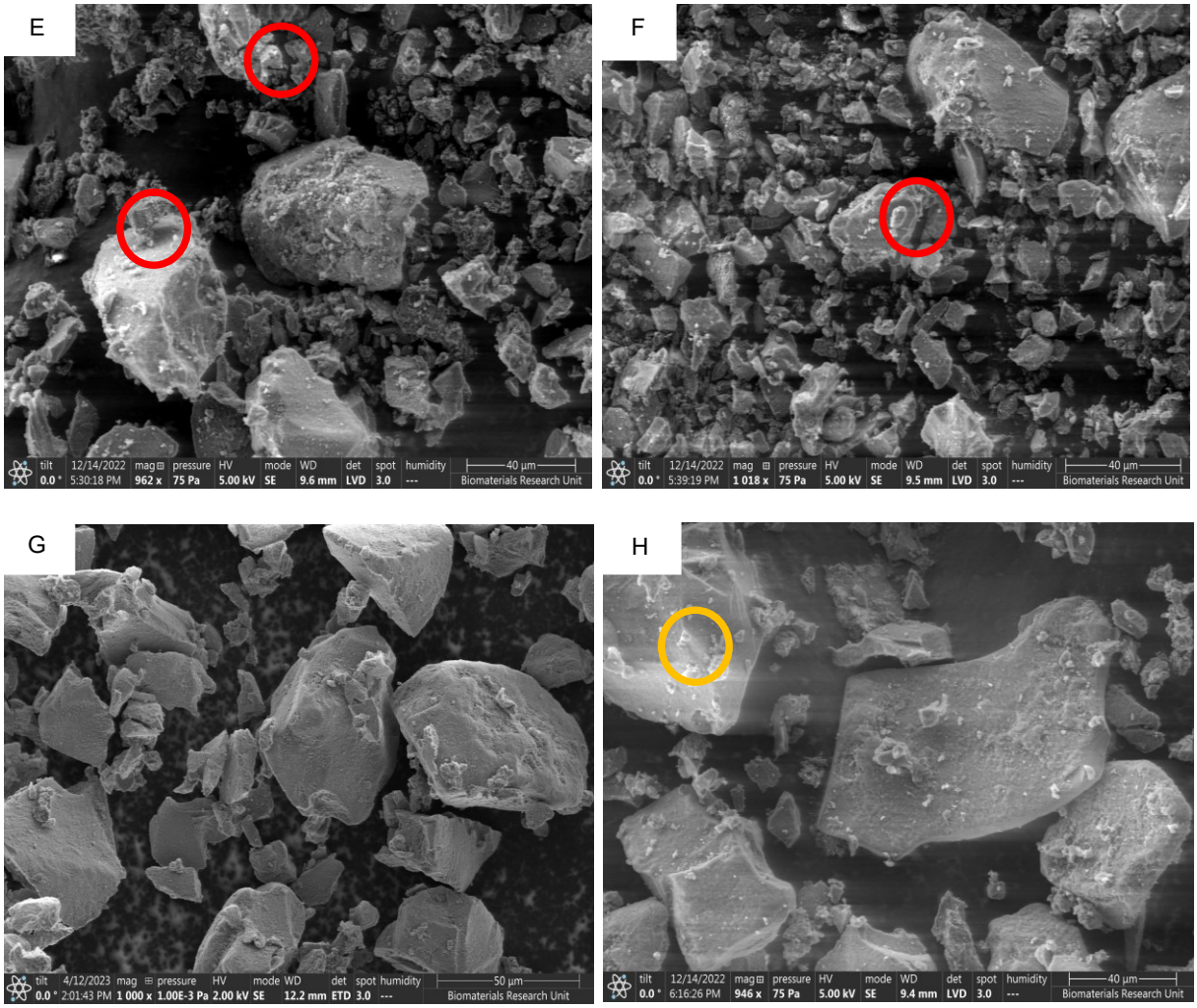

*Figure 4.9. SEM images of different peptide-silica complexes identifying the surface morphology and protein crystal adherence. SYLOID XDP 3050 low magnification (A), and high magnification (B), octreotide acetate (C), BSA (D), octreotide 20% w/w in methanol (E), octreotide 20% w/w in ethanol (F), octreotide 20% w/w in water (G), and BSA 20% w/w in water (H). The red and orange circles are highlighting protein crystals adhering on the surface for octreotide and BSA. * BSA samples in methanol and ethanol were not imaged due to the low solubility of the protein in both solvents.*

Figures 4.9 E, F, and G represent octreotide 20% w/w loading in methanol, ethanol and water, respectively, while H is BSA 20% w/w loading in water. As seen from the figures above, in comparison to the plain carrier (B), small crystal structures seem adhered on the surface of SYLOID' surface in 4.9 E and F (red circles), while G does not. This is related to octreotide crystalising on the surface from both methanol and ethanol due to the low polar properties of both solvents compared to water (G). These crystal-like structures could have contributed to the high recovery from both solvents, as discussed earlier, where water presented the lowest value. These findings further support the fluorescence intensity results, where water-based loading presented the lowest fluorescence intensity. On the other hand, BSA formulation (H) contains small crystals that adhere to the surface (orange circle), which might be related to the small amount of BSA being adsorbed.

Conclusions

This chapter reports the formulation of silica-protein complexes using mesoporous silica microparticles (SYLOID) and two proteins with different molecular weights (BSA and octreotide).

Both proteins were loaded into the silica carrier via a solvent evaporation method in different loading concentrations and solvents with varying polarities (methanol, ethanol, and water). The highest recovery (71%) was associated with octreotide loaded in methanol at 20% w/w, while the lowest (0%) is related to BSA loaded with ethanol and methanol at 5% w/w. This is attributed to the polarity of the solvents, viscosity, solubility, and protein molecular weight.

Octreotide solubility was the highest in methanol and the lowest in ethanol, where the solubility in methanol assisted in loading. In addition, the loading phase viscosity contributed to loading as the diffusivity is disproportional to viscosity according to the Stokes-Einstein equation. Furthermore, BSA did not dissolve in methanol and ethanol and produced large aggregates that were analysed using laser diffraction where their size was in the micro range (231.06 μm).

The molecular size of the protein has affected the loading efficiency as diffusion is also disproportional to the molecular size. BSA's molecule radius was calculated to be 2.69 nm, while octreotide's is 0.67 nm. Upon calculating the diffusivity of the proteins, the highest diffusion value was related to octreotide in methanol, while the lowest was BSA in ethanol.

The diffusion of proteins was further characterised using fluorescence imaging via confocal microscopy. The method involved generating 3D images of the silica-protein particle and assessing the fluorescence intensity of the middle plane. The results showed that octreotide had diffused evenly into SYLOID's porous structure, and its diffusion efficiency was concentration-dependent. Upon using ethanol and water, the diffusion decreased and became more centred around the edges of the particle, with the lowest being in water at 5% w/w, which supported the recovery and diffusivity values. As for BSA, the protein was centred around the edges of the carrier regardless of the solvent. This is related to the large radius of BSA, which hinders the molecules from entering the porous structure and the low solubility in both ethanol and methanol.

The pore volume and surface area of the silica-protein complexes were analysed using nitrogen porosimetry to support previous findings. The results showed that increasing the loading concentration has decreased the pore volume and the surface area, which is related to the protein being incorporated inside the silica carrier as well as crystallising on the surface. Additionally, the lowest pore volume for octreotide samples correlates to the 20% w/w

methanol loading, and the highest was with 5% in water. This further supported our previous findings, which showed that octreotide in methanol diffused more efficiently and occupied the porous structure. Additionally, in BSA-based formulations, the largest pore volume was associated with methanol loading at 5% w/w, while the smallest was for the formulation made with water at 20%.

SEM was used to study the morphology of both SYLOID and the formulations. The images showed that at loading concentrations of 20% w/w for octreotide, the protein seemed to crystallise on the surface of the silica carrier. However, this observation was not evident in water-based loading due to the low diffusion of octreotide into SYLOID based on the abovementioned reasons. Furthermore, BSA also seemed to crystallise on SYLOID's surface, as it is related to the protein not being able to penetrate the porous structure as much as octreotide.

Based on the aforementioned findings, the next chapter will focus on designing tablets using a mesoporous silica-protein complex. This complex will be made according to what has been reported here. Additionally, the next chapter's work will focus on overcoming the barriers to silica tabletting.

Chapter 5

Designing and Characterising of Mesoporous Silica-Protein-Based Tablets for Oral Delivery

Introduction

Tablets are the most common drug delivery systems (DDS) due to their easy manufacturing, as they are acquired through several techniques, including dry compression (DC) and granulation. However, despite the feasibility of direct compression and the reduced costs since no additional step is included, like granulation, less than 20% of products are manufactured using this method (Fayed et al., 2022). This is because both the active pharmaceutical ingredients (API) and the excipients should possess good compactability and compressibility properties to be considered for this approach (Fayed et al., 2022, Sohail Arshad et al., 2021, Choi du et al., 2013). Therefore, many additives and carriers are included in the powder mixture for tabletting to enhance the product properties.

Drug carriers and excipients in the pharmaceutical industry have undergone significant advancements, leading to the utilization of various types. Inorganic-silica-based carriers provide a suitable candidate for drug delivery since they are biocompatible and nontoxic (Wu et al., 2007).

The use of silica in the pharmaceutical industry can take many forms. For instance, they are used in tablets to improve compactability by increasing the surface roughness of the particles, which increases bonding strength (Qu et al., 2017). In addition, using colloidal silica has been widely reported in the literature for improving powder flowability. Nano-sized silica is used in formulations, where they are arranged on the diluent surface. This arrangement decreases the surface area of the interparticle contact between the diluent particles, reducing electrostatic interactions, and thus enhancing the powder mix's flowability and tablet properties (Tran et al., 2019).

Furthermore, tablets made with silica-based mesoporous carriers have been reported in the literature. For example, Parekh et al. (2023) reported the use of SYLOID 244 (mesoporous silica microparticle) as a glidant to reduce tablet sticking on the punch. They found that using SYLOID at a concentration of 2% has significantly reduced tablet sticking. In addition, Kunnath et al. (2018) found that using nano silica as an excipient for dry coating a cohesive API can enhance tabletting properties by facilitating the rearrangement of particles during compression, where the interparticle forces are decreased.

Furthermore, the tablet disintegration can be increased by mesoporous silica addition as the porous carrier coats the other excipients in the formulation. This reduces their adherence and aggregation and allows capillary wetting. In addition, it absorbs more significant amounts of water compared to non-porous carriers, which facilitates additional interactions between the

powder particles and the dissolution medium, resulting in an enhanced disintegration (El-Setouhy et al., 2015).

Using mesoporous silica-based carriers as excipients for tablet manufacturing has been reported where the mesoporous carrier is used as the carrier for the API, rather than an additive for enhancing flow properties. However, many factors affect the final tablet properties that are related to silica addition. These factors include the amount of silica, diluents presence in the formulation, size of silica, and the carrier type.

The amount of mesoporous silica affects the tablet's properties. For instance, silica can be included as a glidant for enhancing the flowability properties of the powder mix, as mentioned earlier. However, if the amount exceeds 1% of the tablet weight, the high surface area of silica will cause an increase in the cohesive forces among the silica particles in the powder blend, affecting the compression as a result by decreasing flowability (Hentzschel et al., 2012). Furthermore, the inclusion of mesoporous silica within the powder blend enhances the disintegration, according to Bhattacharyya and Ramachandran (2022). This is due to the high porosity of silica inside the formulation, prompting it to absorb more water and create an expansion in volume, generating hydrostatic pressure that assists in disintegration. One crucial factor to consider regarding the effect of silica amount on tablet compression is how the compression force affects the carrier's structure upon increasing pressure. For instance, the internal porous structure of the carrier, as well as the pores, can deteriorate and collapse in the absence of plastically deforming materials like microcrystalline cellulose (MCC) (Baumgartner and Planinsek, 2021). In addition, Vialpando et al. (2011) found that increasing tabletting pressures on mesoporous silica carriers causes small fragments to break off the individual carrier surface. They also found that the morphological structure was heavily affected, and the distribution of the pores was heavily damaged, even though some pores remained intact. They attributed the structural deterioration to the increasing pressure that collapses the carrier and decreases the specific area and volume.

The addition of diluents with silica in the formulation affects the properties of the resulting tablets. The use of mesoporous silica Aeroperl® as an additive for tablets through direct compression without diluents results in poor tabletability, which is due to its large size and poor compaction properties (Baumgartner and Planinsek, 2021, Sun et al., 2018). Additionally, according to Tahvanainen et al. (2012), MCC and lactose are usually added to tablets in different ratios considering their good compaction properties and porosity, which enhances the tabletability since porous fillers absorb high compression forces and protect particles from fragmentation (Vialpando et al., 2011). In addition, Vialpando et al. (2011) found that using MCC helps maintain the silica structure upon compression due to its plastic deformation, which

assists in dissipating the compression energy, and counteracting the pore collapse. Furthermore, the type of diluent and amount affect the disintegration. The most commonly used diluents in the pharmaceutical industry are lactose monohydrate, which is a water-soluble material, and avicel 102, also known as (MCC) that is non-water soluble, with both excipients having good tabletability properties (Alzoubi et al., 2021, Sun and Sun, 2020). Yet, increasing the amount of MCC increases disintegration time due to its low solubility, the formation of non-soluble condensed structures with silica, as well as its low swelling properties (Vialpando et al., 2011, Kumar et al., 2002).

The size of added silica has a crucial role in the tablet's properties. For instance, mesoporous silica nanoparticles (MSNs) enhance disintegration due to their small size, resulting in a large surface area and absorption of larger amounts of the solvent (El-Setouhy et al., 2015). Also, small-size silica carriers have low density, leading to a higher quantity of particles per dosage form, causing the diluent mixture to be in full contact with water, further enhancing disintegration (Li et al., 2018). The silica particle size also affects the tablet's compactability and hardness. This is due to the increased number of bonds formed between silica particles inside the tablet as their size decreases, which increases compactability (Wunsch et al., 2021). Additionally, according to Mura et al. (2019) the hardness of the resulting tablet is affected by the size, where small-size particles result in tablets with higher hardness values. This can be attributed to the previous reason concerning the large number of formed bonds.

As for the carrier type, it refers to the chemical structure and bonds between atoms within the mesoporous carrier. According to Kovacevic et al. (2022), the type of carrier affects the final properties of the tablet, where magnesium aluminosilicates tend to form stronger interparticle bonds compared to carriers containing the silanol group, like SYLOID. This difference results in silanol-based silica tablets having lower hardness values than aluminosilicates at the same compression force (Baumgartner and Planinsek, 2021). This causes tablets containing silanol-based silica to have lower compactability compared to the aluminosilicate, which Mura et al. (2019) found by comparing Nesulsin US2 with SYLOID. In addition, silanol-based silica have low compressibility compared to silicates, where the former forms channels inside the tablet that is suitable for water penetration and accelerating disintegration (Yu et al., 2021). The factors that affect silica tabletting are summarized in figure 5.1 below.

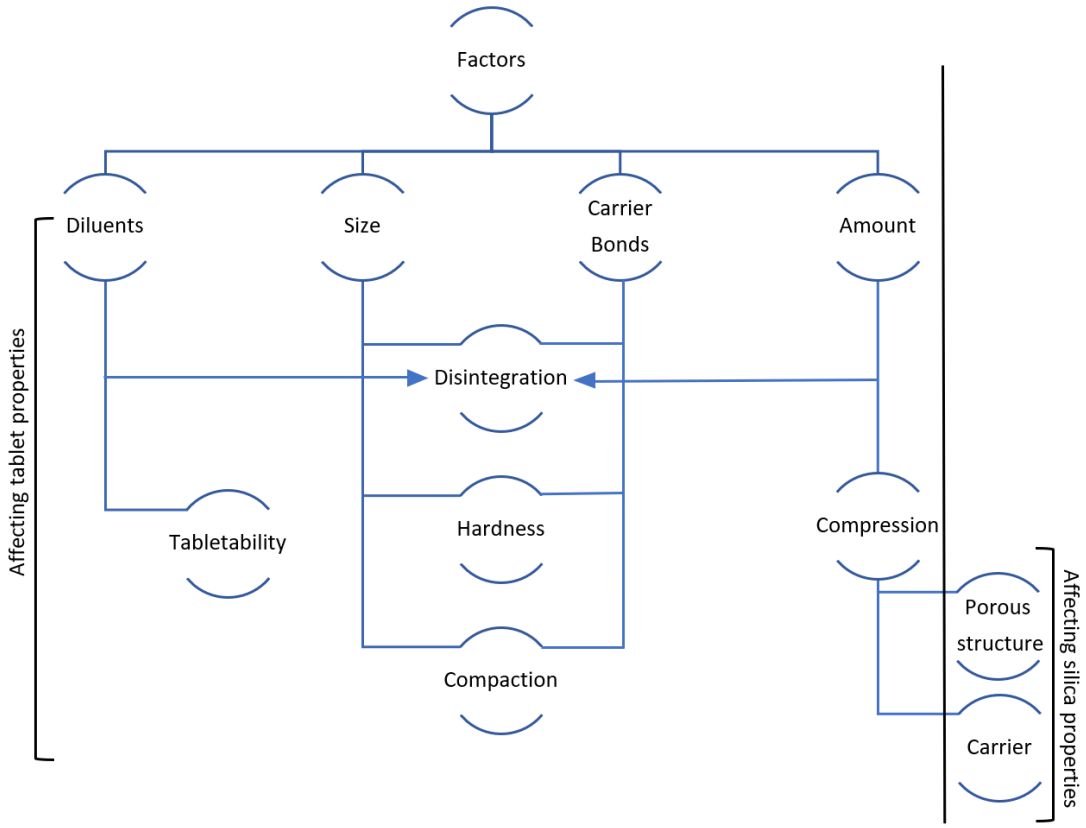

Figure 5.1. Factors affecting silica tabletting and the effects of these factors on tablet properties and the silica carrier.

This chapter aims to design tablets containing mesoporous silica-peptide complex for oral delivery. The silica-peptide will be constructed using a commercially available mesoporous silica microparticle (SYLOID XDP 3150) and a model protein (BSA). The silica carrier will be added into different ratios of diluents and additives to present compactable tablets that disintegrate within expected specifications for immediate release tablets.

Objectives are to:

- Assess the different effects of compression on the morphological properties of SYLOID.
- Investigate the factors that govern mesoporous silica microparticles tabletting.
- Design a tablet containing silica-peptide for oral delivery by investigating different silica concentrations and excipients.
- Examine the effects of different excipients and silica ratios on tabletting properties.

5.2. Materials and Methods

5.2.1. Materials

Bovine serum albumin (BSA) fraction V molecular weight 68 kDa, (Hydroxypropyl)methyl cellulose (average M_n ~10,000), croscarmellose sodium, acetonitrile 99.8% (HPLC grade), and phosphate buffered saline (PBS) tablets were purchased from Sigma-Aldrich (Dorset, UK). Mesoporous silica microparticles SYLOID XDP 3150 were kindly provided by W.R. Grace and Co (Worms, Germany). Lactose monohydrate 316 fast flow was purchased from Foremost Farms (USA). Avicel PH-102 was kindly provided by FMC (Philadelphia, USA). Polyvinylpyrrolidone (PVP), average Mw 40.000 was purchased from Fisher Scientific (Belgium). Magnesium stearate (3.8-5% Mg) was purchased from Acros Organics (Netherlands). Polypropylene containers were purchased from Agar scientific (Essex, UK).

5.2.2. Methods

5.2.2.1. Preparation of mesoporous silica-BSA complex:

The SYLOID-BSA complex was prepared via the solvent evaporation method using distilled water. BSA was dissolved in the solvent at concentrations ranging between 0.5 – 2 mg/ml, followed by SYLOID XDP 3150 addition. The mixture was left on a magnetic stirrer for 2 hours while covered. The suspension mixture was transferred into a watch glass and left in the fume hood for the solvents to evaporate for 24 hours. After solvent evaporation, the samples were kept in plastic containers for characterisation. The theoretical loading of BSA to SYLOID was 10, 20, and 40% w/w.

5.2.2.2. Drug load quantification

Actual drug loaded was calculated using the same method in section 3.1.2.9.

5.2.2.3. HPLC method for analysis

HPLC analysis for BSA was conducted similar to the method in section 4.1.2.3.

5.2.2.4. Particle size analysis using laser diffraction.

Particle size analysis was conducted using the same method in section 2.1.2.3.

5.2.2.5. Particle sizing for silica dispersions in liquid

The particle size for dispersed particles was assessed using same method in section 4.1.2.7.

5.2.2.6. Fourier-transform infrared spectroscopy (FTIR)

The molecular inetarctions were assessed using same method from section 2.1.2.5.

5.2.2.7. Fluorescence imaging

Fluorescence imaging was conducted using same method in section 4.1.2.5. without assessing the fluorescence intensity in the middle plane.

5.2.2.8. Tablet formulation to investigate powder composition and silica on tablet properties.

Different ratios of Avicel and lactose monohydrate (25:75, 50:50, and 75:25) were mixed, followed by the addition of SYLOID XDP 3150 at concentrations of (0, 20, and 40% w/w) of the tablet weight. Afterwards, magnesium stearate was added at 1% w/w, followed by mixing the powder for 5 minutes. The powder mixture was used to prepare 500 mg -13 mm in diameter flat-faced tablets using Power 8T automatic press from Specac (Orpington, UK). Tablets were compressed at a 3-Ton force using 13 mm evacuable pellet die. 30 tablets were made for each batch, and the formulations are explained in table 5.1 below.

Table 5.1. Preliminary formulations containing different ratios of avicel:lactose and SYLOID amounts.

Formulation number	Composition
1	Avicel:lactose monohydrate (25:75)
2	SYLOID 20% + Avicel:lactose monohydrate (25:75)
3	SYLOID 40% + Avicel:lactose monohydrate (25:75)
4	Avicel:lactose monohydrate (50:50)
5	SYLOID 20% Avicel:lactose monohydrate (50:50)
6	SYLOID 40% Avicel:lactose monohydrate (50:50)
7	Avicel:lactose monohydrate (75:25)
8	SYLOID 20% Avicel:lactose monohydrate (75:25)
9	SYLOID 20% Avicel:lactose monohydrate (75:25)

5.2.2.9. Tablet formulation to investigate the influence of binders and disintegrants on tablet friability and disintegration

PVP was added to formulations that had high friability at a concentration of 5% w/w. The binder was added to the SYLOID-diluent powder and mixed for 5 minutes followed by the addition of magnesium stearate at a concentration of 1% w/w. The powder mixture was used to prepare 500 mg 13mm flat-faced tablets. As for the disintegrants, croscarmellouse in concentrations of (1-2%) was added to the powder mixture of SYLOID and avicel:lactose in different concentrations.

5.2.2.10. Tablet porosity

Tablet porosity was measured using helium pycnometry, the instrument was Multipycnometer from Quantachrome (Syosset, USA). One tablet with the weight of 0.5 g was put in micro sample cell and the true volume V_t was calculated based on Archimedes principle of fluid displacement, while the fluid is the helium gas that is able to penetrate the porous structure of the tablet to the pores of an 10^{-10} m of size, and is inert towards materials at normal temperatures (Columbu et al., 2021). The true volume V_t was calculated using the equation 5.1 below:

$$V_t = V_c - V_R (P_1/P_2 - 1)$$

Equation 5.1. True volume.

Where V_c is the sample cell volume (11.6029), V_R is the reference volume (6.2581), P_1 is the atmospheric pressure, and P_2 is the pressure change. V_T will be used to calculate the true density of the tablet according to the equation 5.2 below:

$$\text{True density} = \text{Tablet weight}/\text{True volume}$$

Equation 5.2. True density.

The porosity of the tablet is calculated using this equation 5.3:

$$\text{Porosity} = [1 - (\text{Bulk density}/\text{True density})] * 100$$

Equation 5.3. Tablet porosity.

The bulk density is calculated through this equation 5.4:

$$\text{Bulk denisty} = \text{Tablet weight}/\text{Volume}$$

Equation 5.4. Bulk density.

The volume is the tablet can be calculated considering that is takes the shape of a cylinder using equation 5.5:

$$Volume = \pi * r^2 * h$$

Equation 5.5. Tablet volume.

Where r is the radius, and h is the tablet's thickness.

5.2.2.11. Tablet hardness

Tablet hardness was assessed using Copley TBF 1000 (Copley Scientific, UK). The instrument was calibrated prior to testing and three tablets were tested. Tensile strength (σ) was calculated using the following equation 5.6 :

$$\sigma = \frac{2 * hardness}{\pi * d * h}$$

Equation 5.6. Tablet hardness.

Where σ is the tensile strength, d is the tablet diameter, and h is thickness of the tablet. All Measurements were done in triplicate and values reported as mean ± SD.

5.2.2.12. Tablet disintegration:

Tablet disintegration time was tested using DTG 100i from Copley Scientific (UK) USP basket apparatus that was equipped with a temperature control unit to maintain temperature at 37 ± 2 ℃. One tablet was placed in the disintegration basket, which moved at 30 cycles/min. Distilled water was the disintegration medium and its temperature was kept at 37 ± 2 ℃. Three tablets per batch were tested, and the time of disintegration was recorded when the tablet fractions had passed through the mesh of the basket.

5.2.2.13. Tablet friability

Tablets friability was assessed using a friabilator from J. Engelsmann AG (Ludwigshafen, Germany). The procedure used 8 tablets where they were weighed prior to testing and rotated in the drum at 25 rpm for 4 min. Tablets were dusted carefully to remove any excess powder, and the friability was calculated as follows (equation 5.7):

$$(weight_{before} - weight_{afetr}) / weight_{before} * 100$$

Equation 5.7. Tablet friability.

5.2.2.14. Tablet dissolution study

Percentage drug release (%) was performed on tablets containing silica-BSA via a USP Apparatus 2 Erweka light (Heusenstamm, Germany), and using a 100 ml small volume vessel (COPLEY, UK). The release medium was PBS, the volume was 100 ml, and the paddle speed was 100 rpm. The sample volume was 1 ml and samples were taken at these time intervals: 0, 30, 60, 90, 120, 150, and 180 minutes, followed by solvent resubstituting. Samples were filtered using 0.25 µm nylon filter (Chromacol ltd, Hertfordshire, UK) prior to analysis.

5.2.2.15. Morphological properties powder

Images were taken using the Environmental Scanning Electron Microscope (SEM) mode of the ThermoFisher Scientific Quattro S microscope equipped with a field emission filament (FEG). The images were taken in low vacuum mode in variable pressure between 85 and 105 Pa, with an acceleration voltage of 3 kV and 3 -3.5 spot size.

5.2.2.16. Statistical analysis

Statistical analyses of data were assessed using same methos in section 2.1.2.10.

5.3. Results and discussion

The SYLOID-BSA complex was made via the solvent evaporation method as reported in the previous chapter.

5.3.1. Actual drug load quantification

As mentioned above, the SYLOID-BSA complex was made using water as the solvent and in three loading concentrations (10, 20, and 40%) BSA w/w. The actual drug load quantification of BSA was investigated via HPLC, and the results are shown in figure 5.2 below.

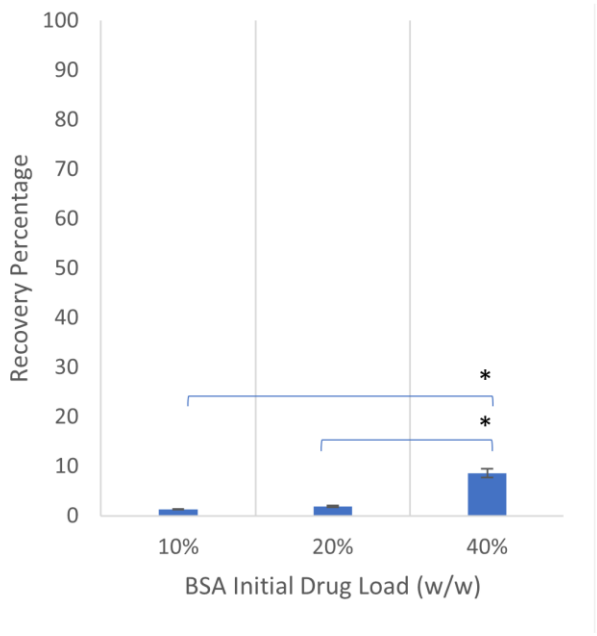

Figure 5.2. Recovery percentage of SYLOID-BSA after 2 hours at different theoretical loadings, 10%, 20% and 40% drug load w/w, with error bars representing standard deviation and (*) representing significant difference ($p<0.05$).

As seen from figure 5.2 above, the recovery of BSA was relatively low as the loading concentrations presented different percentages, with the highest value being 8%. Additionally, increasing BSA loading amount has significantly increased the recovery percentage ($P<0.05$). This is related to several factors; for instance, BSA molecular weight is 67 kDa, where the loading is related to the API molecules diffusing into the carrier, which is governed by the Stokes-Einstein equation (equation 4.1) (Thompson and Williams, 2021). Additionally, using highly polar solvents decreases loading efficiency due to the interaction between the polar solvent and the silica surfaces, where water (highly polar) will compete with BSA to interact with the negatively charged SYLOID surface and form hydrogen bonds (Hillerström et al., 2014, He et al., 2017). Moreover, using glass could decrease loading efficiency due to its

interaction with BSA, causing the latter to adhere to glass surfaces (Krajewski et al., 1996). However, this effect is negligible, and the main reasons for low recovery are BSA's radius and water's polarity (please refer to Chapter 4 for more information).

Following the drug load quantification, FTIR was used to investigate the presence of BSA within the silica carrier.

5.3.2. Molecular interactions of BSA-SYLOID formulations.

FTIR was used to investigate the presence of BSA within the carrier. Figure 5.3 below presents the spectrums of SYLOID-BSA in three loading concentrations with SYLOID and BSA as references.

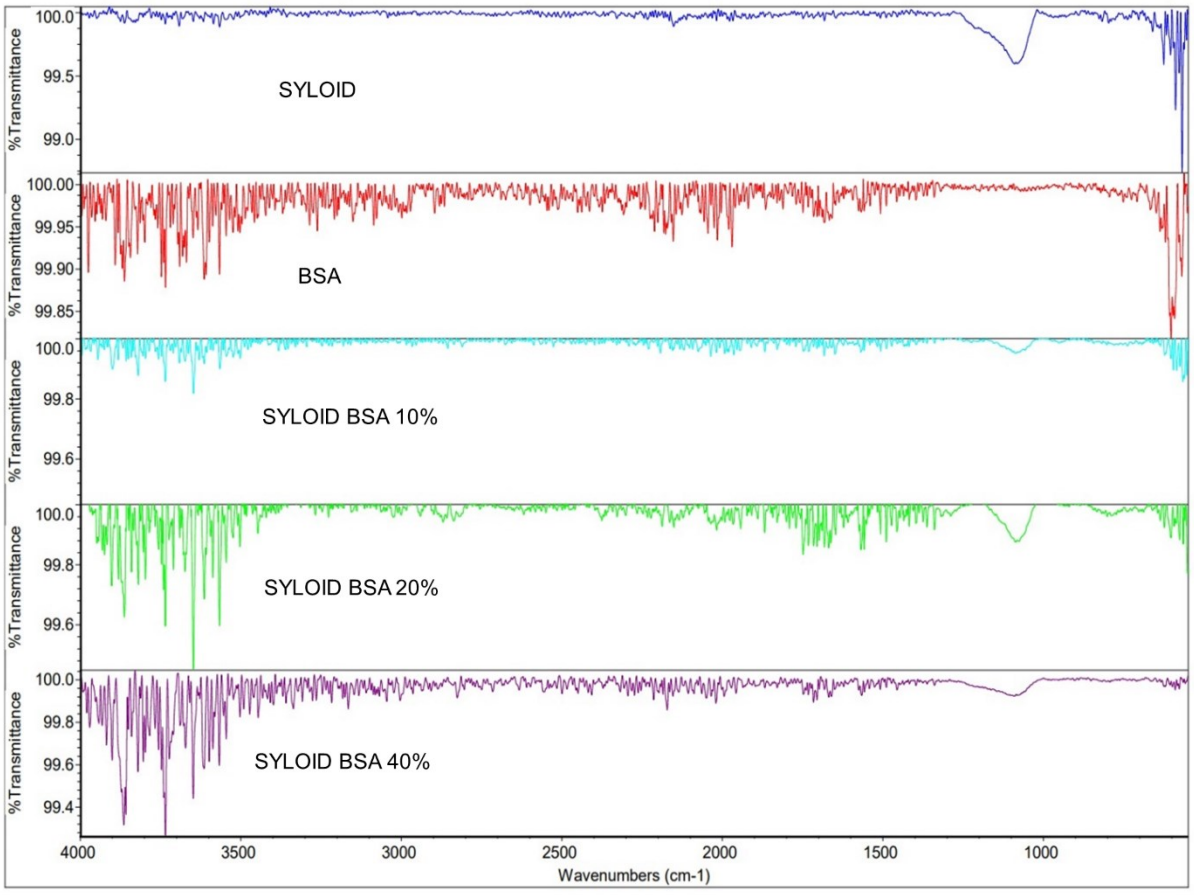

Figure 5.3. FTIR profile for formulations containing different concentrations of BSA.

The FTIR spectrum for both BSA and SYLOID has been reported in sections 2.2.1. and 4.2.5.

Confocal imaging was used to support the presence of BSA in SYLOID, and 3D images were generated of the SYLOID-BSA complexes.

5.3.3. Fluorescence imaging

The chemical structure of BSA contains the amino acid tryptophan, which assists in detecting the fluorescence presence of BSA and diffusion into SYLOID (Sy et al., 2001, Vivian and Callis, 2001). 3D images were generated of the three formulations, and a picture of the combined planes was taken to present the fluorescence pattern. They are presented in figure 5.4 (A-C) below.

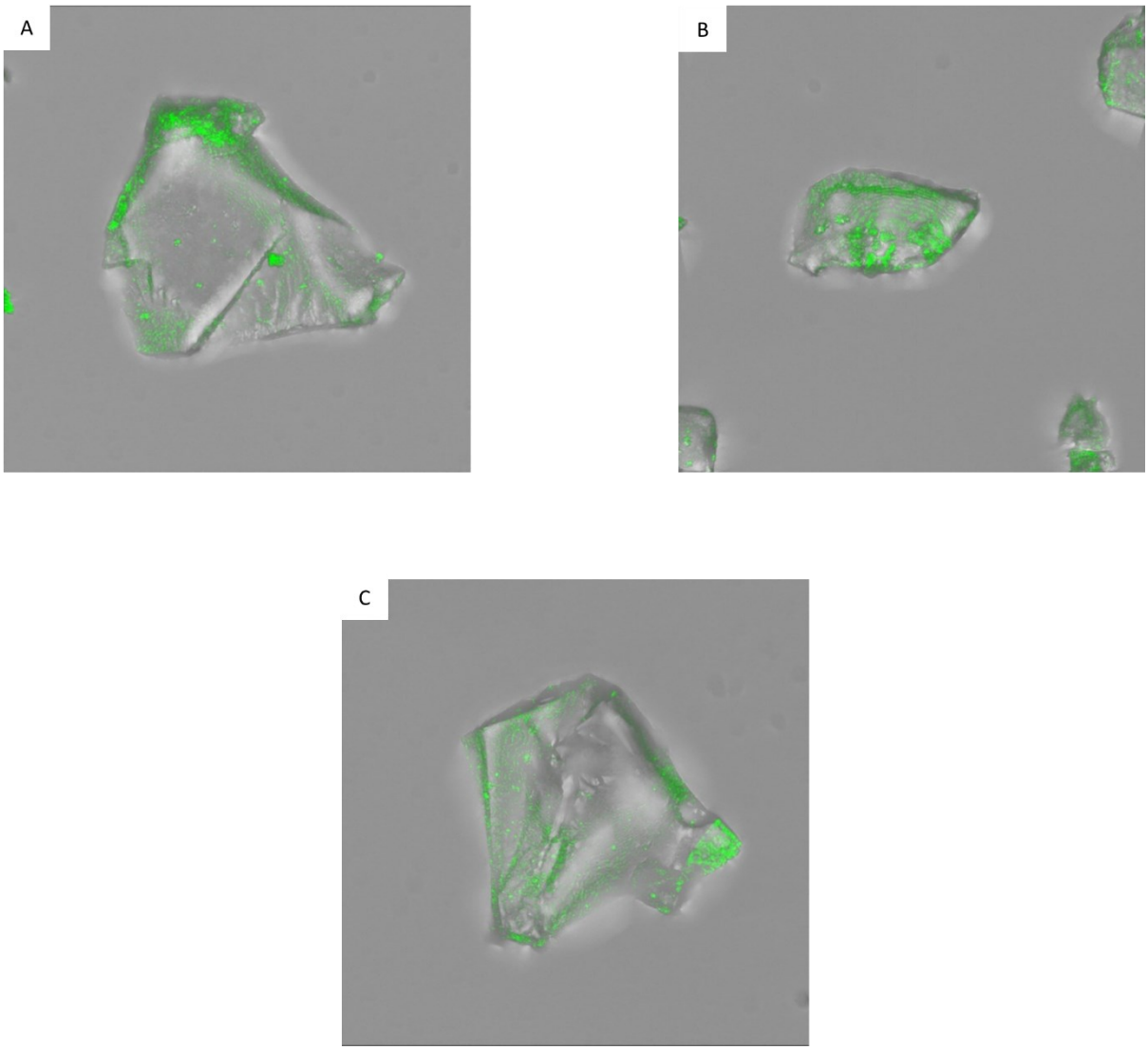

Figure 5.4. 3D confocal imaging of SYLOID-BSA in different initial loading concentrations showing BSA presence on the surface of the carrier; SYLOID-BSA 10% (A), SYLOID-BSA 20% (B), and SYLOID-BSA 40% (C).

SYLOID XDP is a non-ordered mesoporous silica carrier that shows no fluorescence properties. However, BSA is fluorescent, making it detectable on SYLOID via confocal microscopy. As seen from figure 5.4 above, BSA seems to be concentrated on the particle's surface. This is related to the radius (2.69 nm) of BSA (as calculated in the previous chapter), which makes diffusion to the silica carrier quite challenging as diffusion would depend on the size of the protein according to the Stokes-Einstein equation (Thompson and Williams, 2021). Furthermore, for efficient diffusion, the pore size should be at least ten times larger than the molecule's radius, However, BSA radius is 2.69 nm while SYLOID's is 20 nm, which decreases the efficiency of diffusion into the porous carrier (Wagner et al., 2017, Waters et al., 2018).

The formulation with 40% BSA w/w was selected for tabletting due to its better recovery in comparison with formulations made with 10 and 20% BSA w/w.

5.3.4. SYLOID tabletting and compression

Manufacturing of the SYLOID-based tablet commenced with compressing tablets entirely made from SYLOID. SYLOID-based tablets were incompressible due to their stickiness, as they were inclined to get stuck in the die even though external lubrication was applied (magnesium stearate in acetone at a concentration of 5% w/v). Different compression forces (1, 2, and 3 Tons) were applied, and the SYLOID powder was either noncompressible at 1 and 2 Tons or the tablet would be ejected as accumulated fragments and powders, as seen in figure 5.5 below.

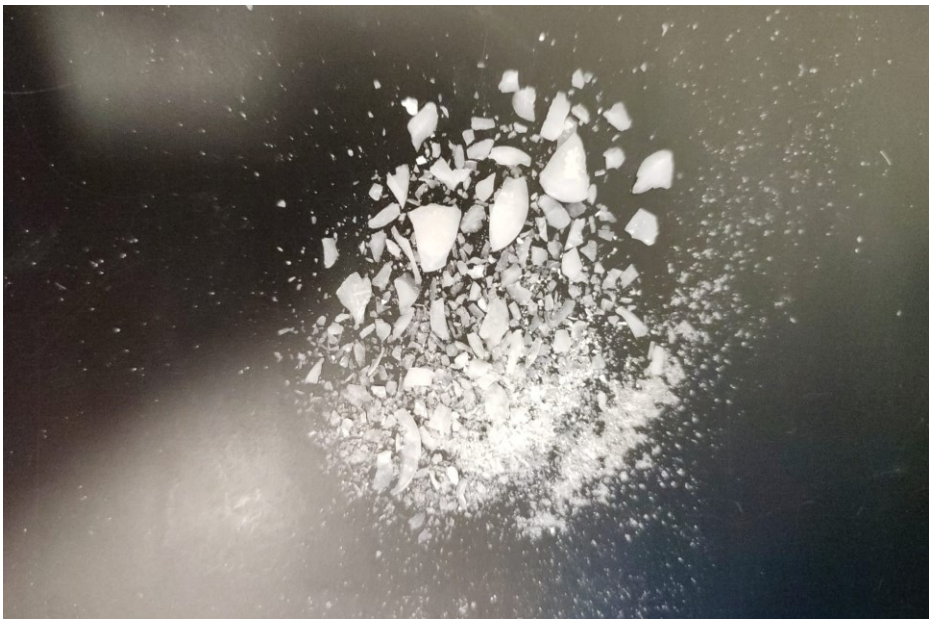

Figure 5.5. SYLOID fragments after tabletting at 3 Tons showing large aggregates of SYLOID and fine powder.

SYLOID XDP is a mesoporous silica microparticle that is composed of SiO_2 groups, and during tablet compression, the porous carriers are susceptible to an event called ‘’squeezing’’. This is the point at which their porous structure and morphology are susceptible to deterioration, leading to the release of their components. This sensitivity is attributed to the high external pressure applied by the die (Koch et al., 2023). Furthermore, mesoporous carriers made from silicates-based materials, especially aluminosilicates, result in tablets with high hardness due to the high compressibility of silicates in comparison to SiO_2 groups (Sander and Holm, 2009). Therefore, the low compressibility of SYLOID can be attributed to the presence of SiO_2 groups, where silanol groups exhibit less propensity to form interparticle bonds compared to an aluminosilicate-based carrier. Consequently, this leads to tablets with reduced hardness and compressibility (Kovacevic et al., 2022).

Shi and Sun (2010) found that diluents should be added at concentrations exceeding 60% for the successful formation of silica-based tablets. Their findings indicated that silica-based carriers do not show plastic deformation but have high elastic modulus. During decompression, silica particles undergo an elastic recovery process when the pressure decreases from the highest point to zero. This will cause the tablet to cap or fail to be compressed in the absence of a material that will undergo plastic deformation to accommodate silica particle recovery. Additionally, when the tablet does not contain any binders or diluents, silica particles will come together, forming macro defects in the tablet matrix and compromising the bonding network. Furthermore, the inclusion of an excipient in the powder mixture can create a continuous bonding network in the tablet that spans the entire tablet, where the excipients could coat or fill the voids between the silica particles, thus producing a tablet with appreciable strength (Blattner et al., 1990).

In order to evaluate the effects of compression on the silica carrier, the loose powder after compression attempts of SYLOID were analysed for its particle size and compared against non-compressed SYLOID. The particle size of the SYLOID powder after crushing was found to be 34.69 ± 8.13 μm compared to 117.3 ± 0.56 of non-crushed powder. Additionally, since the particle size of the powder has changed, the morphology of the silica carrier could have changed upon compression. Therefore, SEM imaging was conducted for SYLOID prior to and after compression.

Figures 5.6 (A-D) below represent the particle population and surface of SYLOID before and after compression at 3 Tons.

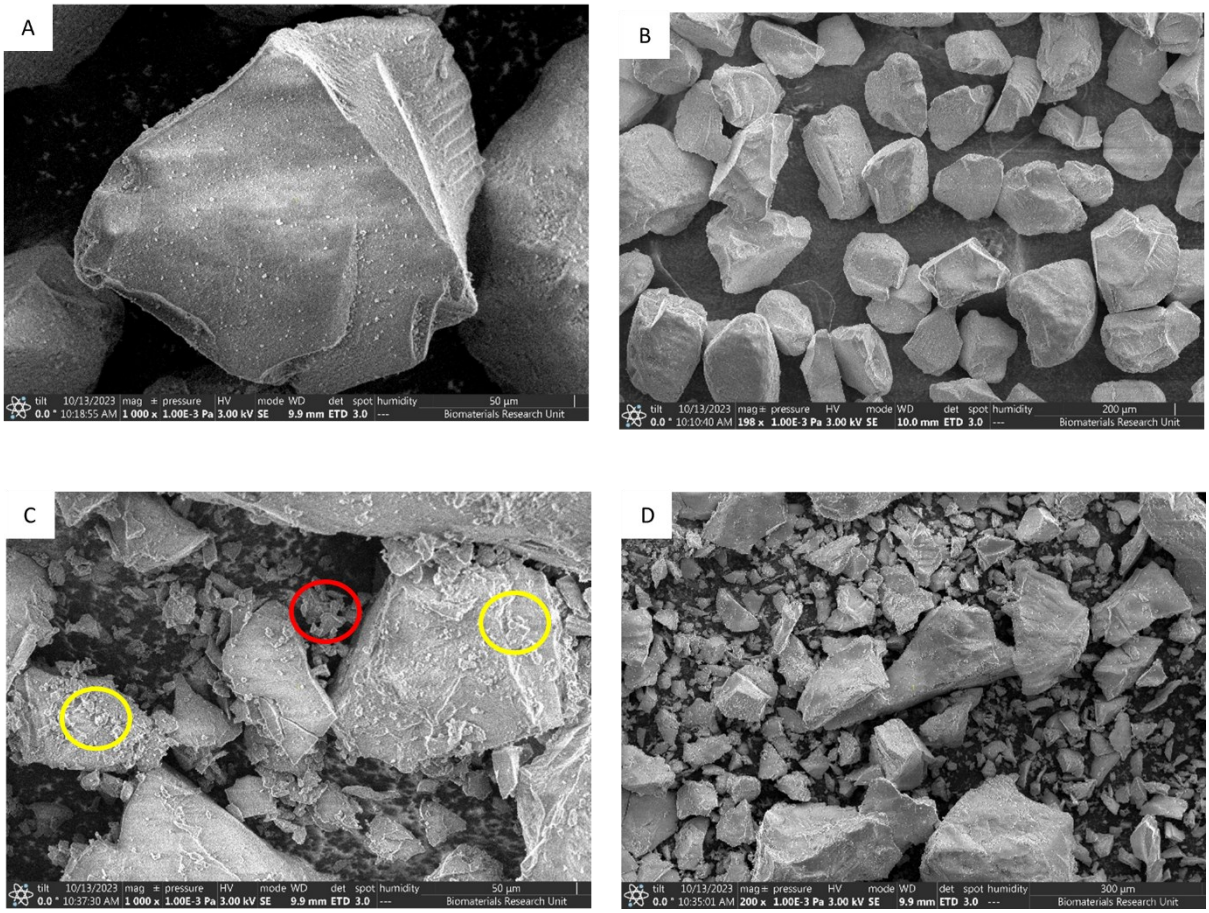

Figure 5.6. SEM imaging of SYLOID XDP 3150 at different magnifications showing the effects of compression force on the morphology of SYLOID morphology before and after compressing at 3 Tons; SYLOID before compressing low magnification (A), powder population (B), after compression (C), and after compression for the powder population (D). The red circles represent the small fragments of SYLOID and the yellow present the cracks deformations on the carrier surface.

SYLOID is a non-ordered mesoporous silica microparticle with shapes differing from other spherical mesoporous microparticles (Waters et al., 2018). Additionally, it has a particle size of around 115 µm compared to other SYLOID carriers like XDP 3050. As seen from figures 5.6 (A-B) above, SYLOID has a large shape (A and B) where the particles are non-spherical, and the surface is smooth and does not show any cracks or deformations.

However, upon tabletting, the particle shapes seem to change where there are small fragments of silica (red circles), and the surface presents some cracks and deformations (yellow circles), which are related to the applied pressure (C). Furthermore, upon compression, small pieces from SYLOID are present in the sample (D), which is related to the carrier shattering due to its low plastic deformation (Mura et al., 2019). The particles are in direct contact with each other, and high-pressure forces cause SYLOID to break upon

compression. Additionally, SYLOID as a carrier has silanol groups, granting the carrier more hardness properties than silicate (Vialpando et al., 2011). This enhanced hardness will contribute to hard tabletting since materials with high plastic deformation enhance compressibility and compactability as they increase bonding strengths and particle bonding areas upon compression (Haruna et al., 2020).

5.3.5. Designing the SYLOID-based tablet

Considering the low tabletability of SYLOID, two diluents were used: Avicel and lactose monohydrate in different ratios; avicel:lactose (75:25, 50:50, and 25:75), and different amounts of SYLOID in the tablet 20 and 40% w/w. The effects of the diluent ratio and SYLOID amount on the tablet properties will be investigated. The tablet weight was 500 ± 1 mg and the previous materials were mixed with magnesium stearate at 1% w/w that was the lubricant. The tablets were made, and their properties are mentioned in table 5.2 below.

Table 5.2. Properties of the tablets made using different ratios of avicel:lactose and different concentrations of SYLOID. All formulations contained magnesium stearate at a concentration of 1%. The disintegration, thickness, hardness, friability, and porosity are reported. The tablets containing 40% with (avicel:lactose ratio of 25:75) were not included as they were very brittle and disintegrated instantly upon ejection.

Formulation	Disintegration time (s)	Thickness (mm)	Hardness (N)	Friability (%)	Porosity (%)
avicel:lactose 25:75	115.33 ± 1	2.43 ± 0.02	158.6 ± 6.4	1.38 ± 0.23	21.93 ± 1.02
SYLOID 20% avicel:lactose 25:75	838.66 ± 4	2.94 ± 0.06	85.7 ± 3.5	6.46 ± 1.76	40.22 ± 1.54
SYLOID 40% avicel:lactose 25:75	Tablets were brittle and disintegrated instantly upon ejection.				
avicel:lactose 50:50	429.33 ± 4	2.55 ± 0.01	282.6 ± 4.3	0.5 ± 0.1	19.08 ± 1.28
SYLOID 20% avicel:lactose 50:50	1520 ± 20	2.73 ± 0.04	123.6 ± 7.2	2.79 ± 0.56	40.87 ± 1.2
SYLOID 40% avicel:lactose 50:50	Did not	3.16 ± 0.06	116.7 ± 5.7	17.01 ± 1.45	52.28 ± 0.78
avicel:lactose 75: 25	1680 ± 15	2.61 ± 0.01	376.8 ± 10.5	0.2 ± 0.02	17.32 ± 1.19
SYLOID 20% avicel:lactose 75:25	2300 ± 33	3 ± 0.08	197.2 ± 1.4	1.3 ± 0.39	37.34 ± 0.96
SYLOID 40% avicel:lactose 75:25	Did not	3.39 ± 0.02	184.2 ± 5.2	3.49 ± 0.15	57.73 ± 0.85

The effects of the diluent composition (avicel:lactose) and the presence and amount of SYLOID in the tablet formulation on each of the tablet mentioned above properties will be discussed in the following sections.

5.3.6. Effects of excipient compositions and silica amount on tablet porosity

Graph 5.7 below presents the porosity values of the tablet formulations containing different avicel:lactose compositions and SYLOID amounts. The tablet containing 40% SYLOID with avicel:lactose 25:75 was not included as it disintegrated and crumbled instantly upon ejection.

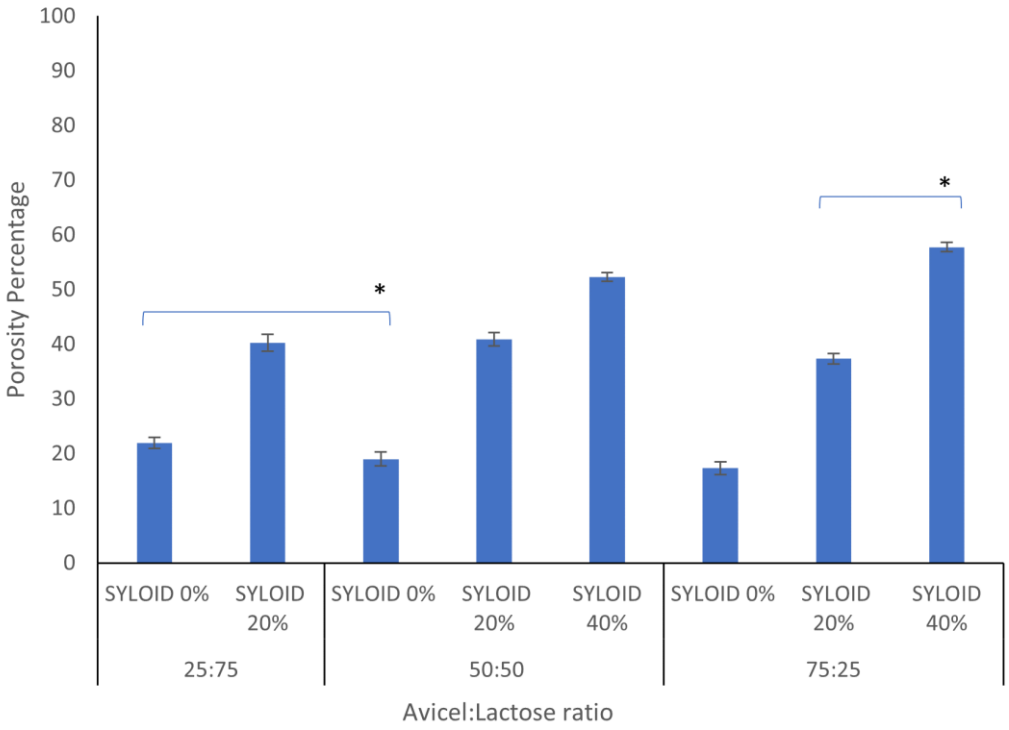

Figure 5.7. The effects of the diluent composition and SYLOID amount on the porosity of the tablets. The formulation containing 40% with (avicel:lactose ratio of 25:75) is not included as it disintegrated instantly upon ejection. Error bars representing standard deviation and (*) representing significant difference ($p<0.05$).

As seen from graph 5.7 above, the porosity of the tablet significantly decreased ($p<0.05$) as the ratio of avicel increased, where it decreased gradually from 21 to 17% when the ratio of avicel within the diluent increased from 25 to 75. This is related to the ability of avicel to form compacted formations compared to lactose and the higher porosity of lactose (Vialpando et al., 2011, Kumar et al., 2002). Moreover, the high interparticle bonding between MCC particles and its effects on cohesive forces due to packed glucose units contribute towards porosity decrease (Nsor-Atindana et al., 2017, Thoorens et al., 2014).

Additionally, according to graph 5.7 above, the porosity of the tablet increased with SYLOID increase, where increasing SYLOID amount from 0-40%, has significantly increased the porosity values, as they were 17, 37, and 57% for SYLOID amounts of 0, 20, and 40% when the diluent composition was avicel:lactose 75:25. The same observation is evident in the other avicel:lactose ratios. This could be related to the nature of the added materials. SYLOID is a

non-ordered mesoporous carrier with a pore volume of 1.7 cm^3/g (Waters et al., 2018). The presence of SYLOID in the tablet contributes to its porosity. This will affect the friability, disintegration, and tablet thickness of the tablet, which will be discussed in the following sections.

5.3.7. Effects of the excipient compositions and silica amount on disintegration time

The formulations had varying disintegration times according to table 5.2 above. Figure 5.8 below shows the disintegration time of the formulations made using different avicel:lactose ratios (25:75, 50:50, and 75:25) and silica amounts (0, 20, and 40% w/w). The formulation made using avicel:lactose 25:75 and containing 40% SYLOID was very brittle and disintegrated instantly upon ejection. Additionally, the formulations that contained 40% SYLOID and were made using avicel:lactose at both ratios of 50:50 and 75:25 did not disintegrate after 50 minutes, therefore their bars were not included.

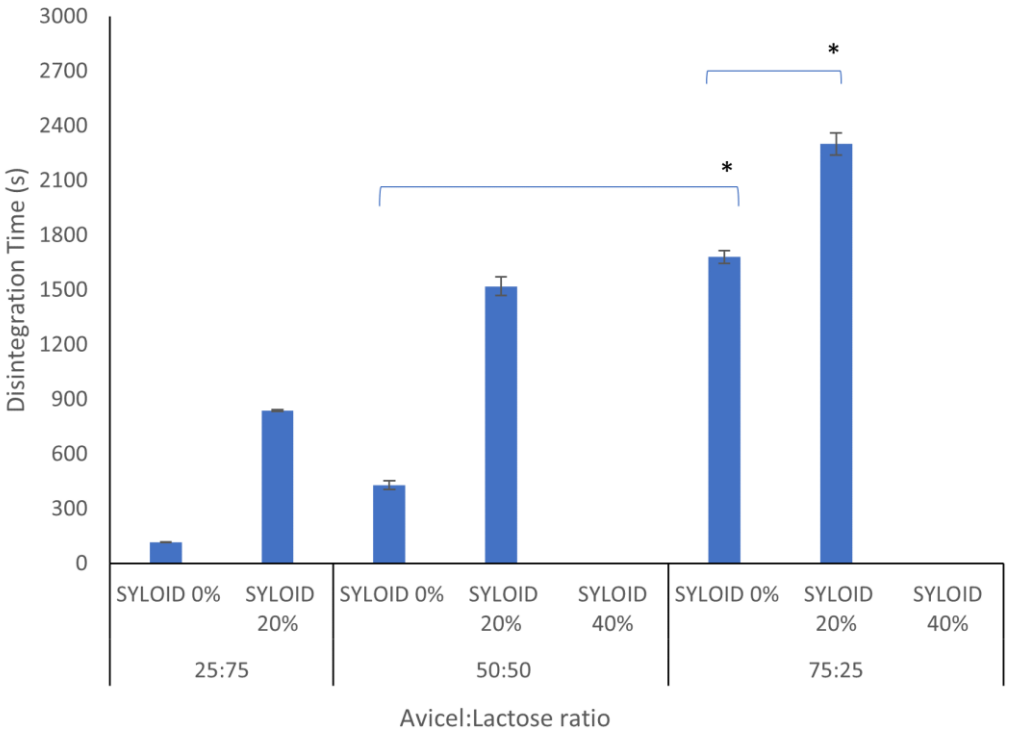

As

Figure 5.8. The effects of the diluent composition and SYLOID amount on the disintegration time of the tablets. The tablets with 40% SYLOID and made using both avicel:lactose ratios of 50:50 and 75:25 was not added as they did not disintegrate after 50 minutes. The formulation containing 40% with (avicel:lactose ratio of 25:75) is not included as it disintegrated instantly upon ejection. Error bars representing standard deviation and (*) representing significant difference ($p<0.05$).

seen from figure 5.8 above, increasing avicel amount in the formulation significantly increased the disintegration time when SYLOID amount was 0%, where it was 115 seconds at 25:75 avicel:lactose and increased to 429 and 1680 seconds at avicel ratios of 50:50 and 75:25, respectively. The last tablet, with the time of 1680 seconds, did not meet the requirements of immediate release tablets regarding disintegration time, as it exceeded 15 minutes (British Pharmacopeia, 2021). Additionally, the increase of SYLOID amount, regardless of the

avicel:lactose ratio has significantly increased the disintegration time ($p<0.05$). For instance, increasing SYLOID from 0 to 20% in the three concentrations has significantly increased disintegration from 115 to 838, 429 to 1520, and 1680 to 2300 (s) for avicel:lactose ratios of 25:75, 50:50, and 75:25, respectively. However, upon increasing SYLOID amount to 40%, the tablet was very brittle and disintegrated directly upon ejection (25:75) or did not disintegrate even after 50 minutes (both 50:50 and 75:25). There are several possible reasons for these observations: diluent materials and their composition as well as the silica presence and its amount in the formulation.

The diluent mixture for the formulations is composed of two materials: lactose monohydrate, which is a water-soluble sugar. The other material is avicel 102, also known as microcrystalline cellulose (MCC), a non-water soluble excipient with good tabletability properties (Alzoubi et al., 2021, Sun and Sun, 2020). Increasing avicel amount in the formulation increases the disintegration time as found by Vialpando et al. (2011), since it forms more compacted formations with other excipients (silica) which is related to its low swelling properties (Kumar et al., 2002). In regard to lactose, Patel et al. (1994) found that increasing the amount of lactose monohydrate increases disintegration time considering its solubility in water. Moreover, lactose monohydrate does not impede water penetration into the tablet, as it does not create a saturated lactose layer around the powder bed. Such a layer could potentially hinder disintegration, as reported by Janssen et al. (2022).

As for the effect of SYLOID, MSNs are usually added into the tablet formulation to enhance the disintegration. This occurs due to their small size and larger surface area, making them absorb a larger amount of the solvent and, thus, enhancing disintegration (El-Setouhy et al., 2015). However, the used carrier is a micro-sized silica with a size of a 115 µm. This causes the surface area to be lower than MSNs'. Additionally, low particle-sized silica powders possess low density, which leads to a higher quantity of particles per dosage form (tablet), and the diluent mixture will be in full contact with water, thus, enhancing disintegration (Li et al., 2018). However, SYLOID is a micro-sized carrier with high density that results in less particles to be inside the tablet. This consumes larger volume which lengthens disintegration time. In addition, the difference in disintegration for samples not containing SYLOID, can be attributed to the amount of diluents and porosity. For instance, tablet porosity affects disintegration as higher porosity relates to liquid penetration of the solvent into the tablet. Furthermore, swelling or dissolution of the tablets will commence after the initial disintegration phase, which will cause a faster disintegration if the components are easily dissolved. This is attributed to the water-soluble materials (lactose) dissolving and leaving larger voids inside the tablet, which non-dissolving materials will consume (Maclean et al., 2021).

The analogy could be that the higher the amount of SYLOID inside the tablet, the more compact it might be, regardless of the thickness. This causes the diluent mixture, especially MCC (considering its insolubility in water) to form a non-permeable layer around the silica particles. This action will prevent water from penetrating, causing the delay in disintegration. Figure 5.9 below presents three tablets made using avicel:lactose 75:25 with different SYLOID ratios that were left in to disintegrate for 25 minutes and then acquired.

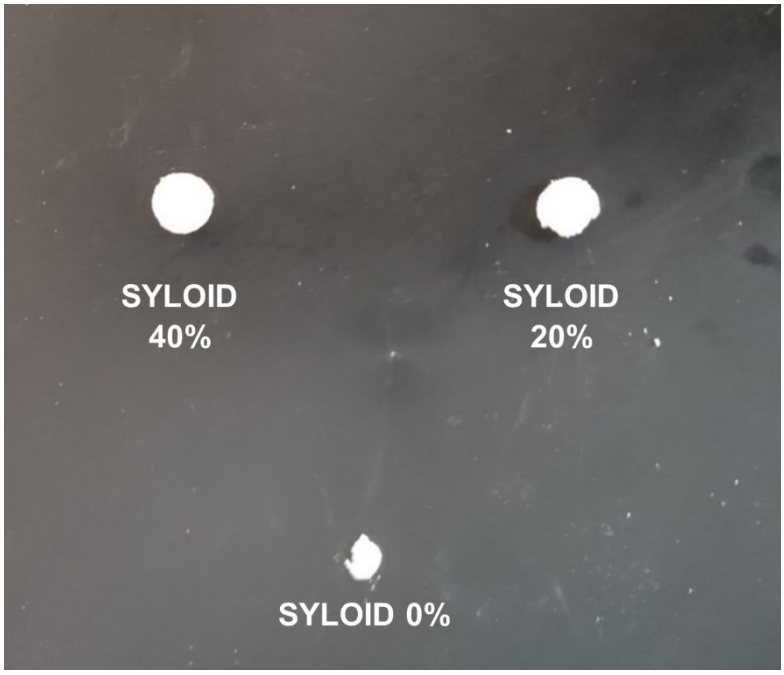

Figure 5.9. The disintegration and size decrease of tablets made with avicel:lactose 75:25 and different concentrations of SYLOID after leaving for 25 minutes.

As seen from the figure above, the tablet with 40% SYLOID seems to be the least eroded and disintegrated compared to those with 0 and 20%. This supports our finding that the tablets with high amounts of SYLOID had longer disintegration time (SYLOID 20% 38 minutes) than those without SYLOID that disintegrated within 28 minutes (graph 5.9). As the effects of silica amount and the diluent composition on disintegration were investigated, the next section focuses on their effects on the tablet hardness.

5.3.8. Effects of the excipient compositions and silica amount on hardness and friability

Figure 5.10 below presents the hardness values for all the tablet formulations except for the one containing 40% w/w SYLOID with Avicel:lactose 25:75, considering that it was very brittle and disintegrated upon ejection.

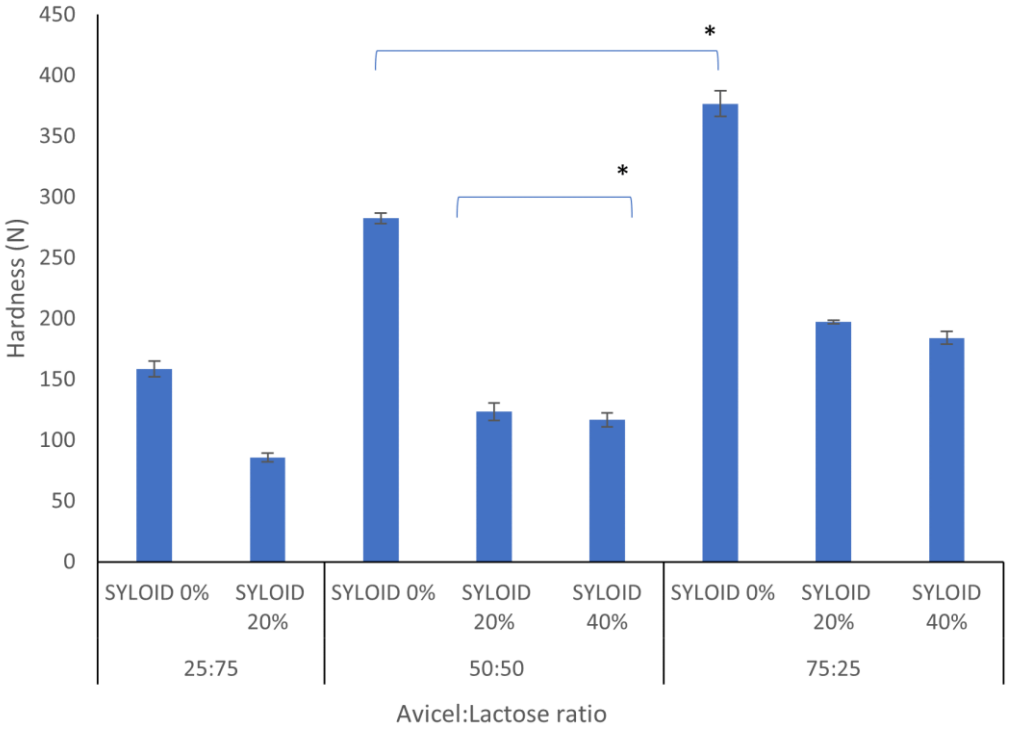

Figure 5.10. The effects of the diluent composition and SYLOID amount on the hardness of the tablets. The formulation containing 40% with (avicel:lactose ratio of 25:75) is not included as it disintegrated instantly upon ejection. Error bars representing standard deviation and (*) representing significant difference ($p<0.05$).

As seen from figure 5.10 above, the tablet hardness increased as the diluent composition shifted towards higher amounts of avicel. This was evident when the hardness was 158 N and increased to 282, then 376 N upon changing Avicel composition from 25:75 to 50:50 and 75:25, respectively. This is related to avicel properties and plasticity in which the particles deform and maximise interparticle bonding (Tran et al., 2019). Moreover, the presence of hydrogen groups on the surface of MCC enables the formation of hydrogen bonds that enhance the tablet's strength and cohesive properties (Thoorens et al., 2014). This can also be related to the packed nature of the linear glucose within MCC units that form a crystal structure (Nsor-Atindana et al., 2017). In addition, tabletability properties are enhanced with MCC due to the mechanical interlocking of irregular shapes and elongated MCC particles (Doelker, 2008).

Additionally, as mentioned above, MCC presents plastic deformation, where the contact area between particles increases, contributing to strong bonding and thus, higher hardness values and hard compacts (Jivraj et al., 2000). Another factor that might affect the hardness is the size of the carrier. For instance, using MSNs improves tablet strength due to the small size of the silica that affects the rearrangement of the diluents, creating a higher surface area that equates to an additional bonding area during tablet compression (Gao et al., 2022). This supports our findings since the used silica carrier is a microporous type with a size of 115 µm, lowering the tablet strength as a result.

Moreover, the hardness of the tablets decreased as the amount of SYLOID increased in the formulation. The hardness of the tablets made using avicel:lactose 75:25 significantly decreased from 376 to 197 N when SYLOID amount increased from 0 to 20% ($p < 0.05$). These results align with Bhattacharyya and Ramachandran (2022) findings, where they found that increasing SYLOID amount decreased hardness and increased the friability. Also, the silanol groups that makeup SYLOID provide it with a hard shell and less compactability than other silica carriers (Yu et al., 2021). The same observation was also seen for both formulations made using avicel:lactose 25:75 and 50:50.

The friability of the tablet indicates the amount of powders lost and is usually associated with hardness. Figure 5.11 below presents the friability percentage for the formulations. The formulation with avicel:lactose 25:75 and 40% SYLOID was not included because it was lost during ejection.

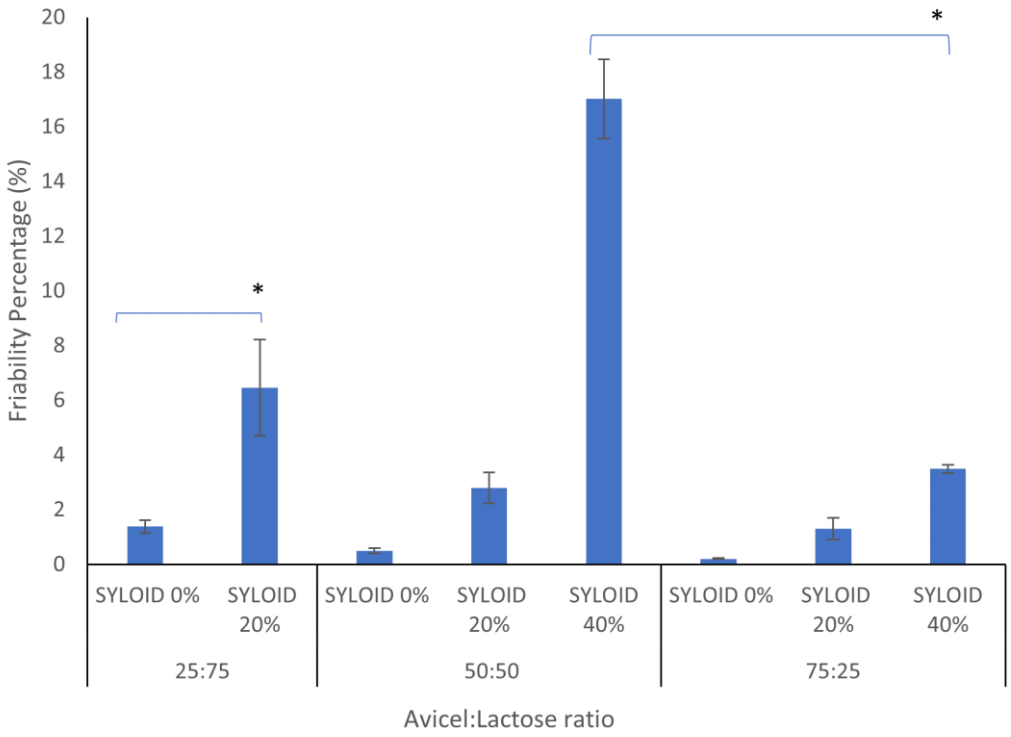

Figure 5.11. The effects of the diluent composition and SYLOID amount on the friability of the tablets. The formulation containing 40% with (avicel:lactose ratio of 25:75) is not included as it disintegrated instantly upon ejection. Error bars representing standard deviation and (*) representing significant difference ($p<0.05$).

As seen from figure 5.11 above, the highest friability value is associated with the formulation containing 40% SYLOID at avicel:lactose 50:50 ratio (17%), while the lowest value is for the formulation that only contained avicel:lactose 75:25 (0.2%). According to figure 5.11 above, the friability percentage seems to decrease as diluent composition shifts towards higher amounts of avicel. For instance, the values significantly decreased ($P<0.05$) from 1.38 to 0.5 and 0.2% when avicel amount increased from 25, 50, and 75, respectively. This is related to the effects of avicel on hardness, as discussed in the previous section. Additionally, increasing SYLOID amount in the formulation significantly increased the friability percentage. The values changed from 2.79 to 17.01% and 1.3 to 3.49% when SYLOID amount increased from 20 to 40% w/w at avicel ratios of 50:50 and 75:25, respectively.

This could be related to the hard shell of SYLOID and the lack of plastic deformity for this carrier. Furthermore, increasing SYLOID amount in the formulation will decrease the amount of the diluent mixture, which will have fewer protective properties and less plastic deformation. This will also impact their effect the diluent's effects to dissipate the pressure around the SYLOID particles and cause the tablet to be less compacted (Vialpando et al., 2011).

5.3.9. Effects of the excipient compositions and silica amount on tablet thickness

The thickness of the formulations was assessed, and the data is included in graph 5.12 below, except for the tablet that was made with avicel:lactose 25:75 and 40% SYLOID as it disintegrated upon ejection.

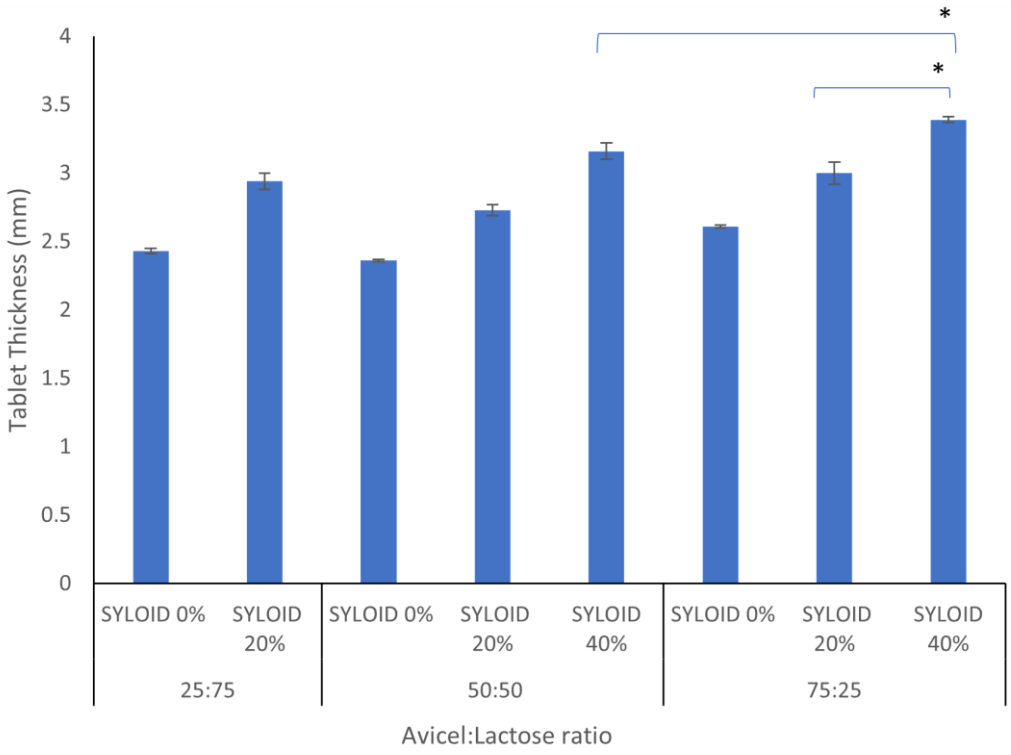

Figure 5.12. The effects of the diluent composition and SYLOID amount on the thickness of the tablets. The formulation containing 40% with (avicel:lactose ratio of 25:75) is not included as it disintegrated instantly upon ejection. Error bars representing standard deviation and (*) representing significant difference ($p<0.05$).

As seen from graph 5.12 above, the thickness of the tablets significantly increased ($p < 0.05$) upon increasing Avicel amount above 25% in the mix, which could relate to the increased amount of Avicel requiring less consolidation and less force. This finding aligns with Patel et al. (1994) results, where their 50% Avicel-containing tablets had higher thickness compared to 25%. Furthermore, lactose monohydrate comes in the form of fine crystals containing a plastically deforming amorphous matrix, where the tablet volume upon compression is reduced due to partial plastic deformation (Janssen et al., 2022). Based on what is mentioned above, the presence of lactose monohydrate in the powder mixture decreases tablet thickness and enhances disintegration, which further supports the results where formulations with high lactose content (Avicel:Lactose 25:75) presented the smallest tablets.

In addition, according to graph 5.12, the thickness of the tablet significantly increases as the amount of SYLOID increases. The highest recorded thickness is associated with the formulation containing 40% SYLOID (3.39 mm) with avicel:lactose ratio of 75:25. This is related to the composition of the tablet as the presence of both avicel and lactose dissipates the pressure that is applied on the silica particles, and they plastically deform to present the tablet. However, due to the hard surfaces and structure of SYLOID, which is due to its silanol groups and porous structure, SYLOID compression is hard and requires higher pressure (Yu et al., 2021, Mura et al., 2019). Yet, applying additional pressure will cause the silica structure to crumble and the particles to break down, as seen in figures 5.6 C-D (Vialpando et al., 2011).

The previous sections and tests show that all the tablets containing SYLOID in different amounts and avicel:lactose compositions have failed to pass the immediate release tablets criteria regarding disintegration and friability (British Pharmacopeia, 2021). Yet, the formulation containing 20% SYLOID at avicel ratio of 75:25 was chosen for further adjustments where its friability and disintegration will be adjusted so the value will be below 1% and tablets disintegrate within 15 minutes.

Croscarmellose sodium (CMC Na) was chosen as a superdisintegrant to enhance the disintegration of the tablet, while PVP was chosen as a binder to decrease the powder loss during friability testing. PVP was added to the powder mixture at a concentration of 5% w/w, while CMC Na was added at two concentrations 1 and 2% w/w. The properties of the new tablets with binder and disintegrants are included in table 5.3 below.

5.3.10. The formulation of SYLOID-BSA tablet

The tablet containing SYLOID 20% at avicel:lactose ratio of 75:25 was chosen for further adjustments as it showed the least friability value (1.3%) (Table 5.2). PVP was added as a binder at a concentration of 5% and croscarmellose was added in two concentrations (1 and 2%) to enhance the disintegration. The properties of the new tablets are mentioned in table 5.3 below.

Table 5.3. Tablet properties after the addition of the binder (PVP) at a concentration of 5% w/w, and the superdisintigrant (croscarmellose Na) at two concentrations (1, 2%) w/w.

Formulation	Disintegration time (s)	Thickness (mm)	Hardness (N)	Friability (%)	Porosity (%)
SYLOID 20% avi:lact 75:25	1680 ± 15	3 ± 0.08	197.2 ± 1.4	1.3 ± 0.39	37.34 ± 0.96
SYLOID 20% avi:lact 75:25 Croscarmellouse Na 1%	69.66 ± 1.52	2.99 ± 0.03	210.6 ± 24.2	2.36 ±	39.27 ± 3.61
SYLOID 20% avicel:lactose 75:25 Croscarmellouse Na 2%	41 ± 1	3.02 ± 0.01	231.9 ± 6.3	1.21 ± 0.33	42.55 ± 1.23
SYLOID 20% avicel:lactose 75:25 PVP 5%	2100 ± 13	3.04 ± 0.06	274.4 ± 4.9	0.72 ± 0.02	37.19 ± 0.39
SYLOID 20% avicel:lactose 75: 25 PVP 5% crosscarmellouse 2%	239.33 ± 4.04	3.04 ± 0.02	252.3 ± 7.5	0.51 ± 0.18	33.73 ± 0.28
(SYLOID+BSA 40%) 20% avicel:lactose 75: 25 PVP 5% crosscarmellouse 2%	501.33 ± 3.21	2.85 ± 0.00	332.6 ± 5.3	0.1 ± 0.02	33.47 ± 1.65

As seen from the table above, the friability of the tablets has significantly decreased (Anova $P< 0.05$) upon adding PVP into the formulation, where it was 1.3% and decreased to 0.72%. This is related to the binding effect of PVP as it promotes better powder agglomeration and enhances compressibility (Luo et al., 2021). However, the disintegration time remained above 15 minutes, which required the addition of CMC Na. Furthermore, the addition of CMC Na significantly decreased the disintegration time below one minute when the concentration was 2% (41 seconds). This is related to the effect of CMC Na in breaking the compacts of tablets,

as Vialpando et al. (2011) reported. Upon adding both PVP at a concentration of 5% w/w and CMC Na at 2%, the tablet passed all the tests required for immediate release tablets.

The tablet was then loaded with the preprepared SYLOID-BSA 40%, which was discussed in previous sections (section 5.3.1). The ratio of SYLOID-BSA is the same to the ratio of SYLOID in the previous formulations (20%) w/w of the tablet weight. The properties of the tablet containing the model SYLOID-protein are mentioned in table 5.3 above. In addition, the formulation that contained (SYLOID-BSA 40%) at a concentration of 20% presented a longer disintegration time. This could be related to BSA's presence as crystals inside the tablet that affect disintegration. Furthermore, the amount of SYLOID in that formulation has decreased, and the tablet's thickness has increased, indicating that the tablet is more tightly packed, which leads to longer disintegration since the tablet structure is denser (Limnell et al., 2011).

5.3.11. Dissolution of SYLOID-BSA tablet

The release of the model protein (BSA) was assessed through a dissolution study to determine whether the high applied pressure affected the protein inside the carrier. This was conducted on the tablet as well as on a capsule containing 100 mg of SYLOID 40%. The dissolution study was conducted in a 100-ml small dissolution vessel for 3 hours and the results are reported in graph 5.13 below.

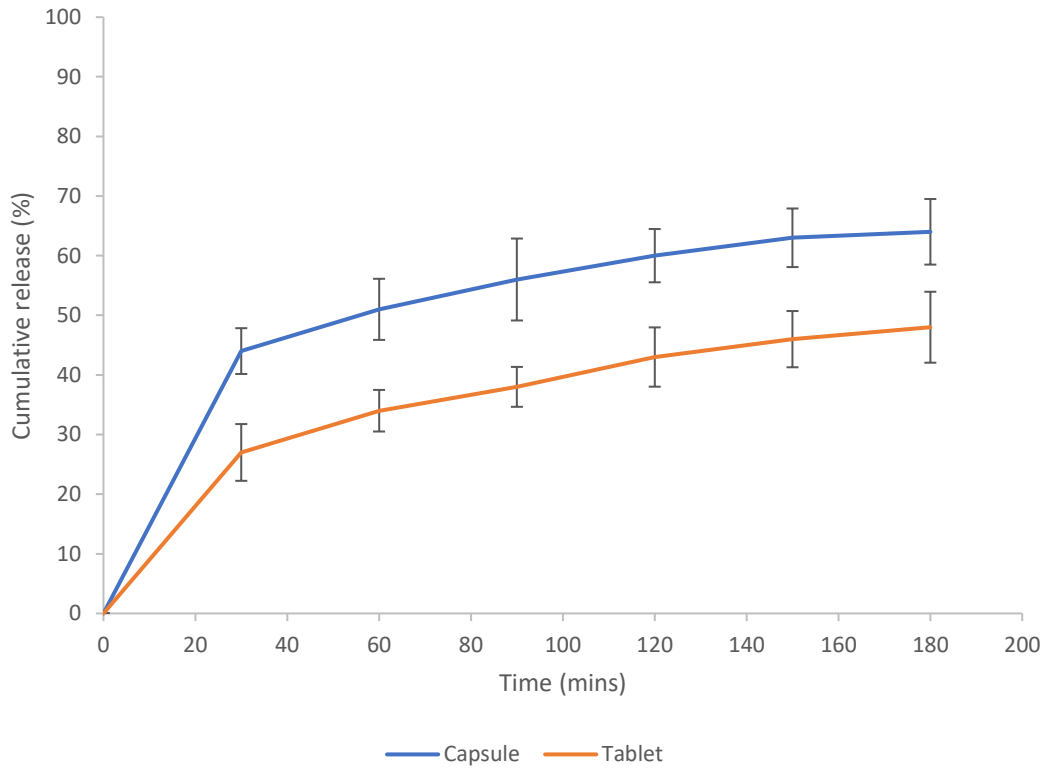

Figure 5.13. Release study of the BSA from a tablet and capsule containing SYLOID 40%. The Y axis represent the cumulative release (%), and the X axis represent the experiment running time (mins). Error bars represent standard deviation.

The tablet has disintegrated within 7.5 minutes while the capsule has fully dissolved within 5 minutes. As seen from the figure above, the tablet and the capsule have released the drug (BSA) over the duration of the study. The capsule released the drug and the maximum cumulative amount achieved was 64% after 3 hours. However, the tablet has achieved a 48% cumulative release after the same time. This variation could indicate that the compression force might have affected the protein and decreased the released amount.

Conclusions

This chapter reports the development of a mesoporous silica-protein-based tablet for oral delivery. The used silica is a micro-sized carrier (SYLOID XDP 3150), and the model protein was BSA.

BSA was loaded into SYLOID via a solvent evaporation method using water as the loading solvent at three concentrations (10, 20, and 40%) w/w, which were further characterised. The formulation with the 40% concentration was chosen for tabletting due to its highest recovery.

Tabletting SYLOID as a carrier without additives was not achieved due to the large size of the carrier and its low compressibility. Using high-pressure forces of 3 Tons has resulted in fragmenting the silica carrier.

Tablets were made using two diluents in different ratios (avicel:lactose monohydrate 25:75, 50:50, and 75:25), as well as different SYLOID concentrations (0, 20, and 40%) w/w of the tablet weight (500 mg), followed by characterising the tablet properties.

The porosity of the tablet decreased with avicel's amount increase, attributed to the high interparticle bonding between Avicel particles, leading to a reduction in porosity. Additionally, the porosity percentage increased with SYLOID concentration increase, which is related to the porous structure of SYLOID that contributes to the tablet porosity.

The diluent composition affected the disintegration time, where increasing lactose ratio enhances disintegration. This is due to the soluble nature of lactose compared to avicel. Additionally, increasing SYLOID amount has decreased the disintegration time, which is related to the large size of SYLOID as well as the binder mixture forming a barrier-like layer around the particles restricting water penetration. Furthermore, the formulations containing 40% SYLOID that were made with avicel ratios above 50% did not disintegrate after 50 minutes. This is due to the higher amount of avicel and SYLOID and the barrier-like layer around SYLOID particles.

The hardness was found to be the highest in formulations made using avicel at a ratio of 75:25. This is due to avicel's plasticity and hydrogen groups on the cellulose surface that maximise interparticle bonding. Furthermore, increasing SYLOID concentration in the tablet decreased hardness as SYLOID does not plastically deform and has poor compressibility.

The friability of the tablets was dependent on avicel amount, in which formulations with a high avicel ratio resulted in low friability. On the other hand, high SYLOID concentration in the tablet resulted in a high friability due to its poor compressibility and decreased hardness of the tablet.

All the formulations containing SYLOID failed to make compactable tablets that disintegrate within the expected specifications for immediate release tablets. However, that tablet that contained 20% SYLOID and made using avicel:lactose 75:25 was chosen for further adjustments. The addition of a PVP at 5% w/w and croscarmellose at 2% w/w has resulted in the formulation passing all the requirements for immediate release tablets. SYLOID was substituted with the previously prepared SYLOID-BSA 40%, and the tablet dissolution was conducted to investigate BSA release. The tablet was compared to a capsule in regard to BSA release. However, the released amount from the tablet was lower than that from the capsule, which indicates that the tabletting process could have affected the release. In summary, the development of silica-based tablets is achievable despite the low compressibility properties of SYLOID XDP 3150. Yet, this is attainable upon the utilisation of diluents in substantial proportions (80% of tablet weight) and application of high pressure (3 Tons).

Chapter 6

Conclusions and Future Work

Conclusions

The oral delivery of peptides is challenging due to the harsh pH environment across the GIT that decreases the bioavailability of proteins. Additionally, the physiochemical properties of the proteins affect the absorption into the GIT, where high molecular weights decrease absorption. Furthermore, there are numerous barriers to absorption that include mucus and absorption routes (paracellular and transcellular) with the tight junctions between cells. Therefore, many research efforts have been introduced to enhance the bioavailability and absorption of oral peptides. These consisted of using polymers for enhancing absorption and interaction with intestinal epithelium, lipid-based carriers, nanocarriers comprising mesoporous silica nanoparticles (MSNs), and excipients involving permeation enhancers (PEs).

Mesoporous silica carriers are GRAS-listed materials that have been highly studied for delivery due to their characteristics. For instance, their porous structure, high surface area, and versatile and easily functionalised structure make them great candidates for loading. They have been reported to enhance the dissolution of materials by incorporating them in their amorphous form. PEs enhance the absorption of drugs by operating either on the transcellular route or the paracellular via adjusting the tight junctions. Several PEs have GRAS status, like Salcaprozate sodium and sodium caprylate, which have been introduced into FDA-approved drugs of Rybelsus and Mycapssa, respectively. These two formulations were manufactured for the delivery of octreotide acetate in Mycapssa and semaglutide in Rybelsus. In addition, scientists have worked on developing several technologies and devices that enhance drug absorption and bioavailability. Noteworthy among these innovations are orally ingested needle-based delivery devices. These include LUMI and SOMA that deliver insulin to the intestinal lumen and stomach lining, respectively. Yet, these techniques might present a disadvantage concerning the use of non-biodegradable needles and devices. In addition, the literature has reported that lipids are used to enhance the interaction with cell membranes in a a non-destructive manner, which might be a good substitute for non-biodegradable needles.

As mentioned previously, Mycapssa is used for the oral delivery of octreotide acetate for the treatment of acromegaly virus. Octreotide is an octapeptide that is poorly absorbed due to its hydrophilic properties and high molecular weight (1kDa). The overall aim of the project is to design a novel mesoporous silica-lipid-based carrier for the oral delivery of peptides. The designed carrier was fabricated using SYLOID XDP 3050 as the mesoporous silica microparticle, subsequently coated with needle-like structures composed of lipids (stearic acid).

The first part of the project aimed at developing a mesoporous silica-lipid carrier. The factors that affect the formulation of the SYLOID-lipid complex were investigated. Stearic acid crystallised on the surface at concentrations exceeding the maximum loading capacity of SYLOID pores to form needle-like structures. SEM imaging has shown that stearic acid capped the pores of SYLOID, and the pore filling increased as stearic acid concentration increased. The utilisation of confocal microscopy proved highly valuable in confirming the presence of stearic acid inside the porous structure of SYLOID and on the surface due to the autofluorescence properties of stearic acid. Moreover, the pore filling of SYLOID was also confirmed by nitrogen porosimetry, where the smallest pore size was associated with the highest stearic acid loading concentration. Additionally, the thermal properties of the SYLOID-lipid carrier were assessed, and the needle-like structures were found to be stearic acid recrystallising on the surface, which was subsequently confirmed via XRD analysis.

Following the development of the SYLOID-stearic carrier, the next step focused on incorporating a protein inside the carrier complex for permeability studies. The chosen protein was octreotide, and an HPLC method was developed and validated according to ICH guidelines for octreotide analysis. The complex carrier that is composed of SYLOID, stearic acid, and octreotide has been found to maintain the needle-like structures on the surface. Additionally, compact-like structures have been found embedded between the needles which were related to octreotide recrystallisation during formulation. Fluorescence imaging has confirmed the presence and positioning of both octreotide compacts and stearic needles, where octreotide was found to be incorporated inside the carrier and between the needle-like structures of stearic. Subsequently, the permeability of octreotide was assessed, where the use of the new formed complex with different permeability enhancers was reported. Indeed, octreotide had a low permeability, which might be due to its hydrophilic properties and molecular weight. The permeability and absorption of octreotide across Caco-2 cells has significantly increased upon using the complex for delivery. Additionally, the apparent permeability closely resembled the value observed with the utilization of permeation enhancers (SNAC), suggesting that the complex possesses the potential for enhancing drug permeability. The hypothesis is based on the needle-like structures interacting with the cells and enhancing the absorption of octreotide.

The Subsequent phase of the project after the successful increase of octreotide absorption using the newly developed complex, involved evaluating the factors that affect silica loading. The work involved studying the interactions between the solvent-carrier (SYLOID) and carrier-protein. The chapter work comprises studying the loading of two proteins with different molecular weights (octreotide and BSA) while using three solvents (water, ethanol, and methanol). Protein Diffusion was found to be governed by the Stokes-Einstein equation, where

the viscosity and protein size are disproportional to diffusivity. Due to its low molecular size, octreotide diffused into SYLOID more efficiently than BSA. Interestingly, methanol was found to be the most efficient solvent for octreotide loading as it has the lowest viscosity and its lower interaction with the silica surface compared to water. Loading BSA with alcohol-based solvents forms insoluble micro aggregates, affecting loading efficiency. In this chapter, we reported the relationship between protein fluorescence intensity and diffusion based on generated 3d images via confocal microscopy. This method proved valuable as it indicated protein positioning inside the carrier, and on the surface which was later confirmed using SEM. Based on this method, we found that the positioning of octreotide depends on the solvent used, where it diffuses evenly and occupies the porous structure upon loading with methanol. However, BSA was found to be crystallised on the surface of the carrier with minimal diffusion due to its large size.

The final part of the project explored the factors that govern silica tabletting and the design of a silica-based tablet for the oral delivery of proteins. Silica-based tablets are challenging to manufacture due to the low compressibility of silica particles. The type and size of these carriers are crucial factors in tabletting processes, influencing the resultant tablet's hardness, friability, disintegration, and thickness. Furthermore, tabletting silica without the inclusion of diluents or binders is ineffective due to its hard shell and the absence of materials that can dissipate pressure for the formation of a successful tablet. This was evident in the case of SYLOID, as the mesoporous carrier has deformed and lost various aspects of its morphological properties due to the high applied pressure. The hurdles mentioned above were successfully overcome by designing SYLOID-based tablets with different ratios and compositions of diluents. Prior to the tablet design, the composition of the powder mix was investigated by choosing lactose and avicel, considering their ability to dissipate pressure and maintain tablet integrity. Increasing the avicel ratio in the tablet increases the tablet's disintegration time, thickness, and hardness.
On the other hand, it decreases friability percentage and porosity. These effects are related to avicel’s chemical structure that is rich with hydroxyl group, its insolubility in water, and lower plastic deformation compared to lactose. Following the successful formulation of a tablet meeting the criteria for immediate release tablets, the substitution of SYLOID with pre-formulated SYLOID-BSA was implemented to devise a silica-based tablet intended for the oral delivery of proteins. The newly developed BSA-based product was manufactured and has also met the criteria for immediate release tablets, eventhough though the manufacturing process might have affected the release properties of BSA from SYLOID.

Future work

The project focused on developing a novel mesoporous silica carrier for the oral delivery of octreotide. Yet, it has not been examined for other entities. Therefore, the potential applications of this platform for alternative proteins can be investigated.

The proposed hypothesis for the enhanced octreotide absorption was the interaction between stearic acid-based needles and the cells. Hence, future work can focus on examining the specific interaction mechanism with cells that led to enhanced permeability and absorption. Furthermore, *In vitro* tests can be conducted to assess the efficiency of the developed complex in delivering octreotide.

The release behaviour of octreotide from the silica-protein tablet could be further investigated, where the factors that hindered its release can be examined. Furthermore, the use of this newly developed complex with different oral drug delivery systems can be assessed. Additionally, incorporating the complex in a tablet-based delivery system can be studied, in which the factors that ensure the preservation of needle-like structures are investigated.

References

ABDULKARIM, M., SHARMA, P. K. & GUMBLETON, M. 2019. Self-emulsifying drug delivery system: Mucus permeation and innovative quantification technologies. *Adv Drug Deliv Rev,* 142**,** 62-74.

ABEER, M. M., MEKA, A. K., PUJARA, N., KUMERIA, T., STROUNINA, E., NUNES, R., COSTA, A., SARMENTO, B., HASNAIN, S. Z., ROSS, B. P. & POPAT, A. 2019. Rationally Designed Dendritic Silica Nanoparticles for Oral Delivery of Exenatide. *Pharmaceutics,* 11.

ABEER, M. M., REWATKAR, P., QU, Z., TALEKAR, M., KLEITZ, F., SCHMID, R., LINDEN, M., KUMERIA, T. & POPAT, A. 2020. Silica nanoparticles: A promising platform for enhanced oral delivery of macromolecules. *J Control Release,* 326**,** 544-555.

AGORAM, B., WOLTOSZ, W. S. & BOLGER, M. B. 2001. Predicting the impact of physiological and biochemical processes on oral drug bioavailability. *Adv Drug Deliv Rev,* 50 Suppl 1**,** S41-67.

AGUIRRE, T. A., TEIJEIRO-OSORIO, D., ROSA, M., COULTER, I. S., ALONSO, M. J. & BRAYDEN, D. J. 2016. Current status of selected oral peptide technologies in advanced preclinical development and in clinical trials. *Adv Drug Deliv Rev,* 106**,** 223-241.

AHADIAN, S., FINBLOOM, J. A., MOFIDFAR, M., DILTEMIZ, S. E., NASROLLAHI, F., DAVOODI, E., HOSSEINI, V., MYLONAKI, I., SANGABATHUNI, S., MONTAZERIAN, H., FETAH, K., NASIRI, R., DOKMECI, M. R., STEVENS, M. M., DESAI, T. A. & KHADEMHOSSEINI, A. 2020. Micro and nanoscale technologies in oral drug delivery. *Adv Drug Deliv Rev,* 157**,** 37-62.

AHMADI, F., SODAGAR-TALEGHANI, A., EBRAHIMNEJAD, P., POUYA HADIPOUR MOGHADDAM, S., EBRAHIMNEJAD, F., ASARE-ADDO, K. & NOKHODCHI, A. 2022. A review on the latest developments of mesoporous silica nanoparticles as a promising platform for diagnosis and treatment of cancer. *Int J Pharm,* 625**,** 122099.

AJITO, K., NAKAMURA, M., TAJIMA, T. & UENO, Y. 2016. Terahertz Spectroscopy Methods and Instrumentation.

ALKEKHIA, D., HAMMOND, P. T. & SHUKLA, A. 2020. Layer-by-Layer Biomaterials for Drug Delivery. *Annu Rev Biomed Eng,* 22**,** 1-24.

ALMQUIST, B. D. & MELOSH, N. A. 2010. Fusion of biomimetic stealth probes into lipid bilayer cores. *Proc Natl Acad Sci U S A,* 107**,** 5815-20.

ALTAANI, B. M., ALMAAYTAH, A. M., DADOU, S., ALKHAMIS, K., DARADKA, M. H. & HANANEH, W. 2020. Oral Delivery of Teriparatide Using a Nanoemulsion System: Design, in Vitro and in Vivo Evaluation. *Pharm Res,* 37**,** 80.

ALZOUBI, T., MARTIN, G. P., BARLOW, D. J. & ROYALL, P. G. 2021. Stability of alpha-lactose monohydrate: The discovery of dehydration triggered solid-state epimerization. *Int J Pharm,* 604**,** 120715.

AMIDON, S., BROWN, J. E. & DAVE, V. S. 2015. Colon-targeted oral drug delivery systems: design trends and approaches. *AAPS PharmSciTech,* 16**,** 731-41.

AMT. 2023. Available: https://www.fiercebiotech.com/biotech/after-slimming-down-applied-molecular-transport-no-closer-taking-uc-drug-phase-3 [Accessed 30/5/2024].

ANFINSEN, C. B. 1973. Principles that govern the folding of protein chains. *Science,* 181**,** 223-30.

ARAUJO, F., SHRESTHA, N., SHAHBAZI, M. A., FONTE, P., MAKILA, E. M., SALONEN, J. J., HIRVONEN, J. T., GRANJA, P. L., SANTOS, H. A. & SARMENTO, B. 2014. The impact of nanoparticles on the mucosal translocation and transport of GLP-1 across the intestinal epithelium. *Biomaterials,* 35**,** 9199-207.

ARIGA, K., ZHANG, Q., NIKI, M., OKABE, A. & AIDA, T. 2003. Proteosilica - mesoporous silicates densely filling amino acid and peptide assemblies in their nanoscale pores. *In:* PARK, S.-E., RYOO, R., AHN, W.-S., LEE, C. W. & CHANG, J.-S. (eds.) *Studies in Surface Science and Catalysis.* Elsevier.

ARODA, V. R., BLONDE, L. & PRATLEY, R. E. 2022. A new era for oral peptides: SNAC and the development of oral semaglutide for the treatment of type 2 diabetes. *Rev Endocr Metab Disord,* 23**,** 979-994.

AWAD, A., MADLA, C. M., MCCOUBREY, L. E., FERRARO, F., GAVINS, F. K. H., BUANZ, A., GAISFORD, S., ORLU, M., SIEPMANN, F., SIEPMANN, J. & BASIT, A. W. 2022.

Clinical translation of advanced colonic drug delivery technologies. *Adv Drug Deliv Rev,* 181**,** 114076.

BAAN, A., ADRIAENSENS, P., LAMMENS, J., DELGADO HERNANDEZ, R., VANDEN BERGHE, W., PIETERS, L., VERVAET, C. & KIEKENS, F. 2019. Dry amorphisation of mangiferin, a poorly water-soluble compound, using mesoporous silica. *Eur J Pharm Biopharm,* 141**,** 172-179.

BAJRACHARYA, R., SONG, J. G., BACK, S. Y. & HAN, H. K. 2019. Recent Advancements in Non-Invasive Formulations for Protein Drug Delivery. *Comput Struct Biotechnol J,* 17**,** 1290-1308.

BAKHSHIAN NIK, A., ZARE, H., RAZAVI, S., MOHAMMADI, H., TORAB AHMADI, P., YAZDANI, N., BAYANDORI, M., RABIEE, N. & IZADI MOBARAKEH, J. 2020. Smart drug delivery: Capping strategies for mesoporous silica nanoparticles. *Microporous and Mesoporous Materials,* 299.

BAUER, W., BRINER, U., DOEPFNER, W., HALLER, R., HUGUENIN, R., MARBACH, P., PETCHER, T. J. & PLESS, J. 1982. SMS 201–995: A very potent and selective octapeptide analogue of somatostatin with prolonged action. *Life Sciences,* 31**,** 1133-1140.

BAUMGARTNER, A. & PLANINSEK, O. 2021. Application of commercially available mesoporous silica for drug dissolution enhancement in oral drug delivery. *Eur J Pharm Sci,* 167**,** 106015.

BECKMANN, W., BOISTELLE, R. & SATO, K. 1984. Solubility of the A, B, and C polymorphs of stearic acid in decane, methanol, and butanone. *Journal of Chemical & Engineering Data,* 29**,** 211-214.

BEDNAREK, R. 2022. In Vitro Methods for Measuring the Permeability of Cell Monolayers. *Methods Protoc,* 5.

BELOQUI, A., DES RIEUX, A. & PREAT, V. 2016. Mechanisms of transport of polymeric and lipidic nanoparticles across the intestinal barrier. *Adv Drug Deliv Rev,* 106**,** 242-255.

BERG, S., EDLUND, H., W, R. F. G., C, A. S. B. & DAVIES, N. M. 2022. Considerations in the developability of peptides for oral administration when formulated together with transient permeation enhancers. *Int J Pharm,* 628**,** 122238.

BERNKOP-SCHNURCH, A., PINTER, Y., GUGGI, D., KAHLBACHER, H., SCHOFFMANN, G., SCHUH, M., SCHMEROLD, I., DEL CURTO, M. D., D'ANTONIO, M., ESPOSITO, P. & HUCK, C. 2005. The use of thiolated polymers as carrier matrix in oral peptide delivery--proof of concept. *J Control Release,* 106**,** 26-33.

BHATTACHARYYA, S. & RAMACHANDRAN, D. 2022. Solubility enhancement study of lumefantrine by formulation of liquisolid compact using mesoporous silica as a novel adsorbent. *Materials Letters: X,* 16.

BHUTANI, U., BASU, T. & MAJUMDAR, S. 2021. Oral Drug Delivery: Conventional to Long Acting New-Age Designs. *Eur J Pharm Biopharm,* 162**,** 23-42.

BIOCON. 2021. Available: https://www.biocon.com/businesses/novel-biologics/insulin-tregopil/ [Accessed 29/10/2021].

BLACH, C., GRAVELLE, A. J., PEYRONEL, F., WEISS, J., BARBUT, S. & MARANGONI, A. G. 2016. Revisiting the crystallization behavior of stearyl alcohol : stearic acid (SO : SA) mixtures in edible oil. *RSC Advances,* 6**,** 81151-81163.

BLATTNER, D., KOLB, M. & LEUENBERGER, H. 1990. Percolation theory and compactibility of binary powder systems. *Pharm Res,* 7**,** 113-7.

BONENGEL, S., JELKMANN, M., ABDULKARIM, M., GUMBLETON, M., REINSTADLER, V., OBERACHER, H., PRUFERT, F. & BERNKOP-SCHNURCH, A. 2018. Impact of different hydrophobic ion pairs of octreotide on its oral bioavailability in pigs. *J Control Release,* 273**,** 21-29.

BRAUN, K., STÜRZEL, C. M., KIRCHHOFF, F. & LINDÉN, M. 2020. In Vitro Evaluation of a Peptide-Mesoporous Silica Nanoparticle Drug Release System against HIV-1. *Inorganics,* 8.

BRAYDEN, D., CREED, E., O'CONNELL, A., LEIPOLD, H., AGARWAL, R. & LEONE-BAY, A. 1997. Heparin absorption across the intestine: effects of sodium N-[8-(2-hydroxybenzoyl)amino]caprylate in rat in situ intestinal instillations and in Caco-2 monolayers. *Pharm Res,* 14**,** 1772-9.

BRAYDEN, D. J., HILL, T. A., FAIRLIE, D. P., MAHER, S. & MRSNY, R. J. 2020. Systemic delivery of peptides by the oral route: Formulation and medicinal chemistry approaches. *Adv Drug Deliv Rev,* 157**,** 2-36.

BRITISH PHARMACOPEIA 2021. *British Pharmacopeia* London: Stationary Office.

BROWN, N. J. 1990. Octreotide: a long-acting somatostatin analog. *Am J Med Sci,* 300**,** 267-73.

BROWN, T. D., WHITEHEAD, K. A. & MITRAGOTRI, S. 2019. Materials for oral delivery of proteins and peptides. *Nature Reviews Materials,* 5**,** 127-148.

BRUNNER, J., RAGUPATHY, S. & BORCHARD, G. 2021. Target specific tight junction modulators. *Adv Drug Deliv Rev,* 171**,** 266-288.

BUCKLEY, S. T., BAEKDAL, T. A., VEGGE, A., MAARBJERG, S. J., PYKE, C., AHNFELT-RONNE, J., MADSEN, K. G., SCHEELE, S. G., ALANENTALO, T., KIRK, R. K., PEDERSEN, B. L., SKYGGEBJERG, R. B., BENIE, A. J., STRAUSS, H. M., WAHLUND, P. O., BJERREGAARD, S., FARKAS, E., FEKETE, C., SONDERGAARD, F. L., BORREGAARD, J., HARTOFT-NIELSEN, M. L. & KNUDSEN, L. B. 2018. Transcellular stomach absorption of a derivatized glucagon-like peptide-1 receptor agonist. *Sci Transl Med,* 10.

CAI, D., HAN, C., LIU, C., MA, X., QIAN, J., ZHOU, J., LI, Y., SUN, Y., ZHANG, C. & ZHU, W. 2020. Chitosan-capped enzyme-responsive hollow mesoporous silica nanoplatforms for colon-specific drug delivery. *Nanoscale Res Lett,* 15**,** 123.

CALVO, B. & CEPEDA, E. A. 2008. Solubilities of Stearic Acid in Organic Solvents and in Azeotropic Solvent Mixtures. *Journal of Chemical & Engineering Data,* 53**,** 628-633.

CARDOSO, V. M. D. O., BRITO, N. A. P. D., FERREIRA, N. N., BONI, F. I., FERREIRA, L. M. B., CARVALHO, S. G. & GREMIÃO, M. P. D. 2021. Design of mucoadhesive gellan gum and chitosan nanoparticles intended for colon-specific delivery of peptide drugs. *Colloids and Surfaces A: Physicochemical and Engineering Aspects,* 628.

CHALASANI, K. B., RUSSELL-JONES, G. J., YANDRAPU, S. K., DIWAN, P. V. & JAIN, S. K. 2007. A novel vitamin B12-nanosphere conjugate carrier system for peroral delivery of insulin. *J Control Release,* 117**,** 421-9.

CHARNAY, C., BEGU, S., TOURNE-PETEILH, C., NICOLE, L., LERNER, D. A. & DEVOISSELLE, J. M. 2004. Inclusion of ibuprofen in mesoporous templated silica: drug loading and release property. *Eur J Pharm Biopharm,* 57**,** 533-40.

CHATZITAKI, A. T., ELEFTHERIADIS, G., TSONGAS, K., TZETZIS, D., SPYROS, A., VIZIRIANAKIS, I. S. & FATOUROS, D. G. 2023. Fabrication of 3D-printed octreotide acetate-loaded oral solid dosage forms by means of semi-solid extrusion printing. *Int J Pharm,* 632**,** 122569.

CHIASMA. 2021. Available: https://chiasma.com/octreotide-capsules/ [Accessed 29/10/2021].

CHIASMATPE. 2021. Available: https://chiasma.com/our-platform-technology/ [Accessed 29/10/2021].

CHOI DU, H., KIM, K. H., PARK, J. S., JEONG, S. H. & PARK, K. 2013. Evaluation of drug delivery profiles in geometric three-layered tablets with various mechanical properties, in vitro-in vivo drug release, and Raman imaging. *J Control Release,* 172**,** 763-72.

CHOONARA, B. F., CHOONARA, Y. E., KUMAR, P., BIJUKUMAR, D., DU TOIT, L. C. & PILLAY, V. 2014. A review of advanced oral drug delivery technologies facilitating the protection and absorption of protein and peptide molecules. *Biotechnol Adv,* 32**,** 1269-1282.

CHUANG, E. Y., LIN, K. J., LIN, P. Y., CHEN, H. L., WEY, S. P., MI, F. L., HSIAO, H. C., CHEN, C. T. & SUNG, H. W. 2015. Self-assembling bubble carriers for oral protein delivery. *Biomaterials,* 64**,** 115-24.

COLLNOT, E. M., BALDES, C., WEMPE, M. F., HYATT, J., NAVARRO, L., EDGAR, K. J., SCHAEFER, U. F. & LEHR, C. M. 2006. Influence of vitamin E TPGS poly(ethylene glycol) chain length on apical efflux transporters in Caco-2 cell monolayers. *J Control Release,* 111**,** 35-40.

COLUMBU, S., MULAS, M., MUNDULA, F. & CIONI, R. 2021. Strategies for helium pycnometry density measurements of welded ignimbritic rocks. *Measurement,* 173.

COSMOPHARAMCEUTICALS. 2021. Available: https://www.cosmopharma.com/activities/technology [Accessed 29/10/2021].

COUTINHO, A. J., COSTA LIMA, S. A., AFONSO, C. M. M. & REIS, S. 2020. Mucoadhesive and pH responsive fucoidan-chitosan nanoparticles for the oral delivery of methotrexate. *Int J Biol Macromol,* 158**,** 180-188.

CROISSANT, J. G., ZHANG, D., ALSAIARI, S., LU, J., DENG, L., TAMANOI, F., ALMALIK, A. M., ZINK, J. I. & KHASHAB, N. M. 2016. Protein-gold clusters-capped mesoporous silica nanoparticles for high drug loading, autonomous gemcitabine/doxorubicin co-delivery, and in-vivo tumor imaging. *J Control Release,* 229**,** 183-191.

CUI, M., WU, W., HOVGAARD, L., LU, Y., CHEN, D. & QI, J. 2015. Liposomes containing cholesterol analogues of botanical origin as drug delivery systems to enhance the oral absorption of insulin. *Int J Pharm,* 489**,** 277-84.

DAHLGREN, D. & LENNERNAS, H. 2019. Intestinal Permeability and Drug Absorption: Predictive Experimental, Computational and In Vivo Approaches. *Pharmaceutics,* 11.

DAHLGREN, D., OLANDER, T., SJOBLOM, M., HEDELAND, M. & LENNERNAS, H. 2021. Effect of paracellular permeation enhancers on intestinal permeability of two peptide drugs, enalaprilat and hexarelin, in rats. *Acta Pharm Sin B,* 11**,** 1667-1675.

DE JONG, W. H. & BORM, P. J. 2008. Drug delivery and nanoparticles:applications and hazards. *Int J Nanomedicine,* 3**,** 133-49.

DE KRUIF, J. K., LEDERGERBER, G., GAROFALO, C., FASLER-KAN, E. & KUENTZ, M. 2016. On prilled Nanotubes-in-Microgel Oral Systems for protein delivery. *Eur J Pharm Biopharm,* 101**,** 90-102.

DE KRUIF, J. K., VARUM, F., BRAVO, R. & KUENTZ, M. 2015. A Systematic Study on Manufacturing of Prilled Microgels into Lipids for Oral Protein Delivery. *J Pharm Sci,* 104**,** 3351-65.

DE SOUSA, F. F., DA SILVA, L. D. P. & FREITAS, K. H. G. 2017. Electrical and dielectric properties of water. *Scientia Plena,* 13.

DECHER, G. 1997. Fuzzy Nanoassemblies: Toward Layered Polymeric Multicomposites. *Science,* 277**,** 1232-1237.

DENING, T. J. & TAYLOR, L. S. 2018. Supersaturation Potential of Ordered Mesoporous Silica Delivery Systems. Part 1: Dissolution Performance and Drug Membrane Transport Rates. *Mol Pharm,* 15**,** 3489-3501.

DIABETOLOGY. 2021. Available: https://www.diabetology.co.uk/projects/capsulin/ [Accessed 29/10/2021].

DIASOME. 2021. Available: https://www.diasome.com/latest-updates [Accessed 29/10/2021].

DING, X., RATH, P., ANGELO, R., STRINGFELLOW, T., FLANDERS, E., DINH, S., GOMEZ-ORELLANA, I. & ROBINSON, J. R. 2004. Oral absorption enhancement of cromolyn sodium through noncovalent complexation. *Pharm Res,* 21**,** 2196-206.

DIZDAREVIC, A., EFIANA, N. A., PHAN, T. N. Q., MATUSZCZAK, B. & BERNKOP-SCHNURCH, A. 2019. Imine bond formation: A novel concept to incorporate peptide drugs in self-emulsifying drug delivery systems (SEDDS). *Eur J Pharm Biopharm,* 142**,** 92-100.

DOELKER, E. 2008. Comparative compaction properties of various Microcrystalline Cellulose types and Generic Products. *Drug Development and Industrial Pharmacy,* 19**,** 2399-2471.

DORKOOSH, F. A., VERHOEF, J. C., VERHEIJDEN, J. H., RAFIEE-TEHRANI, M., BORCHARD, G. & JUNGINGER, H. E. 2002. Peroral absorption of octreotide in pigs formulated in delivery systems on the basis of superporous hydrogel polymers. *Pharm Res,* 19**,** 1532-6.

DRAGAN, E. S. & DINU, M. V. 2019. Polysaccharides constructed hydrogels as vehicles for proteins and peptides. A review. *Carbohydr Polym,* 225**,** 115210.

DRUCKER, D. J. 2020. Advances in oral peptide therapeutics. *Nat Rev Drug Discov,* 19**,** 277-289.

DUBEY, S. K., PARAB, S., DABHOLKAR, N., AGRAWAL, M., SINGHVI, G., ALEXANDER, A., BAPAT, R. A. & KESHARWANI, P. 2021. Oral peptide delivery: challenges and the way ahead. *Drug Discov Today,* 26**,** 931-950.

DUMONT, C., JANNIN, V., MIOLANE, C., LELONG, Q., VALOUR, J.-P., URBANIAK, S., FESSI, H. & BOURGEOIS, S. 2019. A proof-of-concept for developing oral lipidized peptide Nanostructured Lipid Carrier formulations. *Journal of Drug Delivery Science and Technology,* 54.

DURAN-LOBATO, M., CARRILLO-CONDE, B., KHAIRANDISH, Y. & PEPPAS, N. A. 2014. Surface-modified P(HEMA-co-MAA) nanogel carriers for oral vaccine delivery: design, characterization, and in vitro targeting evaluation. *Biomacromolecules,* 15**,** 2725-34.

EASA, N., ALANY, R. G., CAREW, M. & VANGALA, A. 2019. A review of non-invasive insulin delivery systems for diabetes therapy in clinical trials over the past decade. *Drug Discov Today,* 24**,** 440-451.

EL-SETOUHY, D. A., BASALIOUS, E. B. & ABDELMALAK, N. S. 2015. Bioenhanced sublingual tablet of drug with limited permeability using novel surfactant binder and microencapsulated polysorbate: In vitro/in vivo evaluation. *Eur J Pharm Biopharm,* 94**,** 386-92.

EL MOUKHTARI, S. H., RODRIGUEZ-NOGALES, C. & BLANCO-PRIETO, M. J. 2021. Oral lipid nanomedicines: Current status and future perspectives in cancer treatment. *Adv Drug Deliv Rev,* 173**,** 238-251.

EMA-ICH-Q2R2. 2023. [Accessed 23/6/2023].

ENOVIC. 2021. Available: https://healthcare.evonik.com/en/custom-solutions/oral-drug-delivery/EUDRATEC-PEP [Accessed 29/10/2021].

EREL, G., KOTMAKÇI, M., AKBABA, H., SÖZER KARADAĞLI, S. & KANTARCI, A. G. 2016. Nanoencapsulated chitosan nanoparticles in emulsion-based oral delivery system: In vitro and in vivo evaluation of insulin loaded formulation. *Journal of Drug Delivery Science and Technology,* 36**,** 161-167.

ERFANI JABARIAN, L., ROUINI, M. R., ATYABI, F., FOROUMADI, A., NASSIRI, S. M. & DINARVAND, R. 2013. In vitro and in vivo evaluation of an in situ gel forming system for the delivery of PEGylated octreotide. *Eur J Pharm Sci,* 48**,** 87-96.

ERICKSON, H. P. 2009. Size and shape of protein molecules at the nanometer level determined by sedimentation, gel filtration, and electron microscopy. *Biol Proced Online,* 11**,** 32-51.

FAN, S., GAO, H., DONG, W., TANG, J., WANG, J., YANG, M. & WANG, G. 2017. Shape-Stabilized Phase Change Materials Based on Stearic Acid and Mesoporous Hollow SiO2 Microspheres (SA/SiO2) for Thermal Energy Storage. *European Journal of Inorganic Chemistry,* 2017**,** 2138-2143.

FAN, T., CHEN, C., GUO, H., XU, J., ZHANG, J., ZHU, X., YANG, Y., ZHOU, Z., LI, L. & HUANG, Y. 2014. Design and evaluation of solid lipid nanoparticles modified with peptide ligand for oral delivery of protein drugs. *Eur J Pharm Biopharm,* 88**,** 518-28.

FATTAH, S., ISMAIEL, M., MURPHY, B., RULIKOWSKA, A., FRIAS, J. M., WINTER, D. C. & BRAYDEN, D. J. 2020. Salcaprozate sodium (SNAC) enhances permeability of octreotide across isolated rat and human intestinal epithelial mucosae in Ussing chambers. *Eur J Pharm Sci,* 154**,** 105509.

FAYED, M. H., ALDAWSARI, M. F., ALALI, A. S., ALSAQR, A., ALMUTAIRY, B. K., AODAH, A. H., TAWFEEK, H. M., KHAFAGY, E.-S. & HELAL, D. A. 2022. Design-of-experiment approach to quantify the effect of nano-sized silica on tableting properties of microcrystalline cellulose to facilitate direct compression tableting of binary blend containing a low-dose drug. *Journal of Drug Delivery Science and Technology,* 68.

FEDI, A., VITALE, C., PONSCHIN, G., AYEHUNIE, S., FATO, M. & SCAGLIONE, S. 2021. In vitro models replicating the human intestinal epithelium for absorption and metabolism studies: A systematic review. *J Control Release,* 335**,** 247-268.

FENG, Y., YUAN, D., KONG, B., SUN, F., WANG, M., WANG, H. & LIU, Q. 2022. Structural changes and exposed amino acids of ethanol-modified whey proteins isolates promote its antioxidant potential. *Current Research in Food Science*.

FISHERSCI-POLARITY. 2023. Available: https://www.fishersci.co.uk/gb/en/scientific-products/technical-tools/summary-key-physical-data-solvents.html [Accessed 10/4/2023].

FLOREA, B. I., THANOU, M., JUNGINGER, H. E. & BORCHARD, G. 2006. Enhancement of bronchial octreotide absorption by chitosan and N-trimethyl chitosan shows linear in vitro/in vivo correlation. *J Control Release,* 110**,** 353-361.

FRALLICCIARDI, J., MELCR, J., SIGINOU, P., MARRINK, S. J. & POOLMAN, B. 2022. Membrane thickness, lipid phase and sterol type are determining factors in the permeability of membranes to small solutes. *Nat Commun,* 13**,** 1605.

FRICKER, G., DREWE, J., VONDERSCHER, J., KISSEL, T. & BEGLINGER, C. 1992. Enteral absorption of octreotide. *Br J Pharmacol,* 105**,** 783-6.

FRITSCH, C., ORIAN-ROUSSEAUL, V., LEFEBVRE, O., SIMON-ASSMANN, P., REIMUND, J. M., DUCLOS, B. & KEDINGER, M. 1999. Characterization of human intestinal stromal cell lines: response to cytokines and interactions with epithelial cells. *Exp Cell Res,* 248**,** 391-406.

GACI, N., BORREL, G., TOTTEY, W., O'TOOLE, P. W. & BRUGERE, J. F. 2014. Archaea and the human gut: new beginning of an old story. *World J Gastroenterol,* 20**,** 16062-78.

GAO, R., STREHLE, S., TIAN, B., COHEN-KARNI, T., XIE, P., DUAN, X., QING, Q. & LIEBER, C. M. 2012. Outside looking in: nanotube transistor intracellular sensors. *Nano Lett,* 12**,** 3329-33.

GAO, Y., HE, Y., ZHANG, H., ZHANG, Y., GAO, T., WANG, J. H. & WANG, S. 2021. Zwitterion-functionalized mesoporous silica nanoparticles for enhancing oral delivery of protein drugs by overcoming multiple gastrointestinal barriers. *J Colloid Interface Sci,* 582**,** 364-375.

GAO, Y., ZHANG, Y., HONG, Y., WU, F., SHEN, L., WANG, Y. & LIN, X. 2022. Multifunctional Role of Silica in Pharmaceutical Formulations. *AAPS PharmSciTech,* 23**,** 90.

GARTI, N., WELLNER, E. & SARIG, S. 1980. Stearic acid polymorphs in correlation with crystallization conditions and solvents. *Kristall und Technik,* 15**,** 1303-1310.

GEDAWY, A., MARTINEZ, J., AL-SALAMI, H. & DASS, C. R. 2018. Oral insulin delivery: existing barriers and current counter-strategies. *J Pharm Pharmacol,* 70**,** 197-213.

GEENS, M. M. & NIEWOLD, T. A. 2011. Optimizing culture conditions of a porcine epithelial cell line IPEC-J2 through a histological and physiological characterization. *Cytotechnology,* 63**,** 415-23.

GLEESON, J. P., FEIN, K. C. & WHITEHEAD, K. A. 2021. Oral delivery of peptide therapeutics in infants: Challenges and opportunities. *Adv Drug Deliv Rev,* 173**,** 112-124.

GOEBEL-STENGEL, M., STENGEL, A., TACHE, Y. & REEVE, J. R., JR. 2011. The importance of using the optimal plasticware and glassware in studies involving peptides. *Anal Biochem,* 414**,** 38-46.

GONÇALVES, F. A. M. M., TRINDADE, A. R., COSTA, C. S. M. F., BERNARDO, J. C. S., JOHNSON, I., FONSECA, I. M. A. & FERREIRA, A. G. M. 2010. PVT, viscosity, and surface tension of ethanol: New measurements and literature data evaluation. *The Journal of Chemical Thermodynamics,* 42**,** 1039-1049.

HALBERG, I. B., LYBY, K., WASSERMANN, K., HEISE, T., ZIJLSTRA, E. & PLUM-MÖRSCHEL, L. 2019. Efficacy and safety of oral basal insulin versus subcutaneous insulin glargine in type 2 diabetes: a randomised, double-blind, phase 2 trial. *The Lancet Diabetes & Endocrinology,* 7**,** 179-188.

HAN, Y., GAO, Z., CHEN, L., KANG, L., HUANG, W., JIN, M., WANG, Q. & BAE, Y. H. 2019. Multifunctional oral delivery systems for enhanced bioavailability of therapeutic peptides/proteins. *Acta Pharm Sin B,* 9**,** 902-922.

HARUNA, F., APEJI, Y. E., OPARAECHE, C., OYI, A. R. & GAMLEN, M. 2020. Compaction and tableting properties of composite particles of microcrystalline cellulose and crospovidone engineered for direct compression. *Future Journal of Pharmaceutical Sciences,* 6.

HE, S., LIU, Z. & XU, D. 2019. Advance in oral delivery systems for therapeutic protein. *J Drug Target,* 27**,** 283-291.

HE, Y., LIANG, S., LONG, M. & XU, H. 2017. Mesoporous silica nanoparticles as potential carriers for enhanced drug solubility of paclitaxel. *Mater Sci Eng C Mater Biol Appl,* 78**,** 12-17.

HE, Y., WANG, M., ZHANG, H., ZHANG, Y., GAO, Y. & WANG, S. 2020. Protective properties of mesocellular silica foams against aggregation and enzymatic hydrolysis of loaded proteins for oral protein delivery. *J Colloid Interface Sci,* 560**,** 690-700.

HENTZSCHEL, C. M., ALNAIEF, M., SMIRNOVA, I., SAKMANN, A. & LEOPOLD, C. S. 2012. Tableting properties of silica aerogel and other silicates. *Drug Dev Ind Pharm,* 38**,** 462-7.

HILLERSTRÖM, A., ANDERSSON, M., SAMUELSSON, J. & VAN STAM, J. 2014. Solvent strategies for loading and release in mesoporous silica. *Colloid and Interface Science Communications,* 3**,** 5-8.

HONG, S., SHEN, S., TAN, D. C., NG, W. K., LIU, X., CHIA, L. S., IRWAN, A. W., TAN, R., NOWAK, S. A., MARSH, K. & GOKHALE, R. 2016. High drug load, stable, manufacturable and bioavailable fenofibrate formulations in mesoporous silica: a comparison of spray drying versus solvent impregnation methods. *Drug Deliv,* 23**,** 316-27.

HUANG, J., SHU, Q., WANG, L., WU, H., WANG, A. Y. & MAO, H. 2015. Layer-by-layer assembled milk protein coated magnetic nanoparticle enabled oral drug delivery with high stability in stomach and enzyme-responsive release in small intestine. *Biomaterials,* 39**,** 105-13.

HUO, L., HAN, X., ZHANG, L., LIU, B., GAO, R., CAO, B., WANG, W.-W., JIA, C.-J., LIU, K., LIU, J. & ZHANG, J. 2021. Spatial confinement and electron transfer moderating Mo N bond strength for superior ammonia decomposition catalysis. *Applied Catalysis B: Environmental,* 294.

HUSSAIN, T., WATERS, L. J., PARKES, G. M. B. & SHAHZAD, Y. 2017. Microwave processed solid dispersions for enhanced dissolution of gemfibrozil using non-ordered mesoporous silica. *Colloids and Surfaces A: Physicochemical and Engineering Aspects,* 520**,** 428-435.

IBEANU, N., EGBU, R., ONYEKURU, L., JAVAHERI, H., KHAW, P. T., WILLIAMS, G. R., BROCCHINI, S. & AWWAD, S. 2020. Injectables and Depots to Prolong Drug Action of Proteins and Peptides. *Pharmaceutics,* 12.

JANSSEN, P. H. M., BERARDI, A., KOK, J. H., THORNTON, A. W. & DICKHOFF, B. H. J. 2022. The impact of lactose type on disintegration: An integral study on porosity and polymorphism. *Eur J Pharm Biopharm,* 180**,** 251-259.

JIANG, Z., QING, Q., XIE, P., GAO, R. & LIEBER, C. M. 2012. Kinked p-n junction nanowire probes for high spatial resolution sensing and intracellular recording. *Nano Lett,* 12**,** 1711-6.

JIN, X., LUONG, T. L., REESE, N., GAONA, H., COLLAZO-VELEZ, V., VUONG, C., POTTER, B., SOUSA, J. C., OLMEDA, R., LI, Q., XIE, L., ZHANG, J., ZHANG, P., REICHARD, G., MELENDEZ, V., MARCSISIN, S. R. & PYBUS, B. S. 2014. Comparison of MDCK-MDR1 and Caco-2 cell based permeability assays for anti-malarial drug screening and drug investigations. *J Pharmacol Toxicol Methods,* 70**,** 188-94.

JIN, Y., SONG, Y., ZHU, X., ZHOU, D., CHEN, C., ZHANG, Z. & HUANG, Y. 2012. Goblet cell-targeting nanoparticles for oral insulin delivery and the influence of mucus on insulin transport. *Biomaterials,* 33**,** 1573-82.

JIVRAJ, I. I., MARTINI, L. G. & THOMSON, C. M. 2000. An overview of the different excipients useful for the direct compression of tablets. *Pharm Sci Technol Today,* 3**,** 58-63.

JORGENSEN, J. R., JEPSEN, M. L., NIELSEN, L. H., DUFVA, M., NIELSEN, H. M., RADES, T., BOISEN, A. & MULLERTZ, A. 2019. Microcontainers for oral insulin delivery - In vitro studies of permeation enhancement. *Eur J Pharm Biopharm,* 143**,** 98-105.

KANG, S. K., WOO, J. H., KIM, M. K., WOO, S. S., CHOI, J. H., LEE, H. G., LEE, N. K. & CHOI, Y. J. 2008. Identification of a peptide sequence that improves transport of macromolecules across the intestinal mucosal barrier targeting goblet cells. *J Biotechnol,* 135**,** 210-6.

KANUGO, A. & MISRA, A. 2020. New and novel approaches for enhancing the oral absorption and bioavailability of protein and peptides therapeutics. *Ther Deliv,* 11**,** 713-732.

KAYSER, J. J., ARNOLD, P., STEFFEN-HEINS, A., SCHWARZ, K. & KEPPLER, J. K. 2020. Functional ethanol-induced fibrils: Influence of solvents and temperature on amyloid-like aggregation of beta-lactoglobulin. *Journal of Food Engineering,* 270.

KHALEEL BASHA, S., SYED MUZAMMIL, M., DHANDAYUTHABANI, R. & SUGANTHA KUMARI, V. 2021. Development of nanoemulsion of Alginate/Aloe vera for oral delivery of insulin. *Materials Today: Proceedings,* 36**,** 357-363.

KNEISZL, R., HOSSAIN, S. & LARSSON, P. 2022. In Silico-Based Experiments on Mechanistic Interactions between Several Intestinal Permeation Enhancers with a Lipid Bilayer Model. *Molecular Pharmaceutics,* 19**,** 124-137.

KOCH, N., JENNOTTE, O., GRIGNARD, B., LECHANTEUR, A. & EVRARD, B. 2020. Impregnation of mesoporous silica with poor aqueous soluble molecule using pressurized carbon dioxide: Is the solubility in the supercritical and subcritical phase a critical parameter? *Eur J Pharm Sci,* 150**,** 105332.

KOCH, N., JENNOTTE, O., TOUSSAINT, C., LECHANTEUR, A. & EVRARD, B. 2023. Production challenges of tablets containing lipid excipients: Case study using cannabidiol as drug model. *Int J Pharm,* 633**,** 122639.

KOCH, N., JENNOTTE, O., ZIEMONS, E., BOUSSARD, G., LECHANTEUR, A. & EVRARD, B. 2022. Influence of API physico-chemical properties on amorphization capacity of several mesoporous silica loading methods. *Int J Pharm,* 613**,** 121372.

KOVACEVIC, M., GERMAN ILIC, I., BOLKO SELJAK, K. & ZVONAR POBIRK, A. 2022. High-Shear Wet Granulation of SMEDDS Based on Mesoporous Carriers for Improved Carvedilol Solubility. *Pharmaceutics,* 14.

KRAJEWSKI, A., MALAVOLTI, R. & PIANCASTELLI, A. 1996. Albumin adhesion on some biological and non-biological glasses and connection with their Z-potentials. *Biomaterials,* 17**,** 53-60.

KRUK, M., JARONIEC, M. & SAYARI, A. 1997. Application of Large Pore MCM-41 Molecular Sieves To Improve Pore Size Analysis Using Nitrogen Adsorption Measurements. *Langmuir,* 13**,** 6267-6273.

KRUSKAL, P. B., JIANG, Z., GAO, T. & LIEBER, C. M. 2015. Beyond the patch clamp: nanotechnologies for intracellular recording. *Neuron,* 86**,** 21-4.

KUMAR, S., MALIK, M. M. & PUROHIT, R. 2017. Synthesis Methods of Mesoporous Silica Materials. *Materials Today: Proceedings,* 4**,** 350-357.

KUMAR, V., DE LA LUZ REUS-MEDINA, M. & YANG, D. 2002. Preparation, characterization, and tabletting properties of a new cellulose-based pharmaceutical aid. *Int J Pharm,* 235**,** 129-40.

KUMBHAR, P. S., NADAF, S., MANJAPPA, A. S., JHA, N. K., SHINDE, S. S., CHOPADE, S. S., SHETE, A. S., DISOUZA, J. I., SAMBAMOORTHY, U. & KUMAR, S. A. 2022. D-α-tocopheryl polyethylene glycol succinate: A review of multifarious applications in nanomedicines. *OpenNano,* 6.

KUNNATH, K., HUANG, Z., CHEN, L., ZHENG, K. & DAVE, R. 2018. Improved properties of fine active pharmaceutical ingredient powder blends and tablets at high drug loading via dry particle coating. *Int J Pharm,* 543**,** 288-299.

LAI, S. K., WANG, Y. Y. & HANES, J. 2009. Mucus-penetrating nanoparticles for drug and gene delivery to mucosal tissues. *Adv Drug Deliv Rev,* 61**,** 158-71.

LALE, S. V. & GILL, H. S. 2018. Pollen grains as a novel microcarrier for oral delivery of proteins. *Int J Pharm,* 552**,** 352-359.

LAMBERT, O., AUSBORN, M., PETERSEN, H., LOEFFLER, R. & BONNY, J.-D. 2003. *Pharmaceutical Composition Comprising Octreotide Microparticles*. 11173962.9.

LARSEN, N. W., KOSTRIKOV, S., HANSEN, M. B., HJORRINGGAARD, C. U., LARSEN, N. B., ANDRESEN, T. L. & KRISTENSEN, K. 2024. Interactions of oral permeation enhancers with lipid membranes in simulated intestinal environments. *Int J Pharm,* 654**,** 123957.

LE-VINH, B., LE, N. N., NAZIR, I., MATUSZCZAK, B. & BERNKOP-SCHNURCH, A. 2019. Chitosan based micelle with zeta potential changing property for effective mucosal drug delivery. *Int J Biol Macromol,* 133**,** 647-655.

LE, T. T., ELZHRY ELYAFI, A. K., MOHAMMED, A. R. & AL-KHATTAWI, A. 2019. Delivery of Poorly Soluble Drugs via Mesoporous Silica: Impact of Drug Overloading on Release and Thermal Profiles. *Pharmaceutics,* 11.

LEI, C., CHEN, B., LI, X., QI, W. & LIU, J. 2013. Non-destructively shattered mesoporous silica for protein drug delivery. *Microporous Mesoporous Mater,* 175**,** 157-160.

LERIDA-VISO, A., ESTEPA-FERNANDEZ, A., GARCIA-FERNANDEZ, A., MARTI-CENTELLES, V. & MARTINEZ-MANEZ, R. 2023. Biosafety of mesoporous silica nanoparticles; towards clinical translation. *Adv Drug Deliv Rev,* 201**,** 115049.

LI, P., FENG, B., JIANG, H., HAN, X., WU, Z., WANG, Y., LIN, J., ZHANG, Y., YANG, M., HAN, L. & ZHANG, D. 2018. A Novel Forming Method of Traditional Chinese Medicine Dispersible Tablets to Achieve Rapid Disintegration Based on the Powder Modification Principle. *Sci Rep,* 8**,** 10319.

LI, Y., HU, Y., LOGSDON, D. L., LIU, Y., ZHAO, Y. & COOKS, R. G. 2020. Accelerated Forced Degradation of Therapeutic Peptides in Levitated Microdroplets. *Pharm Res,* 37**,** 138.

LI, Z., CHEN, J., SUN, W. & XU, Y. 2010. Investigation of archaeosomes as carriers for oral delivery of peptides. *Biochem Biophys Res Commun,* 394**,** 412-7.

LIMNELL, T., SANTOS, H. A., MAKILA, E., HEIKKILA, T., SALONEN, J., MURZIN, D. Y., KUMAR, N., LAAKSONEN, T., PELTONEN, L. & HIRVONEN, J. 2011. Drug delivery formulations of ordered and nonordered mesoporous silica: comparison of three drug loading methods. *J Pharm Sci,* 100**,** 3294-3306.

LIN, Y., WANG, X., HUANG, X., ZHANG, J., XIA, N. & ZHAO, Q. 2017. Calcium phosphate nanoparticles as a new generation vaccine adjuvant. *Expert Rev Vaccines,* 16**,** 895-906.

LIN, Y., ZHU, C. & FANG, G. 2019. Synthesis and properties of microencapsulated stearic acid/silica composites with graphene oxide for improving thermal conductivity as novel solar thermal storage materials. *Solar Energy Materials and Solar Cells,* 189**,** 197-205.

LIU, J., LENG, P. & LIU, Y. 2021. Oral drug delivery with nanoparticles into the gastrointestinal mucosa. *Fundam Clin Pharmacol,* 35**,** 86-96.

LIU, J., SHIN, Y., NIE, Z., CHANG, J. H., WANG, L.-Q., FRYXELL, G. E., SAMUELS, W. D. & EXARHOS, G. J. 2000. Molecular Assembly in Ordered Mesoporosity: A New Class of Highly Functional Nanoscale Materials. *The Journal of Physical Chemistry A,* 104**,** 8328-8339.

LU, S., SONG, Z. & HE, J. 2011. Diffusion-controlled protein adsorption in mesoporous silica. *J Phys Chem B,* 115**,** 7744-50.

LUNDQUIST, P. & ARTURSSON, P. 2016. Oral absorption of peptides and nanoparticles across the human intestine: Opportunities, limitations and studies in human tissues. *Adv Drug Deliv Rev,* 106**,** 256-276.

LUO, Y., HONG, Y., SHEN, L., WU, F. & LIN, X. 2021. Multifunctional Role of Polyvinylpyrrolidone in Pharmaceutical Formulations. *AAPS PharmSciTech,* 22**,** 34.

MA, X. Y., PAN, G. M., LU, Z., HU, J. S., BEI, J. Z., JIA, J. H. & WANG, S. G. 2000. Preliminary study of oral polylactide microcapsulated insulin in vitro and in vivo. *Diabetes Obes Metab,* 2**,** 243-50.

MACLEAN, N., WALSH, E., SOUNDARANATHAN, M., KHADRA, I., MANN, J., WILLIAMS, H. & MARKL, D. 2021. Exploring the performance-controlling tablet disintegration mechanisms for direct compression formulations. *Int J Pharm,* 599**,** 120221.

MAHER, S. & BRAYDEN, D. J. 2021. Formulation strategies to improve the efficacy of intestinal permeation enhancers(). *Adv Drug Deliv Rev,* 177**,** 113925.

MAHER, S., GEOGHEGAN, C. & BRAYDEN, D. J. 2021. Intestinal permeation enhancers to improve oral bioavailability of macromolecules: reasons for low efficacy in humans. *Expert Opin Drug Deliv,* 18**,** 273-300.

MAHER, S., MRSNY, R. J. & BRAYDEN, D. J. 2016. Intestinal permeation enhancers for oral peptide delivery. *Adv Drug Deliv Rev,* 106**,** 277-319.

MAJOREK, K. A., POREBSKI, P. J., DAYAL, A., ZIMMERMAN, M. D., JABLONSKA, K., STEWART, A. J., CHRUSZCZ, M. & MINOR, W. 2012. Structural and immunologic characterization of bovine, horse, and rabbit serum albumins. *Mol Immunol,* 52**,** 174-82.

MAKHLOF, A., FUJIMOTO, S., TOZUKA, Y. & TAKEUCHI, H. 2011. In vitro and in vivo evaluation of WGA-carbopol modified liposomes as carriers for oral peptide delivery. *Eur J Pharm Biopharm,* 77**,** 216-24.

MALKOV, D., ANGELO, R., WANG, H. Z., FLANDERS, E., TANG, H. & GOMEZ-ORELLANA, I. 2005. Oral delivery of insulin with the eligen technology: mechanistic studies. *Curr Drug Deliv,* 2**,** 191-7.

MALTA, V., CELOTTI, G., ZANNETTI, R. & MARTELLI, A. F. 1971. Crystal structure of the C form of stearic acid. *Journal of the Chemical Society B: Physical Organic*.

MAMAEVA, V., SAHLGREN, C. & LINDEN, M. 2013. Mesoporous silica nanoparticles in medicine--recent advances. *Adv Drug Deliv Rev,* 65**,** 689-702.

MANDSBERG, N. K., CHRISTFORT, J. F., KAMGUYAN, K., BOISEN, A. & SRIVASTAVA, S. K. 2020. Orally ingestible medical devices for gut engineering. *Adv Drug Deliv Rev,* 165-166**,** 142-154.

MARGOLIS, L. B., VICTOROV, A. V. & BERGELSON, L. D. 1982. Lipid-cell interactions. *Biochimica et Biophysica Acta (BBA) - Molecular Cell Research,* 720**,** 259-265.

MARKOVIC, M., ZUR, M., GARSIANI, S., PORAT, D., CVIJIC, S., AMIDON, G. L. & DAHAN, A. 2022. The Role of Paracellular Transport in the Intestinal Absorption and Biopharmaceutical Characterization of Minoxidil. *Pharmaceutics,* 14.

MASUELLI, M. A. 2013. Study of Bovine Serum Albumin Solubility in Aqueous Solutions by Intrinsic Viscosity Measurements. *Advances in Physical Chemistry,* 2013**,** 1-8.

MAUBON, N., LE VEE, M., FOSSATI, L., AUDRY, M., LE FERREC, E., BOLZE, S. & FARDEL, O. 2007. Analysis of drug transporter expression in human intestinal Caco-2 cells by real-time PCR. *Fundam Clin Pharmacol,* 21**,** 659-63.

MCCARTNEY, F., JANNIN, V., CHEVRIER, S., BOULGHOBRA, H., HRISTOV, D. R., RITTER, N., MIOLANE, C., CHAVANT, Y., DEMARNE, F. & BRAYDEN, D. J. 2019.

Labrasol(R) is an efficacious intestinal permeation enhancer across rat intestine: Ex vivo and in vivo rat studies. *J Control Release,* 310**,** 115-126.

MCCUSKER, L. B., LIEBAU, F. & ENGELHARDT, G. 2003. Nomenclature of structural and compositional characteristics of ordered microporous and mesoporous materials with inorganic hosts. *Microporous and Mesoporous Materials,* 58**,** 3-13.

MEKARU, H., LU, J. & TAMANOI, F. 2015. Development of mesoporous silica-based nanoparticles with controlled release capability for cancer therapy. *Adv Drug Deliv Rev,* 95**,** 40-9.

MINAMI, K., TAKAZAWA, A., TANIGUCHI, Y., HIGASHINO, H., KATAOKA, M., ASAI, T., OKU, N. & YAMASHITA, S. 2020. Challenge for oral delivery of middle-molecular drugs: Use of osmolarity-sensitive liposome as a drug carrier in the GI tract. *Journal of Drug Delivery Science and Technology,* 56.

MINER-WILLIAMS, W. M., STEVENS, B. R. & MOUGHAN, P. J. 2014. Are intact peptides absorbed from the healthy gut in the adult human? *Nutr Res Rev,* 27**,** 308-29.

MITRAN, R. A., BERGER, D. & MATEI, C. 2019. Phase Change Materials Based on Mesoporous Silica. *Current Organic Chemistry,* 22**,** 2644-2663.

MOHSEN-NIA, M., AMIRI, H. & JAZI, B. 2010. Dielectric Constants of Water, Methanol, Ethanol, Butanol and Acetone: Measurement and Computational Study. *Journal of Solution Chemistry,* 39**,** 701-708.

MOLINIER, C., PICOT-GROZ, M., MALVAL, O., LE LAMER-DECHAMPS, S., RICHARD, J., LOPEZ-NORIEGA, A. & GRIZOT, S. 2021. Impact of octreotide counterion nature on the long-term stability and release kinetics from an in situ forming depot technology. *J Control Release,* 336**,** 457-468.

MUHEEM, A., SHAKEEL, F., JAHANGIR, M. A., ANWAR, M., MALLICK, N., JAIN, G. K., WARSI, M. H. & AHMAD, F. J. 2016. A review on the strategies for oral delivery of proteins and peptides and their clinical perspectives. *Saudi Pharm J,* 24**,** 413-28.

MURA, P., VALLERI, M., FABIANELLI, E., MAESTRELLI, F. & CIRRI, M. 2019. Characterization and evaluation of different mesoporous silica kinds as carriers for the development of effective oral dosage forms of glibenclamide. *Int J Pharm,* 563**,** 43-52.

MURRAY, J. E., LAURIERI, N. & DELGODA, R. 2017. Chapter 24 - Proteins. *In:* BADAL, S. & DELGODA, R. (eds.) *Pharmacognosy.* Boston: Academic Press.

NAZIR, I., SHAHZADI, I., JALIL, A. & BERNKOP-SCHNURCH, A. 2020. Hydrophobic H-bond pairing: A novel approach to improve membrane permeability. *Int J Pharm,* 573**,** 118863.

NDAYISHIMIYE, J., POPAT, A., BLASKOVICH, M. & FALCONER, J. R. 2020. Formulation technologies and advances for oral delivery of novel nitroimidazoles and antimicrobial peptides. *J Control Release,* 324**,** 728-749.

NEGAHBAN, Z., SHOJAOSADATI, S. A. & HAMEDI, S. 2021. A novel self-assembled micelles based on stearic acid modified schizophyllan for efficient delivery of paclitaxel. *Colloids Surf B Biointerfaces,* 199**,** 111524.

NIU, N. & WANG, L. 2015. In vitro human cell line models to predict clinical response to anticancer drugs. *Pharmacogenomics,* 16**,** 273-85.

NIU, Z., CONEJOS-SANCHEZ, I., GRIFFIN, B. T., O'DRISCOLL, C. M. & ALONSO, M. J. 2016. Lipid-based nanocarriers for oral peptide delivery. *Adv Drug Deliv Rev,* 106**,** 337-354.

NSOR-ATINDANA, J., CHEN, M., GOFF, H. D., ZHONG, F., SHARIF, H. R. & LI, Y. 2017. Functionality and nutritional aspects of microcrystalline cellulose in food. *Carbohydr Polym,* 172**,** 159-174.

OCTREOTIDE. 2023. Available: https://pubchem.ncbi.nlm.nih.gov/compound/octreotide#section=Biologic-Description [Accessed 13/11/2023].

OMAR, H., CROISSANT, J. G., ALAMOUDI, K., ALSAIARI, S., ALRADWAN, I., MAJRASHI, M. A., ANJUM, D. H., MARTINS, P., LAAMARTI, R., EPPINGER, J., MOOSA, B., ALMALIK, A. & KHASHAB, N. M. 2017. Biodegradable Magnetic Silica@Iron Oxide Nanovectors with Ultra-Large Mesopores for High Protein Loading, Magnetothermal Release, and Delivery. *J Control Release,* 259**,** 187-194.

ORAMED.INC. 2021. Available: https://www.oramed.com/oramed-reaches-25-enrollment-in-its-second-of-two-concurrent-phase-3-oral-insulin-trials/ [Accessed 29/10/2021].

PALUMBO, P., PICCHINI, U., BECK, B., VAN GELDER, J., DELBAR, N. & DEGAETANO, A. 2008. A general approach to the apparent permeability index. *J Pharmacokinet Pharmacodyn,* 35**,** 235-48.

PAMSHONG, S. R., BHATANE, D., SARNAIK, S. & ALEXANDER, A. 2023. Mesoporous silica nanoparticles: An emerging approach in overcoming the challenges with oral delivery of proteins and peptides. *Colloids Surf B Biointerfaces,* 232**,** 113613.

PANDEY, A., SINGH, D., DHAS, N., TEWARI, A. K., PATHAK, K., CHATAP, V., RATHORE, K. S. & MUTALIK, S. 2020. *Complex injectables*, Elsevier.

PANDEY, P., PUROHIT, D. & DUREJA, H. 2018. Nanosponges -A Promising Novel Drug Delivery System. *Recent Pat Nanotechnol,* 12**,** 180-191.

PANSE, N. & GERK, P. M. 2022. The Caco-2 Model: Modifications and enhancements to improve efficiency and predictive performance. *Int J Pharm,* 624**,** 122004.

PAREKH, B. V., SADDIK, J. S., PATEL, D. B. & DAVE, R. H. 2023. Evaluating the effect of glidants on tablet sticking propensity of ketoprofen using powder rheology. *Int J Pharm,* 635**,** 122710.

PARK, E. J. & NA, D. H. 2008. Optimization of octreotide PEGylation by monitoring with fast reversed-phase high-performance liquid chromatography. *Anal Biochem,* 380**,** 140-2.

PARK, K., KWON, I. C. & PARK, K. 2011. Oral protein delivery: Current status and future prospect. *Reactive and Functional Polymers,* 71**,** 280-287.

PATEL, G. B., AGNEW, B. J., DESCHATELETS, L., FLEMING, L. P. & SPROTT, G. D. 2000. In vitro assessment of archaeosome stability for developing oral delivery systems. *Int J Pharm,* 194**,** 39-49.

PATEL, N. K., UPADHYAY, A. H., BERGUM, J. S. & REIER, G. E. 1994. An evaluation of microcrystalline cellulose and lactose excipients using an instrumented single station tablet press. *International Journal of Pharmaceutics,* 110**,** 203-210.

PATTI, A., LECOCQ, H., SERGHEI, A., ACIERNO, D. & CASSAGNAU, P. 2021. The universal usefulness of stearic acid as surface modifier: applications to the polymer formulations and composite processing. *Journal of Industrial and Engineering Chemistry,* 96**,** 1-33.

PENG, T., SHAO, X., LONG, L., LIU, H., SONG, W., HOU, J., ZHONG, H., DING, Y. & HUANG, Y. 2023. Rational design of oral delivery nanosystems for hypoglycemic peptides. *Nano Today,* 53.

PEPTELLIGENCE®. 2021. Available: https://enterisbiopharma.com/peptelligence/ [Accessed 29/10/2023 2023].

PEREIRA, C., COSTA, J., SARMENTO, B. & ARAÚJO, F. 2016. 3.3 - Cell-based in vitro models for intestinal permeability studies. *In:* SARMENTO, B. (ed.) *Concepts and Models for Drug Permeability Studies.* Woodhead Publishing.

PHARMA, P.-I. 2021a. Available: <https://www.intractpharma.com/fomulation-technologies/phloral/> [Accessed 29/10/2021].

PHARMA, S.-I. 2021b. Available: <https://www.intractpharma.com/fomulation-technologies/soteria/> [Accessed 29/10/2021].

PIRES, C. L., PRACA, C., MARTINS, P. A. T., BATISTA DE CARVALHO, A. L. M., FERREIRA, L., MARQUES, M. P. M. & MORENO, M. J. 2021. Re-Use of Caco-2 Monolayers in Permeability Assays-Validation Regarding Cell Monolayer Integrity. *Pharmaceutics,* 13.

PLAVEC, T. V. & BERLEC, A. 2019. Engineering of lactic acid bacteria for delivery of therapeutic proteins and peptides. *Appl Microbiol Biotechnol,* 103**,** 2053-2066.

PLEWE, G., KRAUSE, U., BEYER, J., NEUFELD, M. & DEL POZO, E. 1984. Long-Acting and Selective Suppression of Growth Hormone Secretion by Somatostatin Analogue Sms 201-995 in Acromegaly. *The Lancet,* 324**,** 782-784.

POHL, E., HEINE, A., SHELDRICK, G. M., DAUTER, Z., WILSON, K. S., KALLEN, J., HUBER, W. & PFAFFLI, P. J. 1995. Structure of octreotide, a somatostatin analogue. *Acta Crystallogr D Biol Crystallogr,* 51**,** 48-59.

PREGO, C., TORRES, D., FERNANDEZ-MEGIA, E., NOVOA-CARBALLAL, R., QUINOA, E. & ALONSO, M. J. 2006. Chitosan-PEG nanocapsules as new carriers for oral peptide delivery. Effect of chitosan pegylation degree. *J Control Release,* 111**,** 299-308.

PROXIMA. 2021. Available: http://proximaconcepts.com/axcess [Accessed 14/10/2021 2021].

QI, W., LI, X., CHEN, B., YAO, P., LEI, C. & LIU, J. 2012. Intramesoporous silica structure differentiating protein loading density. *Mater Lett,* 75**,** 102-106.

QU, L., STEWART, P. J., HAPGOOD, K. P., LAKIO, S., MORTON, D. A. V. & ZHOU, Q. T. 2017. Single-step Coprocessing of Cohesive Powder via Mechanical Dry Coating for Direct Tablet Compression. *J Pharm Sci,* 106**,** 159-167.

RAGHAVAN, S. R., WALLS, H. J. & KHAN, S. A. 2000. Rheology of Silica Dispersions in Organic Liquids: New Evidence for Solvation Forces Dictated by Hydrogen Bonding. *Langmuir,* 16**,** 7920-7930.

RAGURAMAN, R., SRIVASTAVA, A., MUNSHI, A. & RAMESH, R. 2021. Therapeutic Approaches Targeting Molecular Signaling Pathways Common to Diabetes and Lung Diseases and Cancer. *Advanced Drug Delivery Reviews*.

RAHMAT, N., ABDULLAH, A. Z. & MOHAMED, A. R. 2010. A Review: Mesoporous Santa Barbara Amorphous-15, Types, Synthesis and Its Applications towards Biorefinery Production. *American Journal of Applied Sciences,* 7**,** 1579-1586.

RAMACHANDRAN, R., PAUL, W. & SHARMA, C. P. 2009. Synthesis and characterization of PEGylated calcium phosphate nanoparticles for oral insulin delivery. *J Biomed Mater Res B Appl Biomater,* 88**,** 41-8.

RANITHERAPEUTICS. 2021. Available: https://www.ranitherapeutics.com/technology/ [Accessed 29/10/2021].

RYU, K.-W. & NA, D.-H. 2009. Stability of Octreotide Acetate in Aqueous Solutions and PLGA Films. *Journal of Korean Pharmaceutical Sciences,* 39**,** 353-357.

SAGIRI, S. S., SINGH, V. K., PAL, K., BANERJEE, I. & BASAK, P. 2015. Stearic acid based oleogels: a study on the molecular, thermal and mechanical properties. *Mater Sci Eng C Mater Biol Appl,* 48**,** 688-99.

SAJEESH, S., BOUCHEMAL, K., MARSAUD, V., VAUTHIER, C. & SHARMA, C. P. 2010. Cyclodextrin complexed insulin encapsulated hydrogel microparticles: An oral delivery system for insulin. *J Control Release,* 147**,** 377-84.

SANCHON, J., FERNANDEZ-TOME, S., MIRALLES, B., HERNANDEZ-LEDESMA, B., TOME, D., GAUDICHON, C. & RECIO, I. 2018. Protein degradation and peptide release from

milk proteins in human jejunum. Comparison with in vitro gastrointestinal simulation. *Food Chem,* 239**,** 486-494.

SANDBORN, W. J., KAMM, M. A., LICHTENSTEIN, G. R., LYNE, A., BUTLER, T. & JOSEPH, R. E. 2007. MMX Multi Matrix System mesalazine for the induction of remission in patients with mild-to-moderate ulcerative colitis: a combined analysis of two randomized, double-blind, placebo-controlled trials. *Aliment Pharmacol Ther,* 26**,** 205-15.

SANDER, C. & HOLM, P. 2009. Porous magnesium aluminometasilicate tablets as carrier of a cyclosporine self-emulsifying formulation. *AAPS PharmSciTech,* 10**,** 1388-95.

SARMENTO, B., ANDRADE, F., DA SILVA, S. B., RODRIGUES, F., DAS NEVES, J. & FERREIRA, D. 2012. Cell-based in vitro models for predicting drug permeability. *Expert Opin Drug Metab Toxicol,* 8**,** 607-21.

SCHINDELIN, J., ARGANDA-CARRERAS, I., FRISE, E., KAYNIG, V., LONGAIR, M., PIETZSCH, T., PREIBISCH, S., RUEDEN, C., SAALFELD, S., SCHMID, B., TINEVEZ, J. Y., WHITE, D. J., HARTENSTEIN, V., ELICEIRI, K., TOMANCAK, P. & CARDONA, A. 2012. Fiji: an open-source platform for biological-image analysis. *Nat Methods,* 9**,** 676-82.

SELJAK, K. B., KOCBEK, P. & GAŠPERLIN, M. 2020. Mesoporous silica nanoparticles as delivery carriers: An overview of drug loading techniques. *Journal of Drug Delivery Science and Technology,* 59.

SEMENOV, A. N., YAKIMOV, B. P., RUBEKINA, A. A., GORIN, D. A., DRACHEV, V. P., ZARUBIN, M. P., VELIKANOV, A. N., LADEMANN, J., FADEEV, V. V., PRIEZZHEV, A. V., DARVIN, M. E. & SHIRSHIN, E. A. 2020. The Oxidation-Induced Autofluorescence Hypothesis: Red Edge Excitation and Implications for Metabolic Imaging. *Molecules,* 25.

SHAJI, J. & PATOLE, V. 2008. Protein and Peptide drug delivery: oral approaches. *Indian J Pharm Sci,* 70**,** 269-77.

SHI, H., LIU, S., CHENG, J., YUAN, S., YANG, Y., FANG, T., CAO, K., WEI, K., ZHANG, Q. & LIU, Y. 2019. Charge-Selective Delivery of Proteins Using Mesoporous Silica Nanoparticles Fused with Lipid Bilayers. *ACS Appl Mater Interfaces,* 11**,** 3645-3653.

SHI, L. & SUN, C. C. 2010. Transforming powder mechanical properties by core/shell structure: compressible sand. *J Pharm Sci,* 99**,** 4458-62.

SHI, Y., YIN, M., SONG, Y., WANG, T., GUO, S., ZHANG, X., SUN, K. & LI, Y. 2021. Oral delivery of liraglutide-loaded Poly-N-(2-hydroxypropyl) methacrylamide/chitosan nanoparticles: Preparation, characterization, and pharmacokinetics. *J Biomater Appl,* 35**,** 754-761.

SHIPP, L., LIU, F., KERAI-VARSANI, L. & OKWUOSA, T. C. 2022. Buccal films: A review of therapeutic opportunities, formulations & relevant evaluation approaches. *J Control Release,* 352**,** 1071-1092.

SHOURNI, S., JAVADI, A., HOSSEINPOUR, N., BAHRAMIAN, A. & RAOUFI, M. 2022. Characterization of protein corona formation on nanoparticles via the analysis of dynamic interfacial properties: Bovine serum albumin - silica particle interaction. *Colloids and Surfaces A: Physicochemical and Engineering Aspects,* 638.

SINGH, N., SHI, S. & GOEL, S. 2022. Ultrasmall Silica Nanoparticles in Translational Biomedical Research: Overview and Outlook. *Adv Drug Deliv Rev***,** 114638.

SOHAIL ARSHAD, M., ZAFAR, S., YOUSEF, B., ALYASSIN, Y., ALI, R., ALASIRI, A., CHANG, M. W., AHMAD, Z., ALI ELKORDY, A., FAHEEM, A. & PITT, K. 2021. A review of emerging technologies enabling improved solid oral dosage form manufacturing and processing. *Adv Drug Deliv Rev,* 178**,** 113840.

SOLEYMANI, F., PAQUET, E., VIKTOR, H., MICHALOWSKI, W. & SPINELLO, D. 2022. Protein-protein interaction prediction with deep learning: A comprehensive review. *Comput Struct Biotechnol J,* 20**,** 5316-5341.

SOLOMON, S., IQBAL, J. & ALBADARIN, A. B. 2021. Insights into the ameliorating ability of mesoporous silica in modulating drug release in ternary amorphous solid dispersion prepared by hot melt extrusion. *Eur J Pharm Biopharm,* 165**,** 244-258.

SOLTYS, M., KOVACIK, P., DAMMER, O., BERANEK, J. & STEPANEK, F. 2019. Effect of solvent selection on drug loading and amorphisation in mesoporous silica particles. *Int J Pharm,* 555**,** 19-27.

SONG, M., LI, L., ZHANG, Y., CHEN, K., WANG, H. & GONG, R. 2017. Carboxymethyl-β-cyclodextrin grafted chitosan nanoparticles as oral delivery carrier of protein drugs. *Reactive and Functional Polymers,* 117**,** 10-15.

SPOORTHI SHETTY, S., HALAGALI, P., JOHNSON, A. P., SPANDANA, K. M. A. & GANGADHARAPPA, H. V. 2023. Oral insulin delivery: Barriers, strategies, and formulation approaches: A comprehensive review. *Int J Biol Macromol,* 242**,** 125114.

SRINIVASAN, B., KOLLI, A. R., ESCH, M. B., ABACI, H. E., SHULER, M. L. & HICKMAN, J. J. 2015. TEER measurement techniques for in vitro barrier model systems. *J Lab Autom,* 20**,** 107-26.

ST. CLAIR, N. L. & NAVIA, M. A. 1992. Cross-linked enzyme crystals as robust biocatalysts. *Journal of the American Chemical Society,* 114**,** 7314-7316.

SUBLIMITY, P. 2021. Available: https://www.sublimitytherapeutics.com/pipeline/ [Accessed 29/10/2021].

SUN, P. D., FOSTER, C. E. & BOYINGTON, J. C. 2004. Overview of protein structural and functional folds. *Curr Protoc Protein Sci,* Chapter 17**,** Unit 17 1.

SUN, W. J., ABURUB, A. & SUN, C. C. 2018. A mesoporous silica based platform to enable tablet formulations of low dose drugs by direct compression. *Int J Pharm,* 539**,** 184-189.

SUN, W. J. & SUN, C. C. 2020. A microcrystalline cellulose based drug-composite formulation strategy for developing low dose drug tablets. *Int J Pharm,* 585**,** 119517.

SY, W., XU, X.-L., QL, L. & XIE, Y. S. 2001. The Application of Fluorescence Spectroscopy in the Study on Protein Conformation. *Progress in Chemistry,* 13**,** 257-260.

TAHVANAINEN, M., ROTKO, T., MAKILA, E., SANTOS, H. A., NEVES, D., LAAKSONEN, T., KALLONEN, A., HAMALAINEN, K., PEURA, M., SERIMAA, R., SALONEN, J., HIRVONEN, J. & PELTONEN, L. 2012. Tablet preformulations of indomethacin-loaded mesoporous silicon microparticles. *Int J Pharm,* 422**,** 125-31.

TAKAHASHI, K., ORITO, N., YANAGISAWA, D., YANO, A., MORI, Y. & INOUE, N. 2020. Eosinophils are the main cellular targets for oral gene delivery using Lactic acid bacteria. *Vaccine,* 38**,** 3330-3338.

TANABE, K., WADA, J., OHKUBO, J., NITTA, A., IKEZAKI, T., TAKEUCHI, M., HANDA, A., TANAKA, M., MURAKAMI, N., KASHII, T. & KITAZAWA, H. 2015. Stability of octreotide acetate decreases in a sodium bisulfate concentration-dependent manner: compatibility study with morphine and metoclopramide injections. *Eur J Hosp Pharm,* 22**,** 171-175.

TATLIĆ, B., ŠEJTO, L., SIRBUBALO ŠAHINOVIĆ, M., TUCAK-SMAJIĆ, A. & VRANIC, E. 2020. Novel Aspects of Drug Delivery: Wireless Electronic Devices.

TEIXEIRA, A. C., FERNANDES, A. C., GARCIA, A. R., ILHARCO, L. M., BROGUEIRA, P. & GONCALVES DA SILVA, A. M. 2007. Microdomains in mixed monolayers of oleanolic and stearic acids: thermodynamic study and BAM observation at the air-water interface and AFM and FTIR analysis of LB monolayers. *Chem Phys Lipids,* 149**,** 1-13.

THANOU, M., VERHOEF, J. C., MARBACH, P. & JUNGINGER, H. E. 2000. Intestinal absorption of octreotide: N-trimethyl chitosan chloride (TMC) ameliorates the permeability and absorption properties of the somatostatin analogue in vitro and in vivo. *J Pharm Sci,* 89**,** 951-7.

THOMPSON, J. W., KAISER, T. J. & JORGENSON, J. W. 2006. Viscosity measurements of methanol-water and acetonitrile-water mixtures at pressures up to 3500 bar using a novel capillary time-of-flight viscometer. *J Chromatogr A,* 1134**,** 201-9.

THOMPSON, S. A. & WILLIAMS, R. O., 3RD 2021. Specific mechanical energy - An essential parameter in the processing of amorphous solid dispersions. *Adv Drug Deliv Rev,* 173**,** 374-393.

THOORENS, G., KRIER, F., LECLERCQ, B., CARLIN, B. & EVRARD, B. 2014. Microcrystalline cellulose, a direct compression binder in a quality by design environment--a review. *Int J Pharm,* 473**,** 64-72.

TOORISAKA, E. & NONAKA, Y. 2018. Development of a Novel Spontaneous Emulsification Method for Peptide Delivery Using Porous Silica Particles. *J Oleo Sci,* 67**,** 303-306.

TRAN, D. T., MAJEROVA, D., VESELY, M., KULAVIAK, L., RUZICKA, M. C. & ZAMOSTNY, P. 2019. On the mechanism of colloidal silica action to improve flow properties of pharmaceutical excipients. *Int J Pharm,* 556**,** 383-394.

TRAVERSO, G., SCHOELLHAMMER, C. M., SCHROEDER, A., MAA, R., LAUWERS, G. Y., POLAT, B. E., ANDERSON, D. G., BLANKSCHTEIN, D. & LANGER, R. 2015. Microneedles for drug delivery via the gastrointestinal tract. *J Pharm Sci,* 104**,** 362-7.

TRZECIAK, K., CHOTERA-OUDA, A., BAK, S., II & POTRZEBOWSKI, M. J. 2021. Mesoporous Silica Particles as Drug Delivery Systems-The State of the Art in Loading Methods and the Recent Progress in Analytical Techniques for Monitoring These Processes. *Pharmaceutics,* 13.

TSAI, L. C., CHEN, C. H., LIN, C. W., HO, Y. C. & MI, F. L. 2019. Development of mutlifunctional nanoparticles self-assembled from trimethyl chitosan and fucoidan for enhanced oral delivery of insulin. *Int J Biol Macromol,* 126**,** 141-150.

TSANG, W.-K., WONG, S.-H., CHU, K.-H., LEE, W., CHEUK, A., TANG, H.-L., FUNG, S. K.-S., CHAN, H. W.-H. & TONG, M. K.-L. 2003. The pharmacokinetics and bioequivalence of Gengraf and Neoral in stable renal transplant recipients. *Hong Kong Journal of Nephrology,* 5**,** 40-43.

TURCO, L., CATONE, T., CALONI, F., DI CONSIGLIO, E., TESTAI, E. & STAMMATI, A. 2011. Caco-2/TC7 cell line characterization for intestinal absorption: how reliable is this in vitro model for the prediction of the oral dose fraction absorbed in human? *Toxicol In Vitro,* 25**,** 13-20.

TWAROG, C., FATTAH, S., HEADE, J., MAHER, S., FATTAL, E. & BRAYDEN, D. J. 2019. Intestinal Permeation Enhancers for Oral Delivery of Macromolecules: A Comparison between Salcaprozate Sodium (SNAC) and Sodium Caprate (C(10)). *Pharmaceutics,* 11.

TWAROG, C., FATTAL, E., NOIRAY, M., ILLEL, B., BRAYDEN, D. J., TAVERNA, M. & HILLAIREAU, H. 2022. Characterization of the physicochemical interactions between exenatide and two intestinal permeation enhancers: Sodium caprate (C(10)) and salcaprozate sodium (SNAC). *Int J Pharm,* 626**,** 122131.

TWAROG, C., LIU, K., O'BRIEN, P. J., DAWSON, K. A., FATTAL, E., ILLEL, B. & BRAYDEN, D. J. 2020. A head-to-head Caco-2 assay comparison of the mechanisms of action of the intestinal permeation enhancers: SNAC and sodium caprate (C(10)). *Eur J Pharm Biopharm,* 152**,** 95-107.

TYAGI, P., TRIVEDI, R., PECHENOV, S., PATEL, C., REVELL, J., WILLS, S., HUANG, Y., ROSENBAUM, A. I. & SUBRAMONY, J. A. 2021. Targeted oral peptide delivery using multi-unit particulates: Drug and permeation enhancer layering approach. *J Control Release*.

UHL, P., GRUNDMANN, C., SAUTER, M., STORCK, P., TURSCH, A., OZBEK, S., LEOTTA, K., ROTH, R., WITZIGMANN, D., KULKARNI, J. A., FIDELJ, V., KLEIST, C., CULLIS, P. R., FRICKER, G. & MIER, W. 2020. Coating of PLA-nanoparticles with cyclic, arginine-rich cell penetrating peptides enables oral delivery of liraglutide. *Nanomedicine,* 24**,** 102132.

UKAI, H., IWASA, K., DEGUCHI, T., MORISHITA, M., KATSUMI, H. & YAMAMOTO, A. 2020. Enhanced Intestinal Absorption of Insulin by Capryol 90, a Novel Absorption Enhancer in Rats: Implications in Oral Insulin Delivery. *Pharmaceutics,* 12.

UMRETHIA, M., KETT, V. L., ANDREWS, G. P., MALCOLM, R. K. & WOOLFSON, A. D. 2010. Selection of an analytical method for evaluating bovine serum albumin concentrations in pharmaceutical polymeric formulations. *J Pharm Biomed Anal,* 51**,** 1175-9.

VARUM, F., FREIRE, A. C., BRAVO, R. & BASIT, A. W. 2020. OPTICORE, an innovative and accurate colonic targeting technology. *Int J Pharm,* 583**,** 119372.

VIALPANDO, M., AERTS, A., PERSOONS, J., MARTENS, J. & VAN DEN MOOTER, G. 2011. Evaluation of ordered mesoporous silica as a carrier for poorly soluble drugs: influence of pressure on the structure and drug release. *J Pharm Sci,* 100**,** 3411-3420.

VIDAURRE-AGUT, C., RIVERO-BUCETA, E., ROMANI-CUBELLS, E., CLEMMENTS, A. M., VERA-DONOSO, C. D., LANDRY, C. C. & BOTELLA, P. 2019. Protein Corona over Mesoporous Silica Nanoparticles: Influence of the Pore Diameter on Competitive Adsorption and Application to Prostate Cancer Diagnostics. *ACS Omega,* 4**,** 8852-8861.

VINAROV, Z., ABRAHAMSSON, B., ARTURSSON, P., BATCHELOR, H., BERBEN, P., BERNKOP-SCHNURCH, A., BUTLER, J., CEULEMANS, J., DAVIES, N., DUPONT, D., FLATEN, G. E., FOTAKI, N., GRIFFIN, B. T., JANNIN, V., KEEMINK, J., KESISOGLOU, F., KOZIOLEK, M., KUENTZ, M., MACKIE, A., MELENDEZ-MARTINEZ, A. J., MCALLISTER, M., MULLERTZ, A., O'DRISCOLL, C. M., PARROTT, N., PASZKOWSKA, J., PAVEK, P., PORTER, C. J. H., REPPAS, C., STILLHART, C.,

SUGANO, K., TOADER, E., VALENTOVA, K., VERTZONI, M., DE WILDT, S. N., WILSON, C. G. & AUGUSTIJNS, P. 2021. Current challenges and future perspectives in oral absorption research: An opinion of the UNGAP network. *Adv Drug Deliv Rev,* 171**,** 289-331.

VIVIAN, J. T. & CALLIS, P. R. 2001. Mechanisms of Tryptophan Fluorescence Shifts in Proteins. *Biophysical Journal,* 80**,** 2093-2109.

VRANIKOVA, B., NIEDERQUELL, A., DITZINGER, F., SKLUBALOVA, Z. & KUENTZ, M. 2020a. Mechanistic aspects of drug loading in liquisolid systems with hydrophilic lipid-based mixtures. *Int J Pharm,* 578**,** 119099.

VRANIKOVA, B., NIEDERQUELL, A., SKLUBALOVA, Z. & KUENTZ, M. 2020b. Relevance of the theoretical critical pore radius in mesoporous silica for fast crystallizing drugs. *Int J Pharm,* 591**,** 120019.

WAGNER, A. M., GRAN, M. P. & PEPPAS, N. A. 2018. Designing the new generation of intelligent biocompatible carriers for protein and peptide delivery. *Acta Pharm Sin B,* 8**,** 147-164.

WAGNER, B. M., SCHUSTER, S. A., BOYES, B. E., SHIELDS, T. J., MILES, W. L., HAYNES, M. J., MORAN, R. E., KIRKLAND, J. J. & SCHURE, M. R. 2017. Superficially porous particles with 1000A pores for large biomolecule high performance liquid chromatography and polymer size exclusion chromatography. *J Chromatogr A,* 1489**,** 75-85.

WAN, Y. & ZHAO, D. 2007. On the controllable soft-templating approach to mesoporous silicates. *Chem Rev,* 107**,** 2821-60.

WANG, D., JIANG, Q., DONG, Z., MENG, T., HU, F., WANG, J. & YUAN, H. 2023. Nanocarriers transport across the gastrointestinal barriers: The contribution to oral bioavailability via blood circulation and lymphatic pathway. *Adv Drug Deliv Rev,* 203**,** 115130.

WANG, J., YADAV, V., SMART, A. L., TAJIRI, S. & BASIT, A. W. 2015. Toward oral delivery of biopharmaceuticals: an assessment of the gastrointestinal stability of 17 peptide drugs. *Mol Pharm,* 12**,** 966-73.

WANG, M., SHAN, F., ZOU, Y., SUN, X., ZHANG, Z. R., FU, Y. & GONG, T. 2016. Pharmacokinetic and pharmacodynamic study of a phospholipid-based phase separation gel for once a month administration of octreotide. *J Control Release,* 230**,** 45-56.

WANG, T., WANG, N., HAO, A., HE, X., LI, T. & DENG, Y. 2010. Lyophilization of water-in-oil emulsions to prepare phospholipid-based anhydrous reverse micelles for oral peptide delivery. *Eur J Pharm Sci,* 39**,** 373-9.

WANG, T., XUE, P., WANG, A., YIN, M., HAN, J., TANG, S. & LIANG, R. 2019a. Pore change during degradation of octreotide acetate-loaded PLGA microspheres: The effect of polymer blends. *Eur J Pharm Sci,* 138**,** 104990.

WANG, W., HU, B., QIN, J. J., CHENG, J. W., LI, X., RAJAEI, M., FAN, J., YANG, X. R. & ZHANG, R. 2019b. A novel inhibitor of MDM2 oncogene blocks metastasis of hepatocellular carcinoma and overcomes chemoresistance. *Genes Dis,* 6**,** 419-430.

WANG, W. & OHTAKE, S. 2019. Science and art of protein formulation development. *Int J Pharm,* 568**,** 118505.

WANG, W., YAN, X., LI, Q., CHEN, Z., WANG, Z. & HU, H. 2020. Adapted nano-carriers for gastrointestinal defense components: surface strategies and challenges. *Nanomedicine,* 29**,** 102277.

WANG, X. Q. & ZHANG, Q. 2012. pH-sensitive polymeric nanoparticles to improve oral bioavailability of peptide/protein drugs and poorly water-soluble drugs. *Eur J Pharm Biopharm,* 82**,** 219-29.

WATERS, L. J., HANRAHAN, J. P., TOBIN, J. M., FINCH, C. V., PARKES, G. M. B., AHMAD, S. A., MOHAMMAD, F. & SALEEM, M. 2018. Enhancing the dissolution of phenylbutazone using Syloid(R) based mesoporous silicas for oral equine applications. *J Pharm Anal,* 8**,** 181-186.

WATFORD, M. & WU, G. 2018. Protein. *Adv Nutr,* 9**,** 651-653.

WONG, C. Y., AL-SALAMI, H. & DASS, C. R. 2018. Microparticles, microcapsules and microspheres: A review of recent developments and prospects for oral delivery of insulin. *Int J Pharm,* 537**,** 223-244.

WU, J., ZHENG, Y., LIU, M., SHAN, W., ZHANG, Z. & HUANG, Y. 2018. Biomimetic Viruslike and Charge Reversible Nanoparticles to Sequentially Overcome Mucus and Epithelial Barriers for Oral Insulin Delivery. *ACS Appl Mater Interfaces,* 10**,** 9916-9928.

WU, Z., JIANG, Y., KIM, T. & LEE, K. 2007. Effects of surface coating on the controlled release of vitamin B1 from mesoporous silica tablets. *J Control Release,* 119**,** 215-21.

WUNSCH, I., FINKE, J. H., JOHN, E., JUHNKE, M. & KWADE, A. 2021. The influence of particle size on the application of compression and compaction models for tableting. *Int J Pharm,* 599**,** 120424.

XU, Y., SHRESTHA, N., PREAT, V. & BELOQUI, A. 2020a. Overcoming the intestinal barrier: A look into targeting approaches for improved oral drug delivery systems. *J Control Release,* 322**,** 486-508.

XU, Y., SHRESTHA, N., PREAT, V. & BELOQUI, A. 2021. An overview of in vitro, ex vivo and in vivo models for studying the transport of drugs across intestinal barriers. *Adv Drug Deliv Rev,* 175**,** 113795.

XU, Y., VAN HUL, M., SURIANO, F., PREAT, V., CANI, P. D. & BELOQUI, A. 2020b. Novel strategy for oral peptide delivery in incretin-based diabetes treatment. *Gut,* 69**,** 911-919.

YANAGISAWA, T., SHIMIZU, T., KURODA, K. & KATO, C. 1990. The Preparation of Alkyltrimethylammonium–Kanemite Complexes and Their Conversion to Microporous Materials. *Bulletin of the Chemical Society of Japan,* 63**,** 988-992.

YILDIRIM, A., OZGUR, E. & BAYINDIR, M. 2013. Impact of mesoporous silica nanoparticle surface functionality on hemolytic activity, thrombogenicity and non-specific protein adsorption. *J Mater Chem B,* 1**,** 1909-1920.

YIN, M., SONG, Y., GUO, S., ZHANG, X., SUN, K., LI, Y. & SHI, Y. 2020. Intelligent Escape System for the Oral Delivery of Liraglutide: A Perfect Match for Gastrointestinal Barriers. *Mol Pharm,* 17**,** 1899-1909.

YOSHIDA, M., KAMEI, N., MUTO, K., KUNISAWA, J., TAKAYAMA, K., PEPPAS, N. A. & TAKEDA-MORISHITA, M. 2017. Complexation hydrogels as potential carriers in oral vaccine delivery systems. *Eur J Pharm Biopharm,* 112**,** 138-142.

YOSHIKAWA, H., HIRANO, A., ARAKAWA, T. & SHIRAKI, K. 2012. Effects of alcohol on the solubility and structure of native and disulfide-modified bovine serum albumin. *Int J Biol Macromol,* 50**,** 1286-91.

YU, Y., ZHAO, L., LIN, X., WANG, Y., DU, R. & FENG, Y. 2021. Research on the powder classification and the key parameters affecting tablet qualities for direct compaction based on powder functional properties. *Advanced Powder Technology,* 32**,** 565-581.

YUAN, H., BAO, X., DU, Y. Z., YOU, J. & HU, F. Q. 2012. Preparation and evaluation of SiO2-deposited stearic acid-g-chitosan nanoparticles for doxorubicin delivery. *Int J Nanomedicine,* 7**,** 5119-28.

ZHANG, A., ZHAO, Y., YOU, S. S. & LIEBER, C. M. 2020. Nanowire probes could drive high-resolution brain-machine interfaces. *Nano Today,* 31.

ZHANG, J., KARMAKAR, S., YU, M., MITTER, N., ZOU, J. & YU, C. 2014. Synthesis of silica vesicles with controlled entrance size for high loading, sustained release, and cellular delivery of therapeutical proteins. *Small,* 10**,** 5068-76.

ZHANG, L., ZENG, Z., HU, C., BELLIS, S. L., YANG, W., SU, Y., ZHANG, X. & WU, Y. 2016a. Controlled and targeted release of antigens by intelligent shell for improving applicability of oral vaccines. *Biomaterials,* 77**,** 307-19.

ZHANG, P., XU, Y., ZHU, X. & HUANG, Y. 2015. Goblet cell targeting nanoparticle containing drug-loaded micelle cores for oral delivery of insulin. *Int J Pharm,* 496**,** 993-1005.

ZHANG, W., LI, Y., ZOU, P., WU, M., ZHANG, Z. & ZHANG, T. 2016b. The Effects of Pharmaceutical Excipients on Gastrointestinal Tract Metabolic Enzymes and Transporters-an Update. *AAPS J,* 18**,** 830-43.

ZHANG, Y., DAVIS, D. A., ABOULFOTOUH, K., WANG, J., WILLIAMS, D., BHAMBHANI, A., ZAKREWSKY, M., MANIRUZZAMAN, M., CUI, Z. & WILLIAMS, R. O., 3RD 2021. Novel formulations and drug delivery systems to administer biological solids. *Adv Drug Deliv Rev,* 172**,** 183-210.

ZHAO, D., FENG, J., HUO, Q., MELOSH, N., FREDRICKSON, G. H., CHMELKA, B. F. & STUCKY, G. D. 1998a. Triblock copolymer syntheses of mesoporous silica with periodic 50 to 300 angstrom pores. *Science,* 279**,** 548-52.

ZHAO, D., HUO, Q., FENG, J., CHMELKA, B. F. & STUCKY, G. D. 1998b. Nonionic Triblock and Star Diblock Copolymer and Oligomeric Surfactant Syntheses of Highly Ordered, Hydrothermally Stable, Mesoporous Silica Structures. *Journal of the American Chemical Society,* 120**,** 6024-6036.

ZHOU, B., ZHEN, L., YANG, Y., MA, W., FU, Y., DUAN, X. & WANG, H. 2022. Novel composite phase change material of high heat storage and photothermal conversion ability. *Journal of Energy Storage,* 49.

ZHOU, M., HOU, T., LI, J., YU, S., XU, Z., YIN, M., WANG, J. & WANG, X. 2019. Self-Propelled and Targeted Drug Delivery of Poly(aspartic acid)/Iron-Zinc Microrocket in the Stomach. *ACS Nano,* 13**,** 1324-1332.

ZHOU, Y., WANG, J., XIAO, Y., WANG, T. & HUANG, X. 2018. The Effects of Polymorphism on Physicochemical Properties and Pharmacodynamics of Solid Drugs. *Curr Pharm Des,* 24**,** 2375-2382.

ZHU, J., ZHANG, Y., CHEN, X., ZHANG, Y., ZHANG, K., ZHENG, H., WEI, Y., ZHENG, H., ZHU, J., WU, F., PIAO, J. G., ZHU, Z. & LI, F. 2021a. Angiopep-2 modified lipid-coated mesoporous silica nanoparticles for glioma targeting therapy overcoming BBB. *Biochem Biophys Res Commun,* 534**,** 902-907.

ZHU, Q., CHEN, Z., PAUL, P. K., LU, Y., WU, W. & QI, J. 2021b. Oral delivery of proteins and peptides: Challenges, status quo and future perspectives. *Acta Pharmaceutica Sinica B*.

ZHU, Q., CHEN, Z., PAUL, P. K., LU, Y., WU, W. & QI, J. 2021c. Oral delivery of proteins and peptides: Challenges, status quo and future perspectives. *Acta Pharm Sin B,* 11**,** 2416-2448.

ZHU, S., PUDNEY, P. D., HEPPENSTALL-BUTLER, M., BUTLER, M. F., FERDINANDO, D. & KIRKLAND, M. 2007. Interaction of the acid soap of triethanolamine stearate and stearic acid with water. *J Phys Chem B,* 111**,** 1016-24.

ZIZZARI, A. T., PLIATSIKA, D., GALL, F. M., FISCHER, T. & RIEDL, R. 2021. New perspectives in oral peptide delivery. *Drug Discov Today,* 26**,** 1097-1105.

ZU, M., MA, Y., CANNUP, B., XIE, D., JUNG, Y., ZHANG, J., YANG, C., GAO, F., MERLIN, D. & XIAO, B. 2021. Oral delivery of natural active small molecules by polymeric

nanoparticles for the treatment of inflammatory bowel diseases. *Adv Drug Deliv Rev*, 113887.